BioMed Research International

Tissue Engineering: From Basic Sciences to Clinical Perspectives

Guest Editors: Pornanong Aramwit, Antonella Motta, and Subhas C. Kundu

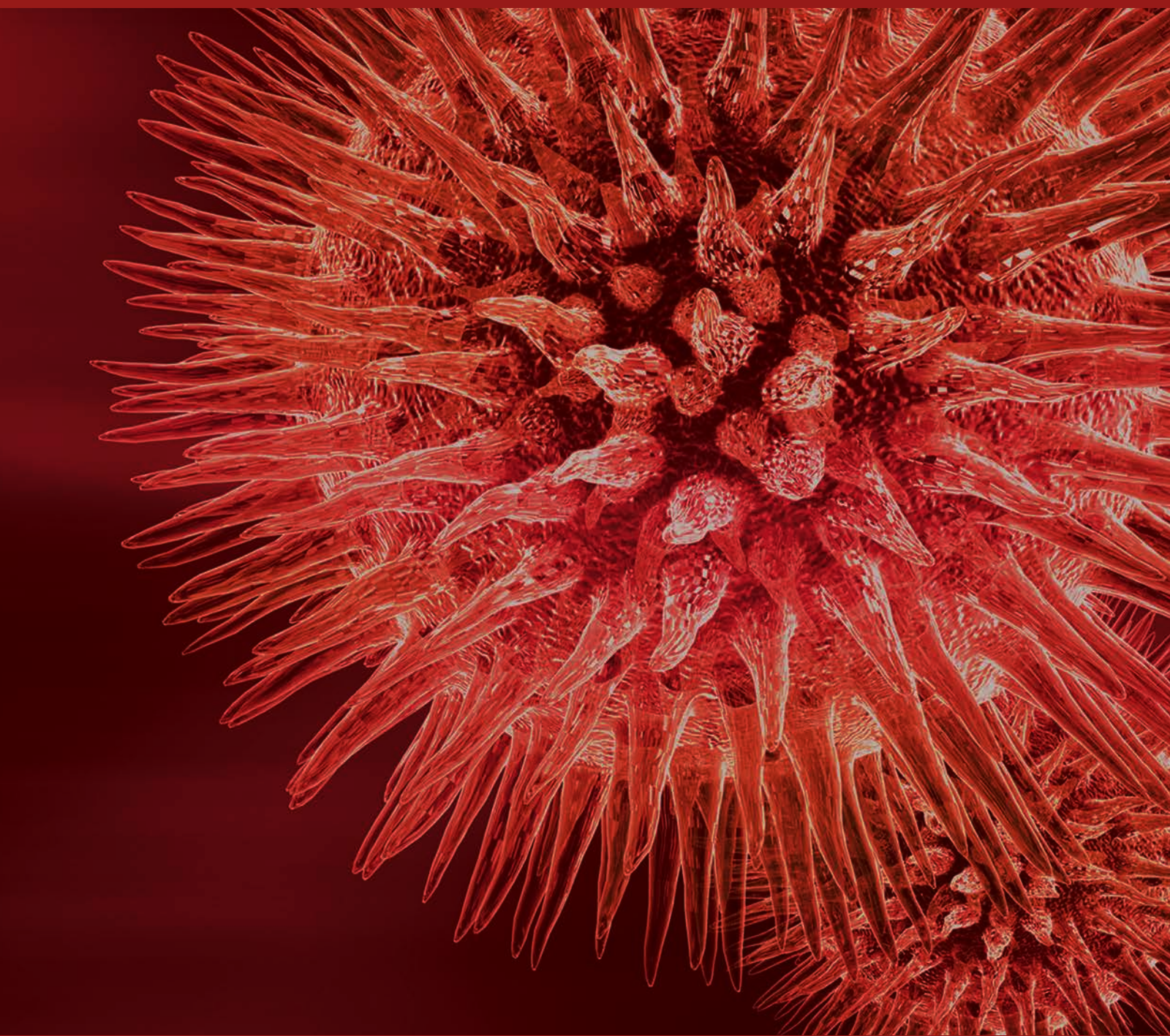

Tissue Engineering: From Basic Sciences to Clinical Perspectives

BioMed Research International

Tissue Engineering: From Basic Sciences to Clinical Perspectives

Guest Editors: Pornanong Aramwit, Antonella Motta, and Subhas C. Kundu

Contents

Hindawi Publishing Corporation
BioMed Research International
Volume 2017, Article ID 8659036, 2 pages
http://dx.doi.org/10.1155/2017/8659036

Editorial

Tissue Engineering: From Basic Sciences to Clinical Perspectives

Pornanong Aramwit,[1] Antonella Motta,[2] and Subhas C. Kundu[3,4]

[1] *Chulalongkorn University, Bangkok, Thailand*
[2] *University of Trento, Trento, Italy*
[3] *Indian Institute of Technology Kharagpur, Kharagpur, India*
[4] *3B Research Group, University of Minho, Braga, Portugal*

Correspondence should be addressed to Pornanong Aramwit; aramwit@gmail.com

Received 18 October 2016; Accepted 18 October 2016; Published 23 January 2017

Tissue engineering and regenerative medicine are interrelated terms and go hand in hand whether we discuss about cells (of any kind especially stem and progenitor cells), biomaterials as matrices (2D films, 3D forms of scaffolds, nanofibers, hydrogels, nanoparticles, aerogel, microcapsules, mats, biogel for 3D printing, blends of naturals and/or synthetics, and others), and addition of bioactive molecules (delivery of growth hormones and drugs) for improvement and/or regeneration of tissues for biomedical applications (in relation to cartilage, shin, bone, blood vessels, nerve conduits, cardiac, adipose, tissue expression, and others). Therefore, it includes basic principles of biological sciences, material chemistry, and relevant engineering subjects. Finally for medical applications after proper clinical verifications of the appropriate films, scaffolds, devices, delivery systems, and other relevant products are needed.

New drugs and innovative devices improve the quality of life for patients with several diseases, which are not necessarily decreased morbidity or mortality in some conditions. Organ replacement is eminently successful but the limitation of available organs made them sparingly used. Tissue engineering and regenerative medicine are proposed as solution by replacing tissue or organ function with constructs that contain specific populations of living cells. Tissue specific stem cells (adult stem cells) become functional cells, which can be used for tissue regeneration (adult stem cell therapy). These cells can replace the defective/damaged cells in different kind of diseases. Therefore, tissue engineering is a new alternate route for the regeneration of damaged/degenerated cells or tissues. This research needs scaffolds (natural and or synthetic), cells (preferably stem cells including induced stem cells), and bioactive molecules (growth hormones). Researchers investigate the possibility of several biomaterials as said using both synthetic and natural substances in the tissue engineering field and regenerative medicines. Different parameters need to be considered before the specific material can be used in clinical investigations.

Due to the advance technology in tissue engineering describing recent findings in this field a few relevant topics are included in this issue. This issue is not a collection of papers based on conferences.

Broad spectrum of tissue engineering-related research work is brought together, for example, potential media supplement for animal cell culture using silk protein sericin, contribution of human umbilical cord blood-derived mesenchymal stem cells towards chondrogenesis, 3D culture of human adult liver cells on hydroxyapatite scaffolds, regenerative peripheral nerve interface for control of a neuroprosthetic limb, and present status in clinical implications of cartilage regeneration in human with adipose tissue-derived stem cells. These areas of research are relevant to the subject of tissue engineering.

It is expected in immediate or near future that there will be development of novel medical devices, artificial organs, cell printing, cell transplantation, and latest combined technologies that will maintain, improve, or restore the functions

of diseased organs, new and multifunctional engineered materials, and novel methodological paradigms that challenge advanced thinking in clinical research, applications, and finally valuable assessments.

Pornanong Aramwit
Antonella Motta
Subhas C. Kundu

Hindawi Publishing Corporation
BioMed Research International
Volume 2016, Article ID 1917394, 13 pages
http://dx.doi.org/10.1155/2016/1917394

Research Article

Proteomic Profiling of Neuroblastoma Cells Adhesion on Hyaluronic Acid-Based Surface for Neural Tissue Engineering

Ming-Hui Yang,[1] Ko-Chin Chen,[2] Pei-Wen Chiang,[3] Tze-Wen Chung,[4] Wan-Jou Chen,[3] Pei-Yu Chu,[5,6] Sharon Chia-Ju Chen,[3] Yi-Shan Lu,[7] Cheng-Hui Yuan,[8] Ming-Chen Wang,[9] Chia-Yang Lin,[3,10] Ying-Fong Huang,[3,10] Shiang-Bin Jong,[3,10] Po-Chiao Lin,[11] and Yu-Chang Tyan[1,3,12,13]

[1] *Center for Infectious Disease and Cancer Research, Kaohsiung Medical University, Kaohsiung 807, Taiwan*
[2] *Department of Pathology, Changhua Christian Hospital, Changhua 500, Taiwan*
[3] *Department of Medical Imaging and Radiological Sciences, Kaohsiung Medical University, Kaohsiung 807, Taiwan*
[4] *Department of Biomedical Engineering, National Yang-Ming University, Taipei 112, Taiwan*
[5] *Department of Laboratory Medicine, Kaohsiung Medical University Hospital, Kaohsiung 807, Taiwan*
[6] *Department of Medical Laboratory Science and Biotechnology, College of Health Sciences, Kaohsiung Medical University, Kaohsiung 807, Taiwan*
[7] *Office of Safety, Health and Environment, Kaohsiung Medical University, Kaohsiung 807, Taiwan*
[8] *Mass Spectrometry Laboratory, Chemical, Molecular and Materials Analysis Center, Department of Chemistry, National University of Singapore, Singapore 119077*
[9] *Department of Biomedical Engineering, Chung Yuan Christian University, Chungli 300, Taiwan*
[10] *Department of Nuclear Medicine, Kaohsiung Medical University Hospital, Kaohsiung 807, Taiwan*
[11] *Department of Chemistry, National Sun Yat-sen University, Kaohsiung 804, Taiwan*
[12] *Graduate Institute of Medicine, College of Medicine, Kaohsiung Medical University, Kaohsiung 807, Taiwan*
[13] *Institute of Medical Science and Technology, National Sun Yat-sen University, Kaohsiung 804, Taiwan*

Correspondence should be addressed to Yu-Chang Tyan; yctyan@kmu.edu.tw

Received 27 June 2016; Revised 10 September 2016; Accepted 5 October 2016

Academic Editor: Pornanong Aramwit

The microenvironment of neuron cells plays a crucial role in regulating neural development and regeneration. Hyaluronic acid (HA) biomaterial has been applied in a wide range of medical and biological fields and plays important roles in neural regeneration. PC12 cells have been reported to be capable of endogenous NGF synthesis and secretion. The purpose of this research was to assess the effect of HA biomaterial combining with PC12 cells conditioned media (PC12 CM) in neural regeneration. Using SH-SY5Y cells as an experimental model, we found that supporting with PC12 CM enhanced HA function in SH-SY5Y cell proliferation and adhesion. Through RP-nano-UPLC-ESI-MS/MS analyses, we identified increased expression of HSP60 and RanBP2 in SH-SY5Y cells grown on HA-modified surface with cotreatment of PC12 CM. Moreover, we also identified factors that were secreted from PC12 cells and may promote SH-SY5Y cell proliferation and adhesion. Here, we proposed a biomaterial surface enriched with neurotrophic factors for nerve regeneration application.

1. Introduction

Nerve injury is an important topic in the world of medicine and there are many nerve injury cases reported every year. These injuries usually have caused a decreased quality of life because of reduction in motor, sensory and autonomic functions [1, 2]. The peripheral nervous system is more permissive to axonal regeneration then the central nervous system; but it is still a challenge to surgery [3]. Despite microsurgical techniques which are more advanced, experimental

and clinical evidences show the results of peripheral nerve recovery are not satisfying [4, 5]. Nerve autograft is the gold standard technique for therapy in peripheral nerve injury. A tubular nerve guidance channel is necessary for nerve autograft. It acts as a physical guide for nerve regeneration and provides a conduit for neurotrophic factor diffusion from the injured nerve stumps [3, 6, 7]. In the past few years, scientists have focused on various conduit materials, including aliphatic polyesters [8, 9], poly(phosphoesters) [10], polyurethanes [11], piezoelectric polymers [12], hydrogel-based nerve guide channels [13], collagen [14], polysaccharides [15], and decellularized biomatrices [3, 16].

Hyaluronan (hyaluronic acid, HA), a component of the extracellular matrix, is a glycosaminoglycan applicable to biomaterial. During embryogenesis, the concentration of HA is at the peak in undifferentiated cells and decreases at the beginning of cell differentiation [17]. Such change is crucial for the angiogenic process regulation and its presence in the extracellular matrix (ECM) is as a naturally occurring polysaccharide [18–20]. HA is vital in the brain development, especially to the postnatal brain in regions adjacent to the lateral ventricles where stem cells reside [21, 22]. It has been reported as a significant factor in a wide range of medical and biological fields, such as reactive oxygen species, angiogenesis, cancer, lung injury, liver injury, kidney injury, brain injury, diabetes, and leukocyte trafficking and in immune regulation [23, 24]. It also plays important roles in neural proliferation, differentiation, migration, survival, and cell signaling [25]. HA-induced signal transduction depends on the interactions of cell surface receptors, including cluster determinant 44 (CD44) and toll-like receptor 4 (TLR4) [26]. In the central nervous system, the HA expression level is elevated at damaged sites. The high molecular weight HA has been digested through hyaluronidases becoming smaller fragments; such products activate downstream signal transduction to regulate progenitor cell differentiation and proliferation to promote nerve repair [25]. It also has advantages as a scaffold material and can be combined with adhesive peptides or other ECM components to provide cell attachment. Previous study indicated that combination scaffolds consisting of fibrin with HA and laminin provide biomaterial properties to enable polymerization with cells. This mimics the native tissue of the brain and supports differentiation of human neural stem/progenitor cell (hNSPC) function [27]. Currently, HA-based biomaterials are used to regulate the cell differentiation and studied for tissue engineering purposes in combination with growth factors or ECM components for tissue repair [28–33].

Cell to cell interaction is important for cell fate determination, providing the first evidence for short-range regulatory mechanisms of cell differentiation. The conditioned medium (CM), which contains growth factors and differentiation regulation factors that are released from the cultured cells, could be used to promote cell differentiation into specific lineages [34]. Previous reports indicated that mouse embryonic stem cells (mESCs) treated with HepG2 CM can enhance mesoderm induction and the subsequent osteogenic differentiation of mESCs [35]. In addition, human marrow stromal cells (hMSC) CM can stimulate the induction of the mesodermal lineage and subsequent differentiation toward the osteogenic and chondrogenic lineage [36]. Differentiation of the human umbilical cord blood neuronal progenitors (HUCBNPs) was achieved by treatment with human SH-SY5Y CM, which showed an increase of the ratio of long outgrowths to cell body diameter and a characteristic of developing neurons [37]. PC12 cells require no supplementary NGF for survival and proliferation because they synthesize and secrete endogenous NGF into the medium as an autocrine regulation, which may be applied for neuron development [38]. The combination of PC12 CM and HA surface biomaterials may synergistically induce the neuronal cell differentiation, offering a new field of vision in nerve regeneration.

In this study, we examined the effects of HA and PC12 CM in SH-SY5Y cells. SH-SY5Y is one kind of human derived cell line which is used in scientific research. The original cell line, called SK-N-SH, was subcloned and isolated from a bone marrow biopsy, which had been taken from a female with neuroblastoma. This cell line has been widely used as a model of neuron diseases as these cells possess many biochemical and functional properties of neurons. SH-SY5Y cells have been widely used as in vitro models of neurological studies, including analysis of neuronal differentiation, metabolism, and function related to neurodegenerative and neuroadaptive processes, neurotoxicity, and neuroprotection. It can be differentiated to a more mature neuron-like phenotype that is characterized by dopaminergic markers and, as such, has been used to study Parkinson's disease [39]. Through the investigation, proteins that influence the responses and later proliferation of SH-SY5Y cells on HA-biopolymer surfaces and PC12 CM were identified. Using proteomic approaches to assess characteristic proteins from HA and PC12 CM treatment found that heat shock protein 60 (HSP60) and E3 SUMO-protein ligase RanBP2 were involved in cell proliferation and attachment regulated the UBC/PI3K/AKT1/mTOR pathway.

2. Materials and Methods

2.1. HA Surfaces Determined by QCM Measurements. The surface of a 9 MHz QCM gold electrode (ANT Tech, Taiwan) was washed with 1 M HCl, rinsed with DI water, followed by drying at room temperature. The frequency of the electrode measured by the QCM (ADS, ANT Tech, Taiwan) was assigned as F_0 and the flow rate was 60 μL/min of phosphate buffered saline (PBS). To prepare QCM-HA layers, HA was adsorbed onto a QCM electrode surface using the layer-by-layer technique. The HA solution (0.5%, Lifecore Biomedical, Inc., USA) was injected into the flow loop of the QCM electrode at flow rate of 60 mL/min and the frequency shifts of the QCM were measured. The frequency shifts determined by the QCM were recorded and the mass of HA adsorption was calculated. To test whether HA layer is stably coated onto the electrode, the frequency of the electrode was measured by the flow of PBS for several minutes. For tested HA-biopolymer, the frequency shift dropped sharply, it was absorbed onto the electrode surface. The detection theory for QCM can be

explained by the Sauerbrey equation (1), which calculates that the mass change is proportional to the oscillation frequency shift of the piezoelectric quartz crystal.

$$\Delta F = -2.3 \times 10^{-6} \frac{F^2 \Delta M}{A} \quad (1)$$

In Sauerbrey equation (1) in gas phase, ΔF is the frequency shift (Hz); F is basic oscillation frequency of piezoelectric quartz (Hz); A is the active area of QCM (cm^2); ΔM is the mass change on QCM (g).

2.2. Culturing SH-SY5Y Cells on the Electrodes Decorated by HA Surfaces. For seeding SH-SY5Y cells, the HA-modified electrodes, decorated by biopolymer layers, were sterilized with 70% (v/v) ethanol and then exposed to ultraviolet light. The 4×10^4 SH-SY5Y cells in serum-free medium were added to each well in the presence of the aforementioned electrodes and incubated at 37°C in 5% CO_2 for 12 hours for investigation of the adhesion of the cells on those electrodes. After the incubations, the electrodes were washed with PBS, and then frequency shifts were measured by the QCM to quantify the adhesions of SH-SY5Y cells on electrodes.

2.3. HA Surface Characterized by FT-IR. The surface characterization of the coverslips decorated with HA was observed using a Fourier transform infrared spectrometer (FT-IR, Spectrum One system, PerkinElmer, USA).

2.4. Cell Culture and Conditioned Media (CM) Collection. For human neuroblastoma cell line, SH-SY5Y cells were cultured in Dulbecco's Modified Eagle Medium: nutrient mixture F-12 (DMEM/F12) medium (Gibco, Invitrogen, USA) with 10% FBS plus 1% antibiotics. In the pheochromocytoma cell line of the rat adrenal medulla, PC12 cells were maintained in DMEM medium with 10% horse serum, 5% FBS plus 1% antibiotics. Those cells were incubated in 5% CO_2 at 37°C for 48 hours.

In this study, PC12 CM were collected, filtered, and mixed with equal volumes of fresh DMEM/F12 medium for SH-SY5Y cells to be cultivated on HA surface. To collect PC12 CM, the PC12 cells were rinsed with phosphate buffer saline (PBS) and then incubated in serum-free DMEM medium for 12 hours. Then, the supernatants of the medium were collected and filtered with 0.22 μm filter.

2.5. Protein Preparation for Proteomic Analysis. SH-SY5Y cell lysates or PC12 CM were transferred into 1.5 mL tubes and reduced with 1 M dithiothreitol (DTT, USB Corporation, USA) in 25 mM NH_4HCO_3 at 37°C. After 3 hours, protein samples were alkylated with 1 M iodoacetamide (IAA, Amersham Biosciences, USA) in the dark at room temperature for 30 min. After the proteins were digested by sequencing-grade modified porcine trypsin (Promega, USA) overnight at 37°C, 2 μL of formic acid was added to each sample.

RP-nano-UPLC ESI-MS/MS analyses (nanoACQUITY UPLC, Waters, Milford, MA, coupled to an ion trap mass spectrometer, LTQ Orbitrap Discovery Hybrid FTMS, Thermo, San Jose, CA) were conducted according to standard procedures described below. Briefly, a sample of the desired peptide digest was loaded into the reverse phase column (symmetry C18, 5 μm, and 180 μm × 20 mm). The RP separation was performed using a linear acetonitrile gradient from 99% buffer A (100% DI water/0.1% formic acid) to 85% buffer B (100% acetonitrile/0.1% formic acid) in 120 min using the micropump at a flow rate of approximately 400 nL/min. The separation was performed on a C18 microcapillary column (BEH C18, 1.7 μm, and 75 μm × 100 mm). As peptides were eluted from the microcapillary column, they were electrosprayed into the ESI-MS/MS with the application of a distal 2.1 kV spraying voltage with heated capillary temperature of 200°C. Each cycle of one full-scan mass spectrum (m/z 400–2000) was followed by three data dependent tandem mass spectra with collision energy set at 35% [40].

All MS and MS/MS data were analyzed and processed using the Mascot software (Version 2.2.1, Matrix Science, London, UK) against the Swiss-Prot database. The search parameters were set as follows: 0.5 Da for MS/MS tolerance, 10 ppm for MS tolerance, carbamidomethylation (C) as the fixed modification, deamidated (NQ), oxidation (M), phospho (ST) and phospho (Y) as the variable modification, and 2 for missing cleavage. Proteins were initially annotated by similar search conditions using UniProtKB/Swiss-Prot databases (SIB Swiss Institute of Bioinformatics, Lausanne, Switzerland). The protein-protein interaction pathways were performed by String 9.1 Web software (SIB Swiss Institute of Bioinformatics, Lausanne, Switzerland) [41].

2.6. Western Blotting of Protein Expression. Confirmation of protein identities was performed by Western blotting. Protein extracts were prepared in lysis buffer and each cell lysate sample (1 μg/μL, 10 μL) was electrophoresed through a precast gel (NuPAGE®Novex® 4–12% Bis-Tris Gel, 1.5 mm, 10 wells, Invitrogen™, Carlsbad, CA). Proteins were transferred from the gel to a polyvinyldifluoride (PVDF) membrane (Millipore, Bedford, CA) by means of the semidry technique using the Criterion Blotter (Bio-Rad) at 100 V for 60 min and blocked with 5% milk in PBS (adjusted to pH 7.4) containing 0.05% Tween-20. The membranes were then separately incubated overnight with primary rabbit antibodies (1 μg/μL). The commercially available primary antibodies used in this study included the following: monoclonal mouse anti-HSP60 (Stressgen, USA) and polyclonal rabbit anti-RanBP2 (Abcam, USA). After washing, the membrane was incubated with HRP-conjugated goat anti-mouse IgG antibodies (purchased from Jackson ImmunoResearch, USA) for 1 hour (1 : 10000). Proteins were detected with an enhanced chemiluminescent (ECL) system, and quantitative analysis of Western blotting was carried out using the ImageQuant-TL-7.0 software, version 2010 (Amersham Biosciences).

2.7. BrdU Assay. The cell viability was determined by BrdU cell proliferation assay kit (Millipore). The assay was performed according to the manufacturer's instructions. Briefly, 1×10^3 SH-SY5Y cells were seeded in a sterile 96-well tissue culture plate and incubated for 24 to 72 hours. Then, cells were

incubated in the culture medium containing BrdU reagent for 2 hours. Fixing solution was added before the absorbance was measured at 450 nm using an ELISA reader (Multiskan EX, Thermo Scientific, Vantaa, Finland).

2.8. Cell Morphology Observed by Immunofluorescence Staining. The SH-SY5Y cells were grown on coverslips in 12-well culture plates. After 24 hours' incubation, the cells were fixed (60% methanol and 40% acetone) at −20°C for 30 min and then permeabilized (0.5% Triton X-100) at room temperature for 5 min. After rinsing with PBS, the cells were blocked (6% bovine serum albumin) and then incubated with primary and secondary antibodies. The nuclei and cytoskeleton of the cells were stained with DAPI (Sigma-Aldrich, USA), vimentin (Vimentin DyLight 488 Antibody, Epitomics, USA), monoclonal mouse anti-HSP60 (Stressgen, USA), and polyclonal rabbit anti-RanBP2 (Abcam, USA), respectively. After rinsing with PBS, the cells were mounted with ProLong® Gold Antifade Reagent (Invitrogen). The images were acquired by a microscope equipped with fluorescence light source (FLoid Cell Fluorescence Imaging Station, Invitrogen).

2.9. Statistical Analysis. All calculations used the SigmaStat statistical software (Jandel Science Corp., San Rafael, CA, USA). All statistical significance was evaluated at 95% of confidence level or better. Data are presented as mean ± standard error.

3. Results and Discussion

3.1. Quantitative Analysis of Adsorbed of HA and Adhesion of SH-SY5Y Cells on Electrodes Using QCM Techniques. In our previous studies, the QCM system was applicable to the quantitative analysis of adsorption of HA and adhesion of cells on electrodes [42, 43]. The QCM frequency variation after HA-biopolymer formation was −212.47 ± 6.33 Hz; the adsorbed HA mass corresponding to those surfaces was 228.11 ± 3.30 ng. To investigate the adhesion of SH-SY5Y cells onto electrodes decorated by HA surface with PC12 CM, SH-SY5Y cells were incubated on the electrodes. The cultivation of SH-SY5Y cells under serum-free conditions after 12 hours herein prevented the apoptosis and proliferation of cells, which were then changed to DMEM/F12 medium without or with PC12 CM. The results concerning the adhesion of SH-SY5Y cells onto the electrode of QCM that was decorated by HA were obtained from the frequency shifts. The frequency shifts for HA-modified surfaces without or with PC12 CM were from -3.68 ± 0.42 to $-10.47 \pm 0.27 \times 10^3$ Hz; the attached cell mass corresponding to HA surface was from 1.13 ± 0.13 to $3.22 \pm 0.08 \times 10^3$ ng, respectively (Table 1, $n = 10$). With treatment of PC12 CM after 48 and 72 hours, the frequency shift was lowered and the mass of cell was increased from that of regular medium. These results indicated that PC12 CM may be beneficial to SH-SY5Y cells adhesion or proliferation.

3.2. Investigation of HA Structure by FT-IR. HA-modified surfaces of coverslips were also routinely characterized using FT-IR spectra. The FR-IR spectra in the range of 500–4000 cm^{-1} for HA surfaces were presented in Figure 1. Expansion of the FT-IR spectra in Figure 1 clearly showed the difference between spectra of nonmodified and HA-modified coverslips. The HA-modified surface showed several sharp peaks such as at 894.9 and 1049.1 cm^{-1} that could be due to the C-O-C stretching, at 1321.0 cm^{-1} that corresponds to the presence of C-O with C=O combination, at 1406.9 cm^{-1} that indicates the presence of NH deformation, at 1616.1 cm^{-1} due to the C=O carboxyl amide I, and at 2893.8 to 3433.8 cm^{-1} that confirms the presence of CH stretching, and NH with C=O combination and OH stretching. Similar peaks were indicated in Table 2. These peaks obtained in the HA-modified surface share a highly similar position when compared to the standard HA.

Table 1: Frequency shifts of QCM and weights of adhered SH-SY5Y cells on the electrodes decorated with HA-modified surface for 24 to 72 hours of cell incubation.

Cell adhesion	ΔF ($\times 10^3$ Hz)	Δm ($\times 10^3$ ng)
DMEM/F12 medium		
24 hrs	−3.68 ± 0.42	1.13 ± 0.13
48 hrs	−4.70 ± 0.48	1.44 ± 0.15
72 hrs	−4.93 ± 0.69	1.51 ± 0.21
DMEM/F12 medium-PC12 CM		
24 hrs	−6.30 ± 1.35	1.94 ± 0.42*
48 hrs	−10.83 ± 0.58	3.33 ± 0.18*
72 hrs	−10.47 ± 0.27	3.22 ± 0.08*

Data are expressed as mean ± standard error, $n = 10$, * $P < 0.05$ (t-test).

Table 2: The assignment of FT-IR bands for HA-modified surface.

Function group	Wavenumber (cm^{-1})
C-O-C stretching, O-H deformation, C=O deformation	894.9
C-O-C, C-O, C-O-H stretching	1049.1
CH_2, CH_3C-O-H deformation, C-O with C=O combination	1321.0
NH deformation	1406.9
C=O carboxyl amide I	1616.1
CH stretching	2893.8
NH with C=O combination	3261.2
NH stretching and OH stretching	3433.8

3.3. Combination Treatment of HA and PC12 CM Increased SH-SY5Y Cell Proliferation. HA is well known to promote fibroblasts proliferation and enhance cell adhesion [42]. To investigate the HA and PC12 CM effect on SH-SY5Y cells, the cell proliferation was assessed. The 4×10^4 SH-SY5Y cells were seeded and grown on HA-modified and nonmodified coverslips. The cell proliferation was measured by BrdU assay for 24, 48, or 72 hours and the baseline of cell proliferation was set at 12 hours after seeding. As shown in Figure 2, SH-SY5Y cell proliferation rates on HA-modified coverslips

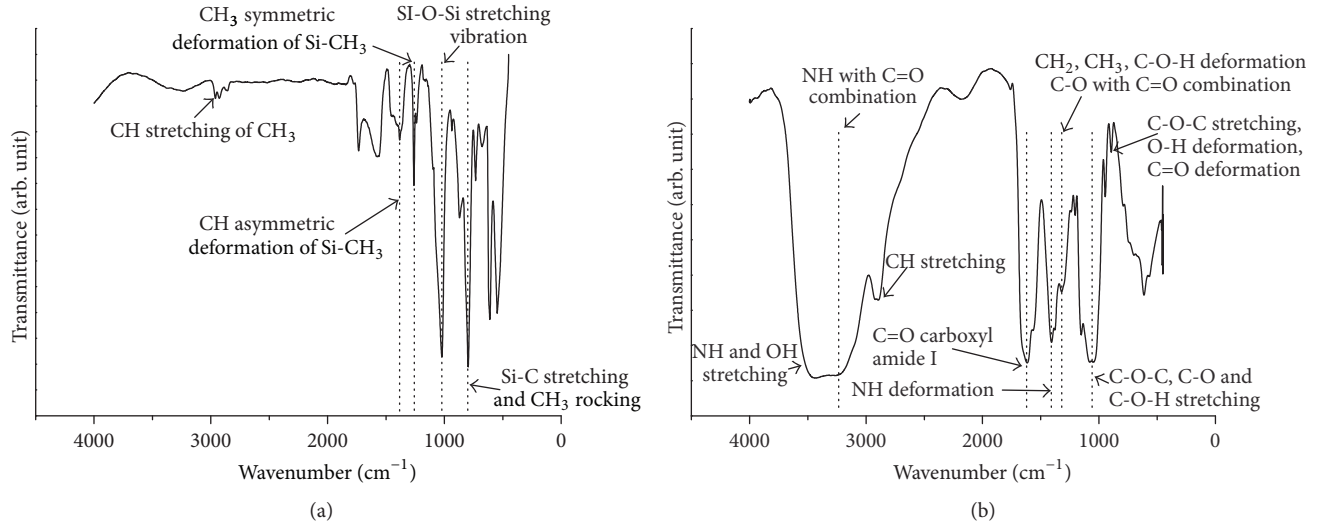

Figure 1: The FT-IR spectra show the frequency region from 4000 to 500 cm^{-1} of modified surfaces and (a) nonmodified and (b) HA-modified coverslips.

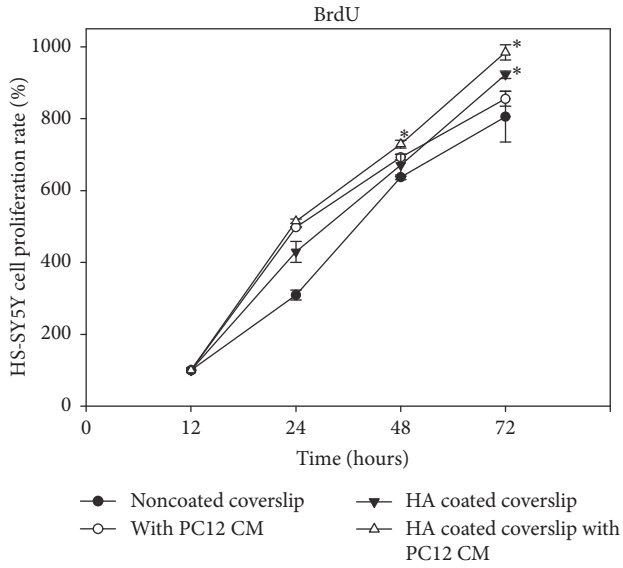

Figure 2: The relative percentage of cell viability obtained from BrdU cell proliferation assay. Differential treatments of SH-SY5Y cells were seeded in 96-well tissue culture plates and incubated for 24 to 72 h. Cells were treated with BrdU reagent for 2 h and fixed before the absorbance was measured at 450 nm.

were similar to those of nonmodified coverslips of 48 hours. However, the SH-SY5Y cell proliferation rate was increased significantly after 72 hours on the HA-modified coverslips.

The PC12 CM was collected and added to the culture medium of the SH-SY5Y cell. After 48 hours' incubation, the results showed that PC12 CM induced SH-SY5Y cell growth and proliferation especially with the HA-modified surface. The HA-modified coverslip combined with treatment of PC12 CM promoted SH-SY5Y cell proliferation after 72 hours' incubation as indicated in Figure 2 using BrdU assay. Therefore, HA and PC12 CM were the two factors with a synergistic effect.

To understand the mechanism and consequence of the increasing of the SH-SY5Y cell proliferation and growth, the proteins in PC12 CM and SH-SY5Y cell lysate were identified by proteomic approaches.

3.4. Identification of Regulator Secreted from PC12. To identify the PC12 secreted proteins related to SH-SY5Y cell proliferation and cell adhesion, the original PC12 CM were collected and the proteins were identified by RP-nano-HPLC-ESI-MS/MS. One hundred seventy-three HA-modified surface proteins were identified and then narrowed down to the number 62, using a threshold of a minimum of three peptides identified in a protein. We found that several proteins (described below) are involved in cell differentiation functions. Table 3 shows the details of the protein identification (protein accession number, protein name, biological process, and molecular function) in PC12 CM.

The expression of Gametogenetin (GGN) was confined to late pachytene spermatocytes and round spermatids, a time window concomitant with the occurrence of meiosis. It was expressed with highest level in diplotene spermatocytes and meiotic germ cells, especially when the nuclear membrane breaks down and the nucleolus is disorganized. In addition to functioning in proliferation of primordial germ cells, POG also involved in spermatogenesis [44].

Adrenomedullin (ADM) is a member of the calcitonin gene-related peptide (CGRP) family, which has shown neuroprotective functions [45]. ADM is secreted in many organs and tissues [46], and so were PC12 cells. ADM mediates downstream signaling through calcitonin receptor-like receptor (CRL)-receptor-activity-modifying proteins (RAMPs) complex [46].

Spermatid perinuclear RNA-binding protein (SPNR) is a microtubule-associated RNA-binding protein [47]. SPNR gene has been detected in the testis, ovary, and brain [48]. Mice deficient for SPNR show neurologic, spermatogenic, and sperm morphological abnormalities [49]. In our study,

Table 3: Proteins identified by the higher confidence level (at least three unique peptide sequences matched) in the PC12 CM which were involved in neuron generation function.

Accession numbers	Protein name	Biological process	Molecular function
Q66HC8	Gametogenetin	Cell differentiation	
		Double-strand break repair	
		Embryo implantation	
		Spermatogenesis	
P43145	ADM	Aging	Adrenomedullin receptor binding
		Androgen metabolic process	
		Calcium ion homeostasis	
		cAMP-mediated signaling	
		Hormone secretion	
		Vasculogenesis	
		Cell proliferation	
		Apoptotic process	
Q9JKU6	Spermatid perinuclear RNA-binding protein	Cell differentiation	DNA binding
		Multicellular organismal development	RNA binding
		Spermatogenesis	
O35569	Pro-neuregulin-2, membrane-bound isoform	Epidermal growth factor receptor signaling pathway	Epidermal growth factor receptor binding
		Intracellular signal transduction	ErbB-3 class receptor binding
		Organ development	
Q62956	Receptor tyrosine-protein kinase erbB-4	Cardiac muscle tissue regeneration	ATP binding
		Cell migration	Receptor signaling protein tyrosine kinase activity
		Nervous system development	Transmembrane receptor protein tyrosine kinase activity
		Apoptotic process	
		Cell proliferation	
		Glucose import	
		Odontogenesis	
		Protein tyrosine kinase Signaling pathway	
P01026	Complement C3	Blood coagulation	C5L2 anaphylatoxin chemotactic receptor binding
		Chemotaxis	Cofactor binding
		Fatty acid metabolic process	Endopeptidase inhibitor activity
		Inflammatory response	Lipid binding
		Glucose transport	
		Triglyceride biosynthetic process	
		Response to progesterone and estrogen	
Q9R172	Neurogenic locus notch homolog protein 3	Cell differentiation	Calcium ion binding
		Multicellular organismal development	
		Notch signaling pathway	
		Regulation of transcription, DNA-templated	
		Tissue regeneration	

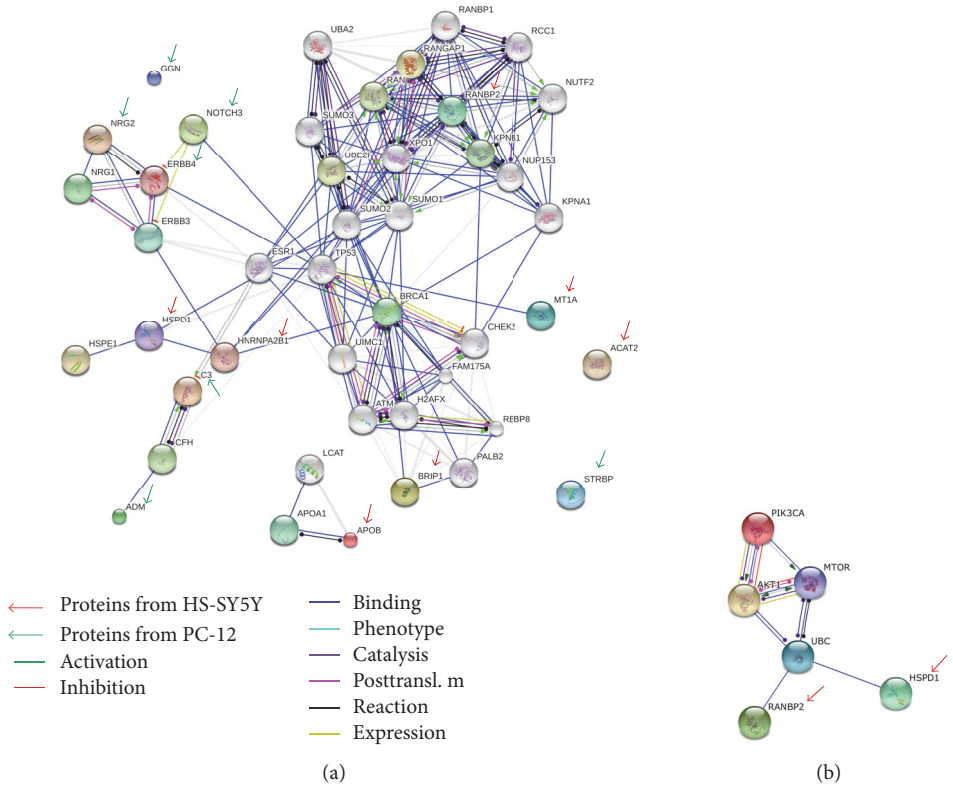

Figure 3: The protein-protein interaction pathways are illustrated. (a) Proteins identified in this study are marked by arrows (red: SH-SY5Y; green: PC12). (b) Two proteins, HSP60 and RanBP2, may turn on the ubiquitin (UBC) pathway, which is responsible for the proliferation and is required for survival of the majority of cells.

SPNR was detected in PC12 CM. This finding indicates that SPNR may be involved in neuron cell development.

The Pro-neuregulin-2 (Nrg2) has played a critical role in the growth and development of multiple organ systems, which was also involved in neural and organ development. In the embryo, the Nrg2 was expressed in the brain where it was found in the telencephalon, but not in the hindbrain. The Nrg2 was direct ligand for ErbB 3 and ErbB 4 tyrosine kinase receptors. Concomitantly recruiting ErbB 1 and ErbB 2 coreceptors, the Nrg2 may result in ligand-stimulated tyrosine phosphorylation and activation of the ErbB receptors, which may also promote the heterodimerization with the EGF receptor [50].

NRG1/ErbB signaling pathways are important in CNS development and may be neuroprotective in brain injury [51]. ErbB4 is predominantly expressed in the brain and well characterized for its function in the CNS [52]. In the CNS, NRG1/ErbB4 signaling is involved in neuronal migration, dendritic spine maturation, and the formation of inhibitory synapses onto excitatory pyramidal neurons [51]. ErbB4 mutant mice were showed to alter the organization and migration of neuroblast chain and display olfactory interneurons deficits in the placement and differentiation [53].

The complement system plays an important role in inflammatory diseases and neurodegenerative processes of the CNS [54]. C3a, one of complement factors, has been shown to be involved in synaptic refinement regulation and neuronal survival during development in the CNS [55].

The interaction of Notch, with its established intercellular signaling pathway, plays a key role in neural development. The Notch-3 activation induces the increase of the progenitor cell number in the central nervous system (CNS) and affects CNS development [56]. The Notch-3 mutation may lead to cerebral autosomal dominant arteriopathy with subcortical infarcts and leukoencephalopathy (CADASIL). CADASIL leads to stroke and dementia and is the main feature of recurrent subcortical ischemic events and vascular dementia. Members of the Notch gene family were thought to be involved as receptors for membrane-bound ligands Jagged1, Jagged2, and Delta1 in the regulation of cell fate in a variety of neurogeneses of embryos, particularly in the developing CNS from the homogenous cell population of the neural tube [57, 58].

Also, in this study, more than one hundred proteins were identified in SH-SY5Y cell lysate and most of these were identified at the minimal confidence level, which was only one unique peptide sequence matched. Experimental results reported a total of six protein identifications with higher confidence levels (at least three unique peptide sequences matched). The protein-protein interaction pathways were performed by String 9.1 Web software, and proteins identified in this study were marked by arrows (red: SH-SY5Y; green: PC12; Figure 3(a)). Using the protein-protein interaction

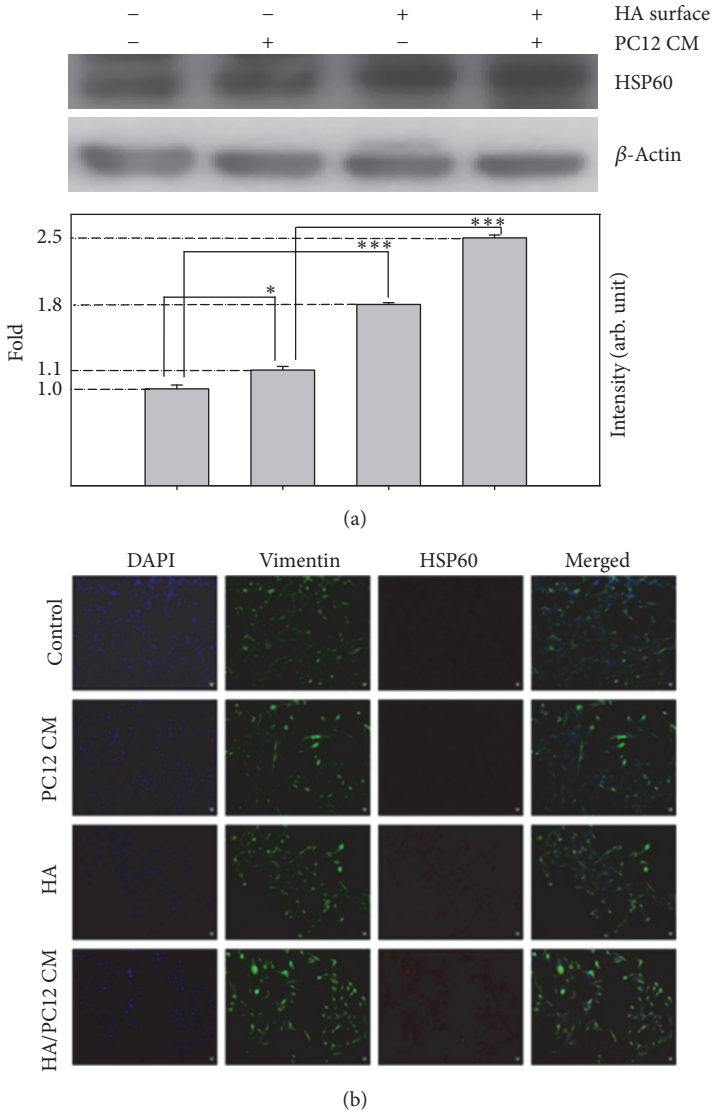

Figure 4: The detection of HSP60 protein expression on SH-SY5Y cells. (a) Western blotting of HSP60 and β-actin from SH-SY5Y cells cultured on different surfaces and/or different medium. The signals were quantified and the data are presented as the means ± SEMs; $p < 0.05$ or 0.001 indicates statistical significance, as determined by unpaired Student's t-test. (b) Analyses of representative samples of SH-SY5Y cells expression of vimentin and HSP60 are shown. Immunochemical stains for DAPI (blue), vimentin (green), and HSP60 (red) for adhered SH-SY5Y cells on indicated surfaces and/or conditioned media for 24 h (scale bars, 10 μm; confocal microscope, 400x). $^{*}p < 0.05$ and $^{***}p < 0.001$.

pathway analysis, the main finding of PC12 CM-treated cells is that the growth factors may focus on the enhancement of the TP53 pathway in SH-SY5Y cells which may result in cell growth (Figure 3(b)).

The TP53 pathway has been famously recognized to be connected to the UBC/PI3K/AKT1/mTOR pathway, which is responsible for the proliferation and is required for survival of the majority of cells. The hypothesis of the mTOR pathway is that it acts as a master switch of cellular catabolism and anabolism, thereby determining whether cells grow and proliferate. In particular, the UBC/PI3K/AKT1/mTOR pathway regulates the import and retention of glucose. It provides substrates for glycolysis and the biosynthetic pathways which rely on the supply of glycolytic intermediates. The mTOR pathway, downstream of AKT signaling, regulates the protein translation rate and accelerates the supply of amino acid biosynthesis to generate the charged tRNAs [59].

To confirm this hypothesis, the proteins in SH-SY5Y cell lysate need to be validated. In addition, there were two proteins, 60 kDa heat shock protein (HSP60, known as HSPD1) and E3 SUMO-protein ligase RanBP2 (RanBP2), identified in SH-SY5Y cell lysate samples, which were involved in cell proliferation, differentiation, development, and cycle regulation. Those two proteins were also involved in the UBC/

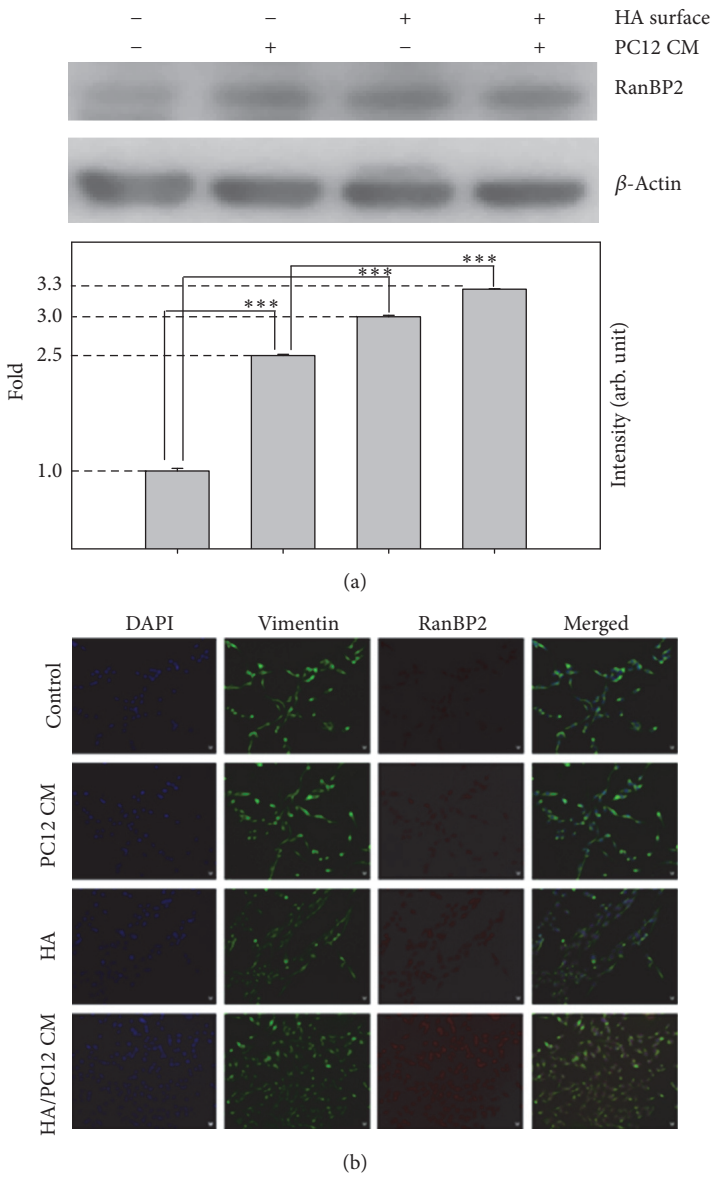

Figure 5: The detection of RanBP2 protein expression on SH-SY5Y cells. (a) Western blotting of RanBP2 and β-actin from SH-SY5Y cells cultured on different surfaces and/or different medium. The signals were quantified and the data are presented as the means ± SEMs; $p < 0.001$ indicates statistical significance, as determined by unpaired Student's t-test. (b) Analyses of representative samples of SH-SY5Y cells expression of vimentin and RanBP2 are shown. Immunochemical stains for DAPI (blue), vimentin (green), and RanBP2 (red) for adhered SH-SY5Y cells on indicated surfaces and/or conditioned media for 24 h (scale bars, 10 μm; confocal microscope, 400x). $^{***}p < 0.001$.

PI3K/AKT1/mTOR pathway (Figure 3(b)). To corroborate the protein candidates identified by RP-nano-HPLC-ESI-MS/MS, the Western blot analysis and immunofluorescence staining were applied to detect the changes in HSP60 and RanBP2.

Heat shock proteins (HSPs) are overexpressed in a wide range of cells and are implicated in cell proliferation, differentiation, and recognition by the immune system. These proteins have molecular chaperone activity, which can be induced by various environmental stresses. Some HSPs were found to be localized in the synapse [60]. HSP60 is widely distributed in the brain and involved in neurodegenerative disorders [61]. When injured, HSP60 can be released to activate microglia in CNS [62]. HSP60 defects can cause neurodegenerative pathologies, such as brain hypomyelination and leukodystrophy [63]. Here, we found the protein expressions of HSP60 were upregulated in HA-modified surface or PC12 CM-treated SH-SY5Y cells compared to control, and the effect was significantly enhanced by the above-mentioned combination (Figure 4(a)). Immunofluorescence staining also showed that cotreatment with HA-modified surface and PC12 CM increased HSP60 expression

in SH-SY5Y cells (Figure 4(b)). These results suggested that HA and PC12 CM may trigger HSP60 as part of its nerve regeneration effects.

RanBP2, located at the nuclear pore complexes (NPCs) [64], is known to modulate CRM1-mediated nuclear protein export [65] and associate with Ubc9 to function as a SUMO E3 ligase [66–68]. RanBP2 also plays a role in neuroprotective regulation [69–71]. RanBP2 associates with RPGRIP1 to implicate retinopathies in amacrine and 661W neurons [72]. RanBP2 mutation has been identified as a key factor in acute necrotising encephalopathy [73, 74]. Here, the protein expression levels of RanBP2 in PC12 CM-treated or HA-modified surface treated SH-SY5Y cells were higher than those from control cells. Cotreatment with HA-modified surface and PC12 CM slightly increased RanBP2 protein expression compared with HA-modified surface or PC12 CM (Figure 5(a)). Immunofluorescence staining also showed the similar results that the expression of RanBP2 was increased in PC12 CM-treated and HA-modified surface with PC12 CM-treated SH-SY5Y cells (Figure 5(b)). Thus, HA and PC12 CM may upregulate RanBP2 protein expression as part of its nerve neuroprotective effects.

In the result, it showed that HA and PC12 CM may regulate protein expression, such as HSP60 and RanBP2 to promote SH-SY5Y cell proliferation and adhesion. These results were similar to Yamada's study, which reported that the combination treatment of SHya and FGF-2 increased NHA proliferation [75]. HA biomaterial surface has been used and reported in a wide range of medical and biological applications and plays an important role in neural development [25, 28]. Due to the activation of UBC/PI3K/AKT1/mTOR, signaling through mutation of pathway components as well as through activation of upstream signaling molecules occurs in a majority of cells contributing to deregulation of proliferation, resistance to apoptosis, and changes in metabolism characteristic of transforming cells.

4. Conclusion

In this study, SH-SYSY cells were used as a model to examine the effects of HA and PC12 CM in neuron regeneration. We found that stimulation of a HA-modified surface with PC12 CM can promote SH-SYSY cell proliferation and adhesion; the combination of both showed synergy effects on SH-SYSY cell regeneration. Our evidences supported that neurotrophic factor proteins enhance HA function in neurogenesis. Biomaterial surface supported with neurotrophic factor proteins may be utilized in nerve autograft application. We used proteomic analysis to analyze the molecular mechanisms of HA-modified surface and PC12 CM stimuli. Among these proteins, HSP60 and RanBP2 were upregulated in SH-SY5Y cells. The UBC/PI3K/AKT1/mTOR pathway was related to the cell growth and proliferation. Future study will be of the molecular regulations and interaction networks governed by biomaterials and combined with neurotrophic factors.

Competing Interests

The authors declare no conflict of interests.

Authors' Contributions

Ming-Hui Yang and Ko-Chin Chen contributed equally to this work.

Acknowledgments

The authors thank S. Sheldon (Medical Technologist, American Society of Clinical Pathology, retired, MT, ASCP) of Oklahoma University Medical Center Edmond for fruitful discussions and editorial assistance. The authors thank the Center of Excellence for Environmental Medicine, Kaohsiung Medical University, for the assistance in protein identification. This work was supported by Research Grants MOST 103-2320-B-037-025 and MOST 105-0210-01-12-01 (Taiwan Protein Project) from the Ministry of Science and Technology, KMU-TP104E12 and KMU-O104003 (Aim for the Top 500 Universities Grant) from Kaohsiung Medical University, 105-CCH-KMU-005 from CCH-KMU Research Project, and NSYSUKMU104-P032 from NSYSU-KMU Research Project, Taiwan.

References

[1] W. Daly, L. Yao, D. Zeugolis, A. Windebank, and A. Pandit, "A biomaterials approach to peripheral nerve regeneration: bridging the peripheral nerve gap and enhancing functional recovery," *Journal of the Royal Society Interface*, vol. 9, no. 67, pp. 202–221, 2012.

[2] A. Muheremu and Q. Ao, "Past, present, and future of nerve conduits in the treatment of peripheral nerve injury," *BioMed Research International*, vol. 2015, Article ID 237507, 6 pages, 2015.

[3] X. Jiang, S. H. Lim, H.-Q. Mao Hai-Quan, and S. Y. Chew, "Current applications and future perspectives of artificial nerve conduits," *Experimental Neurology*, vol. 223, no. 1, pp. 86–101, 2010.

[4] S. Rochkind and Z. Nevo, "Recovery of peripheral nerve with massive loss defect by tissue engineered guiding regenerative gel," *BioMed Research International*, vol. 2014, Article ID 327578, 7 pages, 2014.

[5] X. Navarro, M. Vivó, and A. Valero-Cabré, "Neural plasticity after peripheral nerve injury and regeneration," *Progress in Neurobiology*, vol. 82, no. 4, pp. 163–201, 2007.

[6] T. Sedaghati and A. M. Seifalian, "Nanotechnology and biofunctionalisation for peripheral nerve regeneration," *Neural Regeneration Research*, vol. 10, no. 8, pp. 1191–1194, 2015.

[7] E. O. Johnson and P. N. Soucacos, "Nerve repair: experimental and clinical evaluation of biodegradable artificial nerve guides," *Injury*, vol. 39, S3, pp. S30–S36, 2008.

[8] D. J. Bryan, A. H. Holway, K.-K. Wang et al., "Influence of glial growth factor and Schwann cells in a bioresorbable guidance channel on peripheral nerve regeneration," *Tissue Engineering*, vol. 6, no. 2, pp. 129–138, 2000.

[9] G. R. D. Evans, K. Brandt, A. D. Niederbichler et al., "Clinical long-term in vivo evaluation of poly(L-lactic acid) porous conduits for peripheral nerve regeneration," *Journal of Biomaterials Science, Polymer Edition*, vol. 11, no. 8, pp. 869–878, 2000.

[10] M. Richards, B. I. Dahiyat, D. M. Arm, P. R. Brown, and K. W. Leong, "Evaluation of polyphosphates and polyphosphonates

as degradable biomaterials," *Journal of Biomedical Materials Research*, vol. 25, no. 9, pp. 1151–1167, 1991.

[11] H. J. Hoppen, J. W. Leenslag, A. J. Pennings, B. van der Lei, and P. H. Robinson, "Two-ply biodegradable nerve guide: basic aspects of design, construction and biological performance," *Biomaterials*, vol. 11, no. 4, pp. 286–290, 1990.

[12] R. F. Valentini, T. G. Vargo, J. A. Gardella Jr., and P. Aebischer, "Electrically charged polymeric substrates enhance nerve fibre outgrowth In vitro," *Biomaterials*, vol. 13, no. 3, pp. 183–190, 1992.

[13] P. D. Dalton, L. Flynn, and M. S. Shoichet, "Manufacture of poly(2-hydroxyethyl methacrylate-co-methyl methacrylate) hydrogel tubes for use as nerve guidance channels," *Biomaterials*, vol. 23, no. 18, pp. 3843–3851, 2002.

[14] S. J. Archibald, C. Krarup, J. Shefner, S.-T. Li, and R. D. Madison, "A collagen-based nerve guide conduit for peripheral nerve repair: an electrophysiological study of nerve regeneration in rodents and nonhuman primates," *Journal of Comparative Neurology*, vol. 306, no. 4, pp. 685–696, 1991.

[15] T. Jiang, S. G. Kumbar, L. S. Nair, and C. T. Laurencin, "Biologically active chitosan systems for tissue engineering and regenerative medicine," *Current Topics in Medicinal Chemistry*, vol. 8, no. 4, pp. 354–364, 2008.

[16] C. E. Dumont and V. R. Hentz, "Enhancement of axon growth by detergent-extracted nerve grafts," *Transplantation*, vol. 63, no. 9, pp. 1210–1215, 1997.

[17] B. P. Toole, "Hyaluronan in morphogenesis," *Seminars in Cell and Developmental Biology*, vol. 12, no. 2, pp. 79–87, 2001.

[18] P. Rooney, S. Kumar, J. Ponting, and M. Wang, "The role of hyaluronan in tumour neovascularization (review)," *International Journal of Cancer*, vol. 60, no. 5, pp. 632–636, 1995.

[19] M. Slevin, J. Krupinski, S. Kumar, and J. Gaffney, "Angiogenic oligosaccharides of hyaluronan induce protein tyrosine kinase activity in endothelial cells and activate a cytoplasmic signal transduction pathway resulting in proliferation," *Laboratory Investigation*, vol. 78, no. 8, pp. 987–1003, 1998.

[20] M. Slevin, S. Kumar, and J. Gaffney, "Angiogenic oligosaccharides of hyaluronan induce multiple signaling pathways affecting vascular endothelial cell mitogenic and wound healing responses," *Journal of Biological Chemistry*, vol. 277, no. 43, pp. 41046–41059, 2002.

[21] M. Preston and L. S. Sherman, "Neural stem cell niches: roles for the hyaluronan-based extracellular matrix," *Frontiers in Bioscience—Scholar*, vol. 3, no. 3, pp. 1165–1179, 2011.

[22] R. U. Margolis, R. K. Margolis, L. B. Chang, and C. Preti, "Glycosaminoglycans of brain during development," *Biochemistry*, vol. 14, no. 1, pp. 85–88, 1975.

[23] D. Jiang, J. Liang, and P. W. Noble, "Hyaluronan in tissue injury and repair," *Annual Review of Cell and Developmental Biology*, vol. 23, pp. 435–461, 2007.

[24] J. Liang, D. Jiang, and P. W. Noble, "Hyaluronan as a therapeutic target in human diseases," *Advanced Drug Delivery Reviews*, vol. 97, pp. 186–203, 2016.

[25] L. S. Sherman, S. Matsumoto, W. Su, T. Srivastava, and S. A. Back, "Hyaluronan synthesis, catabolism, and signaling in neurodegenerative diseases," *International Journal of Cell Biology*, vol. 2015, Article ID 368584, 10 pages, 2015.

[26] M. A. Solis, Y.-H. Chen, T. Y. Wong, V. Z. Bittencourt, Y.-C. Lin, and L. L. H. Huang, "Hyaluronan regulates cell behavior: a potential niche matrix for stem cells," *Biochemistry Research International*, vol. 2012, Article ID 346972, 11 pages, 2012.

[27] J. Arulmoli, H. J. Wright, D. T. Phan et al., "Combination scaffolds of salmon fibrin, hyaluronic acid, and laminin for human neural stem cell and vascular tissue engineering," *Acta Biomaterialia*, vol. 43, pp. 122–138, 2016.

[28] J. J. Greene and D. M. Sidle, "The hyaluronic acid fillers. Current understanding of the tissue device interface," *Facial Plastic Surgery Clinics of North America*, vol. 23, no. 4, pp. 423–432, 2015.

[29] P. Moshayedi and S. T. Carmichael, "Hyaluronan, neural stem cells and tissue reconstruction after acute ischemic stroke," *Biomatter*, vol. 3, no. 1, Article ID e23863, 2013.

[30] Z. Z. Khaing, B. D. Milman, J. E. Vanscoy, S. K. Seidlits, R. J. Grill, and C. E. Schmidt, "High molecular weight hyaluronic acid limits astrocyte activation and scar formation after spinal cord injury," *Journal of Neural Engineering*, vol. 8, no. 4, Article ID 046033, 2011.

[31] Z. Z. Khaing and S. K. Seidlits, "Hyaluronic acid and neural stem cells: implications for biomaterial design," *Journal of Materials Chemistry B*, vol. 3, no. 40, pp. 7850–7866, 2015.

[32] G. Lisignoli, S. Cristino, A. Piacentini et al., "Cellular and molecular events during chondrogenesis of human mesenchymal stromal cells grown in a three-dimensional hyaluronan based scaffold," *Biomaterials*, vol. 26, no. 28, pp. 5677–5686, 2005.

[33] N. P. Rhodes, J. K. Srivastava, R. F. Smith, and C. Longinotti, "Metabolic and histological analysis of mesenchymal stem cells grown in 3-D hyaluronan-based scaffolds," *Journal of Materials Science: Materials in Medicine*, vol. 15, no. 4, pp. 391–395, 2004.

[34] P. C. Baer, J. Bereiter-Hahn, C. Missler et al., "Conditioned medium from renal tubular epithelial cells initiates differentiation of human mesenchymal stem cells," *Cell Proliferation*, vol. 42, no. 1, pp. 29–37, 2009.

[35] Y.-S. Hwang, W. L. Randle, R. C. Bielby, J. M. Polak, and A. Mantalaris, "Enhanced derivation of osteogenic cells from murine embryonic stem cells after treatment with HepG2-conditioned medium and modulation of the embryoid body formation period: application to skeletal tissue engineering," *Tissue Engineering*, vol. 12, no. 6, pp. 1381–1392, 2006.

[36] T.-J. Lee, J. Jang, S. Kang et al., "Mesenchymal stem cell-conditioned medium enhances osteogenic and chondrogenic differentiation of human embryonic stem cells and human induced pluripotent stem cells by mesodermal lineage induction," *Tissue Engineering—Part A*, vol. 20, no. 7-8, pp. 1306–1313, 2014.

[37] H. Arien-Zakay, A. Nagler, H. Galski, and P. Lazarovici, "Neuronal conditioning medium and nerve growth factor induce neuronal differentiation of collagen-adherent progenitors derived from human umbilical cord blood," *Journal of Molecular Neuroscience*, vol. 32, no. 3, pp. 179–191, 2007.

[38] J. S. Gill, A. E. Schenone, J. L. Podratz, and A. J. Windebank, "Autocrine regulation of neurite outgrowth from PC12 cells by nerve growth factor," *Molecular Brain Research*, vol. 57, no. 1, pp. 123–131, 1998.

[39] A. Krishna, M. Biryukov, C. Trefois et al., "Systems genomics evaluation of the SH-SY5Y neuroblastoma cell line as a model for Parkinson's disease," *BMC Genomics*, vol. 15, article 1154, 2014.

[40] M.-H. Yang, S.-S. Yuan, T.-W. Chung et al., "Characterization of silk fibroin modified surface: a proteomic view of cellular response proteins induced by biomaterials," *BioMed Research International*, vol. 2014, Article ID 209469, 13 pages, 2014.

[41] M. H. Yang, S. S. Yuan, Y. L. Chen et al., "Mass spectrometry in clinical diagnosis: a preliminary application in tumor cellular proteomics for biomarker discovery," *Journal of Analytical Bioanalytical Techniques*, vol. S2, article 9, 2014.

[42] M.-H. Yang, S.-B. Jong, C.-Y. Lu et al., "Assessing the responses of cellular proteins induced by hyaluronic acid-modified surfaces utilizing a mass spectrometry-based profiling system: over-expression of CD36, CD44, CDK9, and PP2A," *Analyst*, vol. 137, no. 21, pp. 4921–4933, 2012.

[43] T.-W. Chung, Y.-C. Tyan, R.-H. Lee, and C.-W. Ho, "Determining early adhesion of cells on polysaccharides/PCL surfaces by a quartz crystal microbalance," *Journal of Materials Science: Materials in Medicine*, vol. 23, no. 12, pp. 3067–3073, 2012.

[44] B. Lu and C. E. Bishop, "Mouse GGN1 and GGN3, two germ cell-specific proteins from the single gene Ggn, interact with mouse POG and play a role in spermatogenesis," *Journal of Biological Chemistry*, vol. 278, no. 18, pp. 16289–16296, 2003.

[45] C. Cheyuo, W.-L. Yang, and P. Wang, "The critical role of adrenomedullin and its binding protein, AMBP-1, in neuroprotection," *Biological Chemistry*, vol. 393, no. 6, pp. 429–439, 2012.

[46] T. Koyama, T. Sakurai, A. Kamiyoshi, Y. Ichikawa-Shindo, H. Kawate, and T. Shindo, "Adrenomedullin-RAMP2 system in vascular endothelial cells," *Journal of Atherosclerosis and Thrombosis*, vol. 22, no. 7, pp. 647–653, 2015.

[47] J. M. Schumacher, K. Artzt, and R. E. Braun, "Spermatid perinuclear ribonucleic acid-binding protein binds microtubules in vitro and associates with abnormal manchettes in vivo in mice," *Biology of Reproduction*, vol. 59, no. 1, pp. 69–76, 1998.

[48] J. M. Schumacher, K. Lee, S. Edelhoff, and R. E. Braun, "Spnr, a murine RNA-binding protein that is localized to cytoplasmic microtubules," *Journal of Cell Biology*, vol. 129, no. 4, pp. 1023–1032, 1995.

[49] A. Pires-daSilva, K. Nayernia, W. Engel et al., "Mice deficient for spermatid perinuclear RNA-binding protein show neurologic, spermatogenic, and sperm morphological abnormalities," *Developmental Biology*, vol. 233, no. 2, pp. 319–328, 2001.

[50] K. L. Carraway III, J. L. Weber, M. J. Unger et al., "Neuregulin-2, a new ligand of ErbB3/ErbB4-receptor tyrosine kinases," *Nature*, vol. 387, no. 6632, pp. 512–516, 1997.

[51] L. Wu, S. J. Walas, W. Leung, E. H. Lo, and J. Lok, "Neuregulin-1 and neurovascular protection," in *Brain Neurotrauma: Molecular, Neuropsychological, and Rehabilitation Aspects*, F. H. Kobeissy, Ed., pp. 561–568, CRC Press, Boca Raton, Fla, USA, 2015.

[52] L. Mei and W.-C. Xiong, "Neuregulin 1 in neural development, synaptic plasticity and schizophrenia," *Nature Reviews Neuroscience*, vol. 9, no. 6, pp. 437–452, 2008.

[53] E. S. Anton, H. T. Ghashghaei, J. L. Weber et al., "Receptor tyrosine kinase ErbB4 modulates neuroblast migration and placement in the adult forebrain," *Nature Neuroscience*, vol. 7, no. 12, pp. 1319–1328, 2004.

[54] S. Nataf, P. F. Stahel, N. Davoust, and S. R. Barnum, "Complement anaphylatoxin receptors on neurons: new tricks for old receptors?" *Trends in Neurosciences*, vol. 22, no. 9, pp. 397–402, 1999.

[55] H. Lian, L. Yang, A. Cole et al., "NFκB-activated astroglial release of complement C3 compromises neuronal morphology and function associated with Alzheimer's disease," *Neuron*, vol. 85, no. 1, pp. 101–116, 2015.

[56] M. H. Yang, R. R. Krishnamoorthy, S. B. Jong et al., "Protein profiling of human nonpigmented ciliary epithelium cell secretome: the differentiation factors characterization for retinal ganglion cell line," *Journal of Biomedicine and Biotechnology*, vol. 2011, Article ID 901329, 28 pages, 2011.

[57] S. A. Sullivan, L. K. Barthel, B. L. Largent, and P. A. Raymond, "A goldfish Notch-3 homologue is expressed in neurogenic regions of embryonic, adult, and regenerating brain and retina," *Developmental Genetics*, vol. 20, no. 3, pp. 208–223, 1997.

[58] Y. Qu, K. Sakamoto, S. Takeda, T. Kayano, M. Takagi, and K. Katsube, "Differential expression of notch genes in the neurogenesis of mouse embryos," *Oral Medicine & Pathology*, vol. 3, no. 1, pp. 21–28, 1998.

[59] H.-Y. Zhou and S.-L. Huang, "Current development of the second generation of mTOR inhibitors as anticancer agents," *Chinese Journal of Cancer*, vol. 31, no. 1, pp. 8–18, 2012.

[60] K. Ohtsuka and T. Suzuki, "Roles of molecular chaperones in the nervous system," *Brain Research Bulletin*, vol. 53, no. 2, pp. 141–146, 2000.

[61] A. M. Gammazza, R. Colangeli, G. Orban et al., "Hsp60 response in experimental and human temporal lobe epilepsy," *Scientific Reports*, vol. 5, article 9434, 2015.

[62] M. J. Feng, L. Zhang, Z. Liu, P. Zhou, and X. Lu, "The expression and release of Hsp60 in 6-OHDA induced in vivo and in vitro models of Parkinson's disease," *Neurochemical Research*, vol. 38, no. 10, pp. 2180–2189, 2013.

[63] D. Magen, C. Georgopoulos, P. Bross et al., "Mitochondrial Hsp60 chaperonopathy causes an autosomal-recessive neurodegenerative disorder linked to brain hypomyelination and leukodystrophy," *American Journal of Human Genetics*, vol. 83, no. 1, pp. 30–42, 2008.

[64] J. M. Avis and P. R. Clarke, "Ran, a GTPase involved in nuclear processes: its regulators and effecters," *Journal of Cell Science*, vol. 109, pp. 2423–2427, 1996.

[65] R. Bernad, H. van der Velde, M. Fornerod, and H. Pickersgill, "Nup358/RanBP2 attaches to the nuclear pore complex via association with Nup88 and Nup214/CAN and plays a supporting role in CRM1-mediated nuclear protein export," *Molecular and Cellular Biology*, vol. 24, no. 6, pp. 2373–2384, 2004.

[66] H. Saitoh, R. Pu, M. Cavenagh, and M. Dasso, "RanBP2 associates with Ubc9p and a modified form of RanGAP1," *Proceedings of the National Academy of Sciences of the United States of America*, vol. 94, no. 8, pp. 3736–3741, 1997.

[67] A. Pichler, A. Gast, J. S. Seeler, A. Dejean, and F. Melchior, "The nucleoporin RanBP2 has SUMO1 E3 ligase activity," *Cell*, vol. 108, no. 1, pp. 109–120, 2002.

[68] H. Saitoh, M. D. Pizzi, and J. Wang, "Perturbation of SUMOlation enzyme Ubc9 by distinct domain within nucleoporin RanBP2/Nup358," *Journal of Biological Chemistry*, vol. 277, no. 7, pp. 4755–4763, 2002.

[69] K.-I. Cho, H. Yi, A. Yeh et al., "Haploinsufficiency of RanBP2 is neuroprotective against light-elicited and age-dependent degeneration of photoreceptor neurons," *Cell Death and Differentiation*, vol. 16, no. 2, pp. 287–297, 2009.

[70] K.-I. Cho, H. Yi, N. Tserentsoodol, K. Searle, and P. A. Ferreira, "Neuroprotection resulting from insufficiency of RANBP2 is associated with the modulation of protein and lipid homeostasis of functionally diverse but linked pathways in response to oxidative stress," *DMM Disease Models and Mechanisms*, vol. 3, no. 9-10, pp. 595–604, 2010.

[71] K.-I. Cho, K. Searle, M. Webb, H. Yi, and P. A. Ferreira, "Ranbp2 haploinsufficiency mediates distinct cellular and biochemical phenotypes in brain and retinal dopaminergic and glia cells

elicited by the Parkinsonian neurotoxin, 1-methyl-4-phenyl-1,2,3,6-tetrahydropyridine (MPTP)," *Cellular and Molecular Life Sciences*, vol. 69, no. 20, pp. 3511–3527, 2012.

[72] P. Castagnet, T. Mavlyutov, Y. Cai, F. Zhong, and P. Ferreira, "RPGRIP1s with distinct neuronal localization and biochemical properties associate selectively with RanBP2 in amacrine neurons," *Human Molecular Genetics*, vol. 12, no. 15, pp. 1847–1863, 2003.

[73] D. E. Neilson, M. D. Adams, C. M. D. Orr et al., "Infection-triggered familial or recurrent cases of acute necrotizing encephalopathy caused by mutations in a component of the nuclear pore, RANBP2," *American Journal of Human Genetics*, vol. 84, no. 1, pp. 44–51, 2009.

[74] R. R. Singh, S. Sedani, M. Lim, E. Wassmer, and M. Absoud, "RANBP2 mutation and acute necrotizing encephalopathy: 2 cases and a literature review of the expanding clinico-radiological phenotype," *European Journal of Paediatric Neurology*, vol. 19, no. 2, pp. 106–113, 2015.

[75] T. Yamada, R. Sawada, and T. Tsuchiya, "The effect of sulfated hyaluronan on the morphological transformation and activity of cultured human astrocytes," *Biomaterials*, vol. 29, no. 26, pp. 3503–3513, 2008.

Hindawi Publishing Corporation
BioMed Research International
Volume 2016, Article ID 6584054, 10 pages
http://dx.doi.org/10.1155/2016/6584054

Research Article

Cogels of Hyaluronic Acid and Acellular Matrix for Cultivation of Adipose-Derived Stem Cells: Potential Application for Vocal Fold Tissue Engineering

Dongyan Huang, Rongguang Wang, and Shiming Yang

Department of Otolaryngology-Head and Neck Surgery, Clinical Division of Surgery, Chinese PLA General Hospital, Beijing 100853, China

Correspondence should be addressed to Dongyan Huang; huangdy301@163.com

Received 27 June 2016; Revised 10 September 2016; Accepted 29 September 2016

Academic Editor: Pornanong Aramwit

Stem cells based tissue engineering has been one of the potential promising therapies in the research on the repair of tissue diseases including the vocal fold. Decellularized extracellular matrix (DCM) as a promising scaffold has be used widely in tissue engineering; however, it remained to be an important issue in vocal fold regeneration. Here, we applied the hydrogels (hyaluronic acid [HA], HA-collagen [HA-Col], and HA-DCM) to determine the effects of hydrogel on the growth and differentiation of human adipose-derived stem cells (hADSCs) into superficial lamina propria fibroblasts. hADSCs were isolated and characterized by fluorescence-activated cell sorting. The results indicated that HA-DCM hydrogel enhanced cell proliferation and prolonged cell morphology significantly compared to HA and HA-Col hydrogel. Importantly, the differentiation of hADSCs into fibroblasts was also promoted by cogels of HA-Col and HA-DCM significantly. The differentiation of hADSCs towards superficial lamina propria fibroblasts was accelerated by the secretion of HGF, IL-8, and VEGF, the decorin and elastin expression, and the synthesis of chondroitin sulfate significantly. Therefore, the cogel of HA-DCM hydrogel was shown to be outstanding in apparent stimulation of hADSCs proliferation and differentiation to vocal fold fibroblasts through secretion of important growth factors and synthesis of extracellular matrix.

1. Introduction

Injury to the vocal fold can lead to intractable changes in the composition and distribution of extracellular matrix (ECM) in the lamina propria and also cause irreversible vocal scarring through significant fibrosis and deposition of hyperplasia disorderly [1–3]. With the development of tissue engineering, biomaterials and stem cells based regenerative therapy had been shown to be one of the promising alternative methods for the treatment of vocal fold injury [4, 5].

Cells and biomaterials are two indispensable elements in tissue engineering aiming at the construction of complex functional tissues *in vitro*. In previous studies, many different types of cells were used in tissue engineering [6–8]. Adipose-derived stem cells (ADSCs) as a population of pluripotent mesenchymal stem cells were promising in the application of regenerative medicine due to their capability of differentiation towards various lineages. A number of *in vivo* applications of ADSCs have been reported in diverse tissue and organ diseases [9–11]. Xu et al. stated that ADSCs showed a satisfactory effect on regeneration of vocal fold [12]. The injection of ADSCs derived fibroblast-like cells in the injured vocal fold was proved to heal the vocal fold wound through deposition of ECM compositions *in vivo* [13].

In tissue engineering, various hydrogels were applied as scaffolds for ADSCs with great potential, such as fibrin, collagen, and hyaluronic acid (HA) [14–16]. The outstanding scaffolds for tissue engineering should serve the following important duties: (1) supporting cell growth and differentiation of stem cells and (2) restoring the volume of the superficial lamina propria [17]. However, there are still some limitations in the application of only one element from the extracellular matrix (ECM) for cell culture such as the absence of essential growth factors for regulation of cell growth and differentiation of stem cells. In recent years, the application of composite materials in the culture of ADSCs has attracted great

interest from researchers to induce differentiation into targeted cell lineages.

ECMs in vocal fold tissues are composed of an organized porous structure of various matrix macromolecules, mainly proteoglycans and glycosaminoglycans (GAGs), the fibrous proteins that are secreted by vocal fold fibroblasts. Collagen and elastin organized structural components of ECMs [18], while fibronectin and laminin formed the main adhesive elements of ECMs. Besides, in vocal fold lamina propria, hyaluronic acid, as another important ECM constituent involved in the regulation of tissue viscosity, osmosis, and dampening [19], and decorin, distributed throughout the vocal fold lamina propria, enhance the assembly of collagen fibers and bundles.

HA as an abundant component of normal vocal fold was shown to be promising in vocal fold tissue engineering. The scaffolds composed of HA provided physiochemical cues for cell growth and differentiation [17, 20]. Collagen as another major component of ECM was applied in tissue engineering widely, and also the composite biomaterials of collagen and other materials including HA showed unique advantages for cell differentiation [21]. However, collagen hydrogel composed of collagen was still limited to some cytokines and some functional proteins for cell growth and differentiation. Recently, decellularized extracellular matrix (DCM) was shown to be promising in tissue engineering due to its natural derivation and functional factors for cell growth [22–24]. However, there are still few studies about its application in vocal fold regeneration; in order to evaluate the application of DCM in vocal fold tissue engineering, we used cogel of HA-DCM to construct hydrogel-MSCs constructs to understand the growth and differentiation of hADSCs in the 3D environment.

Here, we used cogel of HA-DCM and hADSCs to construct 3D hydrogel-cell constructs and evaluate the effect of HA-DCM hydrogel on the growth and differentiation of hADSCs. Meanwhile, through analyzing the secretion of cytokines and synthesis of ECM, we will figure out how HA-DCM hydrogel affects the differentiation of hADSCs towards vocal fold fibroblasts. This study aims to find a promising cogel to stimulate the differentiation of stem cells towards vocal fold fibroblasts and to be used for regeneration of injured vocal fold.

2. Materials and Methods

2.1. Isolation of hADSCs. hADSCs were isolated from human adipose tissues by digestion of collagenase and filtration using cell strainers as in previous methods [17]. Human abdominoplasty adipose tissues were obtained from 20- to 30-year-old female donors ($n = 5$), and the collected specimens were washed with saline buffer five times to remove blood and free fatty acids. The washed adipose tissues were cut into small blocks and then were digested with Blendzyme (0.3 mg/mL) for 30 min while stirring at 37°C. The incubated tissues were filtered through 100 and 40 μm cell strainers to remove fibrous redundant tissues and then centrifuged at 700 ×g for 10 min. The cells were collected to remove red blood cells using a lysis buffer and then centrifuged again as the previous condition. The collected cells were resuspended in α-MEM and cultured in 37°C, 5% CO_2 humid incubator.

2.2. Characterization of hADSCs. hADSCs were characterized by fluorescence-activated cell sorting (FACS) analysis. In brief, hADSCs were incubated with fluorescent primary antibodies including CD105, CD90, CD34, and CD45 for 30 min at room temperature. The incubated cells were washed by phosphate buffered saline (PBS) buffer containing 5% serum (v/v) three times. The labeled cells were analyzed using a BD FACSCalibur™ system.

2.3. Transduction of hADSCs with Green Fluorescence Protein (GFP). In order to visualize hADSCs in 3D cell culture conditions, the hADSCs were transfected with lentivirus with expression of GFP as in previous methods [17]. Lentivirus expressing GFP was expanded by 293T cells. 500,000 hADSCs were transfected with GFP-lentivirus for 6 h, and the infected efficiency of GFP-lentivirus was examined by GFP expression using FACS (BD Company). The transfected hADSCs showed no apparent difference in the morphology with untreated hADSCs in 2D culture.

2.4. Construction of 3D Constructs of Cells Embedded in Hydrogel. Small intestinal submucosa derived DCM was purchased from Cook Biotech (West Lafayette, IN, USA). HA (Restylane) hydrogel with the concentration 20 mg/mL was formed as the manufacturer's protocol. Collagen type I gel was purchased from BD. DCM solution was prepared by dissolving 1 g DCM powder and 50 mg of pepsin in 0.01 M HCl while stirring for 48 h at room temperature. The solution of DCM was diluted with PBS to 3 mg/mL, and also the pH was modulated to 7.4 with 0.1 N NaOH. Composite hydrogels of HA-collagen and HA-DCM were produced by mixing the composites of HA and collagen or DCM at the ratios of 1 : 1. The HA-Col composite hydrogel was cross-linked as in the provided protocol. 3D cell-hydrogel constructs were obtained by mixing hADSCs (200,000 cells) at passage 3 in 200 μL hydrogels and were cultured for 7 days in H-DMEM with supplementation of 5% FBS in a 37°C, 5% CO_2 incubator. The culture media were replenished every 2 days.

2.5. The Secretion of HGF, IL-8, VEGF, and Chondroitin Sulfate in hADSCs by Analysis of ELISA. ELISA was applied to determine the secretion of HGF, IL-8, and VEGF of hADSCs on the surface of HA, HA-Col, and HA-DCM hydrogel. HA, HA-Col, and HA-DCM hydrogels were coated in 12-well plates, and hADSCs (50,000 cells) at passage 3 were seeded on the surface of HA, HA-Col, and HA-DCM hydrogel individually. Conditioned media from three groups were collected at 72 hours as in previous methods. Human HGF, IL-8, VEGF, and chondroitin sulfate ELISA kits from R&D Systems were used as per the manufacturer's description to analyze the concentration of HGF, IL-8, VEGF, and chondroitin sulfate in the media. All ELISA experiments were repeated three times.

2.6. Proliferation of hADSCs in Hydrogel by DNA Content. In order to determine the proliferation of hADSCs in hydrogel,

3D cell-hydrogel constructs was collected to measure the total DNA content. The PicoGreen kit (Molecular Probes, Eugene, OR) was used as per the manufacturer's instruction. In brief, the extraction buffer containing 1 N NH_4OH and 0.2% Triton X-100 was used to suspend 3D constructs of cell-hydrogel, and a bead beater from BioSpec was used to release DNA. The extract was analyzed using PicoGreen following the manufacturer's instruction after removal of debris through centrifugation at 10,000 ×g for 10 min.

2.7. Immunofluorescence Staining. Immunofluorescence staining of 3D cell-hydrogel constructs was conducted as in a previous method. In brief, the constructs were collected, fixed by 4% paraformaldehyde, and paraffinized. Sections were deparaffinized and antigen was treated by heat for 20 min at 95°C. The sections were blocked with horse serum for 30 min at room temperature and incubated with CD105 primary antibody (Abcam, Cambridge, MA) in a 4°C refrigerator overnight. FITC-conjugated secondary antibody (Abcam, Cambridge, MA) was incubated at room temperature for 2 h in the dark. Nuclei were stained by DAPI for 20 min in the dark. The pictures were observed by a laser microscope (Leica).

2.8. Real-Time-Polymerase Chain Reaction (RT-PCR). The important constituents of ECMs, decorin and elastin, were determined by RT-PCR [17]. Total RNA of cell-hydrogel constructs was prepared using an RNeasy system (Qiagen, Valencia, CA) and a bead beater (BioSpec Products, Bartlesville, OK). The extracted total RNA was treated with DNase for 20 min to remove genomic DNA from the samples. Then, cDNA was synthesized using oligo-dT primers from the total mRNA (Invitrogen), and 200 ng of the cDNA was used for the real-time PCR analysis (AB7500). TaqMan Universal PCR mix, gene-specific primers, and cDNA were mixed, and the PCR reaction was performed at 50°C for 2 min, 95°C for 10 min, and 40 cycles of 95°C for 15 s and 60°C for 1 min. GAPDH was used as the control. The expression of gene level, decorin and elastin, was calculated as the following equation: relative expression = $2/(Ct_{sample} - Ct_{GAPDH})$, where Ct indicates the average cycle threshold (Ct) of three replicates. Three samples from each group were used for gene analysis.

2.9. Statistical Analysis. Average and standard deviations were obtained from three separate experiments. All data are expressed as mean ± standard error of the mean (SEM) unless indicated otherwise and analyzed using one-way analysis of variance (ANOVA) using Tukey's *post hoc* test. Data was considered statistically significant at $p < 0.05$.

3. Results

3.1. Isolation, Culture, and Characterization of hADSCs. Adipose tissue is composed of various types of cells such as endothelial cells, adipose cells, fibroblasts, and adipocyte progenitors. We isolated adipose-derived stem cells using a mixture of collagenase and dispase as in previous methods [17]. Fresh isolated cells were cultured in cell culture dishes at a density of 35,000 cells/mm^2. In order to characterize hADSCs, expression of surface markers in cells was analyzed by FACS after 3 passages as in previous methods [25, 26] (Figure 1(a)). The results showed that more than 90% of cells expressed CD105 (99.4%) and CD90 (99.7%), and most of the cells were shown to be negative for CD34 (16.4%) and CD45 (0.1%) which were the surface markers of hematopoetic stem cells. Meanwhile, cells were shown to be in spindle shape at day 4 of culture (Figure 1(b)).

To further characterize the multipotentiality of hADSCs, the osteogenic and adipogenic differentiation of hADSCs was determined. hADSCs were cultured in the osteogenic media and were positively stained with von Kossa method, which indicated the existence of osteoblasts (Figure 1(c)), while hADSCs showed positive staining with Oil Red-O, indicative of adipocytes (Figure 1(d)). Based on the FACS data and differentiation results, we concluded that the cell populations are enriched with stem cells, which were referred to as hADSCs.

3.2. Cell Morphology of hADSCs in HA-DCM Composite Hydrogel. Cell shape affected the cell proliferation and differentiation of hADSCs towards different lineages. In order to understand the effects of HA-DCM composite hydrogel on the cell morphology of hADSCs, we transfected hADSCs by GFP-lentivirus and visualized the GFP positive cells using light microscope and fluorescence microscope as in a previous method [17] (Figure 2). hADSCs were shown to be round when they were embedded in composite hydrogel on the first day (Figure 2(a)), and hADSCs elongated significantly within HA-DCM composite hydrogel in a time-course manner (Figure 2(b)). Through visualization of GFP, cells exhibited obvious variance in cell shape significantly (Figures 2(c)–2(e)). Some of the hADSCs were shown to have fibroblast-like shape in HA-DCM hydrogel, but apparently more hADSCs with spindle or ellipsoid shape existed in both HA-Col and HA-DCM hydrogel than in HA hydrogel. Furthermore, the ratio of major/minor length through quantification of cell shape by ImagJ2x software indicated that HA-DCM hydrogel induced the change of cell shape of hADSCs with greater ratio of major/minor length of ellipsoid cells significantly compared to HA-Col and HA hydrogel (Figure 2(f)).

3.3. Cell Growth and Differentiation of hADSCs in Hyaluronic Acid/Acellular Matrix Composite Hydrogel. In order to evaluate the cell growth of hADSCs in the HA-DCM hydrogel, we labeled hADSCs with GFP before embedding in hydrogel. DNA was extracted to determine the proliferation of hADSCs in HA-DCM hydrogel at different time points (Figure 3). On day 1, similar DNA contents of hADSCs in HA, HA-Col, and HA-DCM hydrogel were detected, indicating that no significant deviation was produced when incorporating MSCs into HA, HA-Col, and HA-DCM hydrogel. That is, equal quantities of hADSCs were incorporated into the three hydrogels. On day 3 and day 7, a significant increase of DNA contents was detected in HA-based composite hydrogel, indicating a significant cell growth. However, DNA contents from HA hydrogel maintained a similar level to day 1, suggesting that no evident proliferation of incorporated cells occurred.

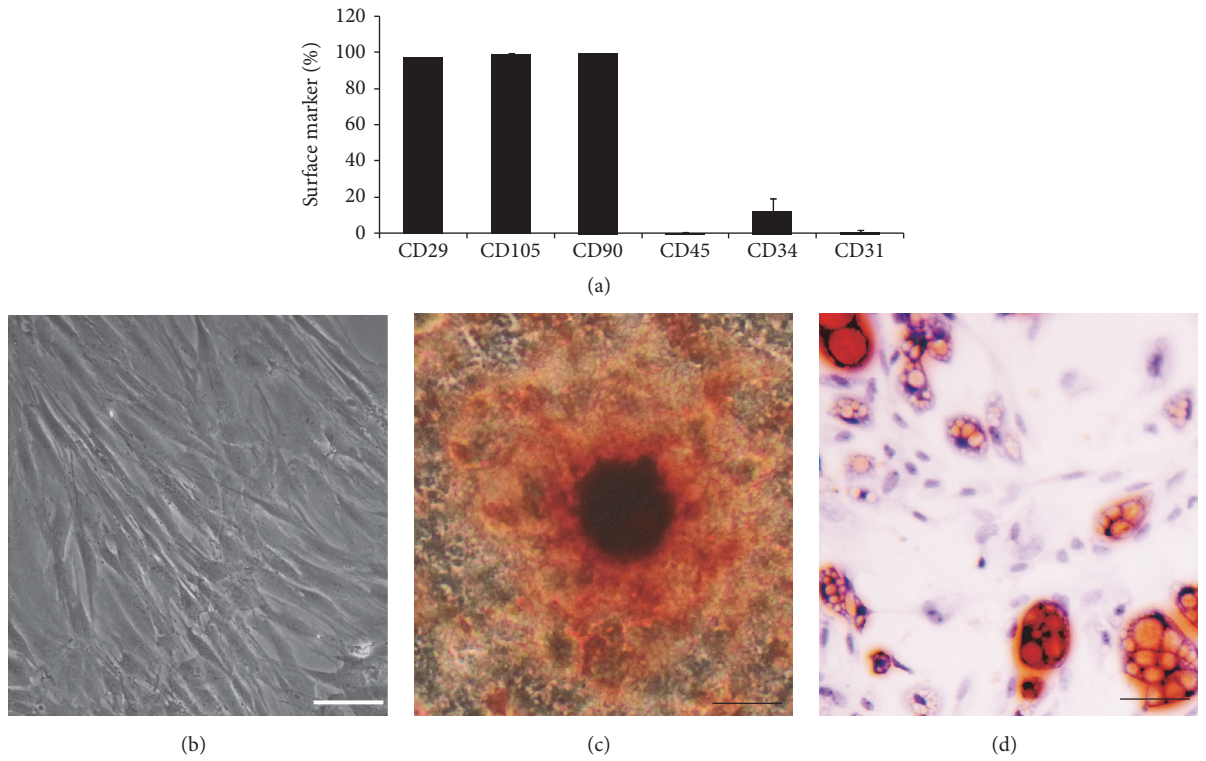

Figure 1: Characterization of isolated hADSCs. (a) Isolated hADSCs were shown to be positive for CD29 (98.9%), CD105 (99.4%), and CD90 (99.7%), while they have been shown to be negative for CD45 (0.1%), CD34 (16.4%), and CD31 (0.1%) in cell population. (b) hADSCs were shown to be in spindle-like shape at passage 3. Scale bar = 50 μm. (c) Osteogenesis of hADSCs was assessed by von Kossa method. (d) Adipogenesis of hADSCs was assessed by Oil Red-O staining.

3.4. Differentiation of hADSCs in Hyaluronic Acid/Acellular Matrix Composite Hydrogel. Through immunofluorescence staining of CD105 (endoglin), we could evaluate the differentiation of hADSCs in varied cultural conditions. CD105 was less expressed in cells in HA-DCM hydrogel than in both HA-Col and HA hydrogel (Figure 4). Expression of CD105 in HA-DCM hydrogel was shown to be the lowest, while the CD105 positive cells in HA composite hydrogel were the most expressed in all the three groups.

3.5. Hyaluronic Acid/Acellular Matrix Composite Hydrogel Increased the Secretion of Cytokines from hADSCs. Secretion of cytokines including HGF, IL-8, and VEGF was analyzed by ELISA assay (Figure 5). The concentration of HGF, IL-8, and VEGF in the media was increased significantly by induction of HA-DCM composite hydrogel comparing to HA-Col and HA hydrogel. hADSCs on HA-DCM composite hydrogel secreted HGF (2450 pg/mL) about 1.8 times more than HA group (1340 pg/mL) and HA-Col group (1504 pg/mL). Meanwhile, the concentration of IL-8 in the media of HA-DCM group (3012 pg/mL) was shown to be about 2 times more than in HA group (1843 pg/mL) and HA-Col group (2100 pg/mL). hADSCs in HA-DCM increased secretion of VEGF (1384 pg/mL) significantly compared to HA group (920 pg/mL) and HA-Col group (1015 pg/mL). Therefore, hADSCs in HA hydrogel secreted HGF, IL-8, and VEGF in a similar level to HA-Col group, while HA-DCM composite hydrogel induced hADSCs to secrete more HGF, IL-8, and VEGF significantly than HA and HA-Col group.

3.6. Functionalization of hADSCs towards Extracellular Matrix-Producing Vocal Fold Fibroblasts. Through qRT-PCR, we further determined the expression of decorin and elastin, which were associated with the vocal fold fibroblasts significantly. The results showed that hADSCs expressed decorin with similar level in HA-Col and HA-DCM hydrogel and increased significantly compared to HA groups. Meanwhile, HA-DCM hydrogel promoted the expression of elastin significantly compared to HA-Col group and HA group. The expression of elastin of hADSCs in HA hydrogel was shown to be the lowest in the three groups (Figure 6). Moreover, the secretion of chondroitin sulfate of hADSCs was promoted by the supplementation of DCM in HA hydrogel significantly compared to hADSCs in HA and HA-Col hydrogel (Figure 7). Therefore, HA-DCM enhanced the differentiation of hADSCs towards vocal fold fibroblasts, which evidenced the notion that HA-DCM hydrogel was promising in vocal fold tissue engineering.

4. Discussion

Cell and hydrogel-based regenerative medicine was shown to be outstanding for regeneration of injured tissues or organs. A variety of stem cells have been applied in tissue engineering

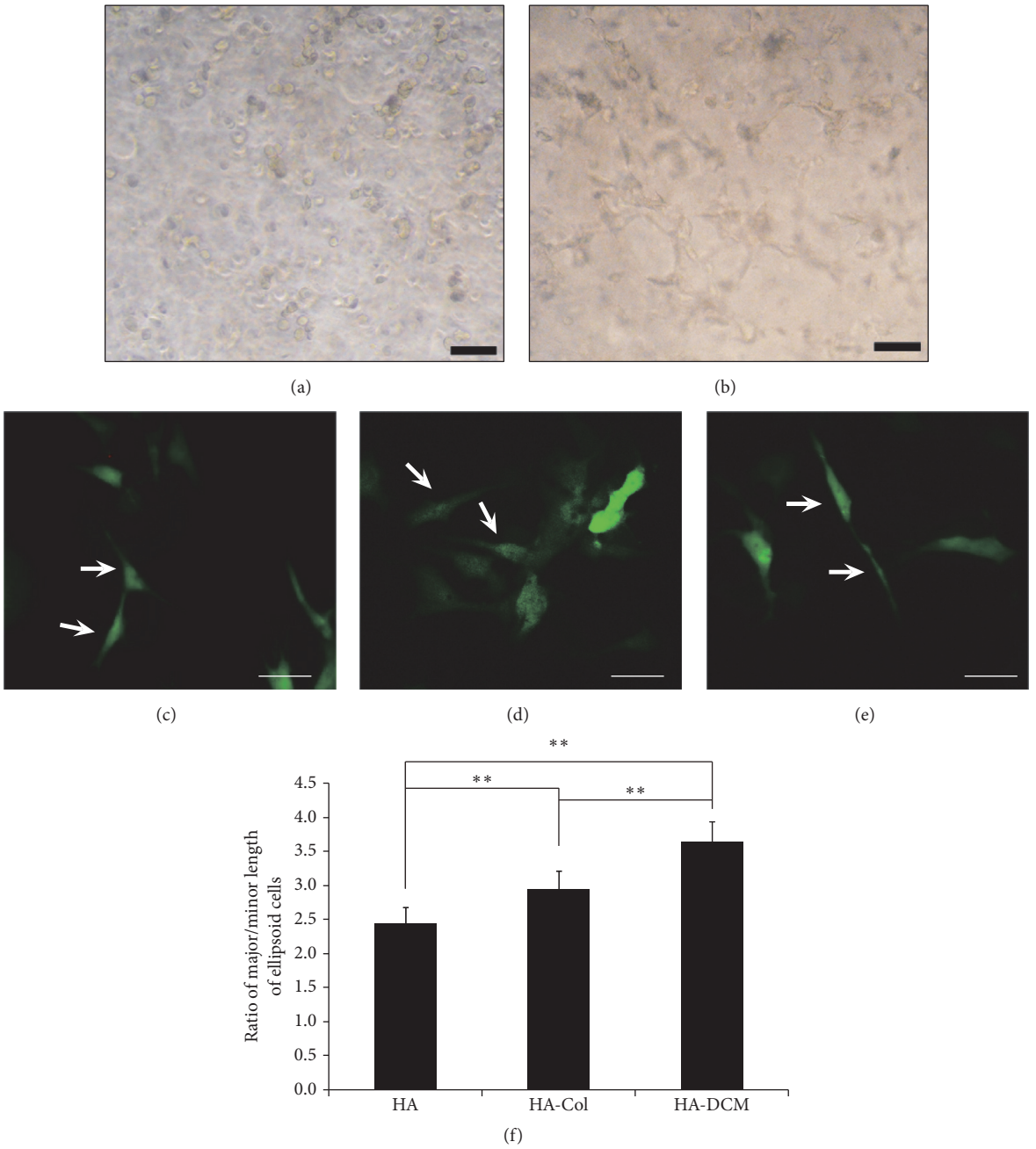

Figure 2: Cell morphology of hADSCs in 3D hydrogel was determined in the cell culture. (a) hADSCs were shown to be circular at 0 h in HA-DCM composite hydrogel; (b) hADSCs developed into spindle cells with fibroblasts-like shape at 24 h; (c–e) cell shape of hADSCs that were labeled with GFP in HA, HA-Col, and HA-DCM hydrogel was observed at the 7th day after cell seeding. The arrows indicated that hADSCs in HA, HA-Col, and HA-DCM hydrogel were shown to be ellipsoid at the 7th day. (f) Quantification of cell shape of hADSCs indicated that the major/minor length of hADSCs in HA-DCM hydrogel was shown to be larger than one in HA-Col hydrogel, and the major/minor length of hADSCs in HA hydrogel was shown to be the smallest in the three groups. ** indicated $p < 0.05$.

to construct engineered tissues [27, 28], and so we focused on human adipose tissue derived stem cells because this kind of stem cells is distributed in the abdominal subcutaneous fat tissue abundantly. Meanwhile, the multipotent nature of hADSCs and putative mesenchymal origin of fibroblasts motivated us to explore the fibroblastic differentiation potential of hADSCs for vocal fold regeneration. Lee et al. stated that the injection hADSCs into vocal folds of canine models promoted the repair of tissues significantly [29].

In tissue engineering, scaffolds providing growth environment including necessary growth factors and 3D spatial environment were shown to be critical for growth and differentiation of stem cells [6]. The extracellular environment determined the potentials of cell growth and differentiation,

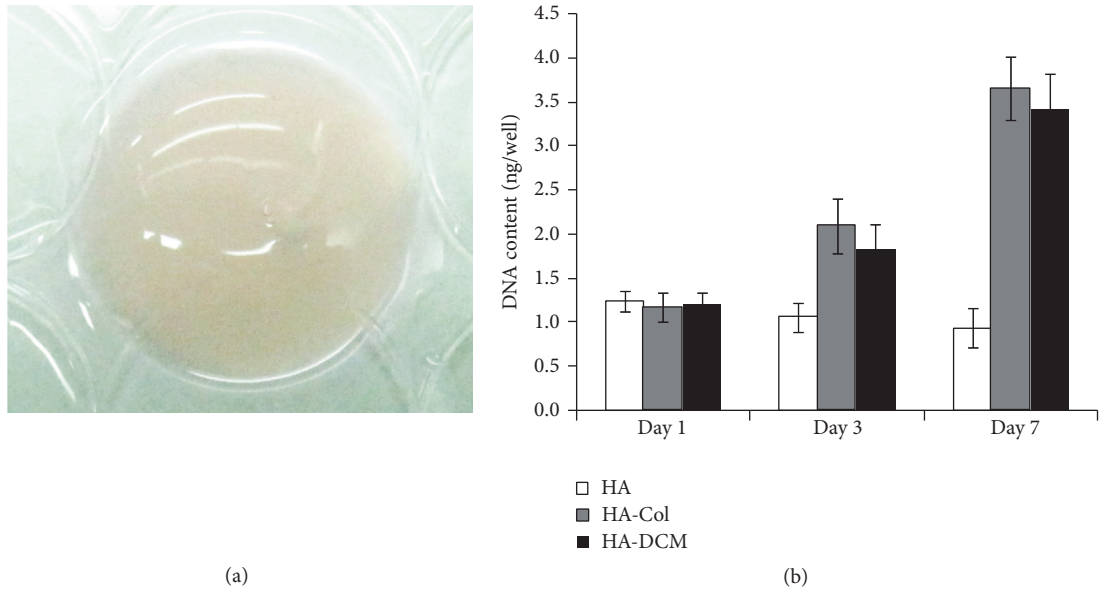

Figure 3: Cell growth of hADSCs in hydrogels. (a) Overall observation of cell-hydrogel constructs indicated that they are transparent. (b) DNA content that was determined by PicoGreen assay indicated that the proliferation of hADSCs in HA-Col and HA-DCM hydrogel was shown to be more than cells in HA-DCM hydrogel significantly.

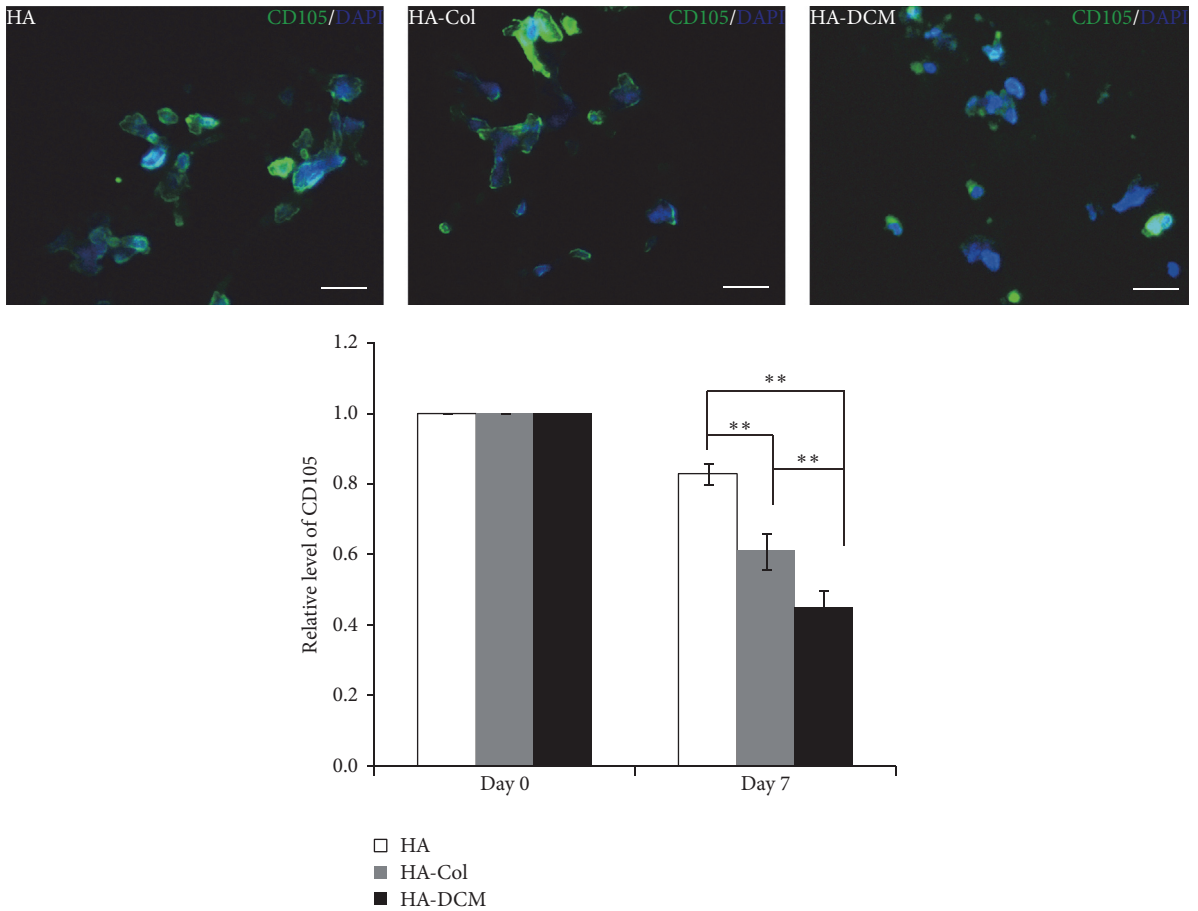

Figure 4: The expression of surface marker CD105 in hADSCs in HA, HA-Col, and HA-DCM hydrogel. The immunofluorescence staining showed CD105 (green) positive cells in HA, HA-Col, and HA-DCM hydrogel. Nuclei were stained by DAPI (blue). Scale bar = 50 μm. The analysis through ImageJ software indicated that cells in HA-DCM hydrogel expressed higher CD105 than cells in HA-Col and HA hydrogel significantly at day 7. ** indicated $p < 0.01$.

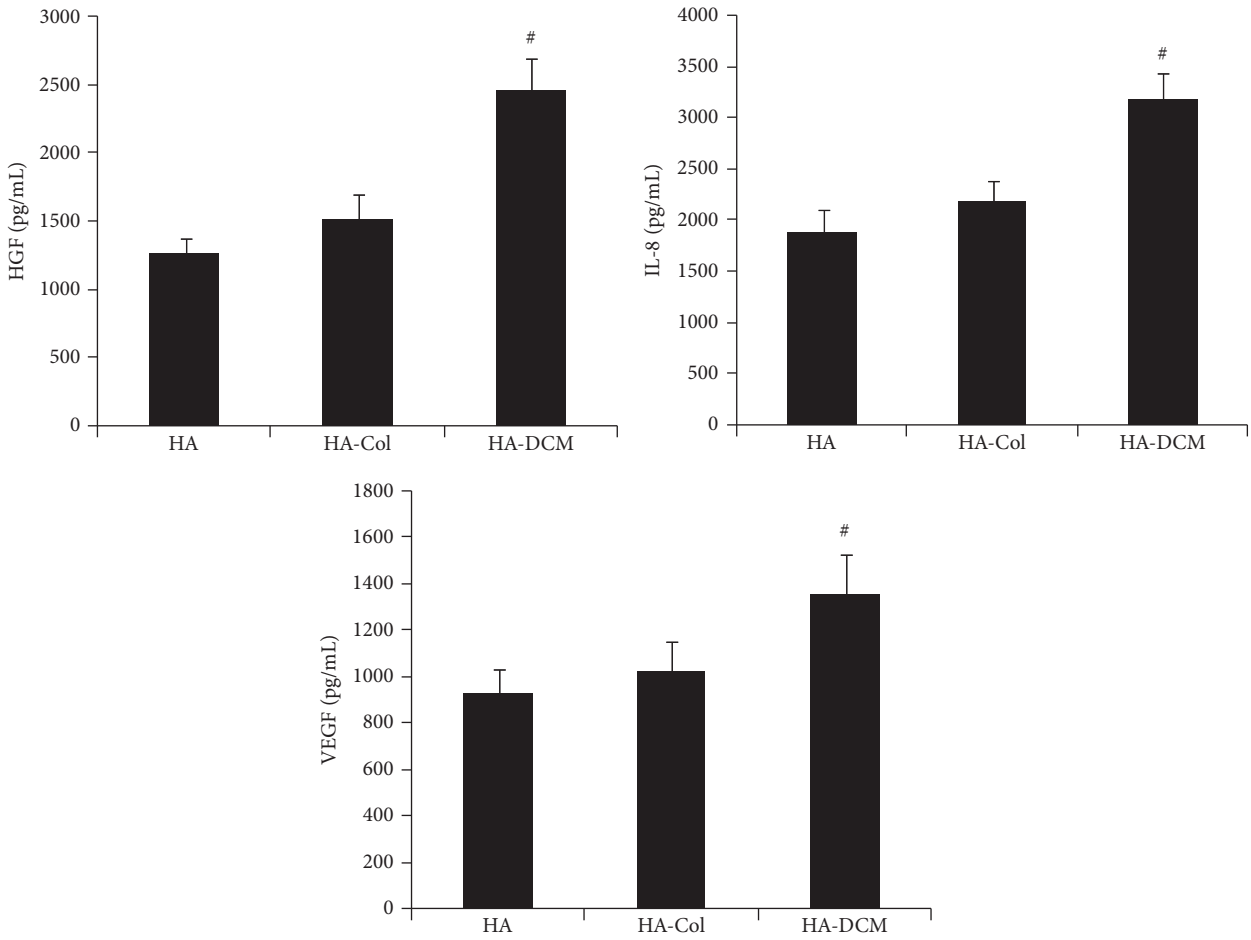

Figure 5: HGF, IL-8, and VEGF release from hADSCs after culture for 3 days in HA, HA-Col, and HA-DCM hydrogel. ELISA assay indicated that hADSCs in HA-DCM composite hydrogel release more HGF, IL-8, and VEGF than cells in HA and HA-Col hydrogel significantly. # indicated $p < 0.01$.

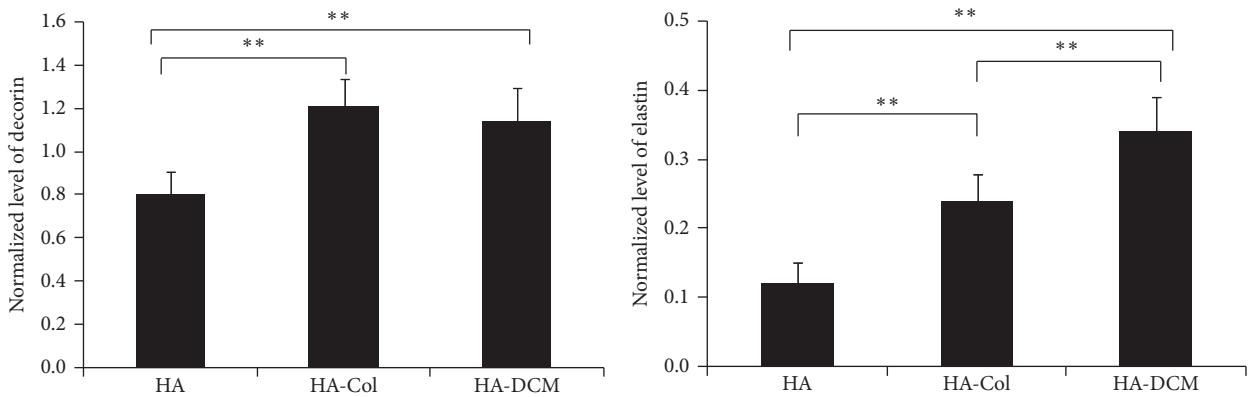

Figure 6: Production of decorin and elastin in hADSCs in HA, HA-Col, and HA-DCM hydrogel. hADSCs in HA-Col and HA-DCM produced more decorin and elastin than cells in HA hydrogel significantly; in particular, the production of elastin was shown to be more than HA-Col and HA hydrogel significantly. ** indicated $p < 0.01$.

such as the stiffness of substrates [30–33]. In the present study, hADSC proliferated evidently in HA-Col and HA-DCM hydrogels, but it was not observed in HA hydrogel (Figure 4). The main reason should be ascribed to the property of the material itself; that is, HA hydrogel alone may have limited biocompatibility or bioactivity to support the proliferation of incorporated hADSCs. Actually, this has been confirmed by a previous report too [17]. The result suggested that though it is

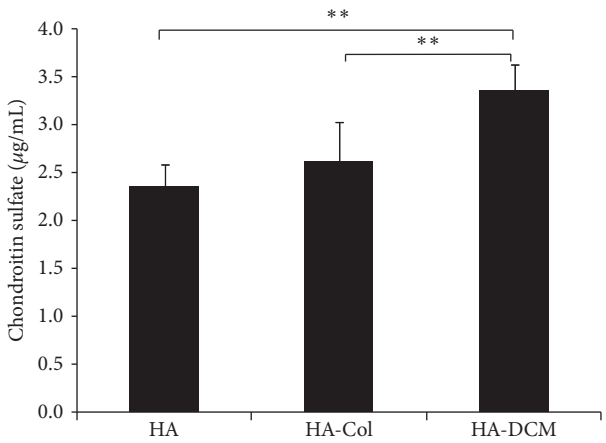

Figure 7: ELISA determined the secretion of chondroitin sulfate of hADSCs in HA, HA-Col, and HA-DCCM hydrogel. The supplementation of DCM in HA hydrogel increased the production of chondroitin sulfate significantly compared to HA-Col and HA hydrogel. ** indicated $p < 0.01$.

an important ECM constituent in vocal fold lamina propria, hyaluronic acid alone may not be suitable to be used as stem cell scaffold for vocal fold tissue engineering. Modifying HA with other hydrogels, or constructing cogels of HA with other hydrogels as investigated in the present and previous study [17], is highly required.

Previously, *in vitro* studies with application of stem cells and hydrogel in vocal fold tissue engineering showed that cogels of HA-Col or HA-fibrin promoted the proliferation, differentiation, and synthesis of elastin [17]. Our results indicated that the supplementation of DCM promoted cell elongation and differentiation significantly compared to HA-Col and HA. We think that this was probably related to the scaffold environment and some signal molecules that were provided by HA-Col hydrogel. As is known, the differentiation of stem cells was mainly regulated by the extracellular environment, signal molecules, and cell-cell interaction [34]. On the one hand, we supposed that HA-DCM hydrogel may provide a more favourable environment than HA and HA-Col hydrogels for hADSC growth and differentiation. On the other hand, DCM has been shown to be with multiple growth factors and functional proteins for cell growth and differentiation, such as bFGF, TGF-β, or BMP4 [35–38]. These proteins may also function as signal molecules stimulating the differentiation of incorporated hADSCs HA-DCM hydrogel. Therefore, hADSCs elongated and differentiated better in HA-DCM hydrogel than in HA and HA-Col hydrogels as observed in the study.

We also found that the supplementation of DCM in HA hydrogel induced the secretion of HGF, IL-8, and VEGF of hADSCs, which might be involved in the promotion of cell growth, elongation, and differentiation by cogel of HA-DCM. Previous studies showed that HGF as an important regulatory factor was secreted by ADSCs *in vitro* significantly to repair the scar fibroblasts of vocal fold [39]. HGF could reduce the deposition of collagen I and increase HA to prevent fibrosis of the vocal fold [40]. The injection of decellularized small intestinal submucosa gel containing HGF repaired and remodeled injured vocal fold *in vivo* significantly [41]. Therefore, the secretion of HGF would increase the therapeutic efficiency of hADSCs significantly.

VEGF as another important paracrine factor was increased by HA-DCM hydrogel, and this suggested that cell-hydrogel constructs may potentially promote ECM remodeling and regulation, angiogenesis, and normal wound-healing process [42]. We observed that the synthesis of important components of ECM such as decorin and elastin has been promoted by cogel of HA-DCM. HGF were confirmed to have a critical effect on the remodeling of injured vocal fold to increase the synthesis of elastin [43].

IL-8 is an important proinflammatory and angiogenic cytokine involved in the regulation of vocal fold remodeling and regeneration. It has been shown that the vocal fold fibroblasts seeding on the surface of Extracel® hydrogels, which resulted from the cross-linking of HA and gelatin, induced proinflammatory cytokines, IL-8 and TNF-α, *in vitro* [44]. With the secretion of IL-8, hADSCs in hydrogel can induce the monocytes and macrophages to repair vocal fold injuries by remodeling of ECMs *in vivo* [45]. As for the exact role of IL-8 in the repair of vocal fold, it will be studied in future work.

This study represents our effort in the evaluation of cogel of HA-DCM to foster the fibroblastic differentiation of hADSCs. In our study, cells embedded in cogels of HA-DCM were cultivated under static conditions. hADSCs upregulated the secretion of HGF, IL-8, and VEGF to promote the differentiation of hADSCs in HA-DCM hydrogel.

5. Conclusion

Cogel of HA-DCM as a promising scaffold supported the proliferation and prolonged the cell shape of hADSCs significantly compared to HA and HA-Col hydrogel. Moreover, the cogel of HA-DCM promoted the differentiation of hADSCs towards vocal fold fibroblasts through stimulation of secretion of HGF, IL-8, and VEGF and synthesis of extracellular matrix such as elastin and decorin. Collectively, these results demonstrated that HA-DCM hydrogel holds a great potential for vocal fold regenerative applications through the increase of cytokine release and ECM synthesis.

Competing Interests

The authors declare that they have no competing interests.

Acknowledgments

This work was supported by the National Natural Science Foundation of China (no. 30700937) and the New-Star of Science and Technology supported by Beijing Metropolis.

References

[1] T. Tateya, I. Tateya, J. H. Sohn, and D. M. Bless, "Histological study of acute vocal fold injury in a rat model," *Annals of*

Otology, Rhinology and Laryngology, vol. 115, no. 4, pp. 285–292, 2006.

[2] I. Tateya, T. Tateya, X. Lim, J. H. Sohn, and D. M. Bless, "Cell production in injured vocal folds: a rat study," *Annals of Otology, Rhinology and Laryngology*, vol. 115, no. 2, pp. 135–143, 2006.

[3] B. Rousseau, S. Hirano, T. D. Scheidt et al., "Characterization of vocal fold scarring in a canine model," *The Laryngoscope*, vol. 113, no. 4, pp. 620–627, 2003.

[4] M. Graupp, S. Bachna-Rotter, C. Gerstenberger et al., "The unsolved chapter of vocal fold scars and how tissue engineering could help us solve the problem," *European Archives of Oto-Rhino-Laryngology*, vol. 273, no. 9, pp. 2279–2284, 2016.

[5] S. Kazemirad, H. K. Heris, and L. Mongeau, "Viscoelasticity of hyaluronic acid-gelatin hydrogels for vocal fold tissue engineering," *Journal of Biomedical Materials Research Part B: Applied Biomaterials*, vol. 104, no. 2, pp. 283–290, 2016.

[6] M. T. Langhans, S. Yu, and R. S. Tuan, "Stem cells in skeletal tissue engineering: technologies and models," *Current Stem Cell Research & Therapy*, vol. 11, no. 6, pp. 453–474, 2016.

[7] R. L. Pisciolaro, M. T. Duailibi, N. F. Novo et al., "Tooth tissue engineering: the importance of blood products as a supplement in tissue culture medium for human pulp dental stem cells," *Tissue Engineering A*, vol. 21, no. 21-22, pp. 2639–2648, 2015.

[8] B. Chuenjitkuntaworn, T. Osathanon, N. Nowwarote, P. Supaphol, and P. Pavasant, "The efficacy of polycaprolactone/hydroxyapatite scaffold in combination with mesenchymal stem cells for bone tissue engineering," *Journal of Biomedical Materials Research Part A*, vol. 104, no. 1, pp. 264–271, 2016.

[9] F. Veronesi, M. Maglio, M. Tschon, N. N. Aldini, and M. Fini, "Adipose-derived mesenchymal stem cells for cartilage tissue engineering: state-of-the-art in in vivo studies," *Journal of Biomedical Materials Research A*, vol. 102, no. 7, pp. 2448–2466, 2014.

[10] Y. S. Choi, K. Matsuda, G. J. Dusting, W. A. Morrison, and R. J. Dilley, "Engineering cardiac tissue in vivo from human adipose-derived stem cells," *Biomaterials*, vol. 31, no. 8, pp. 2236–2242, 2010.

[11] L. Flynn, G. D. Prestwich, J. L. Semple, and K. A. Woodhouse, "Adipose tissue engineering in vivo with adipose-derived stem cells on naturally derived scaffolds," *Journal of Biomedical Materials Research A*, vol. 89, no. 4, pp. 929–941, 2009.

[12] W. Xu, R. Hu, E. Fan, and D. Han, "Adipose-derived mesenchymal stem cells in collagen-hyaluronic acid gel composite scaffolds for vocal fold regeneration," *Annals of Otology, Rhinology and Laryngology*, vol. 120, no. 2, pp. 123–130, 2011.

[13] R. Hu, W. Ling, W. Xu, and D. Han, "Fibroblast-like cells differentiated from adipose-derived mesenchymal stem cells for vocal fold wound healing," *PLoS ONE*, vol. 9, no. 3, Article ID e92676, 2014.

[14] D. Skodacek, U. Arnold, K. Storck, C. P. Alvarez, S. Ratzinger, and R. Staudenmaier, "Chondrocytes suspended in modified fibrin glue for vocal fold augmentation: an in vitro study in a porcine larynx model," *Head and Neck*, vol. 34, no. 5, pp. 667–673, 2012.

[15] T. Long, J. Yang, S.-S. Shi, Y.-P. Guo, Q.-F. Ke, and Z.-A. Zhu, "Fabrication of three-dimensional porous scaffold based on collagen fiber and bioglass for bone tissue engineering," *Journal of Biomedical Materials Research Part B: Applied Biomaterials*, vol. 103, no. 7, pp. 1455–1464, 2015.

[16] D. G. Miranda, S. M. Malmonge, D. M. Campos, N. G. Attik, B. Grosgogeat, and K. Gritsch, "A chitosan-hyaluronic acid hydrogel scaffold for periodontal tissue engineering," *Journal of Biomedical Materials Research B: Applied Biomaterials*, vol. 104, no. 8, pp. 1691–1702, 2015.

[17] H. Park, S. Karajanagi, K. Wolak et al., "Three-dimensional hydrogel model using adipose-derived stem cells for vocal fold augmentation," *Tissue Engineering-Part A*, vol. 16, no. 2, pp. 535–543, 2010.

[18] A. K. Miri, H. K. Heris, U. Tripathy, P. W. Wiseman, and L. Mongeau, "Microstructural characterization of vocal folds toward a strain-energy model of collagen remodeling," *Acta Biomaterialia*, vol. 9, no. 8, pp. 7957–7967, 2013.

[19] P. D. Ward, S. L. Thibeault, and S. D. Gray, "Hyaluronic acid: its role in voice," *Journal of Voice*, vol. 16, no. 3, pp. 303–309, 2002.

[20] X. Q. Jia, Y. Yeo, R. J. Clifton et al., "Hyaluronic acid-based microgels and microgel networks for vocal fold regeneration," *Biomacromolecules*, vol. 7, no. 12, pp. 3336–3344, 2006.

[21] W. Xu, R. Hu, E. Fan, and D. Han, "Adipose-derived mesenchymal stem cells in collagen-hyaluronic acid gel composite scaffolds for vocal fold regeneration," *Annals of Otology, Rhinology and Laryngology*, vol. 120, no. 2, pp. 123–130, 2011.

[22] Y.-C. Chen, R.-N. Chen, H.-J. Jhan et al., "Development and characterization of acellular extracellular matrix scaffolds from porcine menisci for use in cartilage tissue engineering," *Tissue Engineering-Part C: Methods*, vol. 21, no. 9, pp. 971–986, 2015.

[23] F. M. Egydio, L. G. Freitas Filho, K. Sayeg, M. Laks, A. S. Oliveira, and F. G. Almeida, "Acellular human glans extracellular matrix as a scaffold for tissue engineering: in vitro cell support and biocompatibility," *International Brazilian Journal of Urology*, vol. 41, no. 5, pp. 990–1001, 2015.

[24] Y. C. Chen, R. N. Chen, H. J. Jhan et al., "Development and characterization of acellular extracellular matrix scaffolds from porcine menisci for use in cartilage tissue engineering," *Tissue Engineering Part C Methods*, vol. 21, no. 9, pp. 971–986, 2015.

[25] A. Mildmay-White and W. Khan, "Cell surface markers on adipose-derived stem cells: a systematic review," *Current Stem Cell Research & Therapy*, vol. 11, no. 8, 2016.

[26] J.-J. Yang, Z.-Q. Liu, J.-M. Zhang et al., "Real-time tracking of adipose tissue-derived stem cells with injectable scaffolds in the infarcted heart," *Heart and Vessels*, vol. 28, no. 3, pp. 385–396, 2013.

[27] M. V. Hogan, G. N. Walker, L. R. Cui, F. H. Fu, and J. Huard, "The role of stem cells and tissue engineering in orthopaedic sports medicine: current evidence and future directions," *Arthroscopy*, vol. 31, no. 5, pp. 1017–1021, 2015.

[28] C. P. Jackman, I. Y. Shadrin, A. L. Carlson, and N. Bursac, "Human cardiac tissue engineering: from pluripotent stem cells to heart repair," *Current Opinion in Chemical Engineering*, vol. 7, pp. 57–64, 2015.

[29] B. J. Lee, S. G. Wang, J. C. Lee et al., "The prevention of vocal fold scarring using autologous adipose tissue-derived stromal cells," *Cells Tissues Organs*, vol. 184, no. 3-4, pp. 198–204, 2007.

[30] J. H. Wen, L. G. Vincent, A. Fuhrmann et al., "Interplay of extracellular matrix stiffness and tethering in regulating stem cell fate," *Molecular Biology of the Cell*, vol. 25, 2014.

[31] O. B. Vidi and A. F. Bakry, "Correlation between serum extracellular matrix and liver stiffness in liver fibrosis," *Journal of Gastroenterology and Hepatology*, vol. 29, pp. 208–208, 2014.

[32] K. Bhadriraju and L. K. Hansen, "Extracellular matrix- and cytoskeleton-dependent changes in cell shape and stiffness," *Experimental Cell Research*, vol. 278, no. 1, pp. 92–100, 2002.

[33] J. Liu, G. N. Jyothirmayi, M. R. Masurekar, M. M. Lyons, T. J. Regan, and T. Niwa, "Extracellular matrix alterations and normalization of diastolic stiffness in aged dog heart," *Circulation*, vol. 102, no. 18, pp. 312–313, 2000.

[34] A. Solanki, S. Shah, K. A. Memoli, S. Y. Park, S. Hong, and K.-B. Lee, "Controlling differentiation of neural stem cells using extracellular matrix protein patterns," *Small*, vol. 6, no. 22, pp. 2509–2513, 2010.

[35] L. K. Kanninen, P. Porola, J. Niklander et al., "Hepatic differentiation of human pluripotent stem cells on human liver progenitor HepaRG-derived acellular matrix," *Experimental Cell Research*, vol. 341, no. 2, pp. 207–217, 2016.

[36] P. Burra, S. Tomat, M. T. Conconi et al., "Acellular liver matrix improves the survival and functions of isolated rat hepatocytes cultured in vitro," *International Journal of Molecular Medicine*, vol. 14, no. 4, pp. 511–515, 2004.

[37] P. L. Sánchez, M. E. Fernández-Santos, S. Costanza et al., "Acellular human heart matrix: a critical step toward whole heart grafts," *Biomaterials*, vol. 61, pp. 279–289, 2015.

[38] N. M. Patel, Z.-W. Tao, M. A. Mohamed, M. K. Hogan, L. Gutierrez, and R. K. Birla, "Engineering 3D bio-artificial heart muscle: the acellular ventricular extracellular matrix model," *ASAIO Journal*, vol. 61, no. 1, pp. 61–70, 2015.

[39] Y. Kumai, J. B. Kobler, H. Park, M. Galindo, V. L. M. Herrera, and S. M. Zeitels, "Modulation of vocal fold scar fibroblasts by adipose-derived stem/stromal cells," *The Laryngoscope*, vol. 120, no. 2, pp. 330–337, 2010.

[40] S. Hirano, D. Bless, D. Heisey, and C. Ford, "Roles of hepatocyte growth factor and transforming growth factor β1 in production of extracellular matrix by canine vocal fold fibroblasts," *The Laryngoscope*, vol. 113, no. 1, pp. 144–148, 2003.

[41] J.-S. Choi, S. Lee, D. Y. Kim, Y.-M. Kim, M. S. Kim, and J.-Y. Lim, "Functional remodeling after vocal fold injury by small intestinal submucosa gel containing hepatocyte growth factor," *Biomaterials*, vol. 40, pp. 98–106, 2015.

[42] X. Chen and S. L. Thibeault, "Role of tumor necrosis factor-α in wound repair in human vocal fold fibroblasts," *The Laryngoscope*, vol. 120, no. 9, pp. 1819–1825, 2010.

[43] Y. Luo, J. B. Kobler, S. M. Zeitels, and R. Langer, "Effects of growth factors on extracellular matrix production by vocal fold fibroblasts in 3-dimensional culture," *Tissue Engineering*, vol. 12, no. 12, pp. 3365–3374, 2006.

[44] X. Chen and S. L. Thibeault, "Biocompatibility of a synthetic extracellular matrix on immortalized vocal fold fibroblasts in 3-D culture," *Acta Biomaterialia*, vol. 6, no. 8, pp. 2940–2948, 2010.

[45] G. Broughton II, J. E. Janis, and C. E. Attinger, "The basic science of wound healing," *Plastic and Reconstructive Surgery*, vol. 117, no. 7, pp. 12S–34S, 2006.

Hindawi Publishing Corporation
BioMed Research International
Volume 2016, Article ID 1596157, 10 pages
http://dx.doi.org/10.1155/2016/1596157

Research Article

Fabrication of Poly(ε-caprolactone) Scaffolds Reinforced with Cellulose Nanofibers, with and without the Addition of Hydroxyapatite Nanoparticles

Pedro Morouço,[1] Sara Biscaia,[1] Tânia Viana,[1] Margarida Franco,[1] Cândida Malça,[1,2] Artur Mateus,[1] Carla Moura,[1,3] Frederico C. Ferreira,[3] Geoffrey Mitchell,[1] and Nuno M. Alves[1]

[1]*Centre for Rapid and Sustainable Product Development, Polytechnic Institute of Leiria, 2430-028 Marinha Grande, Portugal*
[2]*Coimbra Institute of Engineering, Polytechnic Institute of Coimbra, 3030-199 Coimbra, Portugal*
[3]*Institute for Bioengineering and Biosciences and Department of Bioengineering, Instituto Superior Técnico, Universidade de Lisboa, 1049-001 Lisboa, Portugal*

Correspondence should be addressed to Pedro Morouço; pedro.morouco@ipleiria.pt

Received 1 July 2016; Revised 10 October 2016; Accepted 11 October 2016

Academic Editor: Pornanong Aramwit

Biomaterial properties and controlled architecture of scaffolds are essential features to provide an adequate biological and mechanical support for tissue regeneration, mimicking the ingrowth tissues. In this study, a bioextrusion system was used to produce 3D biodegradable scaffolds with controlled architecture, comprising three types of constructs: (i) poly(ε-caprolactone) (PCL) matrix as reference; (ii) PCL-based matrix reinforced with cellulose nanofibers (CNF); and (iii) PCL-based matrix reinforced with CNF and hydroxyapatite nanoparticles (HANP). The effect of the addition and/or combination of CNF and HANP into the polymeric matrix of PCL was investigated, with the effects of the biomaterial composition on the constructs (morphological, thermal, and mechanical performances) being analysed. Scaffolds were produced using a single lay-down pattern of 0/90°, with the same processing parameters among all constructs being assured. The performed morphological analyses showed a satisfactory distribution of CNF within the polymer matrix and high reliability was obtained among the produced scaffolds. Significant effects on surface wettability and thermal properties were observed, among scaffolds. Regarding the mechanical properties, higher scaffold stiffness in the reinforced scaffolds was obtained. Results from the cytotoxicity assay suggest that all the composite scaffolds presented good biocompatibility. The results of this first study on cellulose and hydroxyapatite reinforced constructs with controlled architecture clearly demonstrate the potential of these 3D composite constructs for cell cultivation with enhanced mechanical properties.

1. Introduction

Tissue engineering (TE) approaches have a high potential for the development of new therapeutic strategies for medical applications, which have led to an increasing number of research and development studies by academic and industry communities. In recent years, the utility of cellulose fibres in biomedical applications has gained distinctive attention by the scientific community, due to the unique combination of its properties such as nontoxicity, biocompatibility, biodegradability, low cost, and high mechanical modulus [1, 2]. This natural polymer is a homopolysaccharide formed by linearly connected D-glucose units condensed through the β (1–4) glycosidic bonds [3, 4]. It is the most available polymer in nature and is widely available from several sources. Furthermore, it can be synthetized by woody plants, several kinds of algae and fungi, grasses, and some species of bacteria [5–7]. The applications of cellulose include coatings, filtration, catalysis, sensors, and medicine [6, 8]. Additionally, its use is particularly interesting for biomedical applications because nanofibers have been successfully used as highly effective reinforced fillers for numerous different polymers,

enhancing the mechanical properties of the composites and improving cell biocompatibility [9–11]. Lastly, the interaction of polymer blends has been of intensive interest due to the number of valuable properties and strong economic incentives.

On the other hand, porous composite scaffolds have been extensively used in TE approaches, as a support for cell attachment, cell growth, and tissue regeneration [12]. An ideal scaffold must be able to provide the essential properties and function to satisfy simultaneously the biological and mechanical requirements for optimal tissue regeneration [13]. To reach these requirements, several studies have been developed based on (i) 3D porous scaffolds with arbitrary architecture (uncontrolled pore size and spatial distribution); (ii) 3D porous scaffolds with hybrid architecture (pore size and spatial distribution partially controlled); and (iii) 3D porous scaffolds with controlled architecture (pore size and spatial distribution) [14]. Each of these approaches have advantages and drawbacks; the fact that having a controlled architecture may bridge the gap between produced scaffolds and native tissue is accepted by the scientific community.

Despite the progress achieved towards the development of structures as biological substitutes, the development of 3D biodegradable scaffolds with improved mechanical and biological properties remains a goal to be achieved. The architecture and mechanical properties of such scaffolds are important to promote further cellular activities and neotissue development. The properties of the scaffolds previously developed aiming at bone regeneration are reviewed elsewhere, with porosities varying widely from 20 to 90% [15]. Importantly, not only a reasonable high porosity, but high pore connectivity and surface area are essential to promote an initial efficient scaffold seeding by cells and metabolite transport and in further states efficient scaffold colonization with formation of continuous tissue across the full scaffolds 3D structure. For bone applications, Rouwkema et al. [16] had pointed out a minimal size of 100 μm to allow oxygen and nutrients diffusion. Likewise, an optimal size of 200–350 μm has been recommended [17] to facilitate both cell attachment and proliferation, for efficient tissue ingrowth.

Poly(ε-caprolactone) (PCL) is one of the most common medical approved linear aliphatic polyesters [18]. It is a hydrophobic and semicrystalline polymer, for which its crystallinity tends to decrease with a molecular weight increase [19]. Furthermore, its good solubility, low melting point (59–64°C), and exceptional blend-compatibility have motivated extensive research over its potential applications in the biomedical field [20]. As cellulose nanofibers (CNF) and PCL are biodegradable and semicrystalline polymers, there are several advantages to blend these two polymers. However, the dispersion of hydrophilic CNF in a hydrophobic thermoplastic to obtain a homogeneous composite is a paramount challenge, demanding more research on methods able to achieve it through the improvement of their interfacial adhesion properties [21]. For the preparation of polymer/cellulose nonhydrosoluble composites, conventional methods, such as solvent casting, usually require cellulose modified by surface coating or grafting to achieve good dispersion [1, 22].

For this research, semicrystalline PCL-based scaffolds with controlled architecture were produced. Aiming to examine the effects of cellulose in those constructs, they were reinforced with cellulose nanofibers with and without the addition of hydroxyapatite nanoparticles (HANP). Scaffolds were produced by extrusion, a layer-by-layer process, which results in a nanocomposite material that gathers unique proprieties: biodegradability resulting from PCL ester bonds breakdown, biocompatibility tailored for bone tissue formation through the use of hydroxyapatite, and mechanical properties provided by a nanostructure obtained with a combination of CNF and HANP. The nanocomposites were characterized by optical microscope, DSC, TGA, compression testing, and *in vitro* cytotoxic techniques. The present work provides a proposal to obtain biodegradable composites which can be further used in biomedical applications.

2. Materials and Methods

2.1. Materials. In this work PCL polymer (CAPA® 6500) from Perstorp Caprolactones (Cheshire, United Kingdom) with a molecular weight of 50 kDa was used. The CNF 3% (w/v) (Curran® Slurry) were provided by the Cellucomp (Burntisland, United Kingdom) and the HANP (≥97%, synthetic) with a particle size less than 200 nm was obtained from Sigma-Aldrich (Saint Louis, USA). Nanocomposites were produced using N,N-Dimethylformamide (DMF) from Merck KGaA® (Germany).

2.2. Composites Preparation. PCL pellets were dissolved in DMF at 50°C. The solution was deposited in Petri dishes and dried at controlled environment on an orbital shaker (KS 4000 i control, IKA, Germany) at 25°C for 48 hours. The PCL/CNF composite was prepared by solvent casting using lyophilized CNF. Cellulose aqueous samples were frozen at −40°C and then freeze-dried under vacuum (2×10^{-3} mbar with a ILMVAC GmbH vacuum pump) at −45°C using a FreeZone 4.5 freeze-drying equipment (from LABCONCO Corporation, Kansas, USA) for 72 hours. The frozen water was removed from the cellulose samples, initially by sublimation (primary drying) and then by desorption (secondary drying).

The corresponding membranes were prepared through the dissolution of PCL pellets (99% (w/w)) and CNF 1% (w/w) in DMF at 50°C, separately. CNF solution preparation includes sonication of the CNF at 100 W for 10 min, using an ultrasonic homogenizer (UP200Ht, Hielscher, Ultrasound Technology). After obtaining two homogeneous solutions, they were mixed using a magnetic stirrer (500 rpm) for 10 min. The PCL/CNF solution was deposited in Petri dishes and dried using the same methodology used for the production of PCL membranes.

The membranes of PCL/CNF/HANP were produced keeping the concentration of CNF at 1% (w/w) and adding 5% (w/w) of HANP in DMF. After complete dissolution, the obtained solution was deposited in Petri dishes and dried

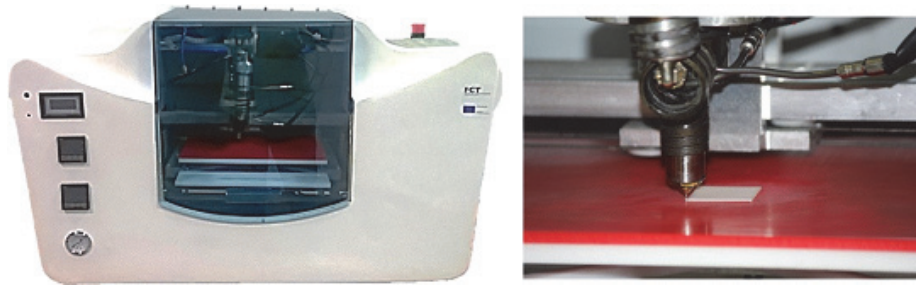

Figure 1: Bioextruder system, developed by the Centre for Rapid and Sustainable Product Development, Polytechnic Institute of Leiria.

in a controlled environment, similar to PCL and PCL/CNF membranes.

2.3. 3D Scaffolds Production. The obtained membranes were processed by extrusion using a Bioextruder® system (Figure 1), developed by the Centre for Rapid and Sustainable Product Development, Polytechnic Institute of Leiria [23]. The 3D scaffolds were produced by fibre deposition with 300 μm diameter, 350 μm pore size, and 0°/90° lay-down pattern. These parameters took in consideration that a minimum pore size of 100 μm is required for the diffusion of nutrients and oxygen for cell survival and proliferation. Furthermore, it has been shown that pore sizes up to 350 μm are optimal for bone tissue ingrowth [24]. The process conditions used for all scaffolds were 20 mm/s of deposition velocity, 50 rpm of screw rotation velocity, and 90°C of liquefier temperature.

2.4. Morphological Analysis. The surface morphology of all produced membranes was examined by optical microscopy (Daffodil MCX100, Micros Austria) at a magnification of 40x. Additionally, micro-computed tomography (Micro-CT) scans of the scaffolds were performed using a SkyScan microtomograph model 1174 by Brucker Company (Brussels, Belgium). The CT system was operated with a rotation step of 0.7 degrees, voltage of 50 kV, exposure time of 2300 ms, and a current of 800 μA with a nominal resolution of 16.65 μm/pixel. The micro-CT analyses allowed the visualization of the internal and external morphologies of the samples as well as the calculation of porosities. The reconstructed set of slices was viewed in SkyScan Data Viewer program, 3D realistic images were made with CTvox software, and porosity values were calculated through CTan software.

2.5. Contact Angle Measurement. The wettability of the scaffolds was evaluated by static contact angle measurement at 10s on a Theta Lite optical tensiometer (Attension, Finland). A water droplet was poured on the surface of solid samples and the contact angle was measured by OneAttension 1.0. software (Attension). Aiming to increase its reliability, 15 measurements were performed for each scaffold type.

2.6. Thermal Analysis. A STA 6000 (Perkin Elmer®) was used for thermal analysis of the materials. Samples of 6 mg were placed in alumina pans and empty pans were used as reference. All samples were first heated at a range of 30–120°C at a heating rate of 10°C/min and held isothermally for 10 min to mitigate any prior thermal history. Afterwards, the samples were cooled to 30°C at 10°C/min and then reheated to 120°C at the same rate. After each test, the melting point region from the thermograph was analysed to determine the heat of fusion (ΔH_m) and the melting temperature (T_m); the crystallization region was analysed to determine the crystallization temperature (T_c) of all samples. To evaluate the thermal degradation of the materials, the samples were exposed to a temperature ramp from 30°C to 600°C, at a heating rate of 10°C/min. The flow rate of nitrogen was 20 mL/min during all the runs.

2.7. Mechanical Analysis. Compression tests were performed to evaluate the effect of CNF and HANP addition on the mechanical properties of the PCL scaffold. The tests were conducted according to ASTM standards, using a ZWICK Z100, with a cross-head displacement speed of 1 mm/min. Mechanical testing was carried out using scaffolds samples in the dry state, with a length of 4 mm, a width of 4 mm, and a height of 8 mm. Stress-strain data were computed from load-displacement measurements and the compressive modulus (E) was determined from the elastic region of the obtained curves.

2.8. Cytotoxicity Assessment. *In vitro* cytotoxicity assessment was performed according to ISO standard 10993-5:2009, as described elsewhere [25]. Direct contact (qualitative) and extract (quantitative) assays were performed. Samples were sterilized in 70% ethanol and UV light overnight and then washed with phosphate buffered saline (PBS, Gibco®). Mouse fibroblasts L929 were cultured in Dulbecco's modified Eagle's medium (DMEM, Gibco), supplemented with 10% Fetal Bovine Serum (FBS, Life Technologies), and seeded on 24-well plates (1.5×10^5 cells/well) to obtain approximately 80% of confluence, that is, well plate surface covered by adherent cells. The plates were incubated overnight (37°C; 21% O_2; 5% CO_2).

Scaffold samples were submersed in the medium and kept in the incubator for 72 hours to obtain the extracting culture media enriched with any eventual solutes that may had leach from the scaffolds. Then, for the extract assay, the culture medium of the cells was discarded and replaced with

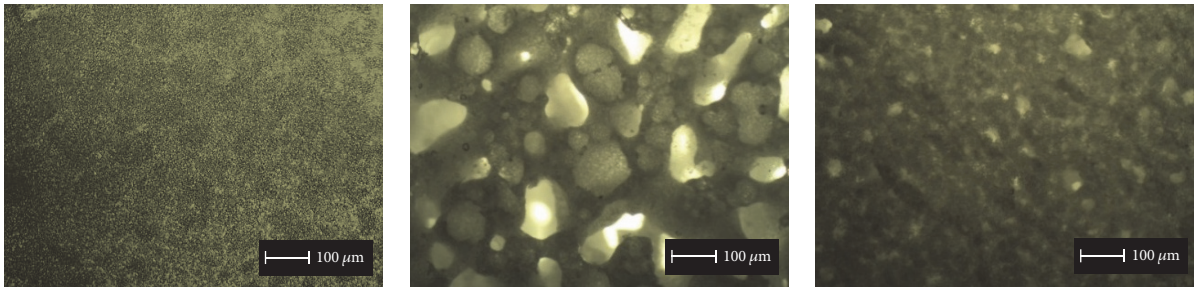

(a) (b) (c)

Figure 2: Micrographs (magnification: 40x) of PCL (a), PCL/CNF (b), and PCL/CNF/HANP (c) membranes.

extracting culture media for further cultivation of the adherent cells for 24 hours. Cell activity of such cultures was assessed by a 3-(4,5-Dimethylthiazol-2-yl)-2,5-diphenyltetrazolium bromide (MTT, Sigma) protocol (extract assay). As controls, fresh medium was used as negative control and latex was used as positive control. All the conditions were tested in triplicate. Direct contact assays were carried out by placing the scaffolds on top of the cells layer at 80% confluence and incubated for another 24 h. After this, photographs were taken in the optical microscope for the direct qualitative contact assay.

2.9. Statistical Analysis. Normality and homoscedasticity assumptions were checked by Shapiro-Wilk and Levene tests, respectively. Descriptive statistics (mean and standard deviation) were calculated for all dependent variables. The significance of differences between types of scaffolds was evaluated by analysis of variance (one-way ANOVA, with Bonferroni *post hoc* test). All statistical procedures were performed using SPSS 23.0 (Chicago, IL, USA) and the G-Power 3.1.9.2 for Windows® (University of Kiel, Germany). The level of statistical significance was set at 95% ($p < 0.05$).

3. Results and Discussion

3.1. Morphological Analysis. Although the addition of CNF in the PCL polymeric matrix significantly influenced the surface morphology of the membranes, micrographs of the produced membranes confirm that the blends obtained by solvent casting were successfully produced, with homogeneous distribution of CNF within the polymer matrix (Figure 2). The adopted strategy of melting the PCL allowed an enhanced interaction between these two polymers. Figure 2(b) clearly shows that the CNF incorporation promotes an increase in pore size. This outcome may be a consequence of the higher cellulose hydrophilicity, thus, potentially higher hygroscopy of the copolymer mixture than PCL alone, which could lead to external surface modification due to the contact with air moisture when the solution is deposited in the Petri dishes. This would lead to the surface energy increase with the addition of CNF, resulting in a pore size increment [26]. Additionally, the incorporation of HANP on the PCL/CNF composite promotes a pore size reduction when compared with PCL/CNF membranes (Figure 2(c)). This reduction was possibly due to HANP filling the observed empty spaces and/or promoting a higher cohesion of PCL and CNF in the solution used for material preparation.

Table 1: Mean ± sd values of the scaffolds porosity.

	PCL	PCL/CNF	PCL/CNF/HANP	p
Porosity (%)	49.0 ± 1.4	49.5 ± 2.1	50.5 ± 2.1	0.749

The scaffolds were successfully produced presenting good geometric accuracy, fully interconnected channel networks, and highly controllable porosity. To verify the interconnectivity of the scaffolds and to calculate their porosity the micro-CT technique was used, as it enables the nondestructive visualization of the internal 3D structure of an object. All the obtained scans were similar, indicating that the proposed approach was precise, once the 3D structures exhibit good and accurate architecture and demonstrate the existence of connectivity between the pores (Figure 3). A high degree of interconnectivity is crucial to achieve a good viability of the inner parts of the scaffold, thus promoting a proper vascularisation of the graft and an effective tissue ingrowth *in vivo* [27].

The calculated porosities are presented in Table 1, showing that all the scaffolds revealed a valid porosity [24]. In fact, optimal balance should be aimed, as increasing porosity reduces the mechanical strength of the scaffold. Porosity is defined as the percentage of void space in a solid, with a morphological property being independent of the material [27]. Although the scaffolds present different compositions, their porosity percentage values were similar ($p = 0.749$), corroborating the geometric accuracy of the structures and the reliability of the extrusion equipment used for their production.

3.2. Surface Wettability of the Scaffolds. The contact angle is a quantitative measure of the wetting of a solid by a liquid and is also dependent on the surface area, with higher surface energies being associated with lower contact angles [28]. The measured contact angles are presented in Figure 4 and it can be noticed that PCL surface had a higher ($p < 0.0001$) contact angle ($82.7 \pm 1.62^{\circ}$), corroborating a hydrophobic nature [29]. Furthermore, CNF are more hydrophilic than PCL; thus, as

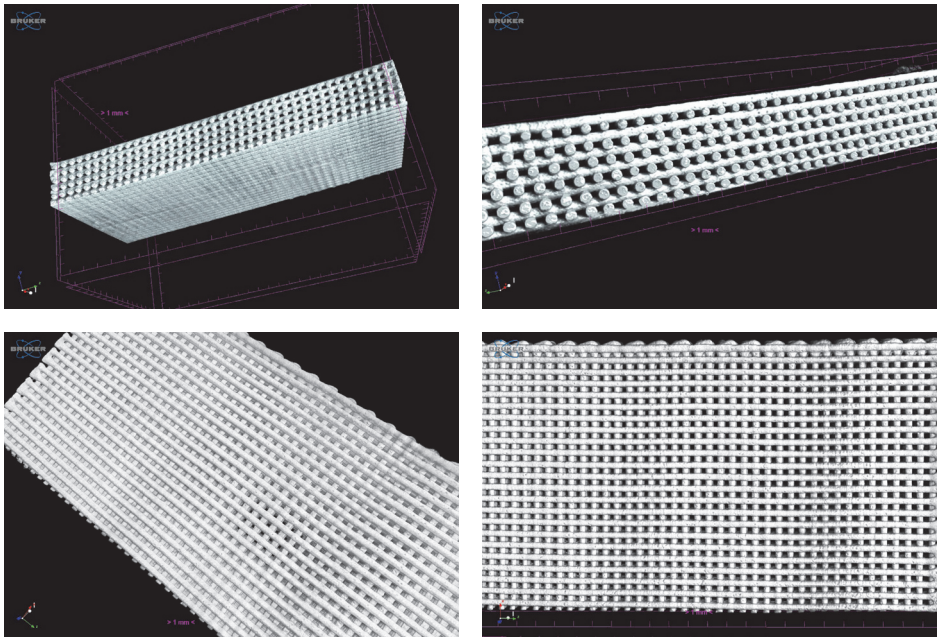

Figure 3: 3D micro-CT images of PCL/CNF scaffolds.

Table 2: Thermal properties of the produced scaffolds.

	PCL	PCL/CNF	PCL/CNF/HANP	p
T_c (°C)	36.6 ± 0.14	38.8 ± 0.30[a]	39.4 ± 0.07[a,b]	*<0.001*
T_m (°C)	58.0 ± 0.23	57.9 ± 0.21	58.2 ± 0.28	*0.158*
ΔH_m (j/g)	58.3 ± 2.01	54.6 ± 2.43	53.1 ± 0.79[a]	*0.019*
X_c	0.42 ± 0.01	0.40 ± 0.02	0.41 ± 0.01	*0.107*
T_d (°C)	386.9 ± 1.75	381.0 ± 3.31[a]	383.4 ± 0.40	*0.038*
Mass loss (%)	98.3 ± 0.25	96.9 ± 0.83[a]	93.6 ± 0.43[a,b]	*<0.001*

[a]Significant difference from PCL; [b]significant difference from PCL/CNF.

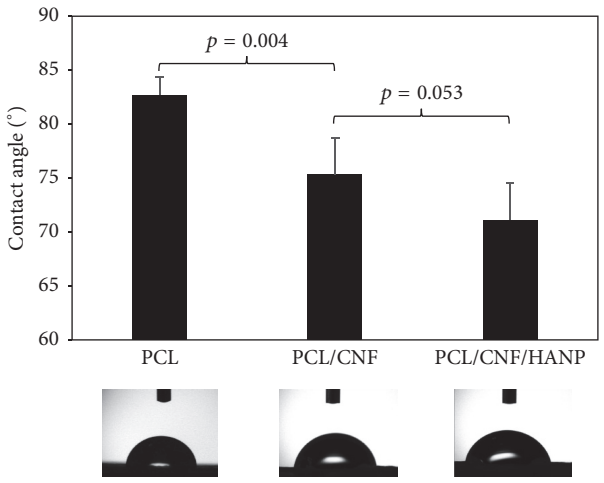

Figure 4: The static water contact angle of the produced nanocomposites.

expected, the addition of CNF increased the surface wettability of the composite scaffolds and, consequently, the contact angle significantly decreased ($p = 0.004$) to 75.3 ± 3.39° [2]. Lastly, the hydrophobicity of the scaffolds was slightly reduced by the incorporation of HANP (71.1±3.41°), without significant differences to the PCL/CNF composites ($p = 0.053$). These results clearly suggest that the addition of CNF on scaffolds may play a significant role in increasing its surface energies, which is beneficial for cell adhesion.

3.3. Thermal Analysis. The thermal behaviour of the nanocomposites was studied by DSC and TGA (Figures 5 and 6) and the thermal parameters, including the melting temperature (T_m), enthalpy of fusion (ΔH_m), crystallization temperature (T_c), degree of crystallinity (X_c), decomposition temperature (T_d), and mass loss, are summarized in Table 2 for all the samples. X_c was calculated using

$$X_c = \frac{\Delta H_m}{w \Delta H_m^o}, \quad (1)$$

where $\Delta H_m^o = 139.5$ J/g is the enthalpy of fusion for 100% crystalline PCL [22] and w is the weight fraction of polymeric matrix in the composite.

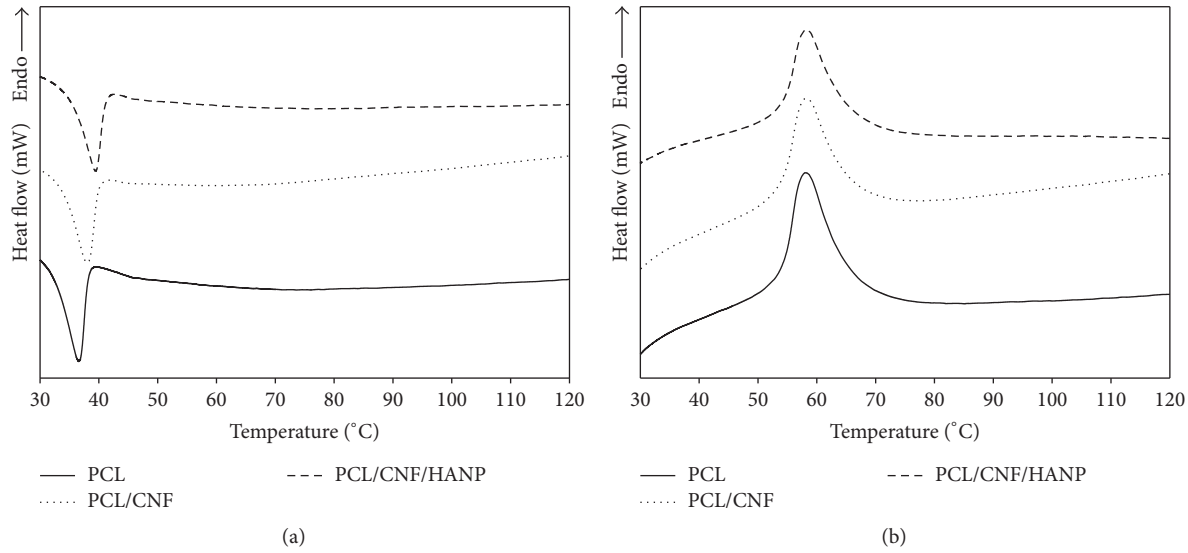

Figure 5: DSC curves of the processed samples: first cooling cycle (a) and second heating cycle (b).

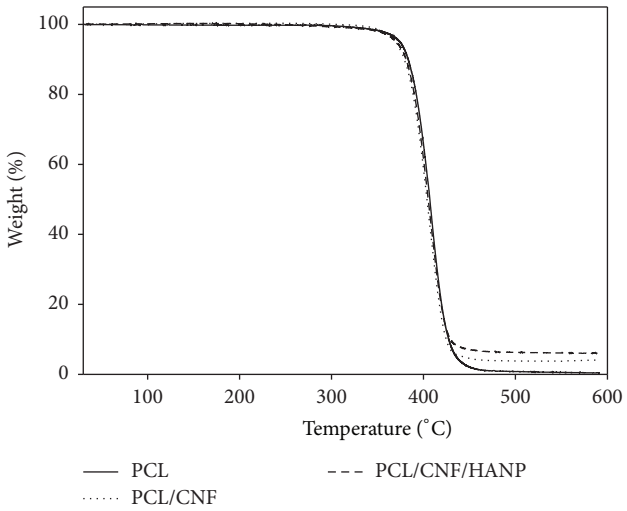

Figure 6: Thermogravimetric analysis of the produced nanocomposites scaffolds.

In Figure 5(a) is presented the crystallization behaviour of the samples. T_c of the PCL/CNF composite slightly shifted to a higher temperature comparatively to pure PCL, suggesting that the crystallization of the PCL in the composite was affected by the addition of CNF. As a consequence, the crystallization started earlier in a nonisothermal process. On the other hand, the incorporation of CNF had no significant effect on T_m of PCL (Figure 5(b)), as supported by previous research [1, 2, 21]. Regarding the nanocomposites crystallinity, the X_c value of the PCL in the composite (PCL/CNF) decreased from 0.42 to 0.40 with the CNF addition. Therefore, CNF can have two different effects on PCL crystallization: (i) CNF may act as nucleating agents and promote PCL crystallization; or (ii) the polymer chain could be restricted by the incorporation of CNF, allowing a decrease in ΔH_m [2, 18, 21].

With the addition of HANP, the thermal behaviour of the nanocomposite did not change significantly. Comparative to PCL alone, results revealed a similar T_m and an increase of T_c. At the same time, a lower heat of fusion (ΔH_m) and nearly similar X_c were also observed. These results suggest that HANP can also change the crystallinity of the polymer and may accelerate the nucleation of the PCL segments [30–33].

The thermal stability of the scaffolds was investigated by thermogravimetric analyses, with a single weight loss step being observed for all the constructs (Figure 6). The decomposition temperature for PCL was consistent with values previously reported in literature [18, 34, 35]; however, the addition of CNF induced a significant decrease (Table 2). Furthermore, regarding mass loss of the nanocomposites, the presence of final residues at 600°C proved that PCL is almost completely degraded, while PCL/CNF and PCL/CNF/HANP composites have residual weights similar to CNF and HANP concentrations. To the best of our knowledge, this is the first study producing PCL scaffolds reinforced with CNF, with controlled architecture. Further research should focus on the behaviour adaptations made by different concentrations of CNF.

3.4. Mechanical Analysis. The influence of CNF and HANP addition on the macromechanical performances of the scaffolds was investigated through compressive mechanical tests. The resultant compressive stress-strain curves, shown in Figure 7, demonstrate that the scaffolds presented the typical stress versus strain response of highly porous polymer scaffolds [12, 36]. The obtained curves are characterized by three different regions: a linear region at lower strain values, suggesting an initial rigid mechanical response, associated with elastic behaviour of the scaffolds; a region with lower stiffness;

Table 3: Compressive mechanical properties of the scaffolds.

	PCL	PCL/CNF	PCL/CNF/HANP	p
Compressive modulus E (MPa)	54.42 ± 2.47	64.58 ± 5.94[a]	70.88 ± 8.60[a]	*0.004*
Maximum stress σ_{max} (MPa)	10.96 ± 0.92	11.35 ± 1.21	12.12 ± 0.82	*0.215*

[a]Significant difference from PCL.

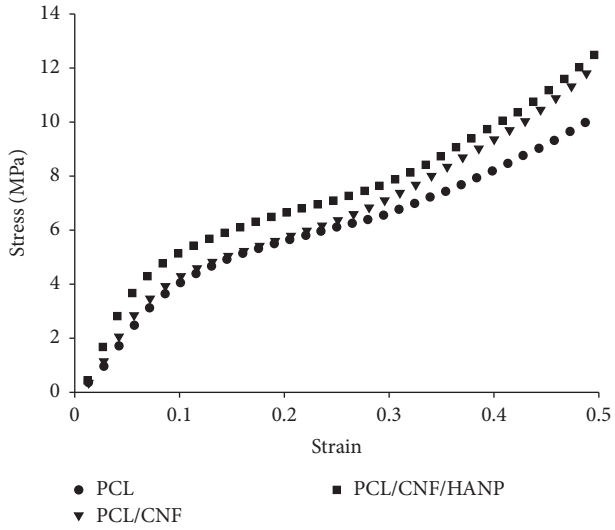

Figure 7: Stress-strain curve of the produced scaffolds.

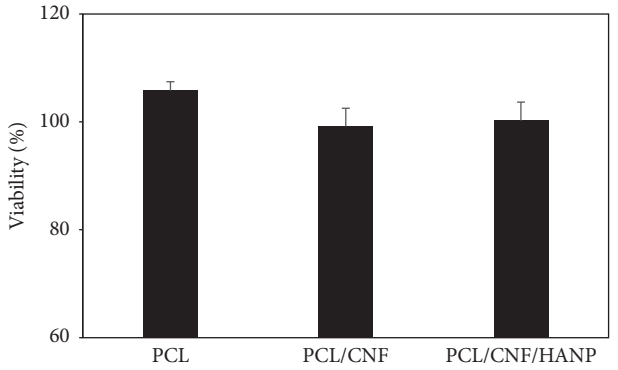

Figure 8: Cytotoxicity assessment: extract results.

and, lastly, a region where a rise of stress with increasing strain is noticed, which is related to densification of the porous scaffolds [12, 35, 37].

The compressive modulus (E) and maximum stress (σ_{max}) values obtained for all different scaffolds are presented in Table 3. The compressive strength of cortical and cancellous bone varies, depending on bone density, from 130 to 180 MPa and 5 to 50 MPa, respectively [38]. For the present study, the obtained values come near to the reported ones of the cancellous bone and significantly lower than the ones in cortical bone. Notwithstanding, the addition of CNF, even in a small amount, influenced the scaffolds mechanical response [21, 39], increasing the mechanical properties of the scaffolds (Table 3). Furthermore, the addition of the ceramic HANP improved the performance of the structures under compressive loads, which is in accordance with previous literature [34, 40, 41]. As previously mentioned, there is a lack of research on 3D structures of controlled architecture with CNF. However, this first study showed that the combination of CNF and HANP provided higher strength and rigidity to the constructed scaffolds.

3.5. Cytotoxicity Assessment. One of the main features for scaffolds production is its biocompatibility. Scaffolds should aim to (i) be the responsible structures to work as substrate to adhesion, proliferation, and cell differentiation; (ii) establish a proper biomechanical environment for an organized tissue regeneration; (iii) allow the diffusion of nutrients and oxygen, and (iv) allow the encapsulation and release of cells and growth factors. As a first study using 3D scaffolds with controlled architecture, with the incorporation of CNF, it was mandatory to analyse their cell viability. The results of the extract assay (Figure 8) showed a viability of approximately 100% for all the conditions tested when compared to the control (105.8 ± 1.9 for PCL; 99.1 ± 3.4 for PCL/CNF; 100.2 ± 3.3 for PCL/CNF/HANP), without significant differences ($p = 0.067$) among constructs. Afterwards, a latex material was used to produce a positive control, showing high cell mortality when those are exposed to toxic lixiviates driven from this material, confirming sensibility of this cytotoxicity test to toxic materials.

Additionally, the contact direct results (Figure 9) corroborate the results obtained in the extract test, showing that cells in contact with scaffolds maintain their morphology and cell death at the interface with the materials was not observed. According to the results obtained it is possible to affirm that these nanocomposites turned out to be biocompatible.

4. Conclusions

In this study poly(ε-caprolactone) membranes reinforced with cellulose nanofibers, with and without the addition of hydroxyapatite nanoparticles, were successfully produced by solvent casting. These membranes exhibit some differences in their morphology and the micrographs of the obtained composite reveal that the membranes had homogeneous distribution of CNF within the polymer matrix. The samples were subsequently processed by extrusion and the produced scaffolds present a fully interconnected network of internal channels and regular pore size, with similar porosity values and regular dimensions.

The incorporation of CNF and HANP into the PCL matrix had effects on surface wettability and thermal properties of the samples. The scaffolds energy surface increased with the addition of CNF and HANP. During cooling DSC

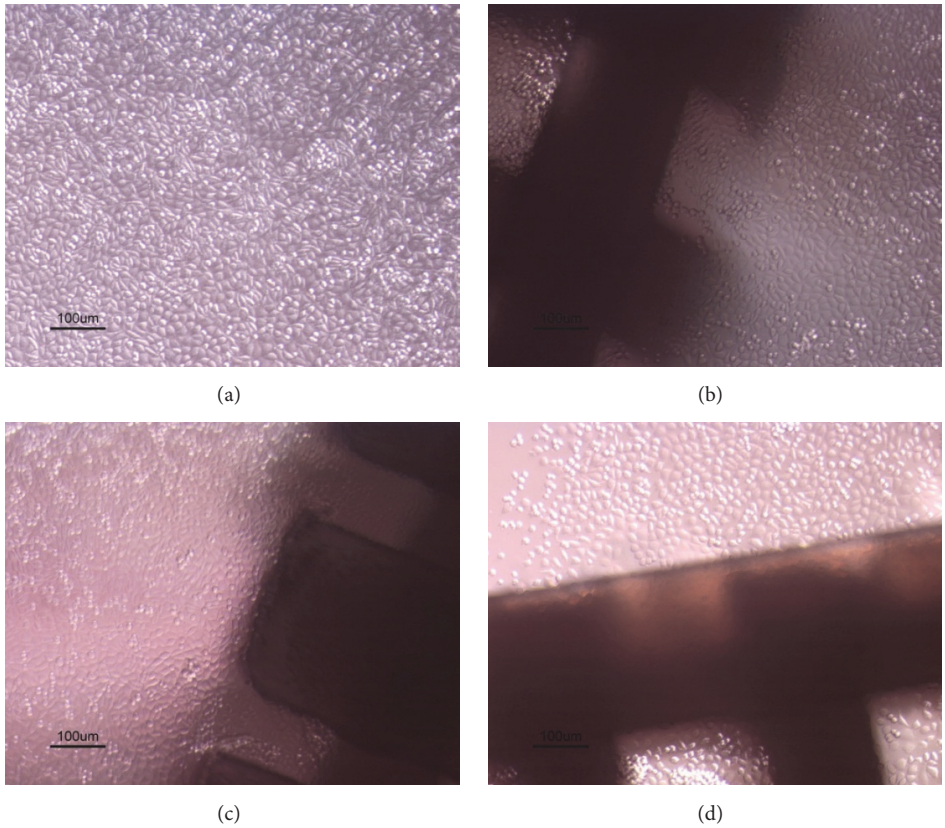

(a) (b)

(c) (d)

Figure 9: Cytotoxicity assessment: direct contact results of control (a); PCL scaffolds (b); PCL/CNF scaffolds (c); and PCL/CNF/HANP scaffolds (d).

scanning, the crystallization temperature of the nanocomposites started at higher temperatures than in the neat polymer. Mechanical compressive tests demonstrated the successful combination between PCL, CNF, and HANP. The mechanical properties of the PCL scaffolds were improved by incorporating CNF and further with HANP addition. The compressive and the elastic modulus of the composite scaffolds proved to be within the range of properties reported for human bone. The addition of CNF and HANP did not impair the biocompatibility of the obtained nanocomposites.

Competing Interests

The authors declare that there is no conflict of interests regarding the publication of this paper.

Acknowledgments

The research is funded by the Projects References (UID/Multi/04044/2013, BioMaTE: PTDC/EMS-SIS/7032/2014, UID/BIO/04565/2013), iBB H3D Grant (iBB/2015/18), and SFRH/BD/73970/2010 from the Portuguese Foundation for Science and Technology, as well as PORL (LISBOA-01-0145-FEDER-007317) and POR (no. Proj. N. 007317), funded by ERDF Portugal 2020.

References

[1] A.-L. Goffin, J.-M. Raquez, E. Duquesne et al., "Poly(ε-caprolactone) based nanocomposites reinforced by surface-grafted cellulose nanowhiskers via extrusion processing: morphology, rheology, and thermo-mechanical properties," *Polymer*, vol. 52, no. 7, pp. 1532–1538, 2011.

[2] L. Sheng, R. Jiang, Y. Zhu, and Y. Ji, "Electrospun cellulose nanocrystals/polycaprolactone nanocomposite fiber mats," *Journal of Macromolecular Science, Part B: Physics*, vol. 53, no. 5, pp. 820–828, 2014.

[3] S. Sen, J. D. Martin, and D. S. Argyropoulos, "Review of cellulose non-derivatizing solvent interactions with emphasis on activity in inorganic molten salt hydrates," *ACS Sustainable Chemistry & Engineering*, vol. 1, no. 8, pp. 858–870, 2013.

[4] S. Van de Vyver, J. Geboers, P. A. Jacobs, and B. F. Sels, "Recent advances in the catalytic conversion of cellulose," *ChemCatChem*, vol. 3, no. 1, pp. 82–94, 2011.

[5] K. Kolářová, V. Vosmanská, S. Rimpelová, and V. Švorčík, "Effect of plasma treatment on cellulose fiber," *Cellulose*, vol. 20, no. 2, pp. 953–961, 2013.

[6] K. Novotna, P. Havelka, T. Sopuch et al., "Cellulose-based materials as scaffolds for tissue engineering," *Cellulose*, vol. 20, no. 5, pp. 2263–2278, 2013.

[7] C. Olsson and G. Westman, "Direct dissolution of cellulose: background, means and applications," in *Cellulose—Fundamental Aspects*, vol. 6, InTech, Rijeka, Croatia, 2013.

[8] M. Poletto, V. A. Pistor, and J. Zattera, "Structural characteristics and thermal properties of native cellulose," in *Cellulose—Fundamental Aspects*, vol. 2, pp. 45–68, InTech, 2013.

[9] M. N. Fukuya, K. Senoo, M. Kotera, M. Yoshimoto, and O. Sakata, "Controlling of crystallite orientation for poly(ethylene oxide) thin films with cellulose single nano-fibers," *Polymer (United Kingdom)*, vol. 55, no. 16, pp. 4401–4404, 2014.

[10] C. Zhou, R. Chu, R. Wu, and Q. Wu, "Electrospun polyethylene oxide/cellulose nanocrystal composite nanofibrous mats with homogeneous and heterogeneous microstructures," *Biomacromolecules*, vol. 12, no. 7, pp. 2617–2625, 2011.

[11] C. Zhou and Q. Wu, "Recent development in applications of cellulose nanocrystals for advanced polymer-based nanocomposites by novel fabrication strategies," in *Nanocrystals—Synthesis, Characterization and Applications*, vol. 6, pp. 103–120, INTECH, Rijeka, Croatia, 2012.

[12] W.-Y. Choi, H.-E. Kim, and Y.-H. Koh, "Production, mechanical properties and in vitro biocompatibility of highly aligned porous poly(ε-caprolactone) (PCL)/hydroxyapatite (HA) scaffolds," *Journal of Porous Materials*, vol. 20, no. 4, pp. 701–708, 2013.

[13] P. Pooyan, R. Tannenbaum, and H. Garmestani, "Mechanical behavior of a cellulose-reinforced scaffold in vascular tissue engineering," *Journal of the Mechanical Behavior of Biomedical Materials*, vol. 7, pp. 50–59, 2012.

[14] J. R. Porter, T. T. Ruckh, and K. C. Popat, "Bone tissue engineering: a review in bone biomimetics and drug delivery strategies," *Biotechnology Progress*, vol. 25, no. 6, pp. 1539–1560, 2009.

[15] S. Bose, M. Roy, and A. Bandyopadhyay, "Recent advances in bone tissue engineering scaffolds," *Trends in Biotechnology*, vol. 30, no. 10, pp. 546–554, 2012.

[16] J. Rouwkema, N. C. Rivron, and C. A. van Blitterswijk, "Vascularization in tissue engineering," *Trends in Biotechnology*, vol. 26, no. 8, pp. 434–441, 2008.

[17] C. M. Murphy and F. J. O'Brien, "Understanding the effect of mean pore size on cell activity in collagen-glycosaminoglycan scaffolds," *Cell Adhesion and Migration*, vol. 4, no. 3, pp. 377–381, 2010.

[18] R. Xiong, N. Hameed, and Q. Guo, "Cellulose/polycaprolactone blends regenerated from ionic liquid 1-butyl-3-methylimidazolium chloride," *Carbohydrate Polymers*, vol. 90, no. 1, pp. 575–582, 2012.

[19] M. A. Woodruff and D. W. Hutmacher, "The return of a forgotten polymer—polycaprolactone in the 21st century," *Progress in Polymer Science*, vol. 35, no. 10, pp. 1217–1256, 2010.

[20] L. S. Nair and C. T. Laurencin, "Biodegradable polymers as biomaterials," *Progress in Polymer Science*, vol. 32, no. 8-9, pp. 762–798, 2007.

[21] S.-H. Lee, Y. Teramoto, and T. Endo, "Cellulose nanofiber-reinforced polycaprolactone/polypropylene hybrid nanocomposite," *Composites Part A: Applied Science and Manufacturing*, vol. 42, no. 2, pp. 151–156, 2011.

[22] H.-Y. Mi, X. Jing, J. Peng, M. R. Salick, X.-F. Peng, and L.-S. Turng, "Poly(ε-caprolactone) (PCL)/cellulose nano-crystal (CNC) nanocomposites and foams," *Cellulose*, vol. 21, no. 4, pp. 2727–2741, 2014.

[23] C. Mota, D. Puppi, D. Dinucci, C. Errico, P. Bártolo, and F. Chiellini, "Dual-scale polymeric constructs as scaffolds for tissue engineering," *Materials*, vol. 4, no. 3, pp. 527–542, 2010.

[24] D. Tang, R. S. Tare, L.-Y. Yang, D. F. Williams, K.-L. Ou, and R. O. C. Oreffo, "Biofabrication of bone tissue: approaches, challenges and translation for bone regeneration," *Biomaterials*, vol. 83, pp. 363–382, 2016.

[25] R. F. Canadas, J. M. B. T. Cavalheiro, J. D. T. Guerreiro et al., "Polyhydroxyalkanoates: waste glycerol upgrade into electrospun fibrous scaffolds for stem cells culture," *International Journal of Biological Macromolecules*, vol. 71, pp. 131–140, 2014.

[26] H. Kamal, F. Abd-Elrahim, and S. Lotfy, "Characterization and some properties of cellulose acetate-co-polyethylene oxide blends prepared by the use of gamma irradiation," *Journal of Radiation Research and Applied Sciences*, vol. 7, no. 2, pp. 146–153, 2014.

[27] C. Renghini, V. Komlev, F. Fiori, E. Verné, F. Baino, and C. Vitale-Brovarone, "Micro-CT studies on 3-D bioactive glass-ceramic scaffolds for bone regeneration," *Acta Biomaterialia*, vol. 5, no. 4, pp. 1328–1337, 2009.

[28] V. Leszczak, D. A. Baskett, and K. C. Popat, "Smooth muscle cell functionality on collagen immobilized polycaprolactone nanowire surfaces," *Journal of Functional Biomaterials*, vol. 5, no. 2, pp. 58–77, 2014.

[29] T.-Y. Bak, M.-S. Kook, S.-C. Jung, and B.-H. Kim, "Biological effect of gas plasma treatment on CO_2 gas foaming/salt leaching fabricated porous polycaprolactone scaffolds in bone tissue engineering," *Journal of Nanomaterials*, vol. 2014, Article ID 657542, 6 pages, 2014.

[30] J. Hao, M. Yuan, and X. Deng, "Biodegradable and biocompatible nanocomposites of poly(ε-caprolactone) with hydroxyapatite nanocrystals: thermal and mechanical properties," *Journal of Applied Polymer Science*, vol. 86, no. 3, pp. 676–683, 2002.

[31] C. Guang-Mei, Z. Tie-Mei, C. Lei, and H. Yi-Ping, "Crystallization properties of polycaprolactone induced by different hydroxyapatite nano-particles," *Asian Journal of Chemistry*, vol. 22, no. 8, pp. 5902–5912, 2010.

[32] B. Chen and K. Sun, "Poly (ε-caprolactone)/hydroxyapatite composites: effects of particle size, molecular weight distribution and irradiation on interfacial interaction and properties," *Polymer Testing*, vol. 24, no. 1, pp. 64–70, 2005.

[33] X. Xiao, R. Liu, Q. Huang, and X. Ding, "Preparation and characterization of hydroxyapatite/polycaprolactone-chitosan composites," *Journal of Materials Science: Materials in Medicine*, vol. 20, no. 12, pp. 2375–2383, 2009.

[34] V. Guarino, F. Causa, P. A. Netti et al., "The role of hydroxyapatite as solid signal on performance of PCL porous scaffolds for bone tissue regeneration," *Journal of Biomedical Materials Research Part B: Applied Biomaterials*, vol. 86, no. 2, pp. 548–557, 2008.

[35] A. Salerno, S. Zeppetelli, M. Oliviero et al., "Microstructure, degradation and in vitro MG63 cells interactions of a new poly (ε-caprolactone), zein, and hydroxyapatite composite for bone tissue engineering," *Journal of Bioactive and Compatible Polymers*, vol. 27, no. 3, pp. 210–226, 2012.

[36] D. Milovac, G. Gallego Ferrer, M. Ivankovic, and H. Ivankovic, "PCL-coated hydroxyapatite scaffold derived from cuttlefish bone: morphology, mechanical properties and bioactivity," *Materials Science and Engineering C*, vol. 34, no. 1, pp. 437–445, 2014.

[37] M. Domingos, F. Intranuovo, A. Gloria et al., "Improved osteoblast cell affinity on plasma-modified 3-D extruded PCL scaffolds," *Acta Biomaterialia*, vol. 9, no. 4, pp. 5997–6005, 2013.

[38] S. B. Nicoll, "Materials for bone graft substitutes and osseous tissue regeneration," in *Biomaterials for Tissue Engineering Applications*, pp. 343–362, Springer, Vienna, Austria, 2011.

[39] B. Nasri-Nasrabadi, T. Behzad, and R. Bagheri, "Preparation and characterization of cellulose nanofiber reinforced thermoplastic starch composites," *Fibers and Polymers*, vol. 15, no. 2, pp. 347–354, 2014.

[40] N. Thadavirul, P. Pavasant, and P. Supaphol, "Improvement of dual-leached polycaprolactone porous scaffolds by incorporating with hydroxyapatite for bone tissue regeneration," *Journal of Biomaterials Science, Polymer Edition*, vol. 25, no. 17, pp. 1986–2008, 2014.

[41] G. Wei and P. X. Ma, "Structure and properties of nano-hydroxyapatite/polymer composite scaffolds for bone tissue engineering," *Biomaterials*, vol. 25, no. 19, pp. 4749–4757, 2004.

Hindawi Publishing Corporation
BioMed Research International
Volume 2016, Article ID 7461041, 13 pages
http://dx.doi.org/10.1155/2016/7461041

Research Article

Non-Mulberry and Mulberry Silk Protein Sericins as Potential Media Supplement for Animal Cell Culture

Neety Sahu,[1] Shilpa Pal,[1] Sunaina Sapru,[1] Joydip Kundu,[1] Sarmistha Talukdar,[1] N. Ibotambi Singh,[2] Juming Yao,[3] and Subhas C. Kundu[1]

[1]*Department of Biotechnology, Indian Institute of Technology Kharagpur, West Bengal 721302, India*
[2]*Central Muga Eri Research and Training Institute, Lahdoigarh, Jorhat, Assam 785700, India*
[3]*The Key Laboratory of Advanced Textile Materials and Manufacturing Technology of Ministry of Education, College of Materials and Textiles, Zhejiang Sci-Tech University, Hangzhou 310018, China*

Correspondence should be addressed to Subhas C. Kundu; kundu@hijli.iitkgp.ernet.in

Received 24 February 2016; Revised 25 May 2016; Accepted 6 June 2016

Academic Editor: Max Costa

Silk protein sericins, in the recent years, find application in cosmetics and pharmaceuticals and as biomaterials. We investigate the potential of sericin, extracted from both mulberry *Bombyx mori* and different non-mulberry sources, namely, tropical tasar, *Antheraea mylitta*; muga, *Antheraea assama*; and eri, *Samia ricini,* as growth supplement in serum-free culture medium. Sericin supplemented media containing different concentrations of sericins from the different species are examined for attachment, growth, proliferation, and morphology of fibrosarcoma cells. The optimum sericin supplementation seems to vary with the source of sericins. The results indicate that all the sericins promote the growth of L929 cells in serum-free culture media; however, *S. ricini* sericin seems to promote better growth of cells amongst other non-mulberry sericins.

1. Introduction

Silk protein sericin (glue protein) is a water soluble glycoprotein that shields the fibroin fibres present in the cocoon. This cocoon structure protects the pupae from the different environmental conditions, natural calamities, and predators (particularly for non-mulberry silkworms) stress. The glue-like strong adhesive nature of this protein is attributed to the hydrogen bonding capability of the enormous number of hydroxyl amino acids present in it. The removal of sericin from the silk fibres is carried out by the different processes called degumming. The sericins are mostly discarded as waste products during silk fibre processing in the textile industries, which now find place in economics. If the sericins are recovered and recycled properly, then this may play significant role in social benefits. Sericin recently finds widespread applications in cosmetic industry, as antioxidant and antiapoptotic compound, as support for enzyme immobilization, as supplement in animal cell culture media, as dietary supplement, and also as biomaterial for cell culture, drug, and gene delivery [1–8]. Addition of 0.5% sericin to cell culture medium improved the resistance to oxidative stress and quality of bovine embryos *in vitro* [9].

Sericin is isolated from the silk cocoons by the degumming process, which takes the advantage of the solubility of sericin in boiling aqueous solutions containing reagents like soap, alkali, synthetic detergents, urea, organic acids, and proteolytic enzymes. The most common methods used for the removal of sericin from cocoons are either by heating or by alkali treatment [10]. Mosher and Rayon in 1934 isolated sericin by boiling cocoons in hot water and separated them as water soluble and water insoluble fractions [11]. Usually in the silk industry, degumming of cocoons is carried out by alkaline condition utilizing either Na_2CO_3 or NaOH followed by boiling for 30 mins. Three types of polypeptides of mulberry silk sericin are obtained using isolation buffer, which contains 8 M urea, 1% SDS, and 2% β-mercaptoethanol for 30 mins at room temperature, followed by heating at 80°C [12]. For isolating sericin in the native condition, the cut cocoons and peduncle pieces are soaked in 1% NaCl solution at room

temperature overnight with shaking at 100 rpm followed by precipitation and resolubilization [13–15]. Sericin displays the ability to self-assemble *via* multiple aggregation mechanisms [16].

Sericin obtained from mulberry *Bombyx mori* contains a group of proteins ranging from 20 to 400 kDa and has an unusually high serine content (40%) along with significant glycine content (16%) [6]. Secondary structure of sericin from the cocoons of *B. mori* reveals the presence of β-sheet structure along with random coils [17]. The sericin of Indian non-mulberry tropical silkworm *Antheraea mylitta* has three prominent polypeptides of 70 kDa, 200 kDa, and a higher fraction of more than 200 kDa [14].

Low molecular weight sericin is reported to have myriad applications in biomedical, cosmetic, and pharmaceutical industries, as bioconjugates in drug delivery and graft copolymers. Sericin from *B. mori* mutant silkworm, sericin hope, a mutant of *Bombyx mori* and deficient of fibroin, is shown to be a new natural silk biomaterial for dermal equivalent for grafting. The fibroblast-keratinocyte coculture on 3D sericin hope matrix model is reported to be an alternative to *in vitro* skin replacement grafts [7]. *A. mylitta* sericin coated titanium surfaces are also reported to have potential application in titanium based medical implants [18]. Mulberry sericin is used as blended biomaterial scaffolds to promote healing in injured tissues [19, 20]. Non-mulberry sericin is also used to promote dermal reconstruction [21]. Therefore, the idea that the sericin may have a role in promoting growth and proliferation of cells apart from its uses as a biomaterial holds promise. Sericin from mulberry *B. mori* is shown to accelerate cell proliferation in serum-free mammalian cell culture [22]. Apart from its applications in tissue engineering and healthcare industries, sericin is also reported to act as an alternative to serum in the culture of islet cells [23, 24]. Sericin is shown to prevent cell death and promote cellular growth in Sf9 insect cells after acute serum deprivation [25]. A novel serum-free freezing medium consisting of PBS, 1% (v/w) sericin, 0.5% (v/w) maltose, 0.3% (v/w) proline, 0.3% (v/w) glutamine, and 10% DMSO is developed and is found to be better than the conventional serum containing freezing media for the cryopreservation of P3U1 myeloma cell line, Chinese-hamster ovary cells, human dermal fibroblasts, human epidermal keratinocytes, the rat pheochromocytoma cell line PC12, and insect cell line Sf9 [26]. Bovine embryos are preserved well in sericin supplemented serum-free freezing media [27]. Serum-free medium containing sericin is shown to be suitable not only for cell culture but also for cryopreservation rat islets [28]. It has been shown that sericin may substitute for FBS in the freezing medium for primary hMSCs but cannot substitute for DMSO [29]. Though serum is widely used as a growth supplement in cell culture media, some potential disadvantages of serum limit its use in pharmaceuticals industries. These are (1) higher level of contaminants, the protein concentration in 10% serum being 6,200–10,1000 mg/L; (2) presence of various other components besides growth factors; (3) potential source of infectious agents, viral, bacterial, and fungal contamination of serum; and (4) high cost and availability [30]. The role of sericin in the growth of animal cells holds an advantage over serum. This holds true in cases where high level of purity of recovered cellular products is desired [22]. Moreover, silk sericin is an inexpensive alternative to serum in this regard. The sericins are low-cost abundant waste/by-product of silk textile industries and until now are underutilised. The application of sericin protein as biomaterial is documented in the literature [1, 6]. The useful properties of sericin like being antioxidant and antiapoptotic, hydrophilicity, and potential to promote cell attachment and growth provide the added characteristics for the use of sericin in the fabrication of various matrices (films, mats, 3D scaffolds, hydrogels, and nanoparticles) in diversified fields of tissue engineering and regenerative medicine (6). High solubility and weak structural composition make silk sericin very fragile and unsuitable for fabricating biomedical materials [31]. However, silk sericins are used to fabricate tenable materials for use in tissue engineering by some biochemical modifications [4, 31]. Our and other similar investigations [23, 24] indicate the ability of silk sericin to promote cell proliferation in serum-free culture media. This makes sericin an attractive component in the fabrication of biodegradable materials like hydrogels, films, and scaffolds, especially for the culture of cells that are susceptible to serum.

In this study, we investigate the biochemical, biophysical characteristics and the potential of the silk protein sericins as supplement to animal cell culture medium. The sericins are isolated from mulberry (*Bombyx mori*) and also different non-mulberry species (tropical tasar, *Antheraea mylitta;* muga, *Antheraea assama*; and eri, *Samia ricini*). The results indicate that the sericins may be used as potential supplements in place of serum for animal cell culture. This replacement with sericin may help future cell based tissue engineering and regenerative medicine practices.

2. Experimental

2.1. Materials. Live silk cocoons of mulberry silkworm, *Bombyx mori* (local farm), and non-mulberry Indian tropical tasar, *Antheraea mylitta* (our IIT farm), obtained from West Midnapore District, West Bengal State; non-mulberry muga silkworm *Antheraea assama*/*Antheraea assamensis* obtained from Cooch Behar District, West Bengal State; eri *Samia ricini*/*Philosamia ricini* silk cocoons obtained from Jalpaiguri Silk Farm, West Bengal State, India; and sericin hope (mutant of *B. mori*) obtained from China were collected for this study. The fine chemicals (St. Luisa, Sigma, USA, and Merck, India); protein molecular weight marker (Amersham, UK, Fermentas); Alamar Blue (Invitrogen, USA); cell culture grade chemicals, namely, Dulbecco's modified eagle medium (DMEM), fetal calf serum, trypsin-EDTA, and penicillin-streptomycin antibiotics (Gibco BRL, USA); and rhodamine-phalloidin and Hoechst, 33342 (Molecular Probes, USA), were purchased for this experimentation. Murine fibrosarcoma cell line, L929 (National Centre for Cell Science (NCCS), Pune, India), was maintained in DMEM supplemented with 10% fetal bovine serum (FBS) and 50 μg/mL penicillin-streptomycin in 5% CO_2 incubator till they attained confluency.

2.2. Isolation of Silk Sericins from the Silk Cocoons. The sericins were isolated individually from mulberry (*B. mori*) and non-mulberry (*A. mylitta, S. ricini, A. assama,* and sericin hope (containing about 98% sericin)) silk cocoons following the protocols modified from Zhang et al. [32] and Dash et al. [13]. In brief, the cocoons were cut into small pieces, degummed by boiling the cocoons in deionised water with a mass to liquid ratio (MLR) (w/v) of 1 : 20 under pressure using an autoclave at 110–120°C for 60 mins in cases of non-mulberry species (*A. mylitta, S. ricini,* and *A. assama*) and 30 mins for mulberry species (*B. mori* and sericin hope). Another extraction method as described by Takasu et al. [12] was followed for analysing the different polypeptide fractions of sericins present in the different species. The cocoon pieces were weighed and soaked in 8 M urea containing 2% β-mercaptoethanol and 1% SDS, followed by incubation at 80°C for 5 minutes. The sericin solutions were centrifuged at 800 rpm for 10 minutes and supernatant so obtained was dialyzed using cellulose tubes (3.5 kDa) against deionised water for 8–12 hrs with regular change of water intermittently. They were filtered using 0.45 μm pore size filters. The sericin powders were obtained individually by lyophilizing the sericin solutions and stored at 4°C until use.

2.3. Scanning Electron Microscopy (SEM). SEM images of the degummed cocoons were obtained after gold sputtering using a JEOL JSM-5800 scanning electron microscope with incident electron beam energy of 1 keV and a working distance of 6 mm.

2.4. Characterization of Sericins

2.4.1. Estimation of Molecular Weight through SDS-PAGE. The molecular weight distribution of the sericin obtained using urea method [12] and the autoclave method was verified by SDS-PAGE. About 0.1–0.2 mg of the sericin samples that were isolated from the cocoons of *B. mori, A. mylitta, S. ricini, and A. assama* using hot boil degumming were incubated with Laemmli sample loading buffer. The proteins were loaded onto a 5% stacking gel cast on the top of an 8% SDS polyacrylamide gel (Merck) and electrophoresed. The gel was run at a constant voltage of 80 V for approximately 3 hrs so that the protein is resolved efficiently. After electrophoresis, the gel was stained with Coomassie Brilliant Blue R-250 (Sigma, USA) and destained in a methanol/water 1 : 1 solution that contained 20% acetic acid. To visualize the bands not observed by Coomassie stain, silver staining [33] was performed. Briefly, the gels were immersed in a fixative solution (40% methanol, 10% acetic acid, and 50% deionised water) for 1 hr. They were then washed with 30% ethanol thrice for 20 minutes each after which the gels were sensitized in the reductant (0.02% sodium thiosulphate) for 2 mins and washed thoroughly with deionised water. The gels were then stained with 0.1% silver nitrate (Merck) solution and 0.02% formaldehyde (Merck) for an hour, washed, and developed using 3% sodium carbonate (Sigma), 0.05% formaldehyde (Sigma, USA), and 0.5% sodium thiosulphate (Sigma, USA) until the bands appeared. When the desired intensity was achieved, the reaction was terminated using 5% acetic acid (Merck) solution.

2.4.2. Circular Dichroism (CD) Spectroscopy. The circular dichroism (CD) studies of cocoon sericins from different species were performed on a JASCO J-810 spectropolarimeter using a 0.1 cm path length quartz cell at 20°C. The spectra were corrected for the baseline. The UV spectrum of the individual sericins was collected at a protein concentration of 0.1% (w/v) in water. The data points were recorded with a step resolution of 0.5 nm, time constant of 1 s, sensitivity of 10 m deg, scan speed of 50 nm/min, and spectral bandwidth of 2 nm. In order to reduce error and noise, each spectrum was an average of three scans over 400–190 nm. The background spectra were acquired from the same solvent. The spectra were corrected for the baseline and normalized to protein concentration in order to obtain the mean residue molar (deg cm^2/d mol). The percentages of α-helix, β-sheet, turns, and random coil were determined using the standard protein secondary structure estimation program provided inbuilt with JASCO J-810 spectropolarimeter [34].

2.4.3. Fourier Transform Infrared (FTIR) Spectroscopy. FTIR analysis of the sericin protein (powders) was carried out using an FTIR spectrometer (Thermo Nicolet Corporation NEXUS-870) with a resolution of 2 cm^{-1} with a scan range of 500 cm^{-1} to 2000 cm^{-1}.

2.4.4. Thermogravimetric Analysis. Thermogravimetric analysis (TGA) was run under the flow of nitrogen gas from 30 to 650°C at a scanning speed of 20°C/min using Pyris Diamond.

2.5. Cell Culture. Approximately 10^3 mouse fibrosarcoma cells (L929) per well were seeded in 24-well tissue culture plates with DMEM (Dulbecco's Modified Eagle's Medium), supplemented with 10% fetal bovine serum, and allowed to get attached to the plate surface for 24 hrs. The cells were then starved for 24 hrs by supplying serum-free (incomplete) DMEM. Sericin supplemented medium was prepared initially by adding different concentrations of sericin solution to incomplete DMEM. Finally, media containing 2 different concentrations (0.05% and 0.1%) of sericin of each of the 4 species were prepared and used as supplement in cell culture medium. Each of these sericin supplemented media was filtered under sterile conditions using a 0.22 μm filter. The previously starved cells were treated with the different concentrations of sericin supplemented media over a period of 3 days. L929 cells growing in serum supplemented DMEM and in serum-free DMEM were used as controls.

2.5.1. Cell Viability. The cell viability was estimated by the reduction of Alamar Blue as substrate. The cells grown in sericin supplemented media were incubated with Alamar Blue at 37°C for 3 hrs. At the end of the assay, the supernatant was taken and the absorbance was measured at 570 nm and 600 nm. The percentage of Alamar Blue reduced was plotted as a function of cellular metabolic activity and viability.

Alamar Blue assay was performed after 24 hrs and 72 hrs of sericin treatment of the cells.

2.5.2. Cell Morphology. Morphology of the cells was studied by visualizing the cells under inverted phase contrast microscope and fluorescence microscope (Leica, Germany).

2.5.3. Cell Attachment. L929 cell attachment in sericin supplemented DMEM was studied by measuring the number of cells attached to the surface of tissue culture well as a function of time. Confluent L929 cells grown in serum supplemented DMEM were trypsinized and 10^5 cells per well were seeded onto the wells containing 0.05% sericin supplemented DMEM of *B. mori, A. mylitta*, *A. assama*, and *S. ricini*. The cell attachment study was performed after 2, 4, 6, 8, 10, and 12 hrs of seeding. Media supernatant was removed at every time point and the number of unattached cells was enumerated. The number of cells attached as obtained by deducting the number of unattached cells from total number of cells seeded was plotted against time. (We have not carried out any further work on sericin hope being a mutant cocoon, which contains mostly sericins. This unique bioengineered silk sericin hope needs to be evaluated more on different aspects).

2.6. Statistical Analysis. Experiments were run in triplicate per sample and each experiment was conducted at least thrice. All data were expressed as mean ± standard deviation (SD) for $n = 3$. A single-factor analysis of variance technique was used to determine the statistical significance of the results.

3. Results

3.1. Isolation of Sericin from the Cocoons. Sericins are isolated from the cocoons of *A. mylitta*, *A. assama*, *S. ricini*, and *B. mori* (Figure 1). They are processed, that is, dialyzed to remove salts, fats, and others, and finally concentrated. Different extraction methods produce variable yields of extracted sericin depending on the physical properties of cocoons. Silk sericin can be extracted by degumming silk cocoons using various chemical agents like urea, sodium chloride, sodium carbonate, and sodium hydroxide. Highest sericin yield is reported to be achieved via sodium carbonate treatment while urea method produces lowest amount of sericin [10]. Additionally, different species of silk are also known to have variable yields of sericin for any extraction method [10]. Non-chemical (autoclave) method shows variable degumming ratio in mulberry (18–21%) and non-mulberry species (6–11%). At times, the variation in extracted amount of sericin from non-mulberry is very low and unpredictable even in the same species. What we understand is that several factors are involved in the variation of sericin yields like age/freshness, eco-races/strain, season, place of collection, type of crops (multivoltine/bivoltine), storage conditions, contamination (being wild), rearing procedure, handling of cocoons, and others [10]. The variations in the sericin content in mulberry and non-mulberry silk cocoons result in the differences of sericin yield in these species.

3.2. Scanning Electron Microscopy (SEM). SEM is carried out to observe the effect of degumming on the microstructures of the fibres of the cocoons. Figure 2 shows the SEM micrographs of cocoon pieces before and after degumming by 8 M urea and boiling under pressure (autoclave method). The micrographs of nondegummed silk cocoons have white striations, indicating sericin, between the fibroin fibres, whereas the degummed fibres have minimal sericin between the fibres. The fibres are distinctly visible and well separated from one another due to the removal of the glue protein sericin, which holds them together.

3.3. Characterization of Silk Sericins

3.3.1. Estimation of Molecular Weight through SDS-PAGE. The sericins of different silkworm species extracted by autoclave method appear as smears in the 8% gel after electrophoresis (Figure 3). Heating of the cocoons under high pressure and temperature degrades the protein. On the other hand, sericin isolated by urea method separates the protein into various fractions, which appear as bands in the gel after the run (Figure 3). Marked differences are seen in sericin extracted from mulberry species from that in non-mulberry species. The sericin fractions obtained in case of *B. mori* and *A. mylitta* are comparable to results obtained previously [14]. *B. mori* sericin shows bands of 250 kDa and 130 kDa, some in the range of 120–130 kDa, and a lower fraction of 17 kDa [35]. *A. mylitta* sericin comprised mainly three fractions of approximately 250 kDa, 200 kDa, and 70 kDa. *S. ricini* has two bands, one greater than 300 kDa and one in the range of 200–250 kDa (Figure 3). For *A. assama* one fraction greater than 250 kDa and another approximately 90 kDa are observed. As inferred by SDS-PAGE, sericin represents a family of proteins with a diverse distribution of molecular weights. Distinct fractions of sericin polypeptides are isolated in the urea method. It is shown that L929 cells grown in medium containing sericin extracted by urea method exhibited cytotoxicity [36]; therefore, this method is not used for preparing sericin supplemented medium in our study. However, to illustrate the different bands or fractions of the sericins from *A. mylitta*, *A. assama*, *S. ricini*, and *B. mori* in SDS-PAGE, sericins extracted by urea method are employed. The other methods used for extraction of sericins provide smears in gels [36]. As sericin hope consists of mostly sericin protein, it is therefore employed for comparison with sericin of *B. mori*, *A. mylitta*, and *S. ricini* by SDS-PAGE. No further work, apart from SDS-PAGE, is carried out with sericin hope for comparison. The autoclave method gives a smear in SDS-PAGE indicating that the protein polypeptides are broken into smaller fractions. This autoclave method is chosen for further investigations as it is free of any toxic ions.

3.3.2. Circular Dichroism (CD) Spectroscopy. The CD spectrum of the cocoon sericin solutions of all species shows one sharp negative band at around 200 nm assigned to random

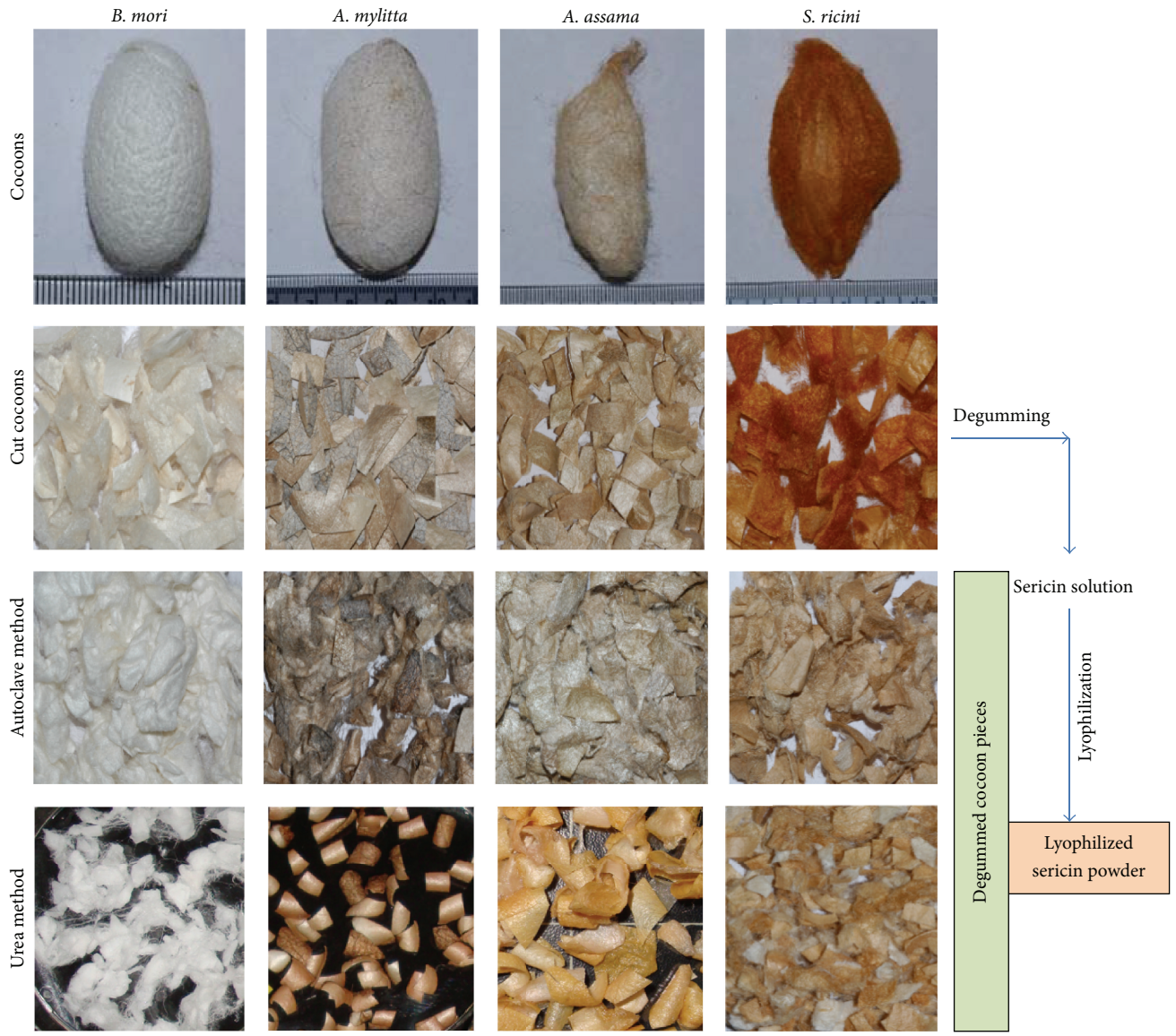

Figure 1: Degumming of silk cocoons of different species of silkworms using different methods of isolation of sericins.

coil conformation (Figure 4(a)). A negative band at 218 nm reveals the presence of β-sheet. The alpha helix content is low because of the absence of double minimum at 222 nm and 208–210 nm and a positive band at 190 nm. The secondary structure data shows that the percentage of random coil is highest in *S. ricini*. Percentage of beta is highest in the wild species *A. assama*, followed by *A. mylitta* and *B. mori,* and the least in *S. ricini.* Small percentages of turns are seen in *S. ricini* and *B. mori*. They are absent in the other two species. Helix is present in very small amount in *A. mylitta* and negligible in *A. assama.* In spite of the presence of higher amount of glutamic acid and lower percentage of tyrosine, CD spectroscopy analysis of the secondary structure of the *A. mylitta* sericin reveals its β-sheet structure in native form. The β-sheet structure may be due to the polar zipper interaction through hydrogen bonding among abundant polar amino acids in the serine-rich repetitive motif [37]. It was reported previously that the β-sheet conformational structure of sericin in aqueous solution is stabilized by the hydration and electrostatic interactions [38].

3.3.3. Fourier Transform Infrared (FTIR) Spectroscopy. All the species have similar peaks at 1656.58 cm^{-1} (Amide I), 1540–1543 cm^{-1} (Amide II), and 1242–1246 (Amide III) (Figure 4(b)). The peak at 1656.58 cm^{-1} suggests the presence of α-helix. The β-sheet aggregates help in stabilizing sericin in water, hence contributing to the strength of the cocoon and suitability as a biomaterial. The CD spectrum of all the species shows the presence of random coil conformation and β-sheets with a low content of alpha helix. In aqueous form, the transition from random coil to β-sheet is quicker whereas anhydrous form has fewer tendencies to change its conformation. Hence, in the FTIR, we find the protein of the

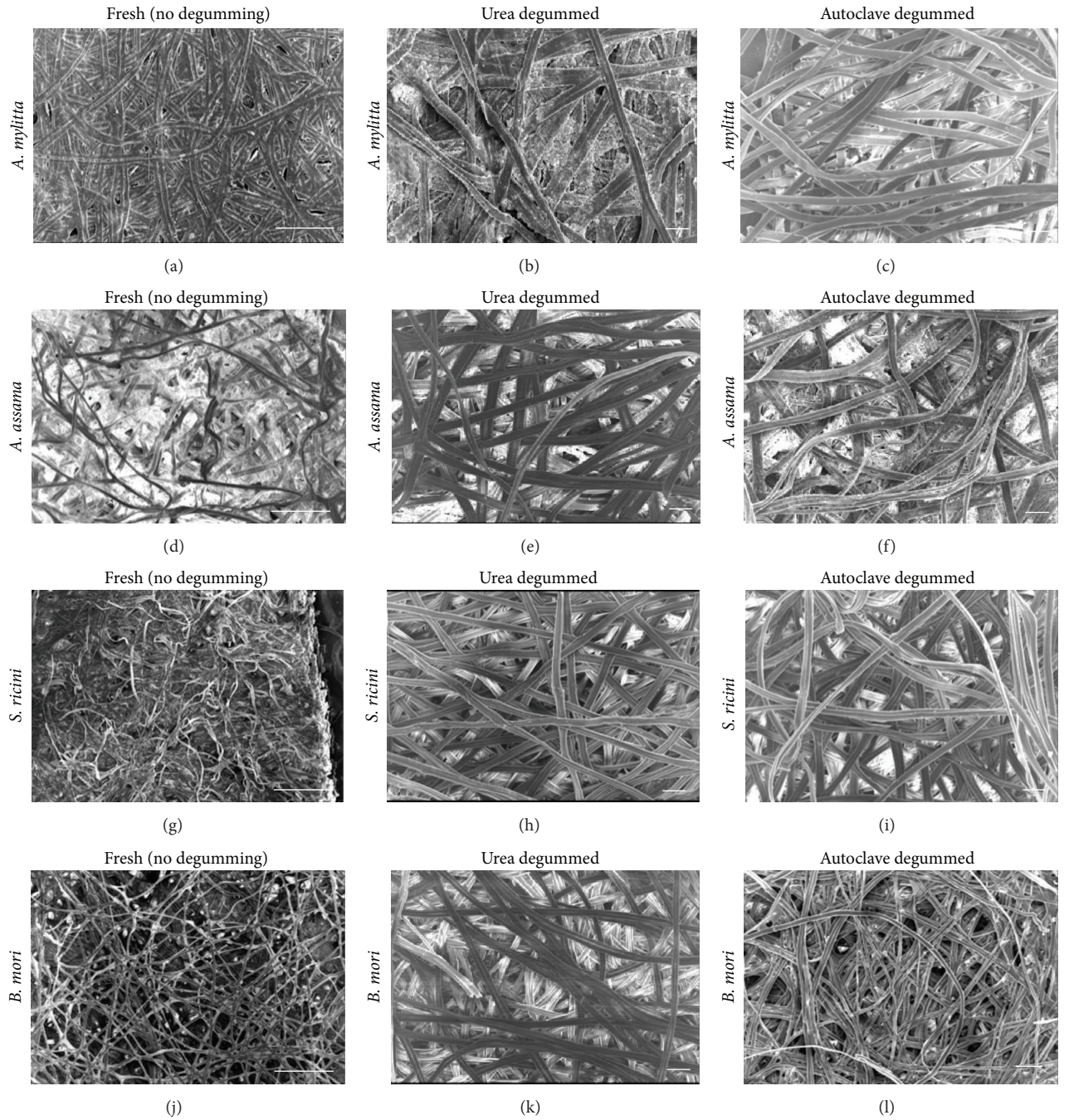

Figure 2: Scanning electron micrographs of the cocoon pieces of mulberry and non-mulberry silks. The cocoons are observed before (50x) and after degumming (100x) using urea and autoclave degumming methods. Scale bar represents 100 μm.

lyophilized powder as random coil and alpha helix, whereas the transition from the random coil to β-sheet is observed in CD results of aqueous solution of sericin.

3.3.4. Thermogravimetric Analysis. The thermogravimetric curves of sericin powders are shown in Figure 4(c). When comparing the graphs for the four samples, it is observed that the peaks in the DTG curve are the smallest for *S. ricini* sample and the largest for *B. mori*. This gives an indication that the rate of change in weight of the sample with time (or temperature) for *S. ricini* is more gradual than that for the sample of *B. mori*. Or in other words, *S. ricini* is thermally more stable than *B. mori*. A lower peak in the DTG curve means that the sample loses weight more steadily. Hence, the corresponding TGA curve is smoother and has lesser slopes at most times (and temperatures). By similar arguments and by observing the plots, the samples can be arranged in the following order of decreasing stability: *S. ricini, A. assama,*

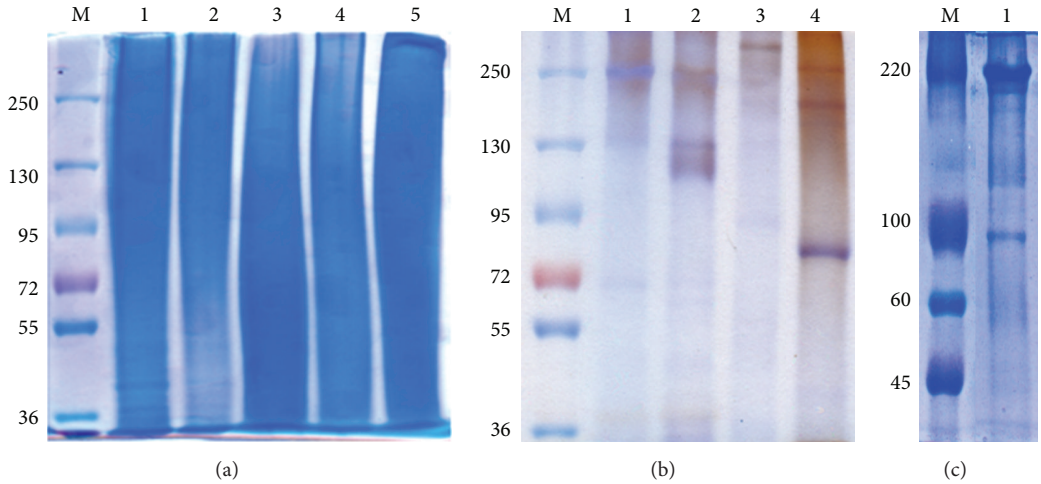

Figure 3: SDS-PAGE (8%) analysis of 0.1% sericin solutions from cocoons of *A. mylitta*, *B. mori*, *S. ricini*, and *A. assama*: (a) isolated by autoclave method: Lane 1: sericin hope, Lane 2: *B. mori,* Lane 3: *S. ricini*, Lane 4: *A. assama*, and Lane 5: *A. mylitta*; (b) isolated by urea method: Lane 1: sericin hope, Lane 2: *B. mori*, Lane 3: *S. ricini*, and Lane 4: *A. mylitta*. (c) Lane 1: *A. assama* isolated by urea method. The protein molecular weight standards are indicated by the numbers on the left. M: molecular weight marker.

A. mylitta, and, lastly, sericin of *B. mori*. *S. ricini* is thermally more stable as compared to that of other species.

3.4. Cell Culture

3.4.1. Cell Attachment. The key in the attachment result is the time taken by cells to reach maximum attachment of cells in DMEM supplemented with 0.05% sericin of *A. mylitta*, *A. assama,* and *S. ricini* is comparable to that in serum supplemented and serum-free DMEM, which show maximum cell attachment at 10 hrs after seeding (Figure 5). For media supplemented with 0.05% sericin of *B. mori*, maximum cell attachment is observed at 12 hrs after seeding, which is in accordance with similar attachment study reported earlier [39]. After 4 hours of cell seeding, the percentage of cells attached in the case of serum-free medium was 99.75% and it remained approximately the same after 12 hours of seeding. However, in case of the cells growing in *B. mori* sericin supplemented medium, 98.5% cells were attached at 4 hours while the number increased to 99.48% after 12 hours. Percentage of the cells attached in non-mulberry sericin supplemented media at 4 hours and 12 hours was similar to that in serum-free media. The attachment of cells in *B. mori* sericin supplemented medium was almost similar in comparison to non-mulberry sericin and serum-free media. We can also say that non-mulberry sericin supported attachment faster than mulberry sericin. The final number of cells attached at 12th hour for cells in serum-free medium and in mulberry supplemented medium does not have a statistical difference (p value $>$ 0.05). So, it can be concluded that somehow the mulberry sericin supplemented medium does promote cell attachment but at a rate slower than serum-free and non-mulberry sericin supplemented media. Furthermore, Tsubouchi et al. [40] reported that attachment is enhanced in mulberry sericin due to a repetitive fraction called sericin M (170 kDa). No sericin protein fraction other than the M fraction contributed to cell attachment. This 170 KDa protein fraction is absent in our SDS-PAGE results. This could be a reason for slower attachment of cells in mulberry supplemented medium.

3.4.2. Cell Morphology. Cell morphology is studied by viewing the cells under inverted phase contrast microscope (Leica, Germany). The cells grown in normal complete DMEM are used as a control. In comparison with the control, the cells grown in sericin supplemented media show a marked morphology change as the concentration of sericin in the media is increased. The morphology of cells, as compared by phase contrast microscope, cultured in sericin supplemented media of *B. mori* and *A. mylitta* is comparable to the cells growing in 10% FBS supplemented control. However, morphology of the cells grown in *S. ricini* and *A. assama* sericin supplemented medium appears to be different (Figure 6(A)). Some morphological changes are observed when cells are cultured with *S. ricini* and *A. assama* sericin supplemented media. However, we have not studied the loss of phenotype or differentiation of cells into other types. The cells growing in control medium are typically spindle shaped. However, the sericin supplemented media did not negatively affect the actin cytoskeleton of the cells; fluorescence images show well-defined nuclei and actin microfilaments comparable to those of the cells grown in serum supplemented media (Figure 6(B)).

3.4.3. Cell Proliferation. Alamar Blue, a water soluble dye, is reduced by the cells growing in the medium, thereby changing the colour of the media from blue to pink which is measured colourimetrically. The number of viable cells correlates with the magnitude of dye reduction and is expressed as percentage of Alamar Blue reduced [41, 42]. Alamar assay conducted on L929 cells grown in sericin supplemented DMEM over a period of 3 days (Figure 7) shows that the

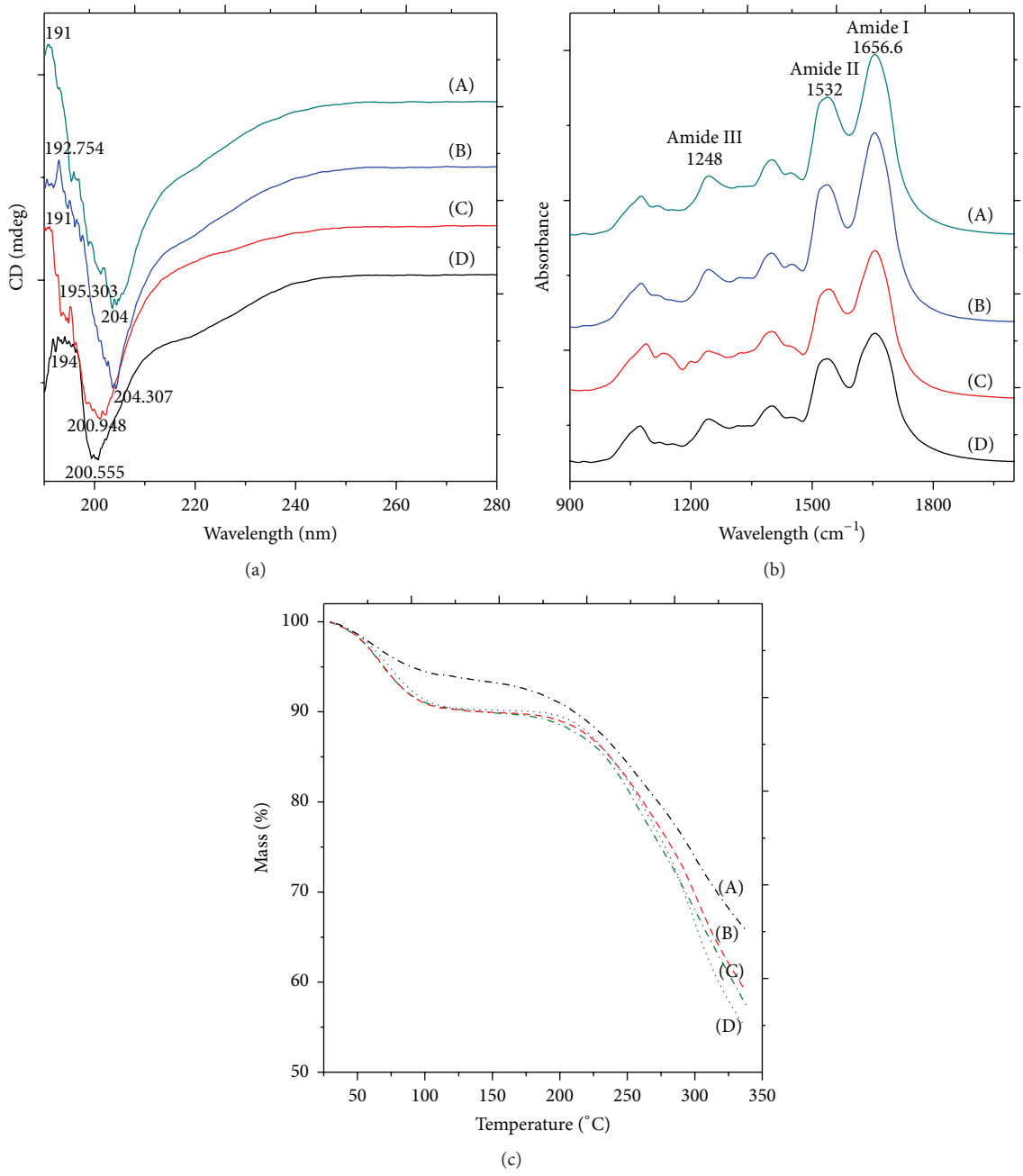

Figure 4: (a) CD spectra of 0.1 % (w/v) sericin solution from cocoons of different species: (A) *A. mylitta*, (B) *A. assama*, (C) *S. ricini*, and (D) *B. mori*. (b) FTIR spectrum of sericin powders from the various species: (A) *A. mylitta*, (B) *A. assama*, (C) *S. ricini*, and (D) *B. mori*. (c) TGA curves of lyophilized sericin powders of (A) *S. ricini*, (B) *A. mylitta*, (C) *A. assama*, and (D) *B. mori*.

cells not only are viable but are also proliferating. This is comparable to that of the cells grown in serum-free DMEM. While sericin of *S. ricini* helps to proliferate the cells better over a period of 3 days, the other non-mulberry and mulberry sericins do not show a marked difference in proliferation. Even the growth of cells in 0.1% *S. ricini* sericin supplemented medium is also significantly greater than the cells growing in 10% serum supplemented medium. This is also found to be true for 0.05% *S. ricini* sericin supplemented medium. Furthermore, the growth of cells in 0.05% *B. mori*, *A. mylitta*, and *A. assama* is found to be better than that of the cells growing in serum-free medium. There is a reduction on the growth of cells in serum-free medium from day one to day three. The cells grown in sericin supplemented media do not reflect the same. Based on the present cell culture assays the sericins of both mulberry and non-mulberry species appear to be beneficial to the growth of cells.

4. Discussion

Different sources of sericin show varied bands of different molecular weights depending on the silkworm species used as

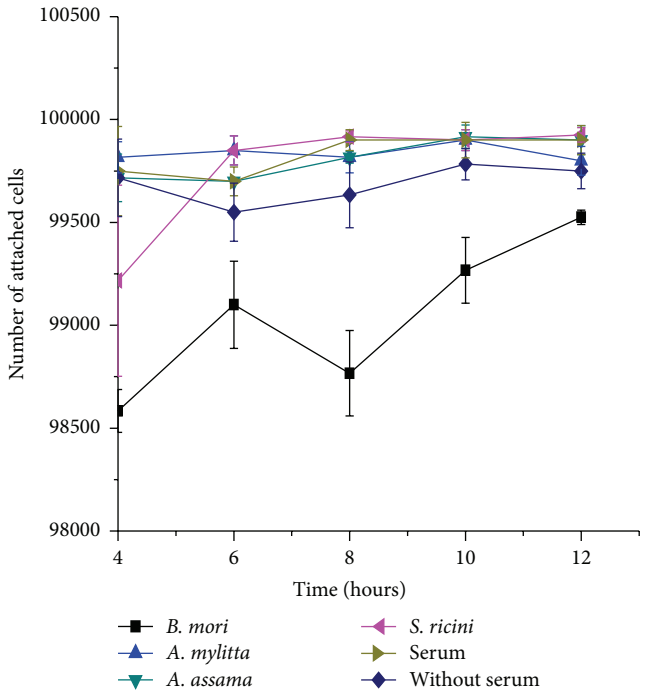

Figure 5: Time-dependent attachment of L929 cells growing in DMEM supplemented with 0.05% sericin of *B. mori, A. mylitta*, *A. assama*, and *S. ricini* sericin. Cells grown in DMEM supplemented with 10% serum and without serum were used as controls (error bars denote standard deviation for $n = 3$).

the source of the protein when extracted using urea. This may lead to different chemical and biological properties, while harsh treatments (high temperature and pressure) tend to degrade the protein leading to the appearance of a smear in the gel. Amongst them the common one is seen around 200–250 kDa along with certain low molecular weight sericin. Sericin-S, a small sericin having molecular weight 5 to 100 kDa of *B. mori*, is believed to act as a mitogenic factor in serum-free media. This accelerates the proliferation of hybridoma cells and T-lymphocyte cells [22]. Novel sericin-GIT medium, devoid of mammalian factors but containing sericin and other nutrients, helps in the proliferation of various cell lines, namely, HepG2, HeLa, SIRC, and L929 [43]. In our study, the silk fibroin fibres are seen to be clear of any remains of sericin when degummed properly indicating efficient extraction of sericin from the silk cocoon. Sericins show random coils and β-sheets in their secondary structures. This may be attributed to the polar interactions among the amino acids in the serine-rich motifs by hydrogen bonding leading to zipper like arrangements [37]. The transition from random coil to β-sheets in solution is stabilized by electrostatic interactions [38]. Thermal stability also differs in sericins. Sericin of *S. ricini* is seen to be most thermally stable amongst all. Sericins of mulberry and non-mulberry species are reported to have different biochemical properties [6]. While *B. mori* sericin comprises polypeptides ranging from 24 to 400 kDa, non-mulberry sericins also differ in molecular weights from one another. One major polypeptide fraction of 66 kDa is identified in sericins of *A. assama* and *S. ricini*, while *A. mylitta* sericin consists of several polypeptide fractions ranging from 30 to 200 kDa [6]. The two ranges of molecular weight-large sericin chain (MW 191–339 kDa) and small-size sericin (MW 61–132 kDa) are investigated for the apoptosis and proliferation of the colon cancer cells [44]. The smaller sericin had higher antiproliferative effects than that of the large sericin but neither of the sericin types (small or large sericin) affects the viability of the cells. So we can assume that the cell attachment will be similar, irrespective of the molecular weight of the sericins. Amino acid composition and secondary structure of *A. mylitta* sericin also vary from those of *B. mori* sericin [13]. Thus, the diversity of biochemical properties of silk sericins among different species of silkworms confers distinct biophysical properties to the sericins. The 400 kDa sericin found in the middle portion of the *B. mori* silk gland, particularly its 170 kDa fraction consisting of serine-rich repetitive domain, is reported to promote skin fibroblast attachment and activity. The sericins of anterior and posterior portions of *B. mori* silk grand show no biological effects in skin fibroblasts even though the posterior sericin has a 170 kDa fraction but no serine-rich amino acid composition [40]. Thus, attachment and proliferation of cells depend not only on the presence of specific polypeptide fractions but also on the amino acid content in the particular fraction. The difference in attachment of cells grown in sericin supplemented medium of different silkworm species in our study may be attributed to the differences in biophysical properties of the sericins.

Sericin has several beneficial properties and has already proved to be one of the natural biomaterials for different biomedical applications [6, 45, 46]. This work indicates that sericin can be used as media supplements. Investigations in the field of tissue engineering and regenerative medicine require growth supplements (growth factors or proteins), which are commonly provided by serum. This work indicates that sericin can support and enhance the cell growth equivalent to serum minimizing the limitation associated with the use of serum.

Replacement of the fetal bovine serum with mulberry *B. mori* sericin is reported to be successful in the culture of rat islet cells [23]. It is known that despite the benefits of serum in cell culture, it hinders the recovery of cellular product from media during downstream processing. The incorporation of sericin in the design of better serum-free media, therefore, may find better place in industries where cellular products of high purity are required. Media used for tissue culture may have significant effects on the growth and morphology of cells [47, 48]. In a departure from similar studies that report the use of *B. mori* sericin as a serum substitute in the growth of fibroblast cells [36, 49], our study shows that the low concentrations of both mulberry and non-mulberry sericin supplemented media can be used as supplements to serum-free media. The differences in the morphology of the cells are observed in cells cultured in media supplemented with sericin of *S. ricini* and *A. assama*. Sericin is known to affect different pathways due to its antioxidant properties [3, 50–52]. The morphological changes may be attributed to the effect of sericin on certain signalling pathway. Sericin

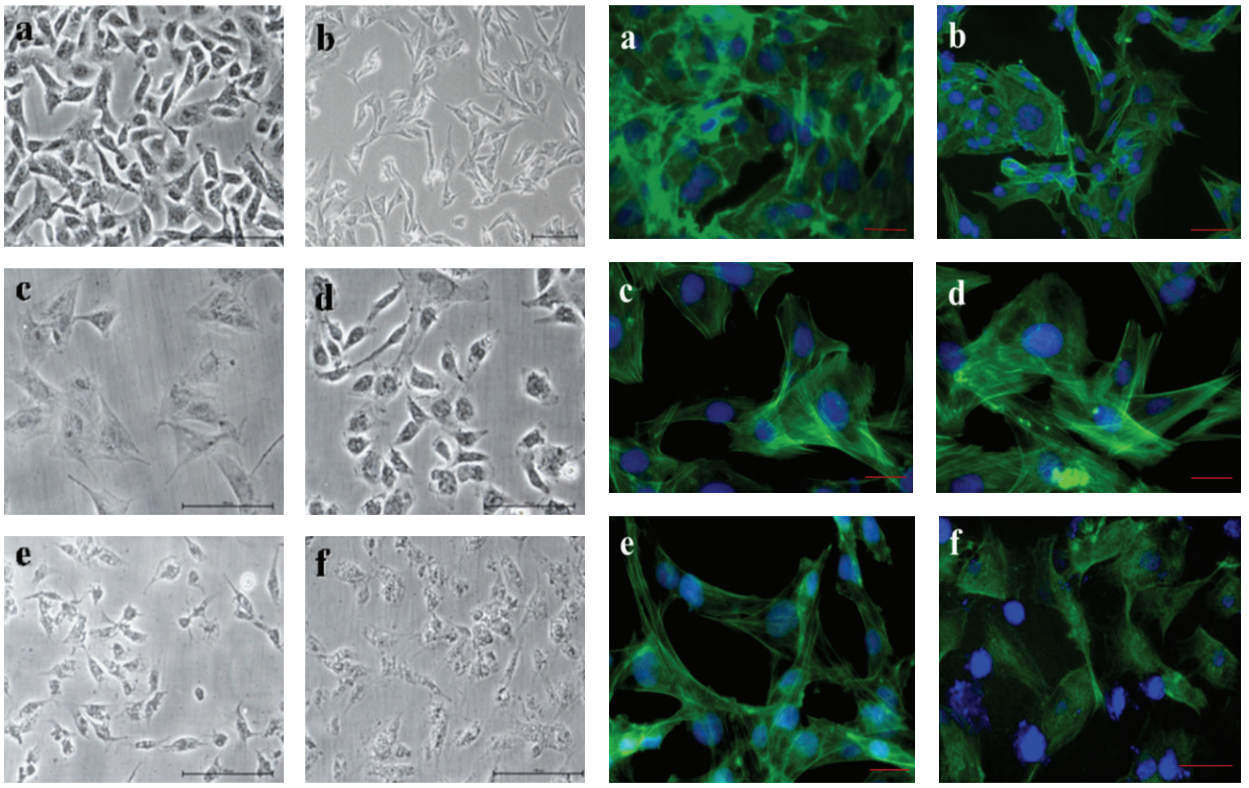

Figure 6: (A) Phase contrast and (B) fluorescence microscopic observations showing L929 fibroblasts growth and attachment on (a) 10% serum supplemented DMEM and (b) serum-free DMEM as controls and in DMEM supplemented with 0.05% silk protein sericins of *B. mori* (c), *A. mylitta* (d), *A. assama* (e), and *S. ricini* (f). Scale bar represents 10 μm.

supplemented media do not seem to negatively affect the actin cytoskeleton of the cells as fluorescence images show well-defined nuclei and actin microfilaments comparable to those of serum supplemented media (Figure 6(B)).

Sericins extracted by different methods were reported to exhibit different physical and biological properties [36]. Sericins consist of different fractions in each species. The extracted quantity of sericins and its fractions depend upon the source of materials, age, storage condition, and extraction protocol [10]. In the autoclave method, we observe only smears in the gels due to extreme conditions used in the extraction procedure. However, the individual fraction can be purified by other extraction methods but the detailed study based on the above parameters is yet to be carried out for each species. The sericins used in the cell culture of this study comprise all the fractions together of a particular species. Out of various methods of extraction, heat-degraded extraction of sericin proved to be least toxic and produced highest collagen in fibroblast cells and a concentration of 100 μg/mL seemed to be optimal for use in serum-free growth medium [51]. Therefore, in our study, heat-extracted sericins were used in serum-free culture medium. The cells grown in sericin supplemented media from *A. mylitta* and *B. mori* depict not only good cell viability but also proper cell morphology that is comparable to serum supplemented media (Figures 6(A)(c, d) and 6(B)(c, d)). Therefore, as low as 0.05% sericins from *B. mori* and *A. mylitta* can be used as potential medium supplements for the culture of L929 fibroblast cells. The authors do not claim at this stage that sericin can completely replace serum supplementation in different kinds of cells. However, in dealing with delicate cell cultures that are prone to serum shock, the sericin may act as a growth supplement. The effects of concentration of sericin in the growth medium are reported to affect the cell viability and growth. In a similar study, mulberry sericin extracted by heat-degradation or autoclave method had been shown to enhance the proliferation of L929 cells in the medium supplemented with 0.03% *B. mori* sericin while the cell viability decreased considerably at higher sericin concentration of 0.3% [53]. Furthermore, Aramwit et al. reported that a low concentration of 8 μg/mL heat-degraded sericin showed highest cell viability in mouse fibroblast cells while higher concentrations of sericin in the medium significantly decreased cell viability [36]. In our study, viability increased when the cells were grown in 0.05% sericin of non-mulberry species during the course of 3 days. *S. ricini* sericin showed the highest increase in viability. However, the viability of cells growing in 0.1% sericin did not change as effectively when compared with cells growing in 0.05% sericin supplemented medium. Thus, the results indicate that the growth and viability of cells depend on the concentration of sericin in the medium. The results indicate that further investigations are to be conducted to determine

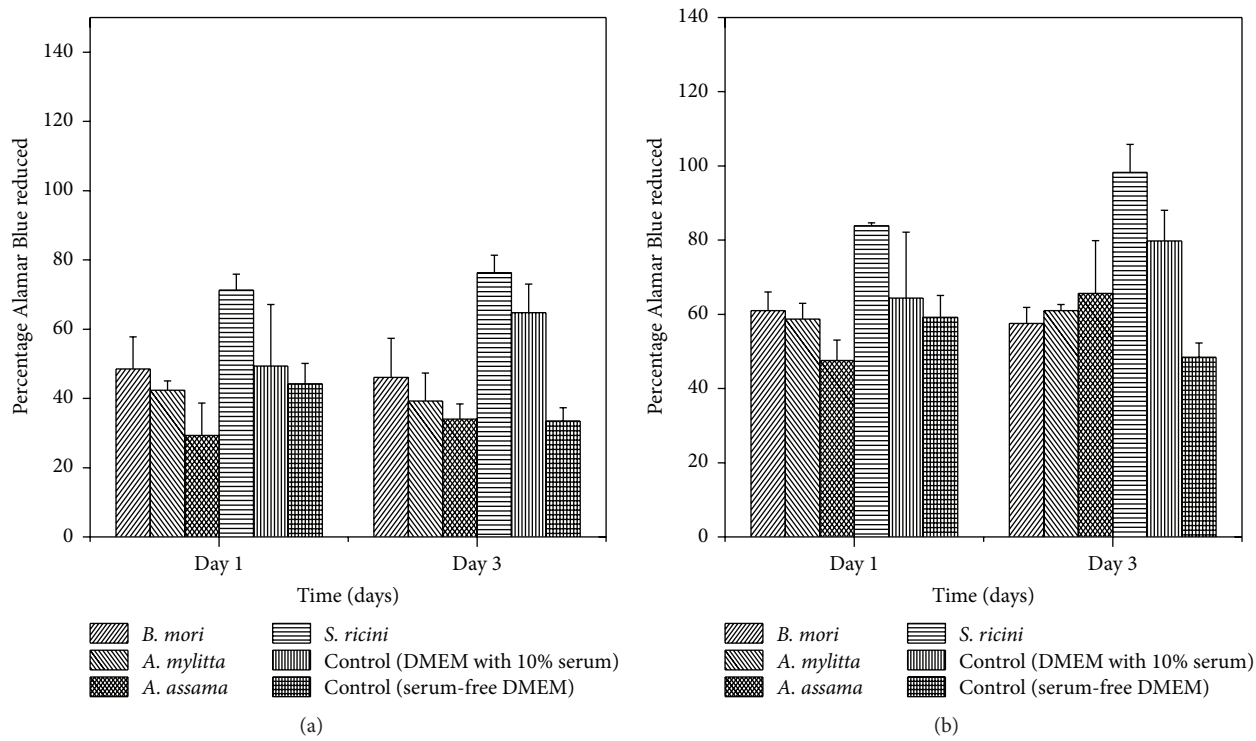

Figure 7: Estimation of cell viability and proliferation by Alamar Blue assay on L929 cells grown on 0.1% (a) and 0.05% (b) concentrations of sericin of *B. mori*, *A. mylitta*, *A. assama,* and *S. ricini,* 10% FBS supplemented DMEM and FBS free DMEM (error bars denote standard deviation for $n = 3$).

how sericin regulates the different cellular morphology and functions. This requires optimizing the dosage for each species of sericin for different cell lines. The present work attempts to present that both mulberry and different non-mulberry silk protein sericins play an important role in cell culture.

5. Conclusion

Sericins from mulberry and different non-mulberry species usually depict that more stable β-sheets conformation is solution, which adds to its integrity in aqueous media. Different molecular weights of sericin may be determining the difference in the properties of sericin from different sources like thermal stability and cytocompatibility. The low concentrations (0.05%) of all the different sources of sericins supplemented media show better cell growth than serum-free media. This indicates that sericin supports both the attachment and growth of the cells. The morphology of cells cultured in sericin supplemented media from mulberry *Bombyx mori* and non-mulberry *Antheraea mylitta* is comparable to that of the cells grown in medium supplemented with 10% FBS. There is a change in the morphology of the cells grown in *Samia ricini* and *Antheraea assama* sericin supplemented media and the cause for the change needs attention. Sericins of both mulberry and non-mulberry species have the potential to be used as a substitute for serum in media for the growth of cells. The sericins are low-cost, abundant, waste/by-product of textile industries and are underutilised materials. Further investigations are needed to understand how sericins aid in the growth and proliferation of cells and their behavior of different sources.

Disclosure

Neety Sahu present address is Department of Chemical and Bimolecular Engineering, 207 Othmer Hall, University of Nebraska-Lincoln, Lincoln, NE 68588-0643, USA. Dr. Joydip Kundu present address is Department of Chemical Engineering, 313 Snell Engineering Centre, Northeastern University, 360 Huntington Avenue, Boston, MA 02115-5000, USA. Dr. Sarmistha Talukdar present address is Virginia Commonwealth University, Institute of Molecular Medicine, Molecular Medicine Research Building, 1220 East Broad Street, 7th Floor, Richmond, VA 23298-0033, USA.

Competing Interests

The authors declare that they have no conflict of interests.

Authors' Contributions

Neety Sahu, Shilpa Pal, and Sunaina Sapru contributed equally to this work.

Acknowledgments

The authors are thankful to Dr. Milli Banerjee, Directorate of Textile (Sericulture), and Mr. Mrinal Dey of State Ericulture Farm, Jalpaiguri, and to Dr. Monoj K. Baidya, Dr. Narayan Biswas, and Mr. Ram Kumar Saha of Central Silk Board, Cooch Behar, West Bengal State of India, for providing the eri and muga cocoons. The authors are also thankful to Sericulture Directorate, West Midnapore, West Bengal State, India, for providing mulberry cocoons. This work is supported by Department of Biotechnology and Indian Council of Medical Research Government of India, New Delhi.

References

[1] L. Lamboni, M. Gauthier, G. Yang, and Q. Wang, "Silk sericin: a versatile material for tissue engineering and drug delivery," *Biotechnology Advances*, vol. 33, no. 8, pp. 1855–1867, 2015.

[2] K. Yanagihara, M. Miki, A. Ogawa, M. Sasaki, H. Yamada, and S. Terada, "Effects of sericin on promoting proliferation and inhibiting apoptosis of mammalian cells," in *Animal Cell Technology: Basic & Applied Aspects*, S. Shirahata, K. Ikura, M. Nagao, A. Ichikawa, and K. Teruya, Eds., vol. 15 of *Animal Cell Technology: Basic & Applied Aspects*, pp. 31–36, 2009.

[3] R. Dash, M. Mandal, S. K. Ghosh, and S. C. Kundu, "Silk sericin protein of tropical tasar silkworm inhibits UVB-induced apoptosis in human skin keratinocytes," *Molecular and Cellular Biochemistry*, vol. 311, no. 1-2, pp. 111–119, 2008.

[4] B. C. Dash, B. B. Mandal, and S. C. Kundu, "Silk gland sericin protein membranes: fabrication and characterization for potential biotechnological applications," *Journal of Biotechnology*, vol. 144, no. 4, pp. 321–329, 2009.

[5] B. B. Mandal and S. C. Kundu, "Self-assembled silk sericin/poloxamer nanoparticles as nanocarriers of hydrophobic and hydrophilic drugs for targeted delivery," *Nanotechnology*, vol. 20, no. 35, Article ID 355101, 2009.

[6] S. C. Kundu, B. C. Dash, R. Dash, and D. L. Kaplan, "Natural protective glue protein, sericin bioengineered by silkworms: potential for biomedical and biotechnological applications," *Progress in Polymer Science*, vol. 33, no. 10, pp. 998–1012, 2008.

[7] S. Nayak, S. Dey, and S. C. Kundu, "Skin equivalent tissue-engineered construct: co-cultured fibroblasts/ keratinocytes on 3D matrices of sericin hope cocoons," *PLoS ONE*, vol. 8, no. 9, article e74779, 2013.

[8] S. K. Das, T. Dey, and S. C. Kundu, "Fabrication of sericin nanoparticles for controlled gene delivery," *RSC Advances*, vol. 4, no. 5, pp. 2137–2142, 2014.

[9] T. Isobe, Y. Ikebata, T. Onitsuka et al., "Effect of sericin on preimplantation development of bovine embryos cultured individually," *Theriogenology*, vol. 78, no. 4, pp. 747–752, 2012.

[10] B. Kundu, N. E. Kurland, V. K. Yadavalli, and S. C. Kundu, "Isolation and processing of silk proteins for biomedical applications," *International Journal of Biological Macromolecules*, vol. 70, pp. 70–77, 2014.

[11] H. Mosher and J. Rayon, "The sericin fractions of silk," *American Silk*, vol. 53, pp. 43–44, 1934.

[12] Y. Takasu, H. Yamada, and K. Tsubouchi, "Isolation of three main sericin components from the cocoon of the silkworm, *Bombyx mori*," *Bioscience, Biotechnology and Biochemistry*, vol. 66, no. 12, pp. 2715–2718, 2002.

[13] R. Dash, S. Mukherjee, and S. C. Kundu, "Isolation, purification and characterization of silk protein sericin from cocoon peduncles of tropical tasar silkworm, *Antheraea mylitta*," *International Journal of Biological Macromolecules*, vol. 38, no. 3–5, pp. 255–258, 2006.

[14] R. Dash, S. K. Ghosh, D. L. Kaplan, and S. C. Kundu, "Purification and biochemical characterization of a 70 kDa sericin from tropical tasar silkworm, *Antheraea mylitta*," *Comparative Biochemistry and Physiology-B Biochemistry and Molecular Biology*, vol. 147, no. 1, pp. 129–134, 2007.

[15] H. Yun, H. Oh, M. K. Kim et al., "Extraction conditions of *Antheraea mylitta* sericin with high yields and minimum molecular weight degradation," *International Journal of Biological Macromolecules*, vol. 52, no. 1, pp. 59–65, 2013.

[16] N. E. Kurland, J. Kundu, S. Pal, S. C. Kundu, and V. K. Yadavalli, "Self-assembly mechanisms of silk protein nanostructures on two-dimensional surfaces," *Soft Matter*, vol. 8, no. 18, pp. 4952–4959, 2012.

[17] J. T. B. Shaw and S. G. Smith, "Amino-acids of silk sericin," *Nature*, vol. 168, no. 4278, p. 745, 1951.

[18] S. Nayak, T. Dey, D. Naskar, and S. C. Kundu, "The promotion of osseointegration of titanium surfaces by coating with silk protein sericin," *Biomaterials*, vol. 34, no. 12, pp. 2855–2864, 2013.

[19] T. Siritienthong, J. Ratanavaraporn, and P. Aramwit, "Development of ethyl alcohol-precipitated silk sericin/polyvinyl alcohol scaffolds for accelerated healing of full-thickness wounds," *International Journal of Pharmaceutics*, vol. 439, no. 1-2, pp. 175–186, 2012.

[20] S. Kanokpanont, S. Damrongsakkul, J. Ratanavaraporn, and P. Aramwit, "An innovative bi-layered wound dressing made of silk and gelatin for accelerated wound healing," *International Journal of Pharmaceutics*, vol. 436, no. 1-2, pp. 141–153, 2012.

[21] B. Kundu and S. C. Kundu, "Silk sericin/polyacrylamide in situ forming hydrogels for dermal reconstruction," *Biomaterials*, vol. 33, no. 30, pp. 7456–7467, 2012.

[22] S. Terada, M. Sasaki, K. Yanagihara, and H. Yamada, "Preparation of silk protein sericin as mitogenic factor for better mammalian cell culture," *Journal of Bioscience and Bioengineering*, vol. 100, no. 6, pp. 667–671, 2005.

[23] M. Morikawa, T. Kimura, M. Murakami, K. Katayama, S. Terada, and A. Yamaguchi, "Rat islet culture in serum-free medium containing silk protein sericin," *Journal of Hepato-Biliary-Pancreatic Surgery*, vol. 16, no. 2, pp. 223–228, 2009.

[24] A. Ogawa, S. Terada, T. Kanayama et al., "Improvement of islet culture with sericin," *Journal of Bioscience and Bioengineering*, vol. 98, no. 3, pp. 217–219, 2004.

[25] M. Takahashi, K. Tsujimoto, H. Yamada, H. Takagi, and S. Nakamori, "The silk protein, sericin, protects against cell death caused by acute serum deprivation in insect cell culture," *Biotechnology Letters*, vol. 25, no. 21, pp. 1805–1809, 2003.

[26] M. Sasaki, Y. Kato, H. Yamada, and S. Terada, "Development of a novel serum-free freezing medium for mammalian cells using the silk protein sericin," *Biotechnology and Applied Biochemistry*, vol. 42, no. 2, pp. 183–188, 2005.

[27] T. Isobe, Y. Ikebata, T. Onitsuka et al., "Cryopreservation for bovine embryos in serum-free freezing medium containing silk protein sericin," *Cryobiology*, vol. 67, no. 2, pp. 184–187, 2013.

[28] K. Ohnishi, M. Murakami, M. Morikawa, and A. Yamaguchi, "Effect of the silk protein sericin on cryopreserved rat islets," *Journal of Hepato-Biliary-Pancreatic Sciences*, vol. 19, pp. 354–360, 2012.

[29] M. Verdanova, R. Pytlik, and M. H. Kalbacova, "Evaluation of sericin as a fetal bovine serum-replacing cryoprotectant during freezing of human mesenchymal stromal cells and human osteoblast-like cells," *Biopreservation and Biobanking*, vol. 12, no. 2, pp. 99–105, 2014.

[30] S. J. Froud, "The development, benefits and disadvantages of serum-free media," *Developments in Biological Standardization*, vol. 99, pp. 157–166, 1999.

[31] B. B. Mandal, A. S. Priya, and S. C. Kundu, "Novel silk sericin/gelatin 3-D scaffolds and 2-D films: fabrication and characterization for potential tissue engineering applications," *Acta Biomaterialia*, vol. 5, no. 8, pp. 3007–3020, 2009.

[32] Y.-Q. Zhang, M.-L. Tao, W.-D. Shen et al., "Immobilization of L-asparaginase on the microparticles of the natural silk sericin protein and its characters," *Biomaterials*, vol. 25, no. 17, pp. 3751–3759, 2004.

[33] H. Blum, H. Beier, and H. J. Gross, "Improved silver staining of plant proteins, RNA and DNA in polyacrylamide gels," *Electrophoresis*, vol. 8, no. 2, pp. 93–99, 1987.

[34] J. T. Yang, C.-S. C. Wu, and H. M. Martinez, "Calculation of protein conformation from circular dichroism," *Methods in Enzymology*, vol. 130, pp. 208–269, 1986.

[35] Y. Takasu, H. Yamada, H. Saito, and K. Tsubouchi, "Characterization of *Bombyx mori* sericins by the partial amino acid sequences," *Journal of Insect Biotechnology and Sericology*, vol. 74, no. 3, pp. 103–109, 2005.

[36] P. Aramwit, S. Kanokpanont, T. Nakpheng, and T. Srichana, "The effect of sericin from various extraction methods on cell viability and collagen production," *International Journal of Molecular Sciences*, vol. 11, no. 5, pp. 2200–2211, 2010.

[37] J. Huang, R. Valluzzi, E. Bini, B. Vernaglia, and D. L. Kaplan, "Cloning, expression, and assembly of sericin-like protein," *The Journal of Biological Chemistry*, vol. 278, no. 46, pp. 46117–46123, 2003.

[38] S. Urushizaki, "The stability of sericin aqueous solution," *Sanshi Kenkyu*, vol. 99, pp. 71–74, 1976.

[39] S. Talukdar, M. Mandal, D. W. Hutmacher, P. J. Russell, C. Soekmadji, and S. C. Kundu, "Engineered silk fibroin protein 3D matrices for *in vitro* tumor model," *Biomaterials*, vol. 32, no. 8, pp. 2149–2159, 2011.

[40] K. Tsubouchi, Y. Igarashi, Y. Takasu, and H. Yamada, "Sericin enhances attachment of cultured human skin fibroblasts," *Bioscience, Biotechnology and Biochemistry*, vol. 69, no. 2, pp. 403–405, 2005.

[41] P. Goegan, G. Johnson, and R. Vincent, "Effects of serum protein and colloid on the alamarBlue assay in cell cultures," *Toxicology in Vitro*, vol. 9, no. 3, pp. 257–266, 1995.

[42] M. M. Nociari, A. Shalev, P. Benias, and C. Russo, "A novel one-step, highly sensitive fluorometric assay to evaluate cell-mediated cytotoxicity," *Journal of Immunological Methods*, vol. 213, no. 2, pp. 157–167, 1998.

[43] M. Kobayashi, A. Sakuma, Y. Kunitomi, M. Sasaki, H. Yamada, and S. Terada, "Development of mammalian factors-free medium for cell culture by using silk protein sericin," *Journal of Bioscience and Bioengineering*, vol. 108, pp. S18–S19, 2009.

[44] W. Kaewkorn, N. Limpeanchob, W. Tiyaboonchai, S. Pongcharoen, and M. Sutheerawattananonda, "Effects of silk sericin on the proliferation and apoptosis of colon cancer cells," *Biological Research*, vol. 45, no. 1, pp. 45–50, 2012.

[45] P. Aramwit, T. Siritientong, and T. Srichana, "Potential applications of silk sericin, a natural protein from textile industry by-products," *Waste Management and Research*, vol. 30, no. 3, pp. 217–224, 2012.

[46] T.-T. Cao and Y.-Q. Zhang, "Processing and characterization of silk sericin from *Bombyx mori* and its application in biomaterials and biomedicines," *Materials Science and Engineering C*, vol. 61, pp. 940–952, 2016.

[47] H. Shafaei, A. Esmaeili, M. Mardani et al., "Effects of human placental serum on proliferation and morphology of human adipose tissue-derived stem cells," *Bone Marrow Transplantation*, vol. 46, no. 11, pp. 1464–1471, 2011.

[48] U. Osuna-Martínez, A. Gómez-Solís, E. Alvarez-Ayala, J. Reyes-Esparza, and L. Rodriguez-Fragoso, "Effect of porcine-serum on viability, proliferation and morphology of hepatic cells," *The FASEB Journal*, vol. 24, no. 1, supplement, p. 965.11, 2010.

[49] T.-T. Cao and Y.-Q. Zhang, "Viability and proliferation of L929, tumour and hybridoma cells in the culture media containing sericin protein as a supplement or serum substitute," *Applied Microbiology and Biotechnology*, vol. 99, no. 17, pp. 7219–7228, 2015.

[50] N. Kato, S. Sato, A. Yamanaka, H. Yamada, N. Fuwa, and M. Nomura, "Silk protein, sericin, inhibits lipid peroxidation and tyrosinase activity," *Bioscience, Biotechnology, and Biochemistry*, vol. 62, no. 1, pp. 145–147, 1998.

[51] J.-B. Fan, L.-P. Wu, L.-S. Chen, X.-Y. Mao, and F.-Z. Ren, "Antioxidant activities of silk sericin from silkworm *Bombyx mori*," *Journal of Food Biochemistry*, vol. 33, no. 1, pp. 74–88, 2009.

[52] P. Qian, S. Ai, H. Yin, and J. Li, "Evaluation of DNA damage and antioxidant capacity of sericin by a DNA electrochemical biosensor based on dendrimer-encapsulated Au-Pd/chitosan composite," *Microchimica Acta*, vol. 168, no. 3, pp. 347–354, 2010.

[53] S. Terada, T. Nishimura, M. Sasaki, H. Yamada, and M. Miki, "Sericin, a protein derived from silkworms, accelerates the proliferation of several mammalian cell lines including a hybridoma," *Cytotechnology*, vol. 40, no. 1–3, pp. 3–12, 2002.

Hindawi Publishing Corporation
BioMed Research International
Volume 2016, Article ID 3827057, 9 pages
http://dx.doi.org/10.1155/2016/3827057

Research Article

Human Umbilical Cord Blood-Derived Mesenchymal Stem Cells Contribute to Chondrogenesis in Coculture with Chondrocytes

Xingfu Li,[1,2] Li Duan,[1,2] Yujie Liang,[3,4] Weimin Zhu,[1,2] Jianyi Xiong,[1,2] and Daping Wang[1,2]

[1]*Shenzhen Key Laboratory of Tissue Engineering, Shenzhen Second People's Hospital (The First Hospital Affiliated to Shenzhen University), Shenzhen, Guangdong 518035, China*
[2]*Department of Orthopedics, Shenzhen Second People's Hospital (The First Hospital Affiliated to Shenzhen University), Shenzhen, Guangdong 518035, China*
[3]*Department of Chemistry, The Chinese University of Hong Kong, Shatin, Hong Kong*
[4]*School of Chemical Biology & Biotechnology, Peking University Shenzhen Graduate School, Shenzhen, Guangdong 518055, China*

Correspondence should be addressed to Jianyi Xiong; jianyixiong@126.com and Daping Wang; dapingwang1963@qq.com

Received 4 February 2016; Revised 28 April 2016; Accepted 22 May 2016

Academic Editor: Subhas C. Kundu

Human umbilical cord blood-derived mesenchymal stem cells (hUCB-MSCs) have been shown as the most potential stem cell source for articular cartilage repair. In this study, we aimed to develop a method for long-term coculture of human articular chondrocytes (hACs) and hUCB-MSCs at low density in vitro to determine if the low density of hACs could enhance the hUCB-MSC chondrogenic differentiation as well as to determine the optimal ratio of the two cell types. Also, we compared the difference between direct coculture and indirect coculture at low density. Monolayer cultures of hUCB-MSCs and hACs were investigated at different ratios, at direct cell-cell contact groups for 21 days. Compared to direct coculture, hUCB-MSCs and hACs indirect contact culture significantly increased type II collagen (COL2) and decreased type I collagen (COL1) protein expression levels. SRY-box 9 (SOX9) mRNA levels and protein expression were highest in indirect coculture. Overall, these results indicate that low density direct coculture induces fibrocartilage. However, indirect coculture in conditioned chondrocyte cell culture medium can increase expression of chondrogenic markers and induce hUCB-MSCs differentiation into mature chondrocytes. This work demonstrates that it is possible to promote chondrogenesis of hUCB-MSCs in combination with hACs, further supporting the concept of novel coculture strategies for tissue engineering.

1. Introduction

Repair of cartilage defects represents a significant orthopedic challenge due to the limited healing capacity of mature cartilage; therefore, the development of new tissue engineering strategies is of major importance for cartilage repair [1]. Autologous chondrocyte implantation (ACI) has long been considered the gold standard to treat cartilage defects [2]. However, use of autologous chondrocytes has disadvantages that limit potential clinical applications, including donor site morbidity and dedifferentiation of the harvested chondrocytes after *ex vivo* monolayer expansion [3]. Recent studies have shifted focus from ACI to mesenchymal stem cell (MSC) therapy, which has been shown as effective for articular cartilage repair [4–11]. Additionally, MSCs have already shown safety and efficacy in a variety of regenerative medicine clinical trials [12–14]. In particular, human umbilical cord blood-derived MSCs (hUCB-MSCs) could serve as a promising cell source for *in vivo* repair of cartilage defects due to advantages of noninvasive collection, high proliferative potential, lower immunogenicity, and chondrogenic potential *in vitro* [15–17].

However, strategies employing hUCB-MSCs for cartilage regeneration are problematic due to the low induction efficiency of hUCB-MSCs alone, in the absence of growth factors and/or gene delivery systems to signal the stem cells to undergo chondrogenesis [18, 19]. An approach that supplements an abundant stem cell source with prochondrogenic signals and cell adhesions needs to be optimized before hUCB-MSCs can be applied therapeutically. Combining progenitors with mature chondrocytes may provide

a solution, as coculture of hUCB-MSCs and chondrocytes *in vitro* has previously been shown to promote hUCB-MSC chondrogenesis and inhibit MSC hypertrophy through specific chondrocyte-secreted factors [20].

It was reported that coculture of HUCB-MSCs and rabbit chondrocytes could induce the differentiation of hUCB-MSCs into human chondrocytes, and the author also obtained the more suitable seed cells ratio [21]. In their study they seeded cells at the density of 2.4×10^6 cells/cm^2. They stated that density of chondrocyte seeding is 1–3 $\times$ 10^4 cells/cm^2; however, this could lead chondrocytes to a fibrotic phenotype. The aim of our study was to explore whether coculture at the density less than 1–3 $\times$ 10^4 cells/cm^2 could induce more chondrocytes and avoid fibrosis. If low density seed cells could induce hUCB-MSCs differentiation into enough chondrocytes for cartilage tissue engineering, the cartilage extracted from patients for chondrocyte proliferation *in vitro* could be greatly lessened.

Direct coculture and indirect coculture are usually adopted in MSCs chondrogenic differentiation induced by articular chondrocytes (ACs). However, the mechanisms of interaction between ACs and MSCs in coculture have not been fully characterized. It is speculated that both physical and paracrine interactions between these two cell types are important in maintaining the chondrogenic phenotype which results in induction of hUCB-MSC chondrogenesis [22]. Chondrocytes also secrete autocrine growth factors such as transforming growth factor-β (TGF-β) and insulin-like growth factor-1 (IGF-1), and the chondrogenic factor (SOX9) can induce chondrogenic cells [23, 24].

The effect of coculture on hUCB-MSC chondrogenesis using hACs, in particular at the low density culture, was investigated in this study. Our work also compared direct cell-cell contact and indirectly coculture of hUCB-MSC and chondrocytes for improving the coculture system. In addition, the role of TGF-β in the coculture system was determined. Results of this study demonstrated that low density coculture model could maintain the chondrocyte phenotype and minimize donor site injury; thus it provided an alternative chondrocytes induction and proliferation system for cartilage tissue engineering.

2. Materials and Methods

2.1. Collection of hUCB and Cartilage. The collection of human umbilical cord blood (hUCB) and cartilage was approved by Shenzhen Second People's Hospital. Informed consent was obtained before the operation from all individuals included in the study. According to the institutional guidelines, hUCB units were obtained from normal full-term and preterm deliveries without complications throughout pregnancy, in a physiological saline system containing heparin anticoagulant, and were processed within 6 hr of collection. The units were stored and transported at 4°C. No complications were encountered upon hUCB collection, and none of the samples had signs of coagulation or haemolysis. Cartilage samples were obtained from donors after trauma patients, in a physiological saline system containing penicillin/streptomycin (P/S), and were processed within 6 hr of collection.

2.2. Isolation and Culture of hUCB-MSCs and hACs. After hUCB was diluted 1 : 1 with 100 U/mL heparin-saline, hUCB-MSCs were isolated using Ficoll-Paque density gradient centrifugation (Amersham Biosciences, Uppsala, Sweden) and resuspended in MesenGro® human mesenchymal stem cell medium (StemRD, America) that was supplemented with 10% fetal bovine serum (FBS) (Gibco, Australia) and 10 μg/L basic fibroblast growth factor (bFGF) (Gibco, Australia). Mononucleated cells were seeded into T25 cell culture flasks (Nunc, USA) at 2×10^4 cells/cm^2 and cultured at 37°C in a 5% CO_2 incubator. Five days after the cells were seeded; nonadherent cells were removed and fresh medium was added to the flasks. Medium replacement was carried out every 72 h until the cells reached an 80% confluent layer. Cells were digested with 0.25% (w/v) trypsin plus 0.02% (w/v) EDTA (HyClone, USA) and subcultured at a density of 1.0×10^4 cells/cm^2. Medium was changed twice a week. The hUCB-MSCs of passage 3 were used for chondrocyte induction [25, 26].

Cartilage specimens were collected, minced to 1 mm^3, and digested in the chondrocyte growth medium containing 1 mg/mL collagenase type II (Worthington Biochemical Corporation) for 8 hr at 37°C in a shaker. After filtration, cells were harvested and plated at a density of 1×10^4 cells/cm^2 and subcultured in chondrocyte growth medium (DMEM-F12, 10% FBS, 10 μg/L bFGF, and 0.1 mg/mL P/S). Chondrocytes of passage 2 were used for chondrocyte induction [27].

2.3. Identification of HUCB-MSCs. hUCB-MSCs were suspended in PBS containing 5% bovine serum albumin (Sigma-Aldrich, USA) at a concentration of 3×10^5 cells/50 μL and stained with CD105, CD73, CD34, and CD45 (BD Biosciences). The appropriate human isotype antibodies were used as controls. Samples were processed using a FACSCanto II flow cytometer (BD Biosciences) and analyzed with FlowJo software (Treestar) [28].

2.4. Chondrogenic Induction of hUCB-MSCs. hACs (P2) and hUCB-MSCs (P3) were used. For coculture with direct cell-cell contact, hACs and hUCB-MSCs were mixed directly at ratio of 1 : 1, 3 : 1, and 5 : 1 (hUCB-MSCs : hACs) [7, 9, 29, 30] and then cultured in basal medium (DMEM-F12, 10% FBS, 100 U/mL penicillin, and 0.1 mg/mL streptomycin). For indirect coculture, hUCB-MSCs and hACs were cultured with supernatants from each other [31]. For growth factor induction in monolayer culture, hUCB-MSCs were maintained in basal medium supplemented with 0.1 mM dexamethasone, 40 mg/mL L-proline, 10 μg/L transforming growth factor beta-1 (TGF-β1, Peprotech, USA), 10 μg/L insulin-like growth factor-1 (IGF-1) (Peprotech, USA), and 1% insulin transferrin selenium (ITS, Invitrogen) [32–35]. hACs and hUCB-MSCs cultured alone with basal medium were used as controls. All cells were incubated for three weeks at 37°C in a humidified atmosphere of 5% CO_2 and the medium changed every three days. The designated groups for this study were listed in Table 1.

Table 1: The seeding cell number of human articular chondrocytes (hACs) and human umbilical cord blood-derived mesenchymal stem cell (hUCB-MSCs).

	Group	hUCB-MSCs (cells/cm^2)	hACs (cells/cm^2)
a	hACs	—	0.6×10^4
b	hUCB-MSCs	0.6×10^4	—
c	hUCB-MSCs cultured with growth factors	0.6×10^4	—
d	Direct coculture (1 : 1)	0.3×10^4	0.3×10^4
e	Direct coculture (3 : 1)	0.45×10^4	0.15×10^4
f	Direct coculture (5 : 1)	0.5×10^4	0.1×10^4
g	Indirect coculture	0.6×10^4	—
h	Indirect coculture	—	0.6×10^4

2.5. Immunofluorescent Staining of COL2. A hyaline cartilage marker protein COL2 was examined using immunofluorescence. All groups were harvested 3 weeks after seeding. The samples were fixed in 4% paraformaldehyde for 15 min at room temperature followed by incubation with PBS containing 0.2% Triton-X100 for 15 min at room temperature (RT); then cells were blocked in 5% bovine serum albumin at RT. Then cells were subsequently incubated overnight at 4°C with mouse mAb to COL2 (1 : 100, R&D Systems). Subsequently, samples were washed and incubated with Goat-Anti-Mouse IgG (1 : 150, Molecular Probes) for 1 h, and nuclei were counterstained with 4,6-diamidino-2-phenylindole DAPI (1 : 1000, Molecular Probes) for 10 min and then rinsed with PBS. The fluorescent signal of cell nuclei and COL2 was visualized using a fluorescent microscope [36].

2.6. RNA Extraction and Quantitative Real-Time Polymerase Chain Reaction. Samples in each group were collected at the time point of 3 weeks of *in vitro* culture ($n \geq 3$ per group). Total RNA was extracted from cell samples using TRIzol reagent (Invitrogen, USA) according to the manufacturer's instructions. cDNA was synthesized from total RNA using an Omniscript RT kit (Qiagen). The mRNA expression levels of SOX9, Col1a1, and Col2a1 were determined by real-time PCR using SYBR Premix EX Taq (Takara, Japan). The forward and reverse primer pairs were shown in Table 2. To normalize mRNA levels, the GAPDH housekeeping gene was used as an internal control [37].

2.7. Western Blotting. The expression levels of SOX9, COL2, and COL1 proteins from cell samples were analyzed as described previously [38]. Samples were lysed in RIPA lysis buffer at 4°C. Samples with equal protein concentration were subjected to SDS-PAGE and transferred to a PVDF membrane. Blots were blocked with 5% skim milk/TBS-Tween 20 for 1 h at room temperature and probed with primary antibodies: mouse anti-SOX9 (Santa Cruz Biotechnology, CA) and mouse anti-COL1 (Abcam, MA) and mouse anti-COL2 (Abcam, MA) and mouse anti-β actin (Abcam, MA) overnight at 4°C. Followed by which blots were washed with PBS-Tween 20 (0.1%) and incubated with horseradish peroxidase-conjugated secondary antibodies (1 : 1000) for 1 h at room temperature. Western blotting images are representative of $N \geq 3$ images.

2.8. ELISA. The TGF-β1 concentration in the supernatant was determined by a human TGF-β1 ELISA kit (R&D Systems). BCA quantifying the total protein was conducted before ELISA; then the same protein quantity was loaded from different culture conditions. Absorbance was measured at a wavelength of 450 and 550 nm. The 450 nm values were subtracted from the 570 nm values for correction of the optical imperfections [39].

2.9. Cell Proliferation Assay. The cell viability was measured using a cell counting kit-8 (CCK-8) (Beyotime, Beijing, China) on days 0, 3, 6, 9, 12, and 15. Briefly, cells were seeded in 96-well plates at a density of 5000 cells/cm^2 in DMEM/F-12 medium. CCK-8 solution (10 μL) was added to each well. The cells were continually cultured for another 4 hours. During this period, viable cells could reduce the CCK-8 to formazan pigment, which was dissolved by 100 μL culture medium. The number of viable cells was measured by recording the formazan pigment optical density at 450 nm by a microplate reader (Bio-Rad 380, USA) [5].

2.10. Statistical Analysis. The statistical significance was analyzed using SPSS statistical analytical software (ver. 18.0; IBM, USA). A Kruskal-Wallis test was used to assess differences among the groups. A *post hoc* test was performed along with a Mann-Whitney U test. P values less than 0.05 were considered to be statistically significant.

3. Results

3.1. Identification of hUCB-MSCs. After the isolation of mesenchymal cells using the adherence criteria, the second passage of hUCB-MSCs was analyzed to confirm their identity. MSCs do not express CD34, CD45, CD117 (cKit), HLA class I, and HLA-DR antigens, whereas they are positive for CD13, CD29, CD44, CD73, CD90, CD105, and CD166 [40]. Surface markers considered positive for the mesenchymal cell lineage (CD73, CD105) and negative for the hematopoietic lineage (CD34, CD45) were used to characterize hUCB-MSCs. As shown in Figure 1, the flow cytometry analysis revealed that the isolated hUCB-MSC population had high expression of CD105 and CD73 and low expression of CD34 and CD45. Furthermore, these cells had acquired the fibroblastic morphology that is characteristic of mesenchymal stem cells, thus confirming the existence of mesenchymal stem cells in human umbilical cord blood. The proportion of stem cells met the identification criteria [41].

3.2. Immunofluorescence Staining of Collagen. COL2 protein was minimally detectable by immunofluorescence staining in cultures containing only hUCB-MSCs, but significant levels of COL2 protein were detected in direct cell-cell contact coculture, indirect coculture, growth factor-supplemented hUCB-MSC culture, and hACs cultured alone. In all groups, COL2 protein was mainly distributed in the extracellular

Table 2: Primer sequences used for real-time PCR.

Genes	Forward primer (5′–3′)	Reverse primer (5′–3′)
SOX9	GACGTGCAAGCTGGGAAA	CGGCAGGTATTGGTCAAACTC
Col2a1	CGCCACGGTCCTACAATGTC	GTCACCTCTGGGTCCTTGTTCAC
Col1a1	GACATGTTCAGCTTTGTGGACCTC	GGGACCCTTAGGCCATTGTGTA
GAPDH	GGCACAGTCAAGGCTGAGAATG	ATGGTGGTGAAGACGCCAGTA

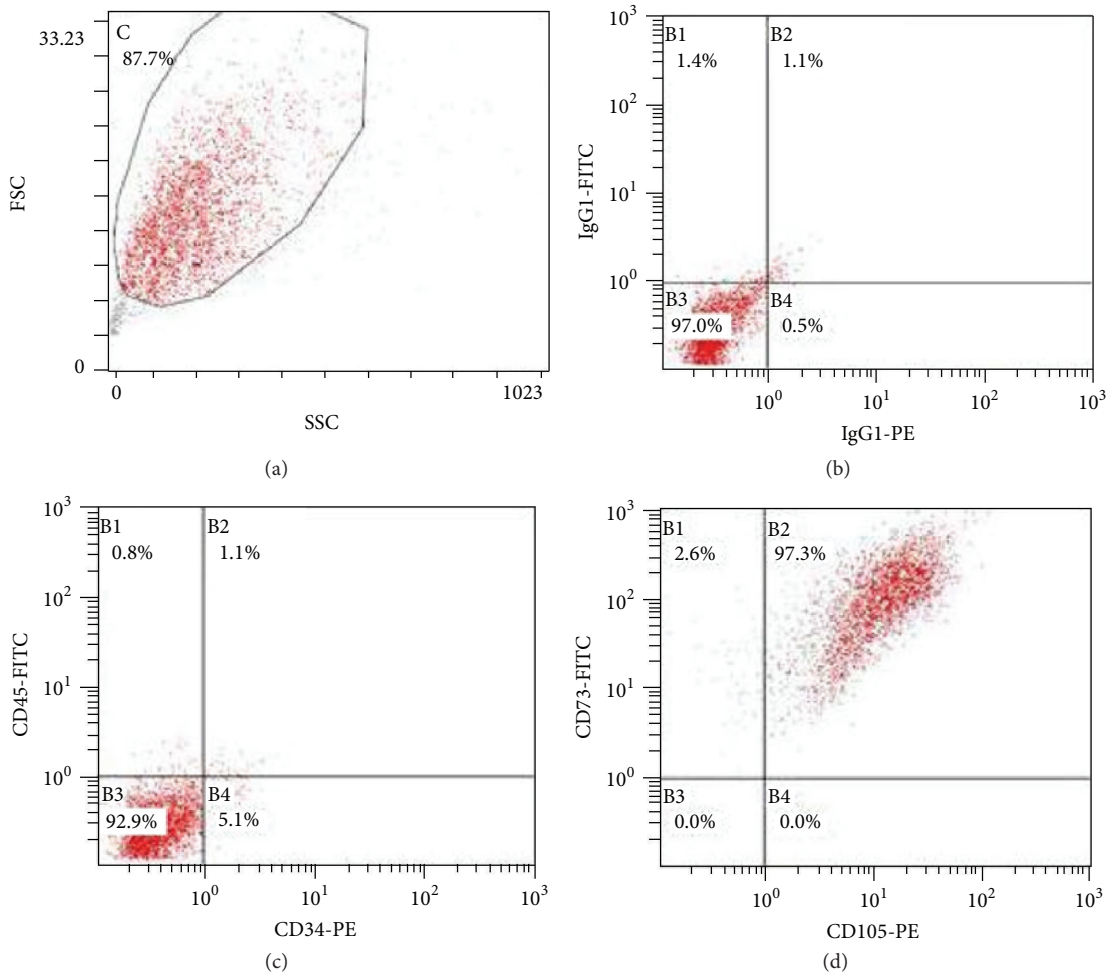

Figure 1: hUCB-MSC cell surface markers were characterized by flow cytometry. (a) Density plot showing the FSC to SSC. (b) IgG1-PE and IgG1-FITC were used as controls. (c) Cells expressing both CD34 and CD45 represented 1.1% of the population. (d) Cells expressing both CD105 and CD73 accounted for 97.3% of the population.

matrix (ECM). Coculture with direct cell-cell contact had stronger COL2 staining than the TGFβ1-induced group. The TGFβ1-induced group exhibited similar staining as compared to the indirect coculture group, and both stained more strongly than hUCB-MSCs cultured alone. The hUCB-MSCs cultured alone exhibited the weakest fluorescent signal among all the experimental groups, indicating that these progenitors do not undergo significant chondrogenesis in the absence of external signals. The hUCB-MSCs and hACs cocultured with direct cell-cell contact in a ratio of 3 : 1 stained stronger than the other ratios and conditions tested. However, all coculture groups with direct cell-cell contact showed signs of fibrosis. Immunofluorescence images of all groups stained for COL2 are shown in Figure 2.

3.3. Quantitative Analysis of mRNA Expression for Chondrocyte and Cartilage-Matrix-Related Genes. To evaluate chondrogenesis, the mRNA levels of several chondrocyte marker genes—*Col2a1*, *Col1a1*, and *SOX9*—were analyzed by quantitative real-time PCR after 3 weeks of culture *in vitro*. The hACs cultured alone had higher *SOX9* expression than hUCB-MSCs cultured alone or any of the cocultured groups

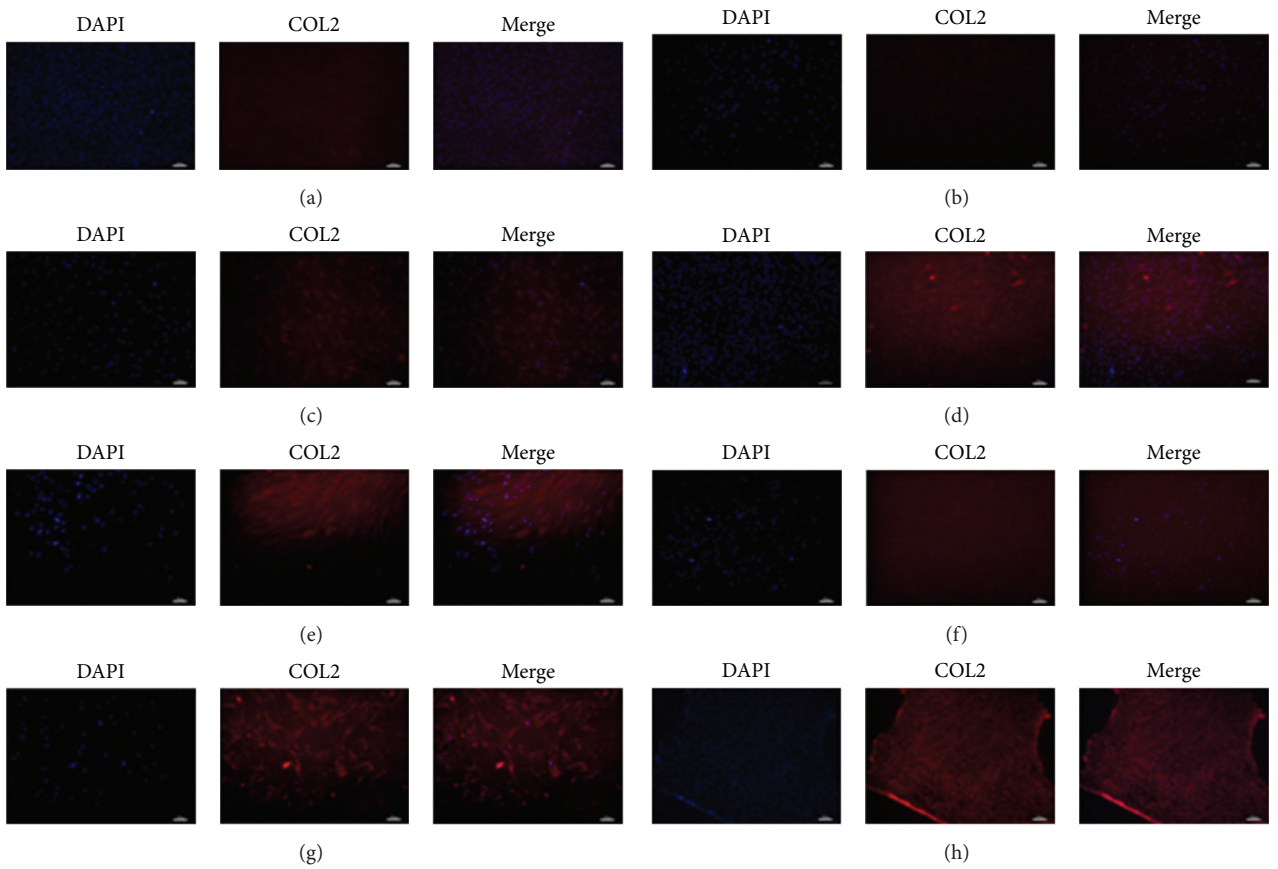

Figure 2: COL2 protein levels were characterized by immunofluorescence. Immunofluorescence staining of COL2 was shown in red. Nuclei were stained with DAPA (4′,6-diamidino-2-phenylindole, blue color). (a) hACs alone; (b) UCB-MSCs alone; (c) hUCB-MSCs cultured with growth factors; (d) direct coculture (1 : 1); (e) direct coculture (3 : 1); (f) direct coculture (5 : 1); (g) indirect coculture (UCB-MSCs); and (h) indirect coculture (hACs). Scale bar is 100 μm. $N = 5$.

($P < 0.05$, Figure 3(A)). *Col2a1* and *Col1a1* expression in the direct cell-cell contact group was significantly upregulated relative to hACs alone (Figures 3(B) and 3(C)). Interesting, the *Col2a1* expression in indirect coculture did not show any significant change relative to hACs and the *Col2a1* expression was higher in the direct group than in the indirect coculture group. The hUCB-MSCs and hACs cocultured with direct cell-cell contact at the ratio of 3 : 1 had the highest *Col2a1* expression overall (Figure 3(C)).

3.4. Analysis of Chondrocyte and Cartilage-Matrix-Related Protein Production. To evaluate chondrogenesis in all groups, the production of chondrocyte marker proteins COL2, COL1, and SOX9 were analyzed by western blotting after 3 weeks of *in vitro* culture. SOX9 and COL2 proteins were upregulated in both direct cell-cell contact and indirect contact cocultures relative to monocultures. All three proteins were more abundant in cocultures with indirect cell-cell contact than in hUCB-MSC monoculture with supplemented growth factors, which actually had the lowest COL2 and SOX9 levels of any group. COL1 levels were highest in hAC monoculture, while indirect cell-cell contacted groups presented higher COL2 content than other groups (Figure 4).

3.5. ELISA Quantification of TGF-β1. The TGF-β1 protein expression level secreted into the medium was measured using ELISA after 3 weeks of *in vitro* culture. Secreted TGF-β1 was significantly upregulated in direct cell-cell contact coculture relative to hUCB-MSC monoculture supplemented with growth factors, which in turn was higher than in the indirect contact coculture ($P < 0.01$). TGF-β1 levels in indirect contact coculture were comparable to those in hACs cultured alone. The hUCB-MSC monoculture had the lowest TGF-β1 levels out of all groups. TGF-β1 concentration in the 3 : 1 direct contact coculture was highest among the groups tested (Figure 5).

3.6. CCK-8 Analysis of Cell Proliferation. Total cellular proliferation in each of the different coculture conditions and with supplemental growth factors was quantified using a CCK-8 cell proliferation assay after 15 days of *in vitro* culture. The cell proliferation rates in the direct and indirect cell-cell contact coculture and hACs monoculture were similar. Cell proliferation was significantly stimulated in both coculture conditions and hAC monoculture relative to hUCB-MSC monoculture with growth factors, which had the lowest cell proliferation rate. Cellular proliferation in the direct cell-cell

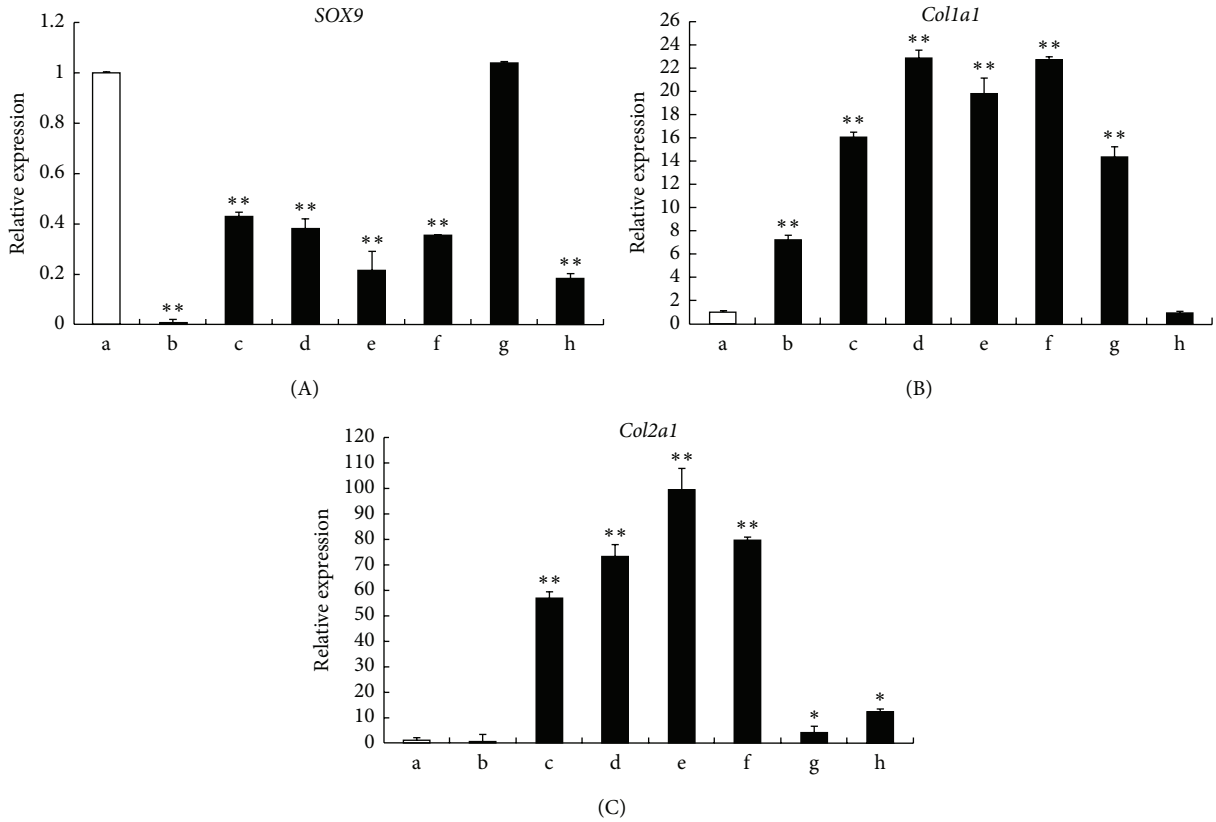

Figure 3: Gene expression was quantified with quantitative polymerase chain reaction. (A) SOX9, (B) Col1a1, and (C) Col2a1. Statistically significant differences were found by one-way ANOVA in all three genes ($^{**}P < 0.01$). (a) hACs alone; (b) UCB-MSCs alone; (c) hUCB-MSCs cultured with growth factors; (d) direct coculture (1 : 1); (e) direct coculture (3 : 1); (f) direct coculture (5 : 1); (g) indirect coculture (UCB-MSCs); and (h) indirect coculture (hACs).

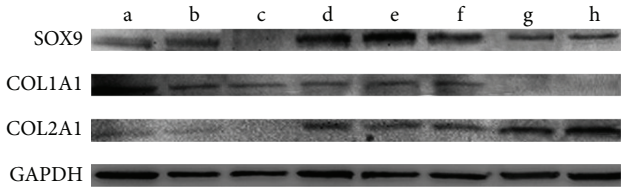

Figure 4: SOX9, COL2, and COL1 protein levels were detected by western blotting. (a) hACs alone; (b) UCB-MSCs alone; (c) hUCB-MSCs cultured with growth factors; (d) direct coculture (1 : 1); (e) direct coculture (3 : 1); (f) direct coculture (5 : 1); (g) indirect coculture (UCB-MSCs); and (h) indirect coculture (hACs).

contact coculture at a ratio of 3 : 1 hUCB-MSCs to hACs was the greatest of all the tested conditions (Figure 6).

4. Discussion

Over the last two decades, there have been great improvements in the tissue engineering field for clinical repair of cartilage defects using autologous chondrocytes. However, the loss of phenotypic functions during chondrocyte expansion in monolayer culture has led to the search for an alternative cell source for cartilage tissue engineering. For example, BMSCs are currently undergoing trials for clinical practice in articular cartilage repair. However, BMSCs collection needs an invasive and painful process. hUCB-MSCs have numerous advantages over BMSCs, including convenient collection, better retention of their multipotency over several passages, reduced immunogenicity, absence of tumor cell contamination, and lower risk of latent virus and pathogenic microorganism transmission.

The hUCB-MSCs can be easily induced to differentiate into mature bone and cartilage cells by stimulation with growth factors, particularly with members of the TGF-β superfamily. Consistent with previous studies, chondrogenic induction by TGF-β1 and ITS could differentiate hUCB-MSCs into chondrocytes *in vitro*, although these cultures exhibited a fibrotic phenotype and limited cell proliferation rate after chondrogenic induction. In our study, COL1A1, a fibrosis marker, was significantly upregulated in hUCB-MSCs cultured with growth factors. The presence of type I collagen could impair the development of cartilage-specific matrix architecture and result in functional impairment. Therefore, our findings indicate that the commonly used chondrogenic induction medium for hUCB-MSCs is not optimal for cartilage regeneration and a better strategy to provide a more stringent control of hUCB-MSC chondrogenic differentiation can be achieved.

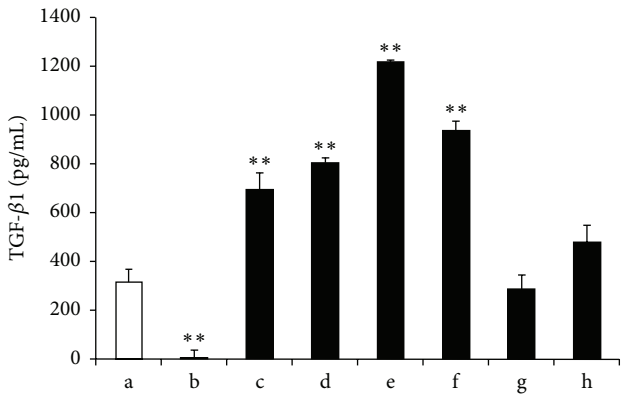

Figure 5: TGF-β1 secreted into the medium was measured using ELISA. Statistically significant differences were found by one-way ANOVA in TGF-β1 concentration. (a) hACs alone; (b) UCB-MSCs alone; (c) hUCB-MSCs cultured with growth factors; (d) direct coculture (1 : 1); (e) direct coculture (3 : 1); (f) direct coculture (5 : 1); (g) indirect coculture (UCB-MSCs); and (h) indirect coculture (hACs). $^{**}P < 0.01$.

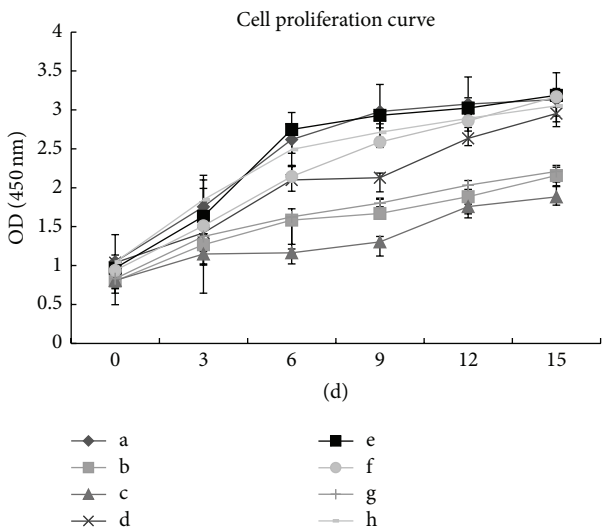

Figure 6: Analysis of cell proliferation. Statistically significant differences were found by one-way ANOVA. (a) hACs alone; (b) UCB-MSCs alone; (c) hUCB-MSCs cultured with growth factors; (d) direct coculture (1 : 1); (e) direct coculture (3 : 1); (f) direct coculture (5 : 1); (g) indirect coculture (UCB-MSCs); and (h) indirect coculture (hACs).

Recently, coculture systems for MSCs and chondrocytes were developed to enhance the chondrogenesis of MSCs [42]. Previous reports have demonstrated that coculture of hUCB-MSCs and rabbit chondrocytes could induce greater differentiation of hUCB-MSCs into chondrocytes [21]. However, the ratio of hUCB-MSCs to chondrocytes is an important element in coculture systems, and establishing the optimal ratio is crucial to successful coculturing and construction of cartilage tissue engineering [29]. But these methods barely exhibit the primary culture of hUCB-MSCs at low densities ($\leq 10^4$ cells/cm^2) for 1 month. We knew that the lower the cell density is, the more difficult it is to maintain the cells in culture. In this study, we performed the low density of hUCB-MSCs at 0.6×10^4 cells/cm^2. The density at 2.4×10^6 cells/cm^2 used by Zhang et al. was much higher than that (about 400-fold) adopted in our study. Our studies showed that low density coculture could induce hUCB-MSCs differentiation into chondrocytes, which resulted in high levels of COL2A1 mRNA and protein as well as increased COL1 expression. Thus, low density direct cell-cell contact could stimulate fibrocartilage-associated Col1a1 expression, which cannot meet the goal of hyaline cartilage for cartilage repair. However, compared with direct coculture, COL-1 expression was lower in the indirect coculture group. Interestingly, western blotting result showed that indirect coculture enhanced COL-2 expression while it inhibited COL-1 expression. Indirect coculture expresses type II collagen but not type I collagen, suggesting that indirect coculture has potential to induce hUCB-MSC differentiation into hyaline chondrocytes.

The mechanisms that contribute to enhancement of chondrogenesis in this hUCB-MSC and chondrocyte coculture system are unclear. Previous studies have shown the crucial role of the signaling cascade activated by TGF-β, which promotes the expression of genes specific to cartilage [23]. In several coculture experiments without direct cell-cell contact, TGF-β or other soluble factors alone contribute to cartilage-matrix formation and promote chondrogenic differentiation of MSCs [29]. Based on our *in vitro* studies, we found that hUCB-MSCs and hACs cocultured with direct cell-cell contact at ratio of 3 : 1 could secrete large amounts of TGF-β1. However, the relative importance of TGF-β1 and direct cell-cell contact in enhancing cartilage-matrix formation remains unclear. In this study, the concentration of TGF-β1 quantified by ELISA in culture media was generally much lower than that used for conventional chondrogenic induction and is most likely too low to induce efficient chondrogenic differentiation of MSCs on their own [24]. Although direct coculture secreted more TGF-β1 compared to indirect coculture, the Col1a1 expression was high, which means that the role of TGF-β1 may be also involved in the induced Col1a1 expression. And we found different expression levels of SOX9 between direct coculture and indirect coculture. Thus SOX9 may be involved in the induced chondrogenic differentiation of indirect coculture group. Additional studies have shown that SOX9 facilitates the COL2 expression, which promotes chondrogenesis [43], while another study found that SOX9 overexpression at high levels could exert an inhibitory effect on Col1a1 gene expression [44]. In this study, the SOX9 expression is higher in indirect coculture than in direct coculture or growth factor-inducing group. And the indirect coculture shows more COL2 expression. Thus, we presume that appropriate SOX9 in indirect coculture group could play an essential role in hUCB-MSC differentiation into chondrocytes and maintain chondrocytes phenotype. However, the exact role of SOX9 in coculture remains undefined, which needs further investigation.

In conclusion, indirect coculture at low density has potential to induce hUCB-MSC differentiation into hyaline

chondrocytes. TGF-β1 may play a role in direct coculture that induces hUCB-MSCs into chondrocytes. SOX9 may be involved in the indirect coculture system that induces hUCB-MSCs into chondrocytes. Indirect coculture at low density could be a promising approach for repair of cartilage lesions.

Ethical Approval

All the studies were approved by Shenzhen Second People's Hospital.

Competing Interests

The authors declare that they have no conflict of interests.

Acknowledgments

This work was supported by the National Natural Science Foundation of China (nos. 81572198 and 81260161), the Natural Science Foundation of Guangdong Province, China (no. 2015A030313772), the Medical Research Foundation of Guangdong Province, China (no. A2016314), and the Shenzhen Science and Technology Innovation Committee (Projects nos. JCYJ20160301111338144, JSGG20151030140325149, JSGG20140519105550503, JCYJ20140414170821200, and JCYJ20140414170821160).

References

[1] E. A. Makris, A. H. Gomoll, K. N. Malizos, J. C. Hu, and K. A. Athanasiou, "Repair and tissue engineering techniques for articular cartilage," *Nature Reviews Rheumatology*, vol. 11, no. 1, pp. 21–34, 2015.

[2] V. V. Kedage, S. Y. Sanghavi, A. Badnre, and N. S. Desai, "Autologous chondrocyte implantation (ACI): an innovative technique for articular cartilage defects," *Journal of Clinical Orthopaedics and Trauma*, vol. 1, no. 1, pp. 33–36, 2010.

[3] K. Elima and E. Vuorio, "Expression of mRNAs for collagens and other matrix components in dedifferentiating and redifferentiating human chondrocytes in culture," *FEBS Letters*, vol. 258, no. 2, pp. 195–198, 1989.

[4] Y.-H. Yang, A. J. Lee, and G. A. Barabino, "Coculture-driven mesenchymal stem cell-differentiated articular chondrocyte-like cells support neocartilage development," *Stem Cells Translational Medicine*, vol. 1, no. 11, pp. 843–854, 2012.

[5] N. Kang, X. Liu, Y. Guan et al., "Effects of co-culturing BMSCs and auricular chondrocytes on the elastic modulus and hypertrophy of tissue engineered cartilage," *Biomaterials*, vol. 33, no. 18, pp. 4535–4544, 2012.

[6] X. He, B. Feng, C. Huang et al., "Electrospun gelatin/polycaprolactone nanofibrous membranes combined with a coculture of bone marrow stromal cells and chondrocytes for cartilage engineering," *International Journal of Nanomedicine*, vol. 10, pp. 2089–2099, 2015.

[7] C. Buhrmann, A. Mobasheri, U. Matis, and M. Shakibaei, "Curcumin mediated suppression of nuclear factor-κB promotes chondrogenic differentiation of mesenchymal stem cells in a high-density co-culture microenvironment," *Arthritis Research & Therapy*, vol. 12, no. 4, article R127, 2010.

[8] A. Lindenmair, T. Hatlapatka, G. Kollwig et al., "Mesenchymal stem or stromal cells from amnion and umbilical cord tissue and their potential for clinical applications," *Cells*, vol. 1, no. 4, pp. 1061–1088, 2012.

[9] V. V. Meretoja, R. L. Dahlin, F. K. Kasper, and A. G. Mikos, "Enhanced chondrogenesis in co-cultures with articular chondrocytes and mesenchymal stem cells," *Biomaterials*, vol. 33, no. 27, pp. 6362–6369, 2012.

[10] E. J. Levorson, M. Santoro, F. Kurtis Kasper, and A. G. Mikos, "Direct and indirect co-culture of chondrocytes and mesenchymal stem cells for the generation of polymer/extracellular matrix hybrid constructs," *Acta Biomaterialia*, vol. 10, no. 5, pp. 1824–1835, 2014.

[11] A. R. Rothenberg, L. Ouyang, and J. H. Elisseeff, "Mesenchymal stem cell stimulation of tissue growth depends on differentiation state," *Stem Cells and Development*, vol. 20, no. 3, pp. 405–414, 2011.

[12] F. Ghobadi, D. Mehrabani, and G. Mehrabani, "Regenerative potential of endometrial stem cells: a mini review," *World Journal of Plastic Surgery*, vol. 4, no. 1, pp. 3–8, 2015.

[13] D. Bhartiya, "Stem cells, progenitors & regenerative medicine: a retrospection," *Indian Journal of Medical Research*, vol. 141, pp. 154–161, 2015.

[14] J. A. Andrades, J. Becerra, R. Muñoz-Chápuli et al., "Stem cells therapy for regenerative medicine: principles of present and future practice," *Journal of Biomedical Science and Engineering*, vol. 7, no. 2, pp. 49–57, 2014.

[15] M. Raoufi, P. Tajik, M. Dehghan, F. Eini, and A. Barin, "Isolation and differentiation of mesenchymal stem cells from bovine umbilical cord blood," *Amsterdamer Beitrage zur Neueren Germanistik*, vol. 46, pp. 95–99, 2010.

[16] P. V. Pham, N. B. Vu, V. M. Pham et al., "Good manufacturing practice-compliant isolation and culture of human umbilical cord blood-derived mesenchymal stem cells," *Journal of Translational Medicine*, vol. 12, article 56, pp. 1–10, 2014.

[17] K. Cooper, A. SenMajumdar, and C. Viswanathan, "Derivation, expansion and characterization of clinical grade mesenchymal stem cells from umbilical cord matrix using cord blood serum," *International Journal of Stem Cells*, vol. 3, no. 2, pp. 119–128, 2010.

[18] R. L. Dahlin, M. Ni, V. V. Meretoja, F. K. Kasper, and A. G. Mikos, "TGF-β3-induced chondrogenesis in co-cultures of chondrocytes and mesenchymal stem cells on biodegradable scaffolds," *Biomaterials*, vol. 35, no. 1, pp. 123–132, 2014.

[19] A. Saraf and A. G. Mikos, "Gene delivery strategies for cartilage tissue engineering," *Advanced Drug Delivery Reviews*, vol. 58, no. 4, pp. 592–603, 2006.

[20] J. Fischer, A. Dickhut, M. Rickert, and W. Richter, "Human articular chondrocytes secrete parathyroid hormone-related protein and inhibit hypertrophy of mesenchymal stem cells in coculture during chondrogenesis," *Arthritis & Rheumatism*, vol. 62, no. 9, pp. 2696–2706, 2010.

[21] P. Zheng, L. Ju, B. Jiang et al., "Chondrogenic differentiation of human umbilical cord blood-derived mesenchymal stem cells by co-culture with rabbit chondrocytes," *Molecular Medicine Reports*, vol. 8, no. 4, pp. 1169–1182, 2013.

[22] Z. Feng, W. Ying-Zhen, Z. Hai-Ning, L. Cheng-Yu, and X. Zong-Yao, "Differentiation of human umbilical cord blood derived-mesenchymal stem cells into chondrocytes induced by supernatants of human chondrocytes," *Journal of Clinical Rehabilitative Tissue Engineering Research*, vol. 17, pp. 7034–7039, 2013.

[23] C. S. De Mara, A. S. S. Duarte, A. Sartori, A. C. Luzo, S. T. O. Saad, and I. B. Coimbra, "Regulation of chondrogenesis by transforming growth factor-β_3 and insulin-like growth factor-1 from human mesenchymal umbilical cord blood cells," *Journal of Rheumatology*, vol. 37, no. 7, pp. 1519–1526, 2010.

[24] X. Liu, H. Sun, D. Yan et al., "*In vivo* ectopic chondrogenesis of BMSCs directed by mature chondrocytes," *Biomaterials*, vol. 31, no. 36, pp. 9406–9414, 2010.

[25] T. G. Koch, T. Heerkens, P. D. Thomsen, and D. H. Betts, "Isolation of mesenchymal stem cells from equine umbilical cord blood," *BMC Biotechnology*, vol. 7, article 26, pp. 1–9, 2007.

[26] M.-S. Seo, Y.-H. Jeong, J.-R. Park et al., "Isolation and characterization of canine umbilical cord blood-derived mesenchymal stem cells," *Journal of Veterinary Science*, vol. 10, pp. 181–187, 2009.

[27] D. H. Rosenzweig, M. Matmati, G. Khayat, S. Chaudhry, B. Hinz, and T. M. Quinn, "Culture of primary bovine chondrocytes on a continuously expanding surface inhibits dedifferentiation," *Tissue Engineering Part A*, vol. 18, no. 23-24, pp. 2466–2476, 2012.

[28] B.-J. Kang, H.-H. Ryu, S. S. Park et al., "Comparing the osteogenic potential of canine mesenchymal stem cells derived from adipose tissues, bone marrow, umbilical cord blood, and Wharton's jelly for treating bone defects," *Journal of Veterinary Science*, vol. 13, no. 3, pp. 299–310, 2012.

[29] Y.-H. Yang, A. J. Lee, and G. A. Barabino, "Coculture-Driven Mesenchymal Stem Cell-differentiated articular chondrocyte-like cells support neocartilage development," *Stem Cells Translational Medicine*, vol. 1, no. 11, pp. 843–854, 2012.

[30] M. E. Cooke, A. A. Allon, T. Cheng et al., "Structured three-dimensional co-culture of mesenchymal stem cells with chondrocytes promotes chondrogenic differentiation without hypertrophy," *Osteoarthritis and Cartilage*, vol. 19, no. 10, pp. 1210–1218, 2011.

[31] S. Giovannini, J. Diaz-Romero, T. Aigner, P. Heini, P. Mainil-Varlet, and D. Nesic, "Micromass co-culture of human articular chondrocytes and human bone marrow mesenchymal stem cells to investigate stable neocartilage tissue formation in vitro," *European Cells and Materials*, vol. 20, pp. 245–259, 2010.

[32] S. Boeuf and W. Richter, "Chondrogenesis of mesenchymal stem cells: role of tissue source and inducing factors," *Stem Cell Research & Therapy*, vol. 1, no. 4, article 31, 2010.

[33] M. Wang, Y. Yang, D. Yang et al., "The immunomodulatory activity of human umbilical cord blood-derived mesenchymal stem cells in vitro," *Immunology*, vol. 126, no. 2, pp. 220–232, 2009.

[34] M. Soleimani, L. Khorsandi, A. Atashi, and F. Nejaddehbashi, "Chondrogenic differentiation of human umbilical cord blood-derived unrestricted somatic stem cells on a 3D beta-tricalcium phosphate-alginate-gelatin scaffold," *Cell Journal*, vol. 16, no. 1, pp. 43–52, 2014.

[35] K. Ma, A. L. Titan, M. Stafford, C. H. Zheng, and M. E. Levenston, "Variations in chondrogenesis of human bone marrow-derived mesenchymal stem cells in fibrin/alginate blended hydrogels," *Acta Biomaterialia*, vol. 8, no. 10, pp. 3754–3764, 2012.

[36] L. Wu, J. Leijten, C. A. van Blitterswijk, and M. Karperien, "Fibroblast growth factor-1 is a mesenchymal stromal cell-secreted factor stimulating proliferation of osteoarthritic chondrocytes in co-culture," *Stem Cells and Development*, vol. 22, no. 17, pp. 2356–2367, 2013.

[37] Q. Chang, W.-D. Cui, and W.-M. Fan, "Co-culture of chondrocytes and bone marrow mesenchymal stem cells in vitro enhances the expression of cartilaginous extracellular matrix components," *Brazilian Journal of Medical and Biological Research*, vol. 44, no. 4, pp. 303–310, 2011.

[38] J. S. Kang, T. Alliston, R. Delston, and R. Derynck, "Repression of Runx2 function by TGF-β through recruitment of class II histone deacetylases by Smad3," *The EMBO Journal*, vol. 24, no. 14, pp. 2543–2555, 2005.

[39] P. Li, X. Wei, Y. Guan et al., "MicroRNA-1 regulates chondrocyte phenotype by repressing histone deacetylase 4 during growth plate development," *The FASEB Journal*, vol. 28, no. 9, pp. 3930–3941, 2014.

[40] M. H. Maurer, "Proteomic definitions of mesenchymal stem cells," *Stem Cells International*, vol. 2011, Article ID 704256, 9 pages, 2011.

[41] T. Revencu, V. Trifan, L. Nacu et al., "Collection, isolation and characterization of the stem cells of umbilical cord blood," *Romanian Journal of Morphology and Embryology*, vol. 54, no. 2, pp. 291–297, 2013.

[42] D.-A. Yu, J. Han, and B.-S. Kim, "Stimulation of chondrogenic differentiation of mesenchymal stem cells," *International Journal of Stem Cells*, vol. 5, no. 1, pp. 16–22, 2012.

[43] S. Kishi, H. Abe, H. Akiyama et al., "SOX9 protein induces a chondrogenic phenotype of mesangial cells and contributes to advanced diabetic nephropathy," *The Journal of Biological Chemistry*, vol. 286, no. 37, pp. 32162–32169, 2011.

[44] M. Kypriotou, M. Fossard-Demoor, C. Chadjichristos et al., "SOX9 exerts a bifunctional effect on type II collagen gene (COL2A1) expression in chondrocytes depending on the differentiation state," *DNA and Cell Biology*, vol. 22, no. 2, pp. 119–129, 2003.

Hindawi Publishing Corporation
BioMed Research International
Volume 2016, Article ID 6040146, 7 pages
http://dx.doi.org/10.1155/2016/6040146

Research Article

Open-Porous Hydroxyapatite Scaffolds for Three-Dimensional Culture of Human Adult Liver Cells

Anthony Finoli,[1] Eva Schmelzer,[2] Patrick Over,[2] Ian Nettleship,[1] and Joerg C. Gerlach[2,3]

[1]*Department of Mechanical Engineering and Materials Science, University of Pittsburgh, Pittsburgh, PA 15261, USA*
[2]*Department of Surgery, McGowan Institute for Regenerative Medicine, University of Pittsburgh, Pittsburgh, PA 15203, USA*
[3]*Department of Bioengineering, McGowan Institute for Regenerative Medicine, University of Pittsburgh, Pittsburgh, PA 15203, USA*

Correspondence should be addressed to Anthony Finoli; anthony.d.finoli@gmail.com

Received 24 February 2016; Accepted 25 May 2016

Academic Editor: Subhas C. Kundu

Liver cell culture within three-dimensional structures provides an improved culture system for various applications in basic research, pharmacological screening, and implantable or extracorporeal liver support. Biodegradable calcium-based scaffolds in such systems could enhance liver cell functionality by providing endothelial and hepatic cell support through locally elevated calcium levels, increased surface area for cell attachment, and allowing three-dimensional tissue restructuring. Open-porous hydroxyapatite scaffolds were fabricated and seeded with primary adult human liver cells, which were embedded within or without gels of extracellular matrix protein collagen-1 or hyaluronan. Metabolic functions were assessed after 5, 15, and 28 days. Longer-term cultures exhibited highest cell numbers and liver specific gene expression when cultured on hydroxyapatite scaffolds in collagen-1. Endothelial gene expression was induced in cells cultured on scaffolds without extracellular matrix proteins. Hydroxyapatite induced gene expression for cytokeratin-19 when cells were cultured in collagen-1 gel while culture in hyaluronan increased cytokeratin-19 gene expression independent of the use of scaffold in long-term culture. The implementation of hydroxyapatite composites with extracellular matrices affected liver cell cultures and cell differentiation depending on the type of matrix protein and the presence of a scaffold. The hydroxyapatite scaffolds enable scale-up of hepatic three-dimensional culture models for regenerative medicine applications.

1. Introduction

Culture of liver cells within three-dimensional (3D) structures provides improved *in vitro* systems for studying hepatic cell differentiation and proliferation. The unfulfilled demand for donor organs for transplantation in chronic liver disease suggests that the development of engineered tissue transplants is necessary to provide additional metabolic capacity. Regenerative medicine techniques are currently being investigated to supplement the need for transplantable tissue. Though the developments are promising, many aspects of such technologies and procedures must be examined. Chief among the unsolved problems is the need for procedures addressing the supply of human liver tissue and cells [1], most likely expanded by proliferation *in vitro* [2]. Once such a cell source has been identified, further applications could be of interest, such as extracorporeal liver support in acute liver failure [3] and pharmacologic *in vitro* screening of hepatic drug candidates [4, 5].

Early mouse liver cell cultures were introduced in monolayer by Evans et al. in the 1950s [6]. Later on, liver cell cultures in suspensions were developed [7]. With the introduction of extracellular matrices as dish coatings for monolayer cultures, the early loss of hepatic functions and viability in culture was somewhat improved. Liver relevant extracellular matrices such as laminin, various collagen types, hyaluronic acid hydrogel, and matrigel were implemented [8–13]. The use of sandwich culture [14–16], that is, the embedding of liver cells between two layers of collagen, was an important step in the enhancement of liver cell culture by mimicking the *in vivo* liver plate architecture. To realistically grow liver tissue from adult liver cells at higher densities and thus approach a more natural tissue situation, the use of a three-dimensional scaffold is advisable and a scale-up

of such techniques may support the cells in cultures at a size suitable for clinical use. Such a scaffold structure must have a high porosity to facilitate cell seeding and fluid flow for mass exchange around the cells but also allow sufficient space for neoendothelialized structures, while being rigid enough to structurally support the mass of the growing tissue.

Ceramic foaming techniques have been developed to create such highly porous, permeable structures [17–19]. Biocompatible calcium phosphates, specifically hydroxyapatite, have successfully been used as scaffolds for culturing several different cell types including liver cells from both human and rat sources [20, 21]. Calcium phosphate ceramics can also be manufactured to be bioresorbable by using tricalcium phosphate or taking advantage of a high temperature decomposition of hydroxyapatite to resorbable calcium phosphate phases. In the present study, we have analyzed two different extracellular matrix proteins, collagen-1 and hyaluronic acid, in combination with previously developed porous hydroxyapatite scaffolds [19]. We investigated the influence of these conditions on longer-term cultures of human adult liver cells to create scaled-up tissue structures.

2. Materials and Methods

2.1. Cell Culture. Hydroxyapatite foam scaffolds were prepared from a 1 mm thick section of an emulsion foam as described in previous work [19]. Scaffolds were placed in polystyrene tissue culture plates (Becton Dickinson Biosciences) and were sterilized by autoclaving. Human total fresh liver cell suspensions from male donors were obtained from discarded grafts (Becton Dickinson Biosciences, Woburn, MA) and cell viability was determined by trypan blue exclusion. Cell number was counted in a Neubauer chamber. The cells were applied to the scaffolds either directly without extracellular matrix, or embedded in extracellular matrix protein. Two different gels of extracellular matrix proteins were prepared for the study. Hyaluronan gel (Glycosan, Alameda, CA) was prepared by dissolving freeze-dried hyaluronan in 1 mL of sterile water at 37°C. To decrease gelation time, a cross-linker (extralink) was added, and the prepared cell fraction was suspended in the mixture at a concentration of 1E6 cells/mL of gel. Collagen-1 gel was prepared by mixing rat-tail collagen type 1 (Becton Dickinson Biosciences) with sterile water, sterile 10x PBS, and sterile 1 M NaOH according to manufacturer's protocol. Cells were suspended at a concentration of 1E6 cells/mL of gel. To each well of a culture plate containing either scaffold or no scaffold, 250 μL of the cell mixtures was added and set at 37°C within 30 minutes. Controls included also cells suspended in 250 μL culture medium without addition of extracellular matrix protein. Again the concentration was 1E6 cells/mL per well. Additionally, 250 μL of supplemented Williams E medium was added to each well. Williams E medium (Life Technologies, Carlsbad, CA) was supplemented with 10% fetal bovine serum, antibiotic/antimycotic mix, 2 mM glutamax (all Life Technologies), 5 μg/L insulin, 10 μg/L transferrin, 30 nM selenium, and 100 nM hydrocortisone (all Sigma-Aldrich, St. Louis, MO). The medium was replaced every 2 to 3 days during culture and the aspirate was saved for future protein analysis. For all experiments, cultures were kept for 5, 15, and 28 days and there were 6 biological repeats, each from a different donor.

2.2. Albumin Enzyme-Linked Immunosorbent Assay. A standard albumin sandwich enzyme-linked immunosorbent assay was used to measure secreted albumin in medium samples. MaxiSorp Immunoplates (Nalgene Nunc International, Penfield, NY) were absorbed with anti-human albumin antibody (Bethyl Laboratories), incubated with samples or standards (Bethyl Laboratories, Montgomery, TX), and conjugated with a goat anti-human albumin horseradish-peroxidase-conjugated antibody (Bethyl Laboratories). Tetramethylbenzidine substrate solution was incubated for 5 min, the enzymatic reaction was stopped with 2 M sulfuric acid (Fisher Scientific, Pittsburgh, PA), and absorbance was read at 450 nm with a Synergy H1 hybrid reader equipped with Gen5 software version 2.00 (Bio-Tek, Winooski, VT). To quantify albumin secretion of cells in culture at longer time points (days 18–28), a linear regression was completed on the data for each sample and for each condition; ANOVA was calculated with the null hypothesis being a slope of 0 (no secretion). A p value of 0.05 was considered statistically significant.

2.3. DNA Quantification and Gene Expression Analysis. DNA was quantified to determine cell numbers of cultures, and RNA was extracted for gene expression analyses. Total DNA and RNA were extracted from cells using the AllPrep DNA/RNA Mini Kit (Qiagen, Valencia, CA). Cells were disrupted in lysis buffer of the kit on QIAshredder columns (Qiagen). Isolated DNA was quantified using the Quant-iT dsDNA BR Assay Kit on a Qubit fluorometer and compared to a sample containing 1E6 human adult liver cells from the donor. RNA was reverse transcribed to cDNA with the High-Capacity cDNA Reverse Transcription Kit (Applied Biosystems). Real-time polymerase chain reaction (PCR) was carried out using the StepOnePlus Real-Time PCR-System equipped with StepOne Software version 2.0 (Applied Biosystems). Predesigned TaqMan probes and primer sets were obtained from Applied Biosystems and used to quantify gene expression for vWF, CK19, CYP3A4, albumin, ASMA, and beta-actin using the ddCt method. Data were normalized against beta-actin expression. Negative PCR controls included no template (water).

2.4. Immunocytochemistry. At each of the three time points, cell culture samples were fixed with 4% para-formaldehyde (Sigma-Aldrich). Portions of these cultures were blocked with 10% goat serum (Sigma-Aldrich) and 1% FCR block (Miltenyi Biotec, Auburn, CA) in phosphate-buffered saline and stained with diamidino-phenylindole dihydrochloride (Sigma-Aldrich) for cell nuclei and AF568-conjugated phalloidin for intracellular actin filaments (Life Technologies). To evaluate CK19 expression cells were stained with mouse anti-CK19 primary antibody (Fisher Scientific) and AF488-conjugated goat anti-mouse secondary antibody (Life Technologies). To examine endothelial cells in culture separate portions were stained with rabbit anti-vWF primary antibody

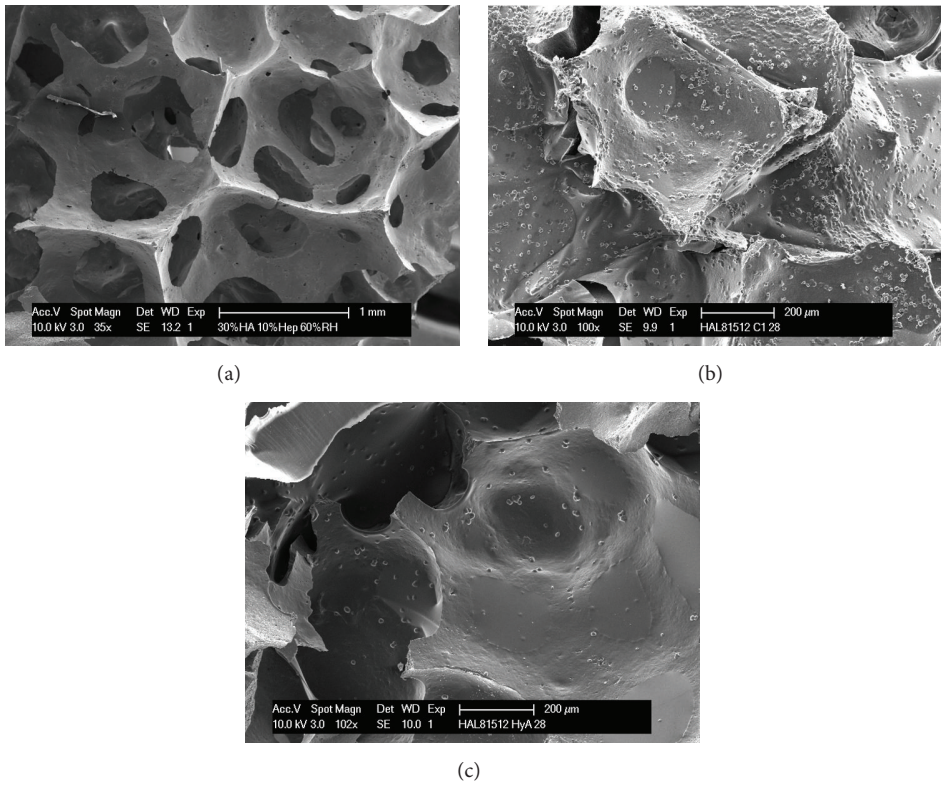

(a) (b)

(c)

Figure 1: Scanning electron microscopy. Porous foamed hydroxyapatite scaffolds (a) were used for cell culture. After 28 days of culture, numerous cells attached to the scaffold could be observed in cultures with collagen-1 (b), whereas considerably less cells were attached to scaffolds in culture with hyaluronan (c).

(Abcam, Cambridge, MA) and AF488-conjugated goat anti-rabbit secondary antibody (Life Technologies). All stainings were analyzed by confocal microscopy using a Fluoview 1000 system (Olympus, Center Valley, PA).

3. Results

3.1. Cell Viability, Attachment, and Number. Human adult liver cell suspensions had viabilities of 65–83%.

After 28 days in culture, cells were analyzed for their attachment on hydroxyapatite scaffolds (Figure 1). In culture with collagen-1, numerous cells could be observed being attached on the scaffold (Figure 1(b)), whereas in culture with hyaluronan considerably fewer cells were attached on the scaffold (Figure 1(c)).

We also investigated cell numbers (based on DNA correlation) in the various culture conditions after 5, 15, and 28 days of culture (Figure 2). Cell numbers in all conditions decreased after 5 days of culture when compared to initial seeding numbers. After 28 days of culture, very few cells could be detected in hyaluronan cultures, both with and without hydroxyapatite scaffold, and were significantly lower than any other condition at day 15 and day 28 ($p < 0.05$). Conversely, cells cultured in collagen-1, both with and without scaffold,

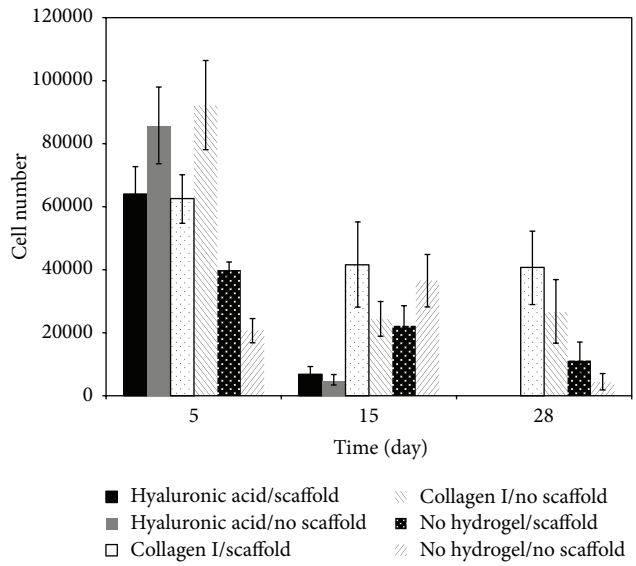

Figure 2: Numbers of liver cells in culture. Cells were cultured for 5, 15, and 28 days with (w) or without (wo) hydroxyapatite scaffolds embedded in hyaluronic acid gel (HyA), collagen-1 gel (C1), or no gel (NG), and cell numbers were determined by correlation with DNA concentration. Data are given as means from 6 biological repeats ± standard deviation.

Table 1: Gene expression of liver cell cultures.

Gene	Culture time (days)	Hyaluronic acid		Collagen I		No hydrogel	
		Scaffold	No scaffold	Scaffold	No scaffold	Scaffold	No scaffold
CK19	5	288.16	95.97	263.85	192.42	164.23	148.33
	15	453.34	202.45*	2063.79*	278.88	391.36	145.73
	28	873.87	791.60	1064.61	309.64	309.73	274.06
vWF	5	1.39	0.84	0.50	0.58	1.18	0.28
	15	0.078<	0.06<	0.93	1.65	4.27*	2.64*
	28	0.12	0.03	0.19<	0.34<	3.62	0.80<
CYP450 3A4	5	63.15	40.56	0.76	0.81	0.26	0.03
	15	5.35<	32.39	4.11	2.14	0.11	0.02
	28	41.87	39.76	0.04	0.04	0.02	0.02
Albumin	5	0.46	0.43	0.56	0.58	0.10	0.20
	15	2.03*	0.34	0.35	0.43	0.15	0.21
	28	0.27<	0.42	0.16	0.12	0.08	0.12
ASMA	5	0.00	0.55	24.62	36.62	17.57	14.69
	15	0.00	10.21*	4.06<	18.34	6.88	3.19<
	28	4.64*	0.00<	2.50	0.99<	1.50	1.37

Cells were cultured for 5, 15, and 28 days with (w) or without (wo) hydroxyapatite scaffolds embedded in hyaluronic acid gel (HyA), collagen-1 gel (C1), or no gel (NG), and gene expression was measured by PCR for cytokeratin-19 (CK19), Von Willebrand Factor (vWF), cytochrome P450 3A4 (CYP3A4), albumin, and Alpha-Smooth Muscle Actin (ASMA). Data are given as means from 6 biological repeats, normalized against beta-actin expression, and significance ($p < 0.05$) is marked by $*$ to indicate a value significantly greater than the previous time point and < to indicate a value significantly less than the previous time point.

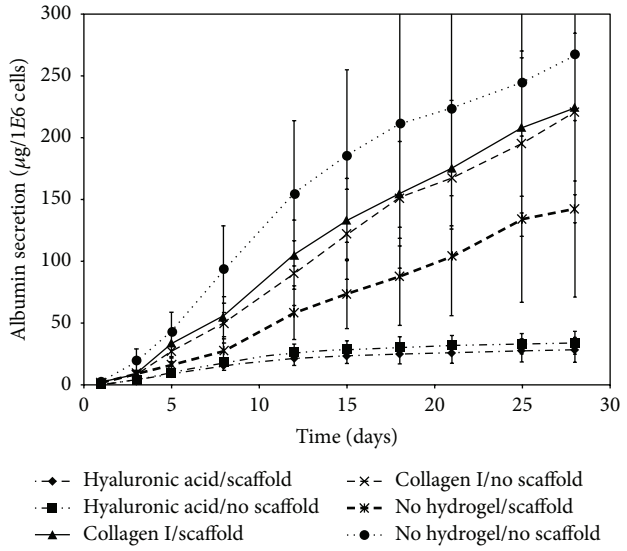

Figure 3: Albumin secretion of liver cell cultures. Cells were cultured for 5, 15, and 28 days with (w) or without (wo) hydroxyapatite scaffolds embedded in hyaluronic acid gel (HyA), collagen-1 gel (C1), or no gel (NG), and albumin secretion was measured by ELISA. Data are given as means from 6 biological repeats ± standard deviation.

showed constant cell numbers between 15 and 28 days. Cultures with the scaffolds were showing slightly higher cell numbers at 28 days than those without (40,643/well on average compared to 26,793/well).

3.2. Albumin ELISA. Albumin secretion of the cultures (Figure 3) varied between samples; however, certain trends developed that were consistent between donors. Of hydrogel conditions, culture in collagen-1 showed consistently higher overall secretion than in hyaluronan. In addition, when hydroxyapatite scaffold was not present the cells ceased significantly albumin secretion after day 15. During the last ten days of culture (days 18–28) only the cells cultured on hydroxyapatite in collagen-1 showed a significant increase in albumin secretion. ANOVA linear regressions of the data demonstrated a nonzero slope in cumulative albumin secretion ($p < 0.01$) in this condition showing significant secretion in the late stages of culture (78.5 ± 40.1 (μg/1E6 cells)/day). No other condition had a slope in cumulative albumin secretion significantly different from zero over the last 10 days of culture.

3.3. Gene Expression. Changes in expressions of genes specific for the various cell types of the liver were analyzed after different time points in culture; data are given relative to freshly isolated cells, which were set as 1. The expression of CK19, a biliary epithelium specific gene, was highly expressed in all samples (Table 1) throughout the 28-day experiment when compared to original cell suspensions. Cells cultured in collagen-1 on scaffolds had the highest expression; after 28 days cells cultured in collagen-1 with scaffold had an expression approximately 1000 times more than that of day 0 donor samples. For the other three conditions (cultures on collagen-1 without scaffold and both no-gel conditions), this expression was around 500 times that of day 0 donor cells and significantly less than cells cultured on collagen-1 with scaffold ($p < 0.05$). The expression of vWF, a mature endothelium specific marker, showed differences between samples (Table 1), with the highest expression after 15 and 28 days in cells cultured

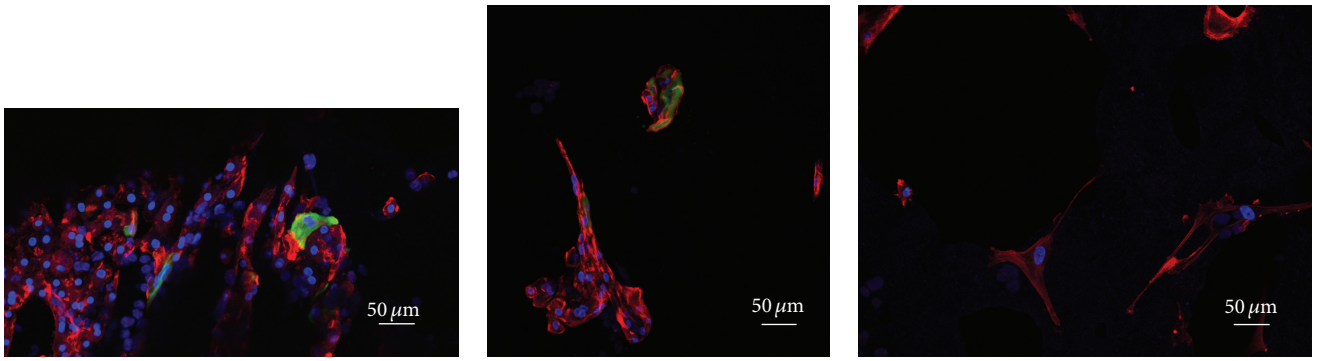

(a) (b) (c)

Figure 4: Immunocytochemistry of liver cell cultures. Liver cells were cultured for 28 days and stained, and images were taken by confocal microscopy. (a) Cells cultured in collagen-1 gel; (b) cells cultured in collagen-1 gel on hydroxyapatite scaffold; (c) cells cultured on hydroxyapatite scaffold only. Blue = DAPI, red = phalloidin, and green = CK19.

without any gel. Cells cultured without any gel on hydroxyapatite had the highest vWF expression, with expression maintained between day 15 and day 28 ($p < 0.05$). The expression of CYP3A4 (Table 1), a cytochrome P450 enzyme of mature hepatocytes, was highest in cultures with hyaluronan. Cells in hyaluronan maintained expression throughout the 28-day culture, significantly greater than all other conditions at day 28 ($p < 0.05$), and cells cultured in collagen-1 gel maintained expression through 15 days and lost expression after 28 days. Cells cultured without hydrogel downregulated expression of CYP3A4 in culture. The gene expression of albumin (Table 1), a secreted protein of mature hepatocytes, was highest in cells cultured in hyaluronan after 28 days, and always lowest in cultures without extracellular matrix addition. The expression of albumin is downregulated with the secretion of albumin, which is why cultures with high albumin secretion seen in ELISA results have lower gene expression. The downregulation of the expression of fibroblastic gene ASMA (Table 1) in most samples during culture suggests that there was no overgrowth of fibroblasts in culture.

3.4. Immunocytochemistry. Cells cultured in collagen-1 gel, regardless of the presence of hydroxyapatite, formed hepatocyte cordlike structures similar to liver plates (Figures 4(a) and 4(b)). Cells were found in small numbers in both hyaluronic acid and the no-gel conditions without the cordlike structures seen in cells cultured in collagen-1. In addition, both collagen-1 conditions also showed many cells positive for CK19 (Figures 4(a) and 4(b)). In those samples containing hydroxyapatite, ring-like structures of CK19 positive cells were found in a few instances (Figure 4(b)), similar to bile ductular structures *in vivo*. Cells cultured on scaffolds without collagen-1 exhibited a much different morphology with cells stretching out over the surface of the ceramic (Figure 4(c)).

4. Discussion

The use of hydroxyapatite ceramic scaffolds should have several advantages for the scale-up of cultures. Previously [18] we reported that a heat treatment process can be used to control the relative amounts of hydroxyapatite and tricalcium phosphate in calcium phosphate scaffolds. This could open new directions in the utilization of such resorbable scaffolds for implantable constructs, as tissue implants which could initially support neovascularization and subsequently disintegrate once perfused tissue is formed. The inherent local liberation of calcium may also be of interest for creation of local calcium gradients around cells immobilized near the scaffolds surface, as calcium is thought to support endothelial structure reformation. Calcium ions contribute to the maintenance of endothelial cells and also the formation of vascularized tissue [22]. Calcium ion concentration has been shown to affect proliferation of adult rat hepatocytes directly in a tight compositional range [23]; their highest proliferation rates *in vitro* were observed at physiological concentrations of 0.4 mM while lower or higher concentrations resulted in lower proliferation rates. Biodegradable ceramic scaffolds have even been seen to influence angiogenesis in bone marrow cell cultures by creating a localized calcium rich environment [24]. The three-dimensional scaffold itself can also be used to induce endothelial cells for culture of vascularized tissue constructs by creating a surface suitable for the actin filaments of the endothelial cells to attach, as well as providing a microenvironment suitable for cell proliferation [25, 26].

Few studies have been published using ceramic structures for liver cell cultures. Ceramic plate-like structures with circular cavities were developed, and rat hepatocytes were demonstrated to attach within the cavities [27]; however, cultures were maintained only for 24 h and no liver specific functions were analyzed. The applicability of cell-seeded hydroxyapatite scaffolds for potential future clinical transplantation studies has been demonstrated by rodent transplantation studies; hydroxyapatite scaffolds seeded with immortalized mouse liver cells were successfully transplanted into the omentum and kidney of mice [21]; transplantation of hydroxyapatite disks seeded with normal rat hepatocytes intraperitoneally into Nagase analbuminemic rats significantly increased albumin secretion within the host [20].

The usefulness of extracellular matrix proteins in the improvement of hepatic cell cultures has been widely discussed in the context of cell structures for implantation or bioreactors for temporary extracorporeal use [28] (for review, see [29]). Extracellular matrix proteins not only provide mechanical stability for cell constructs but also interact directly with cells through receptors influencing their cell type specific function. We used hyaluronan and collagen-1 hydrogels for our studies on establishing culture models involving hydroxyapatite, because these extracellular proteins have been used successfully to culture human adult hepatocytes and other primary cell types [13–15, 30–32]. Of the culture conditions examined, the maintenance of cells in culture was clearly best in the collagen-1/hydroxyapatite composite showing almost two times as many cells after 28 days compared with any other condition. These findings were also supported by the other parameters examined. Although gene expression of albumin, a secreted protein of mature hepatocytes, was highest in cells cultured in hyaluronan after 28 days, actual secretion of albumin protein (as measured by ELISA) was higher in collagen-1 culture. This fact can be explained by the known feedback mechanism of albumin protein on gene expression, by which gene expression of albumin is downregulated with the secretion of albumin protein [33], which is why cultures with high albumin secretion seen in ELISA results have lower gene expression. Collagen-1 hydrogels are a common culture model for liver cells because of the abundance in liver tissue [34, 35]. This extracellular matrix provides an environment on the lowest level of organ structure similar to native liver tissue and might be expected to be the best hydrogel for supporting the culture of adult liver cells *in vitro*. When cells were cultured on porous hydroxyapatite in collagen-1 the composite structure also provided improved cell maintenance during the last two weeks of culture, compared to the negative control and also the collagen-1 sandwich cultures of primary human hepatocytes found in the literature [31]. We have shown previously that such a three-dimensional condition supported hepatic cell differentiation and proliferation in perfusion culture [32, 36]. However, it must be noted that in the model used here the static conditions did not involve medium perfusion, which was found to further enhance culture longevity [37, 38].

Competing Interests

No competing interests were identified for all authors.

Acknowledgments

The authors thank the Center for Biological Imaging (CBI) at the University of Pittsburgh for its support. This study was funded by the National Institutes of Health (Grant no. 1R01HL108631).

References

[1] B. Gridelli, G. Vizzini, G. Pietrosi et al., "Efficient human fetal liver cell isolation protocol based on vascular perfusion for liver cell-based therapy and case report on cell transplantation," *Liver Transplantation*, vol. 18, no. 2, pp. 226–237, 2012.

[2] T. Miki, A. Ring, and J. Gerlach, "Hepatic differentiation of human embryonic stem cells is promoted by three-dimensional dynamic perfusion culture conditions," *Tissue Engineering Part C: Methods*, vol. 17, no. 5, pp. 557–568, 2011.

[3] J. C. Gerlach, K. Zeilinger, and J. F. Patzer II, "Bioartificial liver systems: why, what, whither?" *Regenerative Medicine*, vol. 3, no. 4, pp. 575–595, 2008.

[4] K. Zeilinger, T. Schreiter, M. Darnell et al., "Scaling down of a clinical three-dimensional perfusion multicompartment hollow fiber liver bioreactor developed for extracorporeal liver support to an analytical scale device useful for hepatic pharmacological in vitro studies," *Tissue Engineering—Part C: Methods*, vol. 17, no. 5, pp. 549–556, 2011.

[5] M. Lubberstedt, U. Muller-Vieira, K. M. Biemel et al., "Serum-free culture of primary human hepatocytes in a miniaturized hollow-fibre membrane bioreactor for pharmacological in vitro studies," *Journal of Tissue Engineering and Regenerative Medicine*, vol. 9, no. 9, pp. 1017–1026, 2015.

[6] V. J. Evans, W. R. Earle, E. P. Wilson, H. K. Waltz, and C. J. Mackey, "The growth in vitro of massive cultures of liver cells," *Journal of the National Cancer Institute*, vol. 12, no. 6, pp. 1245–1265, 1952.

[7] L. E. Gerschenson and D. Casanello, "Metabolism of rat liver cells cultured in suspension: insulin and glucagon effects on glycogen level," *Biochemical and Biophysical Research Communications*, vol. 33, no. 4, pp. 584–589, 1968.

[8] K. Hirata, Y. Yoshida, K. Shiramatsu, A. E. Freeman, and H. Hayasaka, "Effects of laminin, fibronectin and type IV collagen on liver cell cultures," *Experimental Cell Biology*, vol. 51, no. 3, pp. 121–129, 1983.

[9] D. M. Bissell, D. M. Arenson, J. J. Maher, and F. J. Roll, "Support of cultured hepatocytes by a laminin-rich gel. Evidence for a functionally significant subendothelial matrix in normal rat liver," *Journal of Clinical Investigation*, vol. 79, no. 3, pp. 801–812, 1987.

[10] S. E. S. Brown, C. P. Guzelian, E. Schuetz, L. C. Quattrochi, H. K. Kleinman, and P. S. Guzelian, "Critical role of extracellular matrix on induction by phenobarbital of cytochrome P450 2B1/2 in primary cultures of adult rat hepatocytes," *Laboratory Investigation*, vol. 73, no. 6, pp. 818–827, 1995.

[11] G. D. Block, J. Locker, W. C. Bowen et al., "Population expansion, clonal growth, and specific differentiation patterns in primary cultures of hepatocytes induced by HGF/SF, EGF and TGFα in a chemically defined (HGM) medium," *Journal of Cell Biology*, vol. 132, no. 6, pp. 1133–1149, 1996.

[12] H. Nakajima and N. Shimbara, "Functional maintenance of hepatocytes on collagen gel cultured with simple serum-free medium containing sodium selenite," *Biochemical and Biophysical Research Communications*, vol. 222, no. 3, pp. 664–668, 1996.

[13] W. S. Turner, E. Schmelzer, R. McClelland, E. Wauthier, W. Chen, and L. M. Reid, "Human hepatoblast phenotype maintained by hyaluronan hydrogels," *Journal of Biomedical Materials Research—Part B Applied Biomaterials*, vol. 82, no. 1, pp. 156–168, 2007.

[14] J. C. Y. Dunn, M. L. Yarmush, H. G. Koebe, and R. G. Tompkins, "Hepatocyte function and extracellular matrix geometry: long-term culture in a sandwich configuration," *FASEB Journal*, vol. 3, no. 2, pp. 174–177, 1989.

[15] J. C. Y. Dunn, R. G. Tompkins, and M. L. Yarmush, "Long-term in vitro function of adult hepatocytes in a collagen sandwich configuration," *Biotechnology Progress*, vol. 7, no. 3, pp. 237–245, 1991.

[16] J. C. Y. Dunn, R. G. Tompkins, and M. L. Yarmush, "Hepatocytes in collagen sandwich: evidence for transcriptional and translational regulation," *Journal of Cell Biology*, vol. 116, no. 4, pp. 1043–1053, 1992.

[17] S. Barg, C. Soltmann, M. Andrade, D. Koch, and G. Grathwohl, "Cellular ceramics by direct foaming of emulsified ceramic powder suspensions," *Journal of the American Ceramic Society*, vol. 91, no. 9, pp. 2823–2829, 2008.

[18] A. Finoli, D. McKeel, J. Gerlach, and I. Nettleship, "Phase transformation behaviour of hydroxyapatite foams subject to heat treatment," *Biomedical Materials*, vol. 5, no. 1, Article ID 015004, 2010.

[19] A. Finoli, N. Ostrowski, E. Schmelzer, I. Nettleship, and J. Gerlach, "Multiscale porous ceramic scaffolds for in vitro culturing of primary human cells," *Advances in Applied Ceramics*, vol. 111, no. 5-6, pp. 262–268, 2012.

[20] S. Higashiyama, M. Noda, S. Muraoka et al., "Transplantation of hepatocytes cultured on hydroxyapatite into Nagase analbuminemia rats," *Journal of Bioscience and Bioengineering*, vol. 96, no. 1, pp. 83–85, 2003.

[21] R. Saito, Y. Ishii, R. Ito et al., "Transplantation of liver organoids in the omentum and kidney," *Artificial Organs*, vol. 35, no. 1, pp. 80–83, 2011.

[22] B. Nilius and G. Droogmans, "Ion channels and their functional role in vascular endothelium," *Physiological Reviews*, vol. 81, no. 4, pp. 1415–1459, 2001.

[23] P. M. Eckl, W. R. Whitcomb, G. Michalopoulos, and R. L. Jirtle, "Effects of EGF and calcium on adult parenchymal hepatocyte proliferation," *Journal of Cellular Physiology*, vol. 132, no. 2, pp. 363–366, 1987.

[24] S. Nakamura, T. Matsumoto, J.-I. Sasaki et al., "Effect of calcium ion concentrations on osteogenic differentiation and hematopoietic stem cell niche-related protein expression in osteoblasts," *Tissue Engineering—Part A*, vol. 16, no. 8, pp. 2467–2473, 2010.

[25] M. I. Santos and R. L. Reis, "Vascularization in bone tissue engineering: physiology, current strategies, major hurdles and future challenges," *Macromolecular Bioscience*, vol. 10, no. 1, pp. 12–27, 2010.

[26] L. H. Nguyen, N. Annabi, M. Nikkhah et al., "Vascularized bone tissue engineering: approaches for potential improvement," *Tissue Engineering Part B: Reviews*, vol. 18, no. 5, pp. 363–382, 2012.

[27] S. Petronis, K.-L. Eckert, J. Gold, and E. Wintermantel, "Microstructuring ceramic scaffolds for hepatocyte cell culture," *Journal of Materials Science: Materials in Medicine*, vol. 12, no. 6, pp. 523–528, 2001.

[28] I. M. Sauer, D. Kardassis, K. Zeillinger et al., "Clinical extracorporeal hybrid liver support—phase I study with primary porcine liver cells," *Xenotransplantation*, vol. 10, no. 5, pp. 460–469, 2003.

[29] J. L. Drury and D. J. Mooney, "Hydrogels for tissue engineering: scaffold design variables and applications," *Biomaterials*, vol. 24, no. 24, pp. 4337–4351, 2003.

[30] K. Y. Lee and D. J. Mooney, "Hydrogels for tissue engineering," *Chemical Reviews*, vol. 101, no. 7, pp. 1869–1879, 2001.

[31] T. S. Weiss, B. Jahn, M. Cetto, K.-W. Jauch, and W. E. Thasler, "Collagen sandwich culture affects intracellular polyamine levels of human hepatocytes," *Cell Proliferation*, vol. 35, no. 5, pp. 257–267, 2002.

[32] E. Schmelzer, F. Triolo, M. E. Turner et al., "Three-dimensional perfusion bioreactor culture supports differentiation of human fetal liver cells," *Tissue Engineering—Part A*, vol. 16, no. 6, pp. 2007–2016, 2010.

[33] A. Pietrangelo, A. Panduro, J. R. Chowdhury, and D. A. Shafritz, "Albumin gene expression is down-regulated by albumin or macromolecule infusion in the rat," *Journal of Clinical Investigation*, vol. 89, no. 6, pp. 1755–1760, 1992.

[34] A. Martinez-Hernandez, "The hepatic extracellular matrix. I. Electron immunohistochemical studies in normal rat liver," *Laboratory Investigation*, vol. 51, no. 1, pp. 57–74, 1984.

[35] A. Martinez-Hernandez and P. S. Amenta, *Morphology, Localization, and Origin of the Hepatic Extracellular Matrix*, Marcel Dekker, New York, NY, USA, 1993.

[36] A. Ring, J. Gerlach, G. Peters et al., "Hepatic maturation of human fetal hepatocytes in four-compartment three-dimensional perfusion culture," *Tissue Engineering—Part C: Methods*, vol. 16, no. 5, pp. 835–845, 2010.

[37] J. C. Gerlach, K. Mutig, I. M. Sauer et al., "Use of primary human liver cells originating from discarded grafts in a bioreactor for liver support therapy and the prospects of culturing adult liver stem cells in bioreactors: a morphologic study," *Transplantation*, vol. 76, no. 5, pp. 781–786, 2003.

[38] K. Zeilinger, G. Holland, I. M. Sauer et al., "Time course of primary liver cell reorganization in three-dimensional high-density bioreactors for extracorporeal liver support: an immunohistochemical and ultrastructural study," *Tissue Engineering*, vol. 10, no. 7-8, pp. 1113–1124, 2004.

Hindawi Publishing Corporation
BioMed Research International
Volume 2016, Article ID 5726730, 8 pages
http://dx.doi.org/10.1155/2016/5726730

Research Article

Development of a Regenerative Peripheral Nerve Interface for Control of a Neuroprosthetic Limb

Melanie G. Urbanchek,[1] Theodore A. Kung,[1] Christopher M. Frost,[1] David C. Martin,[2] Lisa M. Larkin,[3,4] Adi Wollstein,[1] and Paul S. Cederna[1,4]

[1]*Section of Plastic and Reconstructive Surgery, Department of Surgery, University of Michigan Health System, Ann Arbor, MI 48109-5463, USA*
[2]*Department of Materials Science and Engineering, University of Delaware, Newark, DE 19716-1501, USA*
[3]*Department of Molecular and Integrative Physiology, University of Michigan, Ann Arbor, MI 48109-2200, USA*
[4]*Biomedical Engineering, College of Engineering, University of Michigan, Ann Arbor, MI 48109-2110, USA*

Correspondence should be addressed to Melanie G. Urbanchek; melurban@umich.edu

Received 7 January 2016; Revised 5 April 2016; Accepted 17 April 2016

Academic Editor: Antonella Motta

Background. The purpose of this experiment was to develop a peripheral nerve interface using cultured myoblasts within a scaffold to provide a biologically stable interface while providing signal amplification for neuroprosthetic control and preventing neuroma formation. *Methods*. A Regenerative Peripheral Nerve Interface (RPNI) composed of a scaffold and cultured myoblasts was implanted on the end of a divided peroneal nerve in rats ($n = 25$). The scaffold material consisted of either silicone mesh, acellular muscle, or acellular muscle with chemically polymerized poly(3,4-ethylenedioxythiophene) conductive polymer. Average implantation time was 93 days. Electrophysiological tests were performed at endpoint to determine RPNI viability and ability to transduce neural signals. Tissue samples were examined using both light microscopy and immunohistochemistry. *Results*. All implanted RPNIs, regardless of scaffold type, remained viable and displayed robust vascularity. Electromyographic activity and stimulated compound muscle action potentials were successfully recorded from all RPNIs. Physiologic efferent motor action potentials were detected from RPNIs in response to sensory foot stimulation. Histology and transmission electron microscopy revealed mature muscle fibers, axonal regeneration without neuroma formation, neovascularization, and synaptogenesis. Desmin staining confirmed the preservation and maturation of myoblasts within the RPNIs. *Conclusions*. RPNI demonstrates significant myoblast maturation, innervation, and vascularization without neuroma formation.

1. Introduction

Breakthroughs in robotic technology have facilitated the advent of upper extremity prosthetic devices which have the capability to emulate the functions of a native extremity. However, realization of the full potential of these devices has been hindered by the lack of an optimal interface between the patient and the artificial limb. This crucial interface must permit reliable transmission of both efferent motor commands and afferent sensory signals of sufficient amplitude to be detectable above the inherent electrical noise. One of the more popular strategies to achieve prosthetic control involves a variety of experimental intraneural or epineural electrodes placed directly within or on the epineurial surface of peripheral nerves within the residual limb [1]. This technique is particularly attractive because a significant amount of axonal sorting and organization occurs within peripheral nerves; therefore, directly interfacing with residual peripheral nerves provides greatly increased signal specificity as compared to other types of control systems including brain interfaces. However, while many types of peripheral nerve interfaces (PNIs) have been studied and successfully utilized to transduce efferent motor action potentials, they are limited by their lack of long-term stability. The major design concern is to provide a sufficiently robust interface capable of detecting physiologic action potentials while limiting the axonal damage and foreign body reaction which

subsequently leads to loss of signal fidelity [2]. In addition, a relatively unrecognized limitation with existing peripheral nerve interfaces is the inability to control neuroma formation in the residual limb.

The ideal PNI possesses a number of attributes which will consistently provide high-fidelity control of a neuroprosthetic device over a long period of time. The highly conductive interface should provide amplification and stable transmission of relatively low-amplitude nerve signals in order to provide fine motor control. It should promote integration with surrounding tissues to minimize the inevitable scarring and encapsulation which result in signal degradation over time. The PNI should be designed to avoid iatrogenic axonal damage within the peripheral nerve either at the time of implantation or from chronic micromotion. Furthermore, the ideal PNI should mitigate neuroma formation which can not only lead to pain but can also lead to signal interference from misdirected axons and inappropriately low depolarization potentials.

These attributes were carefully considered when conceptualizing the Regenerative Peripheral Nerve Interface (RPNI), a novel experimental nerve interface designed for long-term, stable integration with transected peripheral nerves in a residual limb. In this study, the RPNI was surgically constructed by inserting the distal end of a divided peripheral nerve into a cylindrical scaffold that was populated with cultured myoblasts. Maturation and innervation of the myoblasts within the RPNI provide amplification of neural signals and mitigate neuroma formation. To increase the conductivity of the RPNI construct, an electroconductive polymer can be applied to the scaffold material prior to implantation. This paper details the development of the RPNI and describes the proof-of-concept experiments performed to demonstrate its potential as an effective interface between divided peripheral nerves and neuroprosthetic devices.

2. Methods

All animal care and operative procedures were conducted in accordance with the Guide for the Care and Use of Laboratory Animals [3]. A single RPNI was constructed within the left thigh in each of 25 male F344 rats weighing between 300 and 400 grams (Charles River, Wilmington, MA). Each RPNI consisted of (1) a scaffold material; (2) cultured autogenous myoblasts; (3) the distal end of the divided peroneal nerve; and, in one experimental group, (4) chemically polymerized poly(3,4-ethylenedioxythiophene) (PEDOT) conductive polymer. Three study groups were established based on the scaffold material used to create the RPNI: (1) silicone mesh ($n = 9$), (2) acellular muscle ($n = 10$), and (3) acellular muscle with polymerized conductive polymer ($n = 6$). Silicone mesh and acellular muscle were chosen because both provide a sufficient amount of pliability and permeability while at the same time possessing enough durability to serve as a stable construct for implantation of cultured myocytes. PEDOT was chosen to determine if a conductive polymer polymerized onto the acellular muscle could be used in the setting of an RPNI.

Cell harvesting and culture were performed as previously described [4]. Soleus muscle myoblasts from isogenic female rats were grown in culture in 35 mm plates with growth medium consisting of 400 mL of HAMF-12 nutrient mixture (GibcoBRL) with 100 mL of fetal bovine serum (GibcoBRL) and 100 units/mL of Penicillin G (SIGMA). Serial passage technique was used to isolate and maximize the myoblasts population within the growth plate. Growth medium was replaced every 48 hours after cell plating. The cells were allowed to mature until 75% confluence was reached. At that time, the growth medium was replaced with differentiation medium consisting of 465 mL of DMEM (GibcoBRL) with 35 mL horse serum (GibcoBRL) and 100 units/mL Penicillin G. Differentiation medium induced formation of multinucleated myotubes and after a total culture period of 13 to 17 days the myotubes were ready. Myotubes were considered ready for implantation into the RPNI when the monolayers of myoblast cells were contracting.

Each RPNI was surgically fabricated in the same fashion and allowed to mature in vivo. After using pentobarbital sodium (50 mg/kg) to achieve anesthesia, a longitudinal incision was made on the lateral aspect of the left hind limb. Intramuscular dissection proceeded through the biceps femoris muscle until the common peroneal and tibial nerves were encountered within the midthigh. Meticulous dissection of the common peroneal nerve was performed distally under the operating microscope to the level where it enters the lateral compartment of the lower extremity. A 2 cm length of common peroneal nerve was resected just proximal to the lateral compartment of the lower limb.

In the silicone mesh group (SM), a 15 × 10 mm piece of 0.5 mm thick silicone elastomer was cut to size and was manually meshed using a 1 mm punch biopsy tool to increase permeability, nutrient diffusion, and vascular ingrowth. The silicone was positioned at the distal end of the divided peroneal nerve. Several interrupted 9-0 nylon microsutures were placed through the epineurium and into the scaffold to secure the nerve with approximately 5 mm of overlap between the distal peroneal nerve and the proximal end of the scaffold. The scaffold was then wrapped into the shape of a cylinder and secured with suture. Two 35 mm plates of myotubes (3 million myoblasts by direct counting technique at plating day 7) were gently removed from the culture dish and transferred to each tube. The ends of the scaffold were closed using interrupted 7-0 Prolene sutures (Figure 1). In the acellular muscle group (AM), the scaffold material was prepared using previously described techniques to remove all cellular elements from mouse abdominal wall muscle specimens [5]. The resultant acellular muscle was then used to create an RPNI at the end of the peroneal nerve in the same manner as the silicone mesh. To investigate if the conductivity of the RPNI could be enhanced, PEDOT electroconductive polymer was chemically polymerized onto the acellular muscle scaffold in a separate group of 6 rats (AM+PEDOT) [6]. PEDOT is a biocompatible substance conducive to polymerization with biologic tissues and has been shown to reduce charge density and lower impedance in other experimental settings by increasing surface area [7–9]. After RPNI implantation, all surgical wounds were closed

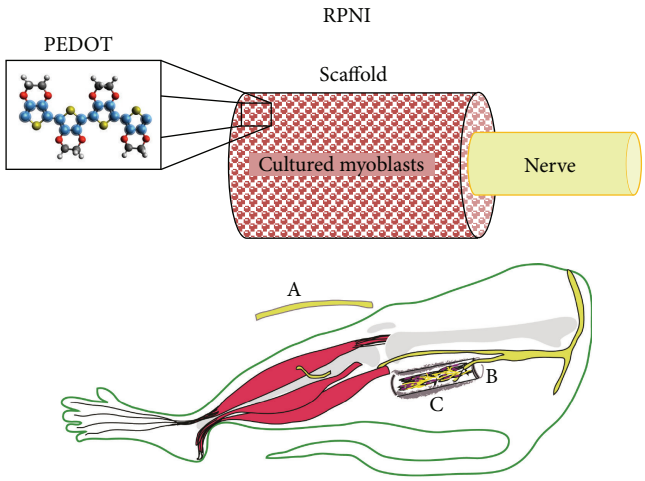

Figure 1: Schematic drawing of a Regenerative Peripheral Nerve Interface (RPNI) which is constructed using scaffold material consisting of either silicone mesh, acellular muscle, or acellular muscle with PEDOT conductive polymer. In this example, the end of the peripheral nerve is wrapped by acellular muscle with PEDOT and the construct is populated with cultured myoblasts. (Below) A 2 cm section of the distal common peroneal nerve is removed (A) and the residual nerve (B) is implanted into the RPNI (C) for a minimum of 2 months.

in a layered fashion and rats were allowed to recover for a minimum of two months.

2.1. Electrophysiological Testing. At the time of sacrifice, rats were anesthetized and the surgical site was reopened. The RPNI and proximal common peroneal nerve were carefully dissected for in situ electrophysiological studies. Electrodiagnostic evaluation of the RPNI was performed using a 26-gauge stainless steel needle (Natus Medical Inc., San Carlos, CA) placed into the central portion of the RPNI (Figure 2). During both deep and light anesthetic conditions, a painful needle stimulus was delivered to the ipsilateral left plantar skin to induce a withdrawal reflex. A deep plane of anesthesia was confirmed by the absence of reflexes to aural and physical stimuli whereas a light plane of anesthesia was defined as preservation of these reflexes but no volitional movement. Electromyographic (EMG) activity in response to this sensory stimulus was recorded by an electrophysiologic monitoring system (Natus Medical Inc., San Carlos, CA). Nerve conduction studies (NCS) were performed using a stimulating shielded bipolar stainless steel hook electrode (Harvard Apparatus, Holliston, MA) placed around the common peroneal nerve at the level of the sciatic notch. Increasing amounts of current were delivered manually to elicit compound muscle action potentials (CMAPs) until supramaximal stimulation was achieved.

2.2. Histology. After testing, animals were euthanized and the RPNI with attached peroneal nerve was removed for histologic examination. Tissue samples were fixed in 10% neural buffered formalin and embedded in paraffin; 5 μm serial sections were subsequently stained with hematoxylin

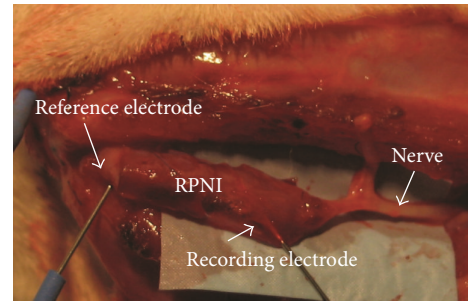

Figure 2: In situ image of Regenerative Peripheral Nerve Interface (RPNI), 4 months after implantation. In this example, 2 × 35 mm plates of myoblasts at culture day 14 were deposited on a one-layer thick sheet (2 cm long) acellular muscle. The common peroneal was transected, a 2 cm length was discarded, and the proximal residual end was tacked to the acellular muscle. The acellular muscle was rolled lengthwise to contain the myoblasts and maintain contact with the transected peroneal nerve. Evoked compound muscle action potential recording with stimulating electrode positioned on the peroneal nerve was 90 μV peak-to-peak.

and eosin. Samples were examined under light microscopy at 100x magnification to evaluate the condition and maturation of muscle fibers, axonal regeneration, extracellular matrix deposition, and neovascularization. Separate sections underwent acetylcholinesterase staining to reveal the presence of neuromuscular junctions within the RPNI specimens [10].

Immunohistochemistry was performed on all RPNI samples to determine the presence of myoblast-specific protein desmin within the various scaffolds, demonstrating the survival of the myotubes from implantation to sacrifice. An antidesmin staining protocol involving polyclonal rabbit antidesmin primary antibody (Thermo Scientific, Waltham, MA) and Cy3-conjugated goat anti-rabbit secondary antibody (Jackson ImmunoResearch Laboratories, Inc., West Grove, PA) was employed with fluorescent microscopy using excitation wavelengths between 515 and 560 nm. An alternative method of visualizing the desmin antibody was to cause a labeled precipitate using 3,3′-diaminobenzidine (ThermoFisher Scientific, Waltham, MA).

2.3. Transmission Electron Microscopy. Tissue was immersion fixed in 3% glutaraldehyde in 0.1 M Sorensen's buffer (pH 7.4) and embedded in Epon epoxy resin. Semithin sections were stained with toluidine blue for tissue identification. Selected regions of interest were sectioned into ultrathin slices 70 nm in thickness and poststained with uranyl acetate and lead citrate. These were examined using a Philips CM100 electron microscope at 60 kV. Images were recorded digitally using Hamamatsu ORCA-HR digital camera system operated using AMT software (Advanced Microscopy Techniques Corp., Danvers, MA).

3. Results

All 25 rats in the study underwent terminal evaluation with electrodiagnostic testing and tissue harvesting. The time from RPNI implantation to euthanasia ranged from 59 days to 111

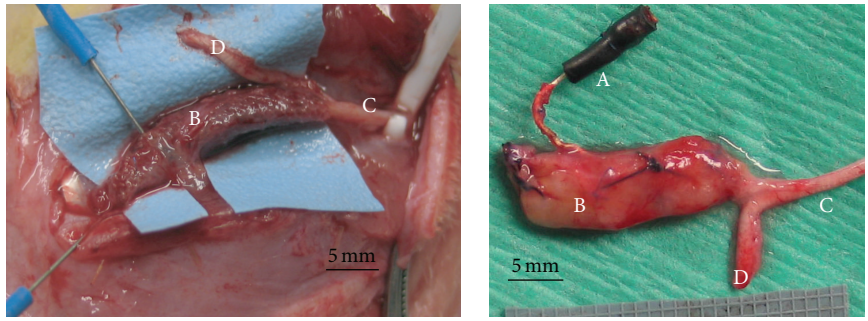

(a) (b)

Figure 3: (a) RPNI constructed with silicone mesh scaffold at postoperative day 111. Note that the myotubes that were implanted within the scaffold have matured and the resultant tissue appears pink and well-vascularized. The silicone mesh remained intact and did not negatively affect viability of the surrounding tissues. (b) RPNI constructed with acellular muscle scaffold at postoperative day 270. (A) implanted electrode; (B) RPNI; (C) peroneal branch of sciatic nerve; and (D) tibial branch of the sciatic nerve.

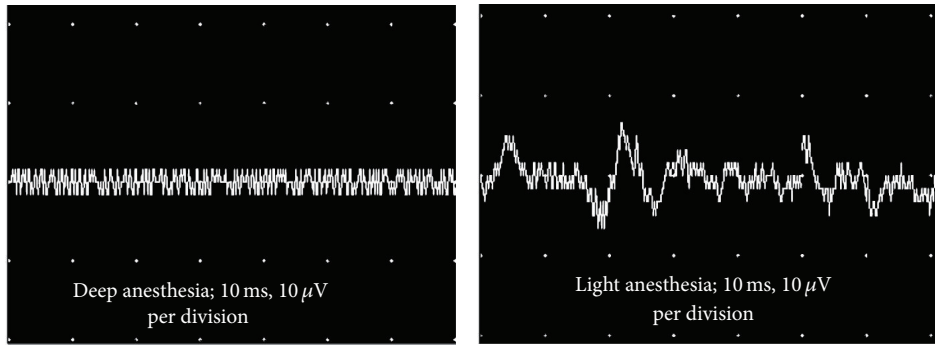

Figure 4: EMG activity recorded from the RPNI in response to painful foot stimulus during deep and light anesthetic conditions.

days with a mean duration of implantation of 93 days. All RPNIs were easily identifiable and clearly vascularized with multiple blood vessels visible on the surface (Figure 3).

3.1. Myoblast-Based RPNIs Can Detect Physiologic Efferent Motor Action Potentials When Interfaced with the Peroneal Nerve. EMG activity was recorded from the RPNI during deep and light anesthetic conditions. During a deep plane of anesthesia, a stimulus to the plantar surface of the foot did not result in any EMG recordings. However, when the anesthesia was lightened, distinct EMG signals were directly elicited from the stimulus (Figure 4). Nerve conduction studies demonstrated that CMAPs could be repeatedly produced and recorded through the RPNI in SM, AM, and AM+PEDOT groups with high fidelity and reproducibility (Figure 5).

3.2. Myoblast-Based RPNIs Develop into Mature Muscle, Are Reinnervated, Revascularized, and Prevent Neuroma on the End of the Divided Peroneal Nerve. Under histologic examination, RPNIs from all groups displayed intact mature muscle fibers and ample numbers of nerve fibers coursing through the substance of the neurotized muscle. Branching blood vessels were readily identified throughout all RPNIs. Occasionally, atrophic or degenerating muscle fibers were recognized, but this was qualitatively similar for all scaffold types. Commonly, groups of regenerated muscle fibers were surrounded by infiltrating connective tissue. Despite the abundance of collagen deposition in all groups, axons were extensively myelinated and no signs of neuromas were detected with light microscopy. In contrast to the SM and AM groups, where axons were identified diffusely throughout the sections, histologic inspection of the AM+PEDOT specimens revealed that regenerating axons were not in close proximity (defined as $<1\,\mu$m) to the PEDOT material. All specimens displayed the presence of neuromuscular junctions on cholinesterase staining, which suggests the development of motor end plates within the myotube-populated RPNI (Figure 6).

On TEM imaging, specimens from all three groups displayed ultrastructural evidence of myogenesis, neovascularization, axonal sprouting, and synaptogenesis (Figure 7). Multinucleated cells with organized sarcomeres indicated the successful differentiation and development of myotubes into mature muscle fibers within the RPNI. Vascular channels were discovered throughout all RPNI specimens, even centrally, away from the peripheral initiation of neovascularization. Neuromuscular junctions were found in the samples of all scaffold groups, suggesting that the regenerating axons within the RPNI are capable of nerve-muscle synaptogenesis with myoblast-derived muscle fibers.

Desmin staining confirmed the survival of myotubes after implantation into the scaffold and supported the premise that

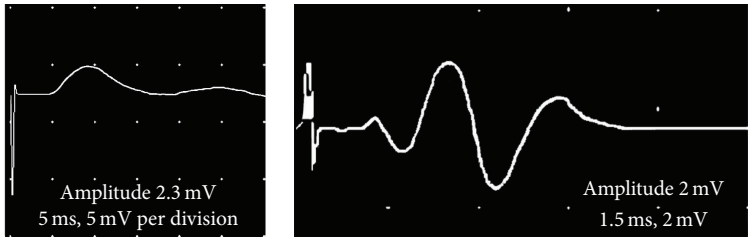

(a) (b)

Figure 5: Nerve conduction studies from acellular muscle scaffold RPNI (a) and acellular muscle+PEDOT scaffold RPNI (b) showing the generation of an elicited compound muscle action potential.

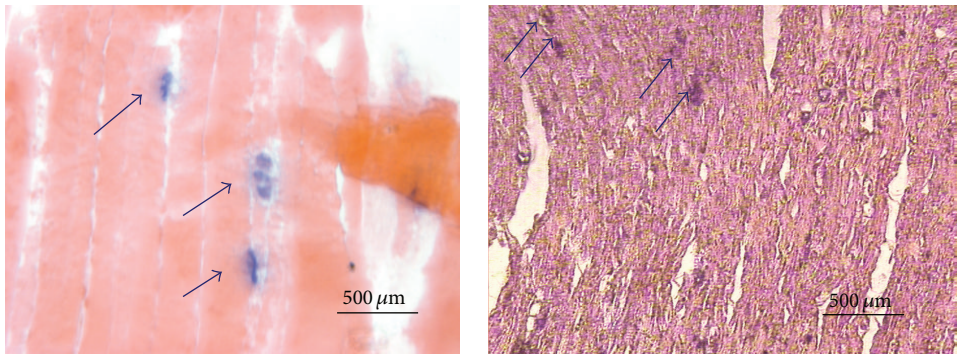

(a) (b)

Figure 6: Histologic localization of acetylcholinesterase (arrows) indicates neuromuscular junctions in an acellular muscle scaffold RPNI (a) and an acellular muscle+PEDOT scaffold RPNI (b). Note the formation of neuromuscular junctions in both specimens which suggests successful nerve-muscle synaptogenesis.

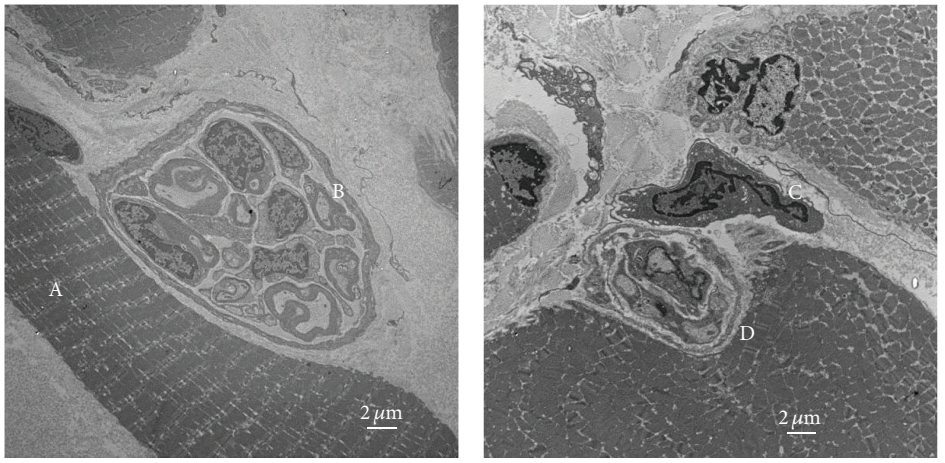

Figure 7: Transmission electron microscopy images of an RPNI created with acellular muscle scaffold at postoperative day 90. Note the presence of mature muscle fibers (A), adjacent regenerating myelinated nerve fibers (B), Schwann cells (C), and the formation of neuromuscular junctions (D).

the muscle fibers found in the RPNI likely originated from the cultured progenitor cells. Desmin-positive mature muscle fibers were identified in all RPNI samples under fluorescent microscopy regardless of the scaffold material (Figure 8). No observational differences were found in desmin staining between the scaffold groups, suggesting that all experimental environments within the RPNIs possessed adequate tissue perfusion and nutrients to promote myotube differentiation into mature muscle fibers. This was true even in the presence of PEDOT polymer within the substance of the acellular muscle.

4. Discussion

High-fidelity control of an upper extremity prosthesis is exceedingly dependent on the crucial interface between the

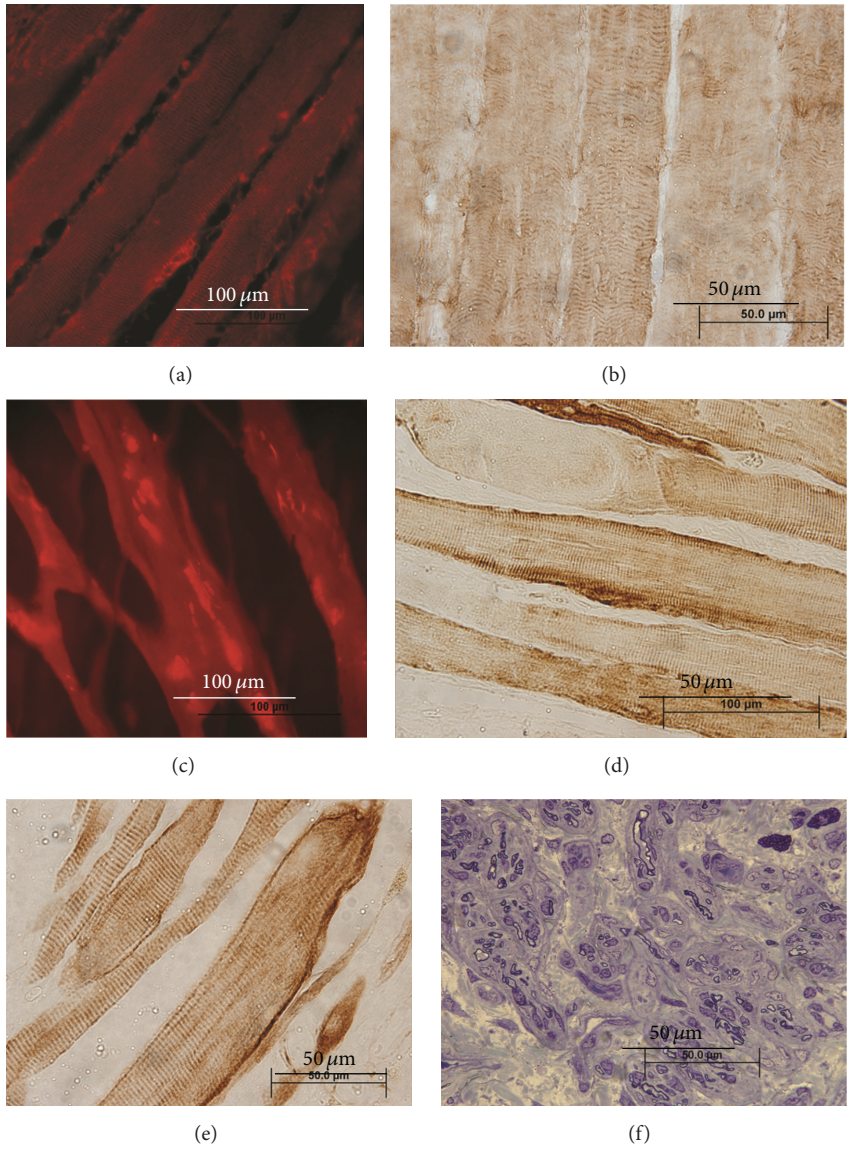

Figure 8: (a–e) Desmin-positive muscle fibers. Desmin staining with striations confirms the survival of myotubes and maturation into muscle fibers after implantation into the RPNI. (a and b) Normal rat muscle fibers. (c) RPNI muscle fibers after maturing inside acellular muscle coated with PEDOT. (d) RPNI muscle fibers after maturing inside acellular muscle. (e) RPNI muscle fibers after maturing inside silicone mesh. Muscle fibers myoblast-derived muscle fibers were found within all RPNI specimens regardless of scaffold material. (f) Example of peroneal nerve cross section at the entrance to the RPNI.

patient and the mechanical device. Several strategies have been proposed to provide this level of prosthetic control. One strategy known as targeted muscle reinnervation involves a surgical procedure which redirects transected peripheral nerves at the site of amputation to proximal muscle groups; upon contraction of these reinnervated muscles, EMG signals can be captured by surface electrodes and used to control a myoelectric prosthesis [11, 12]. To date, this approach provides the most natural, intuitive control for neuroprosthetic devices. Unfortunately, this strategy provides only a limited number of distinct control signals making it difficult to functionally restore many degrees of freedom and permit independent finger, wrist, and elbow motion simultaneously. Other investigators have attempted to provide prosthetic control through direct neural interfacing of the central or peripheral nervous systems [1, 2]. Nevertheless, methods to harness command signals from either the brain or peripheral nerves possess several significant limitations including inadequate signal selectivity and iatrogenic injury to delicate nervous tissue.

The authors present the development of the Regenerative Peripheral Nerve Interface as a new strategy to potentially connect divided peripheral nerves with artificial limbs. As the myoblasts within the RPNI mature into muscle fibers, they are reinnervated by the implanted peroneal nerve, become revascularized, and serve to prevent neuroma formation. In addition, electrical connectivity between the RPNI and peroneal nerve has been demonstrated by CMAPs recorded

after both proximal peroneal nerve stimulation and sensory stimulation to the ipsilateral foot. The RPNI displays unique features which address several of the limitations of other experimental peripheral nerve interfaces. First, the RPNI uses contractile myotubes on a biocompatible scaffold in order to generate electrical activity that can be recorded. With reinnervation, relatively low-amplitude nerve signals traveling through the RPNI result in contraction of the myotubes, generating compound muscle action potentials that are readily measured. In essence, the RPNI transduces nerve signals into muscle signals and facilitates detection of efferent motor action potentials. Second, the application of an implanted electrode on the surface of the RPNI construct, distinctly separate from the peripheral nerve, will reduce the possibility of iatrogenic nerve injury either at the time of implantation or due to micromotion over time. Although chronic micromotion may also produce trauma at the interface between the RPNI and the electrode, we posit that muscle tissue will be comparatively more resilient compared to nerve tissue and that much larger muscle action potentials will remain detectable even with expected fibrosis. Third, a separate RPNI can theoretically be interfaced with individual nerve fascicles, allowing for a much greater degree of signal selectivity compared to other available interfaces. Fourth, living myotubes provide regenerating axons a target for reinnervation, thereby reducing the occurrence of misdirected nerve fibers which leads to neuroma formation.

Signals that are transduced through the RPNI must be detected by an electrode in contact with the RPNI. To increase the conductivity between the RPNI and electrode, a biocompatible conductive polymer may be added to the scaffold material. Previous work demonstrated the ability to polymerize PEDOT onto acellular muscle constructs [5, 13]. Ideally, modification of the RPNI scaffold would enhance conductivity without adversely affecting neuronal regeneration, muscle maturation, muscle reinnervation, and neuroma formation. In this study, we found that RPNIs fabricated with AM+PEDOT could sustain viable cultured myoblasts and allow these cells to undergo differentiation into mature muscle fibers once implanted into the rat thigh. Synaptogenesis was also demonstrated histologically in this study group through identification of neuromuscular junctions seen on immunohistochemical staining. Interestingly, while regenerating axons were found adjacent to muscle fibers in all specimens, compared to the SM and AM groups axons were not found in close proximity to the PEDOT substance on histologic examination. While the biocompatibility of PEDOT has been reported by others [14–16], further investigation is required to ascertain the optimum polymerization methods in order to maximize axonal sprouting and muscle reinnervation within the RPNI, while at the same time limiting the potential for neuroma formation.

Painful neuromas can be problematic after upper extremity amputation and multiple surgical approaches have been described to treat symptomatic cases [17, 18]. Many surgeons choose to excise the distal neuroma bulb and implant the nerve into muscle [19]. The RPNI utilizes this concept to address the problem of neuroma in the setting of limb amputation. Current experimental strategies to interface with residual peripheral nerves require application of electrodes around or within nerves which may lead to other unfavorable consequences such as axonal injury and neuroma-in-continuity [20]. Histologic findings of neuroma have been described and include increased myelinated fiber counts and decreased fiber cross-sectional area [21]. Although objective quantification of these specific factors was not performed, we did not find evidence of neuroma formation within any of the RPNIs on either histology or TEM imaging after variable periods of maturation. This observation lends support to the efficacy of muscle implantation as a valid method to treat neuromas and identifies a unique advantage of the RPNI in its role as a possible prosthetic interface.

The authors acknowledge a number of limitations with this proof-of-concept study. Because this experiment represents an attempt to demonstrate the feasibility and potential of the RPNI, the chosen methods were intended to provide a wide variety of information in an expeditious manner, understanding that subsequent work would be required to validate the observations made in this study. Future studies will elaborate on the health of the RPNI by examining the contractile properties of the mature muscle fibers within the RPNI. Nerve conduction studies can clarify the amount of signal that can be transmitted though the RPNI as well as the degree of signal amplification provided by the muscle tissue. Furthermore, harvested tissues can be analyzed quantitatively through histologic techniques to determine the extent of axonal sprouting and synaptogenesis within the RPNI. Despite the subjective nature of this study, our findings encourage the ongoing investigation of this novel peripheral nerve interface.

5. Conclusions

This study demonstrates the considerable potential of the RPNI as a novel interface between living peripheral nerves and a neuroprosthetic device. The successful conduction of biologic signals through the use of cultured myotubes within a biocompatible scaffold suggests that perhaps autotransplantation of a unit of muscle may serve a similar purpose. Subsequent studies will explore this possibility and seek to optimize the design such that indwelling electrodes can be chronically implanted with RPNIs for long-term, high-fidelity control of neuroprosthetic devices.

Competing Interests

David C. Martin is a founder and owner of Biotectix, a company specialized in the commercialization of conducting polymer materials. This conflict of interests is managed by the University of Michigan Technology Transfer Office. Otherwise, none of the other authors has a financial interest in any of the products, devices, or drugs mentioned in this paper.

Acknowledgments

This work was supported by the Department of Defense Multidisciplinary University Research Initiative (MURI)

Program administered by the Army Research Office (W911NF0610218).

References

[1] X. Navarro, T. B. Krueger, N. Lago, S. Micera, T. Stieglitz, and P. Dario, "A critical review of interfaces with the peripheral nervous system for the control of neuroprostheses and hybrid bionic systems," *Journal of the Peripheral Nervous System*, vol. 10, no. 3, pp. 229–258, 2005.

[2] A. E. Schultz and T. A. Kuiken, "Neural interfaces for control of upper limb prostheses: the state of the art and future possibilities," *PM&R*, vol. 3, no. 1, pp. 55–67, 2011.

[3] National Research Council, *Guide for the Care and Use of Laboratory Animals*, National Academics Press, Washington, DC, USA, 8th edition, 2010.

[4] P. E. Kosnik, J. A. Faulkner, and R. G. Dennis, "Functional development of engineered skeletal muscle from adult and neonatal rats," *Tissue Engineering*, vol. 7, no. 5, pp. 573–584, 2001.

[5] A. Peramo, M. G. Urbanchek, S. A. Spanninga, L. K. Povlich, P. Cederna, and D. C. Martin, "In situ polymerization of a conductive polymer in acellular muscle tissue constructs," *Tissue Engineering Part A*, vol. 14, no. 3, pp. 423–432, 2008.

[6] K. H. Hong, K. W. Oh, and T. J. Kang, "Preparation and properties of electrically conducting textiles by in situ polymerization of poly(3,4-ethylenedioxythiophene)," *Journal of Applied Polymer Science*, vol. 97, no. 3, pp. 1326–1332, 2005.

[7] S. M. Richardson-Burns, J. L. Hendricks, B. Foster, L. K. Povlich, D.-H. Kim, and D. C. Martin, "Polymerization of the conducting polymer poly(3,4-ethylenedioxythiophene) (PEDOT) around living neural cells," *Biomaterials*, vol. 28, no. 8, pp. 1539–1552, 2007.

[8] M. G. Urbanchek, B. S. Shim, Z. Baghmanli et al., "Conduction properties of decellularized nerve biomaterials," in *Proceedings of the 26th Southern Biomedical Engineering Conference (SBEC '10)*, vol. 32 of *IFMBE*, pp. 430–433, May 2010.

[9] K. A. Ludwig, N. B. Langhals, M. D. Joseph, S. M. Richardson-Burns, J. L. Hendricks, and D. R. Kipke, "Poly(3,4-ethylenedioxythiophene) (PEDOT) polymer coatings facilitate smaller neural recording electrodes," *Journal of Neural Engineering*, vol. 8, no. 1, Article ID 014001, 2011.

[10] A. Pestronk and D. B. Drachman, "A new stain for quantitative measurement of sprouting at neuromuscular junctions," *Muscle and Nerve*, vol. 1, no. 1, pp. 70–74, 1978.

[11] T. Kuiken, "Targeted reinnervation for improved prosthetic function," *Physical Medicine and Rehabilitation Clinics of North America*, vol. 17, no. 1, pp. 1–13, 2006.

[12] T. A. Kuiken, G. Li, B. A. Lock et al., "Targeted muscle reinnervation for real-time myoelectric control of multifunction artificial arms," *The Journal of the American Medical Association*, vol. 301, no. 6, pp. 619–628, 2009.

[13] B. M. Egeland, M. G. Urbanchek, A. Peramo et al., "In vivo electrical conductivity across critical nerve gaps using poly(3,4-ethylenedioxythiophene)-coated neural interfaces," *Plastic and Reconstructive Surgery*, vol. 126, no. 6, pp. 1865–1873, 2010.

[14] R. M. Miriani, M. R. Abidian, and D. R. Kipke, "Cytotoxic analysis of the conducting polymer PEDOT using myocytes," in *Proceedings of the Annual International Conference of the IEEE Engineering in Medicine and Biology Society*, pp. 1841–1844, Vancouver, Canada, August 2008.

[15] S. J. Wilks, A. J. Woolley, L. Ouyang, D. C. Martin, and K. J. Otto, "In vivo polymerization of poly(3,4-ethylenedioxythiophene) (PEDOT) in rodent cerebral cortex," in *Proceedings of the Annual International Conference of the IEEE Engineering in Medicine and Biology Society*, pp. 5412–5415, Boston, Mass, USA, August-September 2011.

[16] M. Asplund, E. Thaning, J. Lundberg et al., "Toxicity evaluation of PEDOT/biomolecular composites intended for neural communication electrodes," *Biomedical Materials*, vol. 4, no. 4, Article ID 045009, 2009.

[17] M. Soroush, E. Modirian, M. Soroush, and M. Masoumi, "Neuroma in bilateral upper limb amputation," *Orthopedics*, vol. 31, no. 12, article 1193, 2008.

[18] D. Elliot and A. Sierakowski, "The surgical management of painful nerves of the upper limb: a unit perspective," *The Journal of Hand Surgery, European Volume*, vol. 36, no. 9, pp. 760–770, 2011.

[19] A. L. Dellon and S. E. Mackinnon, "Treatment of the painful neuroma by neuroma resection and muscle implantation," *Plastic and Reconstructive Surgery*, vol. 77, no. 3, pp. 427–436, 1986.

[20] J. D. D. V. Alant, S. W. P. Kemp, K. J. O. L. Khu, R. Kumar, A. A. Webb, and R. Midha, "Traumatic neuroma in continuity injury model in rodents," *Journal of Neurotrauma*, vol. 29, no. 8, pp. 1691–1703, 2012.

[21] P. S. Kim, J. H. Ko, K. K. O'Shaughnessy, T. A. Kuiken, E. A. Pohlmeyer, and G. A. Dumanian, "The effects of targeted muscle reinnervation on neuromas in a rabbit rectus abdominis flap model," *Journal of Hand Surgery*, vol. 37, no. 8, pp. 1609–1616, 2012.

Hindawi Publishing Corporation
BioMed Research International
Volume 2016, Article ID 4702674, 12 pages
http://dx.doi.org/10.1155/2016/4702674

Review Article

Cartilage Regeneration in Human with Adipose Tissue-Derived Stem Cells: Current Status in Clinical Implications

Jaewoo Pak,[1] Jung Hun Lee,[1,2] Wiwi Andralia Kartolo,[3] and Sang Hee Lee[2]

[1]*Stems Medical Clinic, 32-3 Chungdam-dong, Gangnam-gu, Seoul 06068, Republic of Korea*
[2]*National Leading Research Laboratory, Department of Biological Sciences, Myongji University, 116 Myongjiro, Yongin, Gyeonggido 17058, Republic of Korea*
[3]*FMN Wellness & Antiaging Centre, Jalan Sangihe 15A, Jakarta Pusat 10150, Indonesia*

Correspondence should be addressed to Sang Hee Lee; sangheelee@mju.ac.kr

Received 22 October 2015; Revised 12 December 2015; Accepted 20 December 2015

Academic Editor: Pornanong Aramwit

Osteoarthritis (OA) is one of the most common debilitating disorders among the elderly population. At present, there is no definite cure for the underlying causes of OA. However, adipose tissue-derived stem cells (ADSCs) in the form of stromal vascular fraction (SVF) may offer an alternative at this time. ADSCs are one type of mesenchymal stem cells that have been utilized and have demonstrated an ability to regenerate cartilage. ADSCs have been shown to regenerate cartilage in a variety of animal models also. Non-culture-expanded ADSCs, in the form of SVF along with platelet rich plasma (PRP), have recently been used in humans to treat OA and other cartilage abnormalities. These ADSCs have demonstrated effectiveness without any serious side effects. However, due to regulatory issues, only ADSCs in the form of SVF are currently allowed for clinical uses in humans. Culture-expanded ADSCs, although more convenient, require clinical trials for a regulatory approval prior to uses in clinical settings. Here we present a systematic review of currently available clinical studies involving ADSCs in the form of SVF and in the culture-expanded form, with or without PRP, highlighting the clinical effectiveness and safety in treating OA.

1. Introduction

Osteoarthritis (OA) is a common painful and debilitating disorder in the elderly [1, 2]. All current medical treatments for OA, such as nonsteroidal anti-inflammatory drugs (NSAIDs), steroids, and hyaluronic acids (HAs), physical therapy, aim to remedy the symptoms, as opposed to treating the underlying causes. When failed with symptomatic medical treatments, patients usually resort to receiving total knee replacement (TKR) or total hip replacement (THR) surgery. Both TKR and THR surgeries carry relatively high morbidity and mortality rates [1, 2]. Even with improved surgical technique, anesthesia, and rehabilitation, the thirty-day mortality rate after total knee arthroplasty is reported to be 0.18%, and 5.6% of the patients experienced complications [3]. Also, the overall 30- and 90-day mortality rates for total hip arthroplasty are reported to be 0.24% and 0.55%, respectively [4]. These approaches do not address the morbidity associated with early disease or the limitations of arthroplasty surgery, which include the possibility of adverse outcomes and the finite lifespan of prostheses [5].

Mesenchymal stem cells (MSCs) are found in numerous human tissues including bone marrow and adipose tissue [6, 7]. These MSCs have been shown to differentiate into bones, cartilage, muscle, and adipose tissue [6–8]. Because of their potential capabilities in regenerating cartilage, MSCs have been successfully used in animals [9, 10]. In 2008, Centeno et al. have showed successful cartilage regeneration in humans with MSCs [11]. Subsequently, in 2010, the same group also reported safety data of using MSCs in humans for cartilage regeneration [12].

Adipose tissue-derived stem cells (ADSCs) are one type of MSCs. In 2001 and 2002, Zuk et al. showed that adipose tissue in the form of stromal vascular fraction (SVF) contains stem cells that have the capacity to differentiate into cartilage, bone, muscle, and adipose tissue, similar to MSCs [13, 14]. Likewise,

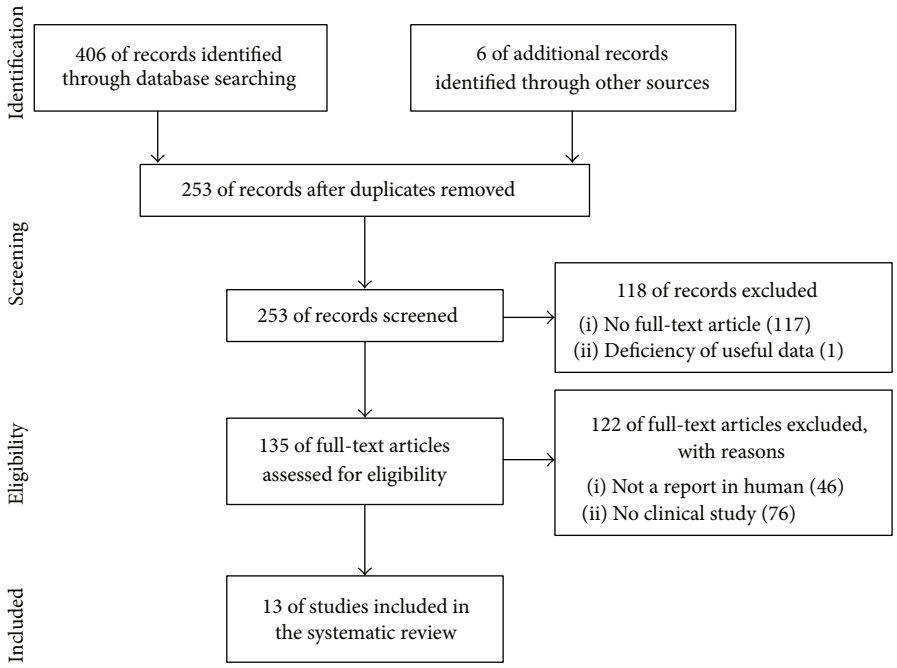

Figure 1: Literature selection process (PRISMA flow diagram).

ADSCs also have been investigated in treatment of cartilage injuries and osteoarthritis in animals. The results from these studies showed evidence of cartilage regeneration by using ADSCs [15–19].

Consequently, in 2011, Pak successfully treated 2 human patients with OA of the knees by using autologous ADSCs in the form of SVF along with platelet rich plasma (PRP) and hyaluronic acid (HA). He documented the regeneration of cartilage-like tissue in these patients through magnetic resonance imaging (MRI) studies [20].

More studies have recently become available, providing more evidence of cartilage regeneration in human patients with OA of the knees [21–23]. Such continued research and interests hold great promises in the field of regenerative medicine.

Although the successful regeneration of cartilage with ADSCs in humans may represent a promising, minimally invasive, nonsurgical alternative, many issues need to be resolved and clarified before the general application of this procedure. The mechanism of regeneration remains unclear: (i) it could be due to the secretory effects of the stem cells injected [24, 25]; (ii) it could be due to direct engraftment and differentiation of the stem cells that were introduced into the diseased joints [26, 27]; or (iii) it could be due to the combination of secretory effects and direct engraftment of the stem cells.

Adipose stem cells excrete a variety of cytokines, chemokines, growth factors, and exosomes [28, 29]. These factors have positive effects on the surrounding progenitor cells. However, there is some evidence that these stem cells injected may actually become engrafted into the tissue and differentiate into tissue-specific stem cells [30]. It is also very possible that these two mechanisms play a role in cartilage regeneration.

Furthermore, the method of the cell transplant needs to be studied in detail: the most optimal dosage of the stem cells to be injected, the best mode of injection, the best method of promoting stem cell adherence to the lesions, and the most potential growth factors (e.g., PRP) to be added, as well as the best scaffolding materials (e.g., HA and extracellular matrix (ECM)).

Here we will present a comprehensive and systematic review of cartilage regeneration in human joints by using ADSCs in the form of adipose SVF and assess the possibility of the clinical application of these stem cells.

2. Method

We used the Preferred Reporting Items for Systematic Review and Meta-Analysis (PRISMA) in our review (Figure 1) [31]. We conducted a systematic literature search in PubMed, Medline, and Embase. We used the keywords as our search terms. We combined terms for selected indications (stem cell, osteoarthritis, and adipose). The literature search included all studies published in English between 2000 and 2015. We identified 253 references after removing duplicates. We independently assessed full-text articles for inclusion in our review. The criteria for the inclusion of studies in our review encompassed clinical studies on ADSC injection conducted on humans for cartilage regeneration. Finally, we found 13 articles showing clinical studies on ADSC treatments for cartilage defects (Figure 1).

3. ADSCs in the Form of SVF along with PRP and/or HA/ECM

At present, most of the ADSCs being used in clinical settings are in the form of SVF. To obtain adipose SVF, liposuction is performed on easily accessible areas of the body, such as the abdomen, buttocks, or thighs. These lipoaspirates are then digested with collagenase to extract stem cells that exist within the matrix of the adipose tissue [13, 14]. The collagenase is then washed off using a centrifuge and dilution method. The pellet, including the bottom portion of the centrifuge, is considered to be SVF [13, 14]. SVF contains a variety of cells in different proportions: ADSCs, a type of mesenchymal stem cells, pericytes, vascular adventitia cells, fibroblasts, preadipocytes, monocytes, macrophages, red blood cells, fibrous tissue, ECM, and so forth [13, 14].

The process of preparing adipose SVF is considered to be a medical procedure in Korea and a few other countries when performed by a physician as a single surgical procedure within the same day and with minimal manipulations [32]. Unlike adipose SVF, culture-expanded stem cells are usually considered to be pharmaceutical products, requiring clinical trials and governmental approval.

3.1. Number of Stem Cells in Human Adipose Tissue. The number of stem cells that can be extracted from each individual varies greatly.

Currently, it is well accepted that ADSCs exist within the matrix of adipose tissue. More specifically, it has been shown that ADSCs exist around blood vessels of adipose matrix [33]. These stem cells can be released from the matrix by processing the lipoaspirate with collagenase. Such stem cells are shown to regenerated cartilage as shown by Zuk et al. [13, 14]. However, the number of stem cells that can be extracted from one gram of adipose tissue can be very variable in different individual patients [13, 34–39].

The number of stem cells that can be obtained from one gram of adipose tissue can range from 5,000 to 200,000 cells [40], which have been measured by flow cytometry and indirect immunofluorescence [41, 42]. Such large individual variability may result in inconsistency of results in treating patients. Patients with high number of stem cells will have great cartilage regeneration. However, patients with low number of stem cells will not a great response, as shown by Jo et al. [21].

3.2. Autologous Platelet Rich Plasma (PRP). Autologous PRP was used in most of 13 articles showing clinical studies on ADSC treatments for cartilage defects.

PRP contains a variety of growth factors: transforming growth factor-β (TGF-β), epidermal growth factor (EGF), and fibroblast growth factor (FGF), along others [43]. These growth factors are known to proliferate stem cells. Centeno et al. used autologous platelet lysate to grow bone marrow-derived stem cells, which were injected in human patients for cartilage regeneration [11]. Likewise, PRP has been used to increase the number of stem cells injected into a joint.

Also, activated PRP may act like a scaffold for stem cells. Autologous PRP has been prepared by centrifuging autologous blood with anticoagulant citrate dextrose solution [11, 44]. When autologous PRP has been activated by adding calcium chloride, thrombin, or collagen [11, 44–46], PRP may become a "curd-like" substance [11], which may function like a scaffold.

3.3. Hyaluronic Acid (HA) and Extracellular Matrix (ECM). Scaffolding materials were used in some [20, 47–49] of the 13 articles showing clinical studies on ADSC treatments for cartilage defects.

HA and ECM are two naturally occurring scaffolding materials. HA has a high affinity for cartilage defects and provides an environment for stem cells to adhere to the lesion and differentiate [50]. ECM also provides an environment for stem cells to adhere and differentiate [51]. When autologous ECM is provided, immune reactions are not likely to occur. In addition, ECM contains a variety of growth factors, which further enhance the growth and differentiation of the injected stem cells [51].

3.4. ADSCs with PRP and/or HA/ECM. The combination of ADSCS with PRP and/or scaffolding materials was used in 13 articles showing clinical studies on ADSC treatments for cartilage defects.

PRP or platelet lysate provides a variety of growth factors for stem cells [11, 43]. HA/ECM scaffolding materials provide the environment for stem cells to adhere and differentiate into cartilage [50, 51]. Together, this combination may provide the best optimal strategy for stem cells to adhere, grow, and differentiate into cartilage [20, 22, 44, 47–49, 52–55].

4. Clinical Applications of ADSCs

The main features of clinical studies on ADSC treatments for cartilage defects were summarized in Table 1.

4.1. Case Report by Pak [20]. This is the very first study that showed the possibility of ADSCs in the form of SVF regenerating cartilage in human patients. Pak used approximately 100 g of adipose tissue obtained from the abdomen. This adipose tissue was digested with collagenase. The collagenase was washed off. The resulting adipose SVF, containing ADSCs, was injected percutaneously with calcium chloride-activated PRP, HA, and dexamethasone into joints of 2 patients with OA. Three months after the injections, the visual analog score (VAS) for pain, functional rating index, and range of motion (ROM) improved along with the MRI evidence of cartilage-like tissue regeneration in these patients.

This study used 100 g of adipose tissue. Thus, the total estimated number of ADSCs injected can range from 500,000 to 20,000,000 [40]. Also, it should be noted that this study used PRP and HA, along with ADSCs.

4.2. Nonrandomized, Retrospective, and Comparative Study by Koh and Choi [52]. This study involved 25 patients with OA of the knees. The patients were injected with adipose SVF derived from approximately 19 g of adipose tissue obtained from the knee fat pad while performing arthroscopic lavage

Table 1: Clinical studies on ADSC treatments for cartilage defects.

Study (yr)	Intervention treatment	Study type	Number of subjects	Subject characteristic [age (yr); gender]	Previous therapy	Concurrent treatment	Follow-up (mo)	Outcome measures	Results	Authors' conclusion
Pak (2011) [20]	Adipose SVF (ADSC) + PRP via percutaneous injections	Case report	2	70 and 79; 2 F with chronic knee pain	Various treatments without any success	None	3	VAS; functions (FRI, ROM); MRI	VAS/function improvements and MRI evidence of cartilage regeneration	ADSC + PRP: potentially effective in regenerating cartilage in humans
Koh and Choi (2012) [52]	Adipose SVF (ADSC) + PRP via percutaneous injections	Nonrandomized, retrospective, comparative study: ADSC + PRP versus PRP alone	25 Study group (ADSC + PRP): 25; control group (PRP alone): 25	Study group: mean 54.1 (range, 34–69); 8 M and 17 F	Various treatments without any success	None	16.4	VAS; functions (Lysholm, Tegner)	ADSC + PRP: more effective than PRP-control group	ADSC + PRP: potentially effective in patients with cartilage defects
Pak et al. (2013) [44]	Adipose SVF (ADSC) + PRP via percutaneous injections	Retrospective cohort study	91	Mean 51.23 ± 1.50 (range, 18–78); 45 M and 46 F	Various treatments without any success	None	26.62 ± 0.32	VAS; functions	Statistically significant improvement in both VAS and functions	ADSC + PRP: safe and potentially effective
Pak et al. (2013) [47]	Adipose SVF (ADSC) + PRP via percutaneous injections	Case series	3	43 and 63; 2 F 54; 1 M All with chronic knee pain	Various treatments without any success	None	3	VAS; functions (FRI, ROM); MRI	VAS/function improvements and MRI evidence of cartilage regeneration	ADSC + PRP: effective in treating chondromalacia patellae patients
Koh et al. (2013) [53]	Adipose SVF (ADSC) + PRP via percutaneous injection	Case series	18	Mean 54.6; 6 M and 12 F	Various treatments without any success	Arthroscopic lavage before knee-fat-pad-derived adipose SVF + PRP injection	24.3	VAS; functions (WOMAC, Lysholm); MRI	VAS/function/MRI improvements	ADSC + PRP: effective in treating OA of knees
Koh et al. (2015) [22]	Adipose SVF (ADSC) + PRP under arthroscopic guidance	Case series	30 for adipose SVF + PRP injection; 16 for second-look arthroscopy	Mean 70.3 (range, 65–80); 5 M and 25 F	Various treatments without any success	Arthroscopic lavage before ADSCs + PRP injection	24	VAS; functions; 2nd-look arthroscopy	VAS/function improvements; improved and maintained cartilage status	ADSCs + PRP: effective in treating elderly patients with OA

Table 1: Continued.

Study (yr)	Intervention treatment	Study type	Number of subjects	Subject characteristic [age (yr); gender]	Previous therapy	Concurrent treatment	Follow-up (mo)	Outcome measures	Results	Authors' conclusion
Pak et al. (2014) [48]	Adipose SVF (ADSC) + PRP via percutaneous injections	Case report	1	32; 1 F with chronic knee pain due to meniscus tear	Various treatments without any success	None	3	VAS; functions (FRI, ROM); MRI	VAS/function improvements and MRI evidence of cartilage regeneration	ADSC + PRP: effective in treating cartilage defect lesions, including meniscus tear
Bui et al. (2014) [54]	Adipose SVF (ADSC) + PRP via percutaneous injections	Case series	21	>18; ND	Various treatments without any success	None	8.5	VAS; functions; MRI	VAS/function/MRI improvements	ADSC + PRP: effective in treating OA of knees
Jo et al. (2014) [21]	Culture-expanded ADSC via arthroscopic injections	Randomized double-blind dose escalation study (a proof-of-concept clinical trial)	18	61–65; 3 M and 15 F	Various treatments without any success	None	6	VAS; functions; MRI; arthroscopy; histology	VAS/function/MRI/ arthroscopic/histological improvements	1.0×10^8 ADSCs into the osteoarthritic knee improved function and pain of the knee joint. Radiological, arthroscopic, and histological measures demonstrated regeneration of hyaline-like articular cartilage
Koh et al. (2014) [23]	Adipose SVF (ADSC) + PRP under arthroscopic guidance	Case series	35 with 37 knee joints	Mean 57.4 (range, 48–69); 14 M and 21 F	Various treatments without any success	Arthroscopic lavage before adipose SVF + PRP injection	12.7	VAS; functions; arthroscopy	94% patients had excellent clinical improvement; 76% had abnormal repair tissue	Scaffolds may be needed to treat patients with large cartilage lesions

Table 1: Continued.

Study (yr)	Intervention treatment	Study type	Number of subjects	Subject characteristic [age (yr); gender]	Previous therapy	Concurrent treatment	Follow-up (mo)	Outcome measures	Results	Authors' conclusion
Koh et al. (2014) [55]	Adipose SVF (ADSC) + PRP under arthroscopic guidance	Comparative study: adipose SVF + PRP versus PRP only	44	ND	Various treatments without any success	Open-wedge high tibial osteotomy	24	VAS; functions; arthroscopy	Adipose SVF + PRP is more effective than PRP alone	ADSC therapy, in conjunction with HTO, mildly improved cartilage healing and showed good clinical results compared with PRP only
Kim et al. (2015) [49]	Adipose SVF (ADSC) under arthroscopic guidance	Comparative study: adipose SVF versus adipose SVF + fibrin glue (as a scaffold)	54	Mean 57.5 ± 5.8; 22 M and 32 F	Various treatments without any success	None	28.6	VAS; functions; arthroscopy	No significant difference	Clinical and arthroscopic outcomes of ADSC implantation were encouraging for OA knees in both groups, although there were no significant differences in outcome scores between groups
Michalek et al. (2015) [56]	Adipose SVF (ADSC) via percutaneous injection	Multicenter case control study	1,114	Median 62 (range, 19–94); 589 M and 525 F	Various treatments without any success	None	Median 17.2	VAS; functions	VAS/function improvements	Adipose SVF is a novel and promising treatment approach for patients with degenerative OA. ADSC is safe and cost-effective

SVF: stromal vascular fraction; ADSC: adipose tissue-derived stem cells; PRP: platelet rich plasma; OA: osteoarthritis; yr: year; mo: month; M: male; F: female; ND: not described; HTO: high tibial osteotomy; VAS: visual analogue scale; FRI: functional rate index; ROM: range of motion; WOMAC: Western Ontario and McMaster Universities osteoarthritis index; Lysholm: Lysholm scores; Tegner: Tegner activity scale.

and debridement. Thereafter, the adipose SVF was percutaneously injected with calcium chloride-activated PRP. A mean of 1.89×10^6 ADSCs was presented in 19 g of adipose SVF. The results showed that the mean Lysholm knee scoring scales, Tegner activity scales, and VAS scores in the study group had improved significantly compared to the control group. No major adverse events were observed.

In this study, the approximate number of ADSCs obtained was little less than 2,000,000, and this was calculated to be little less than 100,000 stem cells per gram of adipose tissue. The study concludes that little less than 2 million of ADSCs with PRP were effective.

4.3. Retrospective Cohort Study by Pak et al. [44]. This is the very first safety report involving human ADSCs in the form of SVF. Between the period of 2009 and 2010, Pak et al. injected joints percutaneously with the autologous, non-culture-expanded ADSCs in 91 patients. In 2013, Pak et al. reported that all 91 patients had no serious side effects and no cancer was reported. However, the study reported that a few minor side effects occurred, mainly swelling and tendonitis, both of which were ameliorated with NSAIDs. The average efficacy reported was 65% at 3 months after the treatment.

All these patients were injected with approximately 100 g of adipose tissue. Thus, the total estimated number of ADSCs injected can range from 500,000 to 20,000,000 [40].

4.4. Case Series by Pak et al. [47]. This study involved 3 patients with chondromalacia patellae of the knees. The patients were treated with ADSCs in the form of SVF, calcium chloride-activated PRP, and HA. The mixture was injected into the knees percutaneously. After 3 months of the treatment, the patients' VAS pain scale, functional rating index (FRI), and ROM had improved. The study also showed positive regeneration of hyaline cartilage-like tissue at the patellofemoral joints of all 3 patients.

This is the very first study showing the possibility of treating chondromalacia patellae with ADSCs with PRP and HA.

4.5. Case Series by Koh et al. [53]. This study involved 18 patients with OA of the knees. The patients received non-culture-expanded ADSCs in the form of SVF obtained from the knee fat pad. The ADSCs were percutaneously injected into the knees with calcium chloride-activated PRP after arthroscopic debridement of the knees. A mean of 1.18×10^6 ADSCs was prepared from approximately 9.1 g of adipose tissue from the knee fat pad. Thereafter, Western Ontario and McMaster Universities osteoarthritis index (WOMAC), Lysholm, and VAS scores were measured and improved. The whole-organ MRI score, particularly the cartilage whole-organ MRI score, also improved. The authors concluded that improvements in the clinical and MRI results were positively related to the number of ADSCs injected.

This study used little over one million ADSCs obtained from mean of 9.1 g of adipose tissue obtained from the knee fat pad along with PRP. The number of ADSCs extracted from 1 g of adipose tissue was approximately 129,700 ADSCs per gram of adipose tissue.

4.6. Case Series by Koh et al. [22]. This study involved 30 patients with OA of the knees. The patients were injected with adipose SVF containing ADSCs extracted from 120 g of adipose tissue from the buttocks. The adipose SVF were injected with calcium chloride-activated PRP under arthroscopic guidance after arthroscopic lavage. Of these patients, 16 patients went through the second-look arthroscopies in a median of 25 months after the initial treatment. At a minimum of 2 years after the operation, almost all patients showed significant improvement in the knee injury, OA outcome scores (KOOS), VAS pain scale, and Lysholm score. In the second-look arthroscopy, 10 patients (63%) had improved cartilage, 4 patients (25%) had maintained the cartilage, and 2 patients (12%) failed in healing cartilage defects.

This study used 120 g of adipose tissue from buttock. Unlike other previous reports, the study reported extracting only little over 4 million ADSCs from 120 g of adipose tissue. However, this study is the very first study showing direct evidence of cartilage regeneration via arthroscope.

4.7. Case Report by Pak et al. [48]. This study involved 1 patient with a meniscus tear of the knee. The patient was treated with autologous adipose SVF containing ADSCs derived from approximately 40 g of packed adipose tissue obtained from the abdomen. The adipose SVF was injected with calcium chloride-activated PRP and HA. After 3 months, the patient's VAS for pain, FRI, and ROM had improved. Furthermore, the meniscus tear had improved, if not entirely disappeared, in the subsequent follow-up MRIs after 3 months.

This is another first case report showing the possibility of treating meniscus tear with ADSCs with PRP and HA.

4.8. Case Series by Bui et al. [54]. This study involved 21 patients with OA of the knees with grades 2 and 3. The patients were treated with autologous ADSCs in the form of SVF obtained from the abdomen. The ADSCs were injected percutaneously into the joints with calcium chloride-activated PRP. All 21 patients showed improved joint function after 8.5 months, measured by VAS pain score and the Lysholm score. In addition, significant improvements were noted in the MRI findings with increased thickness of the cartilage layer.

This study used 50–100 g of lipoaspirates. Thus, the number of ADSCs injected may range from 250,000 to 20,000,000. All these ADSCs were injected with PRP with good response.

4.9. Double-Blind, Randomized Dose Escalation Study by Jo et al. [21]. This is the very first double-blind, randomized clinical trial involving ADSCs in 18 patients. The patients received autologous culture-expanded ADSCs via arthroscopy. No arthroscopic lavage was performed and no PRP was injected. The ADSCs suspended in 3 mL of normal saline were injected. Initially, there were 3 groups: low-dose (1.0×10^7 ADSCs), mid-dose (5.0×10^7 ADSCs), and high-dose (1.0×10^8 ADSCs) groups with 3 patients each. In the high-dose group, there was a significantly increased volume of cartilage regeneration compared to mid-dose and low-dose group. The regeneration of the cartilage was confirmed by MRI and

arthroscopy. Furthermore, the histology of the regenerated tissue was consistent with hyaline cartilage in characteristics. After such results in the first 9 patients, the remaining 9 of the 18 patients received high-dose (1.0×10^8) ADSCs. There were no treatment-related adverse events and the WOMAC score improved.

This is the very first double-blind, randomized study with 3 different dosages of ADSCs. Unlike other studies, Jo et al. used only autologous culture-expanded ADSCs without PRP and without HA. This study clearly shows that ADSCs are effective in regenerating cartilage. This study also showed that higher dosage of ADSCs (100 million) is more efficacious than lower number of ADSCs (10 million).

4.10. Case Series by Koh et al. [23]. This is a second-look arthroscopic study involving 35 patients with a total of 37 knee joints with OA. The patients were treated with ADSCs contained in SVF obtained from a mean of 22.6 g of fat originating from the buttocks. The mean ADSCs obtained from SVF were 3.83×10^6. The ADSCs were injected with calcium chloride-activated PRP under arthroscopic guidance after arthroscopic lavage.

After the mean follow-up period of 12.7 months, second-look arthroscopy was performed. The mean International Knee Documentation Committee (IKDC) and Tegner activity scale scores significantly improved in 94% of the patients. However, 76% of the patients had abnormal repair tissue at second-look arthroscopies. The authors concluded that a scaffolding material may be needed for large lesions.

This study used little less than 4 million ADSCs obtained from 22.6 g of adipose tissue from buttocks. Although PRP was injected with ADSCs, some of the patients did not respond well, necessitating a scaffolding material for better results.

4.11. Comparative Study by Koh et al. [55]. This study involved 44 patients and compared the clinical results and second-look arthroscopic findings of a PRP-only treatment group and ADSCs in the form of SVF with a PRP treatment group. Both groups underwent open-wedge high tibial osteotomies (HTO). ADSCs were obtained from 120 g of adipose tissue and injected with PRP in 23 patients. The other 21 patients who went through HTO were injected with PRP only. After following the patients for 24 months, the ADSC with PRP group showed significantly greater improvement in the VAS for pain and KOOS subscales for pain and symptoms, compared to the PRP-only group. However, the Lysholm score was similarly improved in both groups. Arthroscopic evaluation showed that fibrocartilage was regenerated in 50% of the ADSCs with PRP group. Only 10% in the PRP-only group had their fibrous cartilage regenerated. The authors concluded that ADSCs with PRP are more effective than PRP alone.

This study used 120 g of adipose tissue. Thus, the number of ADSCs injected may range from 600,000 to 24,000,000 cells. This study also showed that ADSCs with PRP are more effective than PRP alone.

4.12. Comparative Study by Kim et al. [49]. This study involved 54 patients with a total of 56 affected knees in comparing the efficacy of ADSCs in the form of SVF-only group to that of ADSCs-with-fibrin-glue group. The fibrin glue was used as a scaffold. Adipose SVF were obtained from 120 g of adipose tissue. A total of 37 patients (39 knees) were treated with ADSCs only, and the other 17 patients were injected with ADSCs with fibrin glue. After a mean follow-up period of 28.6 months, the mean IKDC score and Tegner activity scale in both the groups significantly improved. However, better International Cartilage Repair Society (ICRS) scores were achieved in the ADSCs-with-fibrin-glue group in the second-look arthroscopies.

This study used 120 g of adipose tissue in comparing ADSCs versus ADSCs with fibrin glue as a scaffold. As expected, ADSCs-with-fibrin-glue scaffold were more effective.

4.13. Multicenter Case Control Study by Michalek et al. [56]. This study involved 1,114 patients with OA of the knee and hip from the USA, Czech Republic, Slovakia, and Lithuania. The patients were percutaneously injected with ADSCs in the form of SVF obtained from 20–90 g of adipose tissue. These patients were then followed up for a median of 17.2 months. The clinical effects were measured on the basis of pain, nonsteroid analgesic usage, limping, extent of joint movement, and stiffness. There were no serious side effects reported, including cancer. At the 12 months of follow-up period, approximately 75% of symptom improvement was noticed in 63% of patients and approximately 50% of symptom improvement was documented in 91% of patients.

This is the first study that involves a large number of human patients. The amount of adipose tissue varies: 20–90 g. Thus, the estimated number of ADSCs injected may range from 100,000 to 18,000,000 cells. Further, no PRP nor HA was used. However, the results are encouraging.

5. Discussions

Adipose tissue is considered to be a preferable source of MSCs due to its ease of accessibility and the availability of a large number of stem cells per gram of adipose tissue. In adipose tissue, 1% to 10% of nucleated cells are considered to be ADSCs whereas only 0.0001–0.01% of nucleated cells in the bone marrow are stem cells [14]. In addition, the number of nucleated cells in adipose SVF can range from 500,000 to 2,000,000 cells per gram of adipose tissue [40]. The range of MSCs in 1 g of adipose tissue may be 5,000–200,000 stem cells [40]. Thus, theoretically, 0.5–20 million ADSCs can be extracted from 100 g of adipose tissue. If the number of MSCs in adipose SVF is 5%, approximately 10 million ADSCs can be obtained from 100 g of adipose tissue.

ADSCs, as one specific form of MSCs, have been shown to regenerate cartilage in animals [15, 57, 58]. However, some authors claim adipose SVF alone may not be sufficient to regenerate cartilage in animals [18]. Interestingly, in this review, 11 of thirteen human studies had used autologous PRP in addition to ADSCs in the form of SVF.

Autologous PRP may play an important role in cartilage regeneration. PRP releases a variety of growth factors when activated. Centeno et al. used platelet lysate to grow MSCs that were injected into a human knee for cartilage regeneration [11]. The TGF-β contained in PRP may be necessary for differentiation of MSCs into cartilage cells [43].

Autologous PRP may also play a role as a scaffold, influencing stem cell adherence to lesions, as well as stem cell growth and differentiation. When properly activated, autologous PRP can become a "curd-like" substance and can thus operate as scaffold, as shown by Kim et al. [49]. Although autologous PRP alone may not regenerate cartilage as shown by Koh et al. [55], PRP may enhance ADSCs in SVF to adhere to the cartilage lesion and proliferate.

The randomized, double-blind dose escalation clinical study reported by Jo et al. clearly showed the likelihood of cartilage regeneration with ADSCs alone without any additives such as PRP or HA [21]. In the study, Jo et al. showed a direct relationship between the number of stem cells injected and the amount of cartilage regenerated. The amount of cartilage regenerated was much greater with 100 million ADSCs than 50 million ADSCs injected. This was documented by arthroscopies and MRIs [21].

On the other hand, the study by Michalek et al. did not use any other additives although the numbers of ADSCs injected are estimated to be less than the number of ADSCs used in the study by Jo et al. Also, the study by Michalek et al. did not use PRP or HA. Among all the studies reviewed in this paper, Michalek et al. study is the only one that did not have any visible objective data, such as MRI or arthroscopic photos, although significant clinical improvement has been documented.

Although most of the studies in this review used a relatively large volume (approximately 100 g) of adipose tissue, three studies used a relatively small volume (approximately 20 g) of adipose tissue. However, these three studies used PRP with low amount of adipose tissue and showed clinical improvement in patients. Therefore, it can only be estimated that adipose tissue from different regions of patients' abdomens may contain different number of stem cells.

It has been shown that different individuals have different density in the adipose tissue, indicating different amount of matrix [59]. ADSCs exist within matrix of adipose tissue around the blood vessels. Consequently, it can be concluded that higher density of adipose tissue may contain higher density of matrix and thus yields higher number of stem cells. Furthermore, the method of liposuction may affect the results of ADSCs yield in the SVF. Compared to surgical resection of adipose tissue, liposuction has been shown to produce higher percentage of viable cells in lipoaspirates [60].

In addition to differences in adipose tissue and its extraction, the concentration and incubation time of collagenase are other important factors affecting the yield of ADSCs and their viability in SVF. Since high dosage or exposure to collagenase may be toxic to ADSCs, excess amount of collagenase can decrease the ADSC viability while insufficient amount of collagenase may result in inefficient and inadequate amount of ADSC yield [61].

Based on the study by Jo et al., it is logical to expect higher rates of improvement with a higher amount of ADSCs obtained and used for cartilage regeneration. However, the direct dose relationship was not clearly observed when comparing the 12 studies that involved ADSCs in the form of SVF. This may be due to variability in adipose SVF obtained from different individuals, stem cell viability when processing adipose tissue and injecting SVF, stem cell adherence, and stem cell growth. Also addition of growth factors, such as PRP, and scaffold material, such as HA, may be important as shown by Koh et al. [49, 55]. Dregalla et al. showed that local anesthetics can also have very significant negative effects on stem cell survival and adherence [62].

Another factor can be the scaffolds themselves. HA works as a scaffold [50], and the studies [20, 44, 47, 48] reported by Pak et al. used HA for such purposes. Adipose SVF contains a variety of cell types including ADSCs and extracellular matrix (ECM) [13, 14]. Such ECM contained in the adipose SVF may also work as scaffold and assist ADSCs to adhere to the lesion, proliferate, and differentiate [51]. ECM also may excrete a variety of cytokines and growth factors, affecting the cartilage regeneration by MSCs [51, 63–65].

The mode of injection does not seem be a major determining factor in cartilage regeneration. Most studies reported by Koh et al. used intra-articular injections of adipose SVF under arthroscopic guidance. However, it is unclear whether such an injection is better than a percutaneous injection. Arthroscopic examination of knees requires spinal or general anesthesia; thus, it is not considered to be a minimally invasive procedure. In addition, arthroscopic lavage and debridement for OA of the knee are ineffective [66]. A head-to-head study may be necessary to determine if such an invasive procedure outweighs the efficacy of percutaneous injections.

6. Conclusions

At present, there is no cure for painful OA in stages 2 and 3. For these patients, the intra-articular injection of ADSCs in the form of SVF can be an alternative treatment for now. As described in this review, the joint injection of ADSCs in the form of SVF with PRP can be safe and efficacious. Moreover, obtaining approximately 100 g of adipose tissue and percutaneous joint injections is considered to be a minimally invasive procedure and can be readily accepted by patients. These procedures carry relatively low rates of morbidity and side effects.

Although a large amount of injecting ADSCs is more efficacious in regenerating cartilage, the studies reviewed in this paper have shown that ADSCs in the form of SVF with PRP can be efficacious in symptom improvement.

However, lack of well-designed studies with control on using different methods and components of the injections still leaves many questions unanswered. In addition, the lack of understanding of the mechanism of action of ADSCs dictates the need for more clinical trials.

Conflict of Interests

The authors have no conflict of interests.

Authors' Contribution

Jaewoo Pak and Jung Hun Lee contributed equally to this work.

Acknowledgments

This work was supported by research grants from the National Research Laboratory Program through the National Research Foundation of Korea (NRF) funded by the Ministry of Science, ICT and Future Planning (no. 2011-0027928) and the Next Generation BioGreen 21 Program (no. PJ01103103) of Rural Development Administration in Republic of Korea.

References

[1] L. S. Simon, "Osteoarthritis," *Current Rheumatology Reports*, vol. 1, no. 1, pp. 45–47, 1999.

[2] J. A. Buckwalter, "Articular cartilage injuries," *Clinical Orthopaedics and Related Research*, vol. 402, no. 1, pp. 21–37, 2002.

[3] P. J. Belmont Jr., G. P. Goodman, B. R. Waterman, J. O. Bader, and A. J. Schoenfeld, "Thirty-day postoperative complications and mortality following total knee arthroplasty: incidence and risk factors among a national sample of 15,321 patients," *The Journal of Bone and Joint Surgery*, vol. 96, no. 1, pp. 20–26, 2014.

[4] M. Aynardi, L. Pulido, J. Parvizi, P. F. Sharkey, and R. H. Rothman, "Early mortality after modern total hip arthroplasty," *Clinical Orthopaedics and Related Research*, vol. 467, no. 1, pp. 213–218, 2009.

[5] S. Glyn-Jones, A. J. Palmer, R. Agricola et al., "Osteoarthritis," *The Lancet*, vol. 386, no. 9991, pp. 376–387, 2015.

[6] S. P. Arnoczky, "Building a meniscus. Biologic considerations," *Clinical Orthopaedics and Related Research*, vol. 367, supplement, pp. S244–S253, 1999.

[7] S. J. Szilvassy, "The biology of hematopoietic stem cells," *Archives of Medical Research*, vol. 34, no. 6, pp. 446–460, 2003.

[8] A. I. Caplan, "Mesenchymal stem cells," *Journal of Orthopaedic Research*, vol. 9, no. 5, pp. 641–650, 1991.

[9] D. R. Carter, G. S. Beaupré, N. J. Giori, and J. A. Helms, "Mechanobiology of skeletal regeneration," *Clinical Orthopaedics and Related Research*, vol. 355, supplement, pp. S41–S55, 1998.

[10] B. Johnstone and J. U. Yoo, "Autologous mesenchymal progenitor cells in articular cartilage repair," *Clinical Orthopaedics and Related Research*, supplement, no. 367, pp. S156–S162, 1999.

[11] C. J. Centeno, D. Busse, J. Kisiday, C. Keohan, M. Freeman, and D. Karli, "Increased knee cartilage volume in degenerative joint disease using percutaneously implanted, autologous mesenchymal stem cells," *Pain Physician*, vol. 11, no. 3, pp. 343–353, 2008.

[12] C. J. Centeno, J. R. Schultz, M. Cheever, B. Robinson, M. Freeman, and W. Marasco, "Safety and complications reporting on the re-implantation of culture-expanded mesenchymal stem cells using autologous platelet lysate technique," *Current Stem Cell Research & Therapy*, vol. 5, no. 1, pp. 81–93, 2010.

[13] P. A. Zuk, M. Zhu, H. Mizuno et al., "Multilineage cells from human adipose tissue: implications for cell-based therapies," *Tissue Engineering*, vol. 7, no. 2, pp. 211–228, 2001.

[14] P. A. Zuk, M. Zhu, P. Ashjian et al., "Human adipose tissue is a source of multipotent stem cells," *Molecular Biology of the Cell*, vol. 13, no. 12, pp. 4279–4295, 2002.

[15] F. Toghraie, M. Razmkhah, M. A. Gholipour et al., "Scaffold-free adipose-derived stem cells (ASCs) improve experimentally induced osteoarthritis in rabbits," *Archives of Iranian Medicine*, vol. 15, no. 8, pp. 495–499, 2012.

[16] L. L. Black, J. Gaynor, D. Gahring et al., "Effect of adipose-derived mesenchymal stem and regenerative cells on lameness in dogs with chronic osteoarthritis of the coxofemoral joints: a randomized, double-blinded, multicenter, controlled trial," *Veterinary Therapeutics*, vol. 8, no. 4, pp. 272–284, 2007.

[17] A. Guercio, P. Di Marco, S. Casella et al., "Production of canine mesenchymal stem cells from adipose tissue and their application in dogs with chronic osteoarthritis of the humeroradial joints," *Cell Biology International*, vol. 36, no. 2, pp. 189–194, 2012.

[18] D. D. Frisbie, J. D. Kisiday, C. E. Kawcak, N. M. Werpy, and C. W. McIlwraith, "Evaluation of adipose-derived stromal vascular fraction or bone marrow-derived mesenchymal stem cells for treatment of osteoarthritis," *Journal of Orthopaedic Research*, vol. 27, no. 12, pp. 1675–1680, 2009.

[19] J.-M. Lee and G.-I. Im, "SOX trio-co-transduced adipose stem cells in fibrin gel to enhance cartilage repair and delay the progression of osteoarthritis in the rat," *Biomaterials*, vol. 33, no. 7, pp. 2016–2024, 2012.

[20] J. Pak, "Regeneration of human bones in hip osteonecrosis and human cartilage in knee osteoarthritis with autologous adipose-tissue-derived stem cells: a case series," *Journal of Medical Case Reports*, vol. 7, no. 5, article 296, 2011.

[21] C. H. Jo, Y. G. Lee, W. H. Shin et al., "Intra-articular injection of mesenchymal stem cells for the treatment of osteoarthritis of the knee: a proof-of-concept clinical trial," *STEM CELLS*, vol. 32, no. 5, pp. 1254–1266, 2014.

[22] Y.-G. Koh, Y.-J. Choi, S.-K. Kwon, Y.-S. Kim, and J.-E. Yeo, "Clinical results and second-look arthroscopic findings after treatment with adipose-derived stem cells for knee osteoarthritis," *Knee Surgery, Sports Traumatology, Arthroscopy*, vol. 23, no. 5, pp. 1308–1316, 2015.

[23] Y. G. Koh, Y. J. Choi, O. R. Kwon, and Y. S. Kim, "Second-look arthroscopic evaluation of cartilage lesions after mesenchymal stem cell implantation in osteoarthritic knees," *American Journal of Sports Medicine*, vol. 42, no. 7, pp. 1628–1637, 2014.

[24] H. Nakagami, K. Maeda, R. Morishita et al., "Novel autologous cell therapy in ischemic limb disease through growth factor secretion by cultured adipose tissue-derived stromal cells," *Arteriosclerosis, Thrombosis, and Vascular Biology*, vol. 25, no. 12, pp. 2542–2547, 2005.

[25] L. Cai, B. H. Johnstone, T. G. Cook et al., "Suppression of hepatocyte growth factor production impairs the ability of adipose-derived stem cells to promote ischemic tissue revascularization," *STEM CELLS*, vol. 25, no. 12, pp. 3234–3243, 2007.

[26] K. Mizuno, T. Muneta, T. Morito et al., "Exogenous synovial stem cells adhere to defect of meniscus and differentiate into cartilage cells," *Journal of Medical and Dental Sciences*, vol. 55, no. 1, pp. 101–111, 2008.

[27] E. Ong, M. Chimutengwende-Gordon, and W. Khan, "Stem cell therapy for knee ligament, articular cartilage and meniscal

injuries," *Current Stem Cell Research & Therapy*, vol. 8, no. 6, pp. 422–428, 2013.

[28] A. I. Caplan and J. E. Dennis, "Mesenchymal stem cells as trophic mediators," *Journal of Cellular Biochemistry*, vol. 98, no. 5, pp. 1076–1084, 2006.

[29] R. W. Y. Yeo, R. C. Lai, K. H. Tan, and S. K. Lim, "Exosome: a novel and safer therapeutic refinement of mesenchymal stem cell," *Exosomes and Microvesicles*, vol. 1, no. 7, pp. 1–12, 2013.

[30] F. Ferro, R. Spelat, G. Falini et al., "Adipose tissue-derived stem cell in vitro differentiation in a three-dimensional dental bud structure," *The American Journal of Pathology*, vol. 178, no. 5, pp. 2299–2310, 2011.

[31] D. Moher, A. Liberati, J. Tetzlaff, and D. G. Altman, "The PRISMA Group. Preferred reporting items for systematic reviews and meta-analyses: the PRISMA statement," *Annals of Internal Medicine*, vol. 151, no. 4, pp. 264–269, 2009.

[32] Ministry of Food and Drug Safety (MFDS), *Cell Therapy: Rules and Regulations*, MFDS, Seoul, South Korea, 2009, http://www.mfds.go.kr/index.do?mid=1013&seq=9618&cmd=v.

[33] Y.-J. Ryu, T.-J. Cho, D.-S. Lee, J.-Y. Choi, and J. Cho, "Phenotypic characterization and in vivo localization of human adipose-derived mesenchymal stem cells," *Molecules and Cells*, vol. 35, no. 6, pp. 557–564, 2013.

[34] D. A. De Ugarte, K. Morizono, A. Elbarbary et al., "Comparison of multi-lineage cells from human adipose tissue and bone marrow," *Cells Tissues Organs*, vol. 174, no. 3, pp. 101–109, 2003.

[35] L. Aust, B. Devlin, S. J. Foster et al., "Yield of human adipose-derived adult stem cells from liposuction aspirates," *Cytotherapy*, vol. 6, no. 1, pp. 7–14, 2004.

[36] M. J. Oedayrajsingh-Varma, S. M. van Ham, M. Knippenberg et al., "Adipose tissue-derived mesenchymal stem cell yield and growth characteristics are affected by the tissue-harvesting procedure," *Cytotherapy*, vol. 8, no. 2, pp. 166–177, 2006.

[37] Y. Zhu, T. Liu, K. Song, X. Fan, X. Ma, and Z. Cui, "Adipose-derived stem cell: a better stem cell than BMSC," *Cell Biochemistry and Function*, vol. 26, no. 6, pp. 664–675, 2008.

[38] J. B. Mitchell, K. McIntosh, S. Zvonic et al., "Immunophenotype of human adipose-derived cells: temporal changes in stromal-associated and stem cell-associated markers," *STEM CELLS*, vol. 24, no. 2, pp. 376–385, 2006.

[39] F. Guilak, K. E. Lott, H. A. Awad et al., "Clonal analysis of the differentiation potential of human adipose-derived adult stem cells," *Journal of Cellular Physiology*, vol. 206, no. 1, pp. 229–237, 2006.

[40] P. C. Baer and H. Geiger, "Adipose-derived mesenchymal stromal/stem cells: tissue localization, characterization, and heterogeneity," *Stem Cells International*, vol. 2012, Article ID 812693, 11 pages, 2012.

[41] R. L. R. Van, C. E. Bayliss, and D. A. K. Roncari, "Cytological and enzymological characterization of adult human adipocyte precursors in culture," *The Journal of Clinical Investigation*, vol. 58, no. 3, pp. 699–704, 1976.

[42] J. M. Gimble, A. J. Katz, and B. A. Bunnell, "Adipose-derived stem cells for regenerative medicine," *Circulation Research*, vol. 100, no. 9, pp. 1249–1260, 2007.

[43] E. Anitua, I. Andia, B. Ardanza, P. Nurden, and A. T. Nurden, "Autologous platelets as a source of proteins for healing and tissue regeneration," *Thrombosis and Haemostasis*, vol. 91, no. 1, pp. 4–15, 2004.

[44] J. Pak, J.-J. Chang, J. H. Lee, and S. H. Lee, "Safety reporting on implantation of autologous adipose tissue-derived stem cells with platelet-rich plasma into human articular joints," *BMC Musculoskeletal Disorders*, vol. 14, article 337, 2013.

[45] B. L. Eppley, W. S. Pietrzak, and M. Blanton, "Platelet-rich plasma: a review of biology and applications in plastic surgery," *Plastic and Reconstructive Surgery*, vol. 118, no. 6, pp. 147e–159e, 2006.

[46] D. Fufa, B. Shealy, M. Jacobson, S. Kevy, and M. M. Murray, "Activation of platelet-rich plasma using soluble type I collagen," *Journal of Oral and Maxillofacial Surgery*, vol. 66, no. 4, pp. 684–690, 2008.

[47] J. Pak, J. H. Lee, and S. H. Lee, "A novel biological approach to treat chondromalacia patellae," *PLoS ONE*, vol. 8, no. 5, Article ID e64569, 2013.

[48] J. Pak, J. H. Lee, and S. H. Lee, "Regenerative repair of damaged meniscus with autologous adipose tissue-derived stem cells," *BioMed Research International*, vol. 2014, Article ID 436029, 10 pages, 2014.

[49] Y. S. Kim, Y. J. Choi, D. S. Suh et al., "Mesenchymal stem cell implantation in osteoarthritic knees: is fibrin glue effective as a scaffold?" *The American Journal of Sports Medicine*, vol. 43, no. 1, pp. 176–185, 2015.

[50] M. Uzuki and T. Sawai, "A comparison of the affinity of sodium hyaluronate of various molecular weights for degenerated cartilage: a histochemical study using hyaluronic acid binding protein," *International Congress Series*, vol. 1223, pp. 279–284, 2001.

[51] K. E. M. Benders, P. R. V. Weeren, S. F. Badylak, D. B. F. Saris, W. J. A. Dhert, and J. Malda, "Extracellular matrix scaffolds for cartilage and bone regeneration," *Trends in Biotechnology*, vol. 31, no. 3, pp. 169–176, 2013.

[52] Y. G. Koh and Y. J. Choi, "Infrapatellar fat pad-derived mesenchymal stem cell therapy for knee steoarthritis," *Knee*, vol. 19, no. 6, pp. 902–907, 2012.

[53] Y.-G. Koh, S.-B. Jo, O.-R. Kwon et al., "Mesenchymal stem cell injections improve symptoms of knee osteoarthritis," *Arthroscopy*, vol. 29, no. 4, pp. 748–755, 2013.

[54] K. Bui, T. Duong, N. Nguyen et al., "Symptomatic knee osteoarthritis treatment using autologous adipose derived stem cells and platelet-rich plasma: a clinical study," *Biomedical Research and Therapy*, vol. 1, no. 1, pp. 2–8, 2014.

[55] Y. G. Koh, O. R. Kwon, Y. S. Kim, and Y. J. Choi, "Comparative outcomes of open-wedge high tibial osteotomy with platelet-rich plasma alone or in combination with mesenchymal stem cell treatment: a prospective study," *Arthroscopy*, vol. 30, no. 11, pp. 1453–1460, 2014.

[56] J. Michalek, R. Moster, L. Lukac et al., "Autologous adipose tissue-derivedstromal vascular fraction cells application in patients with osteoarthritis," *Cell Transplantation*, In press.

[57] J. L. Dragoo, G. Carlson, F. McCormick et al., "Healing full-thickness cartilage defects using adipose-derived stem cells," *Tissue Engineering*, vol. 13, no. 7, pp. 1615–1621, 2007.

[58] Q. Li, J. Tang, R. Wang et al., "Comparing the chondrogenic potential in vivo of autogeneic mesenchymal stem cells derived from different tissues," *Artificial Cells, Blood Substitutes, and Biotechnology*, vol. 39, no. 1, pp. 31–38, 2011.

[59] A. D. Martin, M. Z. Daniel, D. T. Drinkwater, and J. P. Clarys, "Adipose tissue density, estimated adipose lipid fraction and whole body adiposity in male cadavers," *International Journal of Obesity and Related Metabolic Disorders*, vol. 18, no. 2, pp. 79–83, 1994.

[60] S. Schreml, P. Babilas, S. Fruth et al., "Harvesting human adipose tissue-derived adult stem cells: resection versus liposuction," *Cytotherapy*, vol. 11, no. 7, pp. 947–957, 2009.

[61] R. A. Soriano, H. Lamblet, S. A. Mohammadi, and H. Torfi, *Optimization of Roche Liberase TM Research Grade (Highly Purified Collagenase) in the Enzymatic Digestion of Human Adipose Tissue for the Isolation of Stem and Regenerative Cells*, Roche Diagnostic Cooperation, Irvine, Calif, USA, 2013, https://lifescience.roche.com/wcsstore/RASCatalogAssetStore/Articles/CellIsolationApplicationNote3.pdf.

[62] R. C. Dregalla, N. F. Lyons, P. D. Reischling, and C. J. Centeno, "Amide-type local anesthetics and human mesenchymal stem cells: clinical implications for stem cell therapy," *Stem Cells Translational Medicine*, vol. 3, no. 3, pp. 365–374, 2014.

[63] K. E. LaBarbera, R. D. Hyldahl, K. S. O'Fallon, P. M. Clarkson, and S. Witkowski, "Pericyte NF-κB activation enhances endothelial cell proliferation and proangiogenic cytokine secretion in vitro," *Physiological Reports*, vol. 3, no. 4, Article ID e12309, 2015.

[64] G. Díaz-Araya, R. Vivar, C. Humeres, P. Boza, S. Bolivar, and C. Muñoz, "Cardiac fibroblasts as sentinel cells in cardiac tissue: receptors, signaling pathways and cellular functions," *Pharmacological Research*, vol. 101, pp. 30–40, 2015.

[65] S. J. O'Carroll, D. T. Kho, R. Wiltshire et al., "Pro-inflammatory TNFα and IL-1β differentially regulate the inflammatory phenotype of brain microvascular endothelial cells," *Journal of Neuroinflammation*, vol. 12, article 131, 2015.

[66] J. B. Moseley, K. O'Malley, N. J. Petersen et al., "A controlled trial of arthroscopic surgery for osteoarthritis of the knee," *The New England Journal of Medicine*, vol. 347, no. 2, pp. 81–88, 2002.